MSc in Physics
Department of Physics
School of Sciences
University of Ioannina

MASTER THESIS

Aspects of False Vacuum Decay

Dimitrios Efstratiou
Registration Number: 781

Supervisor: Leandros Perivolaropoulos

Ioannina
May 2023

Πρόγραμμα Μεταπτυχιακών Σπουδών
στη Φυσική
Τμήμα Φυσικής
Σχολή Θετικών Επιστημών
Πανεπιστήμιο Ιωαννίνων

ΜΕΤΑΠΤΥΧΙΑΚΗ ΔΙΠΛΩΜΑΤΙΚΗ ΕΡΓΑΣΙΑ (Μ.Δ.Ε)

Πτυχές της Διασποράς Ψευδούς Κενού

Δημήτριος Ευστρατίου
Αριθμός μητρώου: 781

Επιβλέπων καθηγητής:
Λέανδρος Περιβολαρόπουλος

Ιωάννινα
Μάιος 2023

Abstract

A field theory can have more than one classically stable vacua. A false vacuum is a state representing a local minimum of the potential (which is not also global), and a true vacuum is the global minimum. When a field is located in the false vacuum state quantum tunneling can make its transition to the true vacuum. This is called false vacuum decay. The passage from one state to the other happens through a first-order phase transition beginning with the nucleation of a bubble of the true vacuum. This bubble can expand asymptotically with the speed of light and gradually eat away more and more of the old-phase space with apocalyptic consequences for the universe.

This master thesis gives an analytic description of various aspects of false vacuum decay. Firstly, we study the fate of the false vacuum decay in zero temperature with and without gravitational effects, and present analytical expressions for the decay rate obtained with the "thin-wall approximation" and numerical solutions of the Euclidean equations of motion, the so-called bounce solutions. Also, the path integral formalism in Euclidean space is used to derive a general expression for the decay rate. Then, we extend our study to modified theories of gravity with a non-minimally coupled scalar field. Furthermore, the finite temperature false vacuum decay is studied, with emphasis on the high-temperature case, where the phase transition takes place through a thermal mechanism instead of quantum tunneling. The final part of this work is a qualitative study of a hypothetical cosmological phase transition of the effective Newton's constant G_{eff} at ultra-late times (during the last $150\,Myrs$). The scale of such a gravitational constant bubble nucleated at recent epochs is calculated with a theoretical model. Then, this scale is compared to the results obtained by the reanalysis of the latest SH0ES data which indicates hints for a transitional behavior in the four modeling parameters of the analysis around $z = 0.01$ (about $150\,Myrs$ ago). A transition of the type Ia supernovae (SnIa) absolute magnitude M_B parameter of the SH0ES data at redshift $z = 0.01$, which can be related to a rapid transition of G_{eff}, could potentially provide a resolution of the Hubble tension which is currently the most important tension of the standard cosmological model ΛCDM.

Περίληψη

Μία θεωρία πεδίου μπορεί να έχει περισσότερα από ένα κλασσικά σταθερά κενά. Ένα ψευδές κενό **(false vacuum)** είναι μια κατάσταση η οποία αντιπροσωπεύει ένα τοπικό ελάχιστο του δυναμικού (το οποίο επίσης δεν είναι ολικό ελάχιστο), ενώ το αληθές κενό **(true vacuum)** είναι το ολικό ελάχιστο. Όταν ένα πεδίο βρίσκεται σε κατάσταση ψευδοκενού το κβαντικό φαινόμενο σήραγγας μπορεί να προκαλέσει την μετάβαση του στο αληθές κενό. Αυτό αποκαλείται διάσπαση ψευδούς κενού **(false vacuum decay)**. Το πέρασμα από τη μία κατάσταση στην άλλη πραγματοποιείται μέσω μιας πρώτης τάξεως μετάπτωσης φάσης **(first-order phase transition)**, η οποία ξεκινά με την πυρήνωση μιας φυσαλίδας **(bubble nucleation)** που εμπεριέχει το αληθές κενό μέσα στο περιβάλλον ψευδούς κενού. Η φυσαλίδα μπορεί να εξαπλωθεί αγγίζοντας την ταχύτητα του φωτός και σταδιακά "καταπίνει" όλο και περισσότερο από το περιβάλλον της αρχικής φάσης με αποκαλυπτικές συνέπειες για το σύμπαν.

Αυτή η μεταπτυχιακή εργασία δίνει μια αναλυτική περιγραφή διάφορων πτυχών της διάσπασης ψευδούς κενού. Πρώτα, μελετάται η διάσπαση ψευδοκενού σε μηδενική θερμοκρασία με και χωρίς τη βαρυτική επίδραση, και παρουσιάζονται αναλυτικές εκφράσεις για τον ρυθμό διάσπασης που λήφθησαν μέσω της προσέγγισης λεπτού τείχους **(thin-wall approximation)** και οι αριθμητικές λύσεις των Ευκλείδειων εξισώσεων κίνησης, οι αποκαλούμενες λύσεις αναπήδησης **(bounce solutions)**. Επίσης, ο φορμαλισμός των ολοκληρωμάτων διαδρομής χρησιμοποιήθηκε για να εξαχθεί μια γενική έκφραση για το ρυθμό διάσπασης. Έπειτα, η μελέτη επεκτείνεται σε τροποποιημένες θεωρίες βαρύτητας με ένα μη ελάχιστα συζευγμένο **(non-minimally coupled)** βαθμωτό πεδίο. Επιπλέον, μελετάται η δίασπαση ψευδοκενού σε περατή θερμοκρασία, με έμφαση στο όριο υψηλής θερμοκρασίας, όπου η μετάπτωση φάσης γίνεται μέσω ενός θερμικού μηχανισμού αντί για το φαινόμενο σήραγγας. Το τελευταίο μέρος αυτής της εργασίας είναι μια ποιοτική μελέτη μιας υποθετικής κοσμολογικής μετάπτωσης φάσης της ενεργής σταθεράς του Νεύτωνα **(effective Newton's constant)** G_{eff} σε παροντικούς χρόνους (μεταξύ των τελευταίων $150\,Myrs$). Το μέγεθος μιας τέτοιας φυσαλίδας βαρυτικής σταθεράς που εμφανίζεται στο πρόσφατο κοσμολογικό παρελθόν υπολογίζεται μέσω ενός θεωρητικού μοντέλου. Στη συνέχεια, αυτο τό μέγεθος συγκρίνεται με αποτελέσματα που ελήφθησαν από την επανανάλυση των τελευταίων δεδομένων SH0ES τα οποία υποδεικνύουν στοιχεία μεταπτωτικής συμπεριφοράς στις τέσσερεις βασικές παραμέτρους μοντελοποίησης της ανάλυσης σε ερυθρά μετατόπιση $z = 0.01$ (περίπου $150\,Myrs$ πριν). Μια μετάπτωση της παραμέτρου απολύτου μεγέθους των σουπερνόβα τύπου Ia (SnIa) M_B στο $z = 0.01$, η οποία μπορεί να συνδέεται με μια ραγδιαία μετάπτωση του G_{eff}, μπορεί ενδεχομένως να επιλύσει την ''ένταση Hubble" (**Hubble tension**), η οποία επί του παρόντος αποτελεί το σημαντικότερο πρόβλημα του καθιερωμένου προτύπου της Κοσμολογίας ΛCDM.

Acknowledgements

First and foremost, I would like to express my deepest appreciation to my supervisor professor Leandros Perivolaropoulos for his precious advice, guidance, and crucial assistance. Without his presence, this thesis would not be accomplished. It was a great challenge to work on spectacular topics of Cosmology, a teenage dream fulfilled, and I am grateful to him for the opportunity he gave me.

I would also like to extend my special thanks to the examination committee members, professor Panagiota Kanti and professor Ioannis Florakis, for their invaluable input and expertise, which significantly contributed to the improvement of this thesis.

Furthermore, I would like to express my gratitude to all the department's theoretical and astrogeophysics division faculty members for their support throughout my M.Sc. journey.

Finally, I would like to say my deepest thanks to my parents, for their unconditional love and for their sacrifices for my education, they mean a lot to me. Also, many thanks to my brother Akis, my grandparents, my girlfriend Dimitra, Petros, Lia, and all my friends for their companionship, emotional and spiritual support, and the unforgettable memories of a great life.

Contents

Appendices

Chapter 1

Introduction

1.1 Prologue

What can anybody say about Cosmology in a few words? Undoubtedly is one of the most exciting fields of physics, an intriguing chapter of science that tries to give answers to fundamental existential questions that arose during the development of human civilization, questions such as "Where do we come from?", "What are we?", "Where are we going?". But it is necessary to give a more appropriate and scientific definition of Cosmology, separating it from its philosophical essence, and state that it is the branch of physical science that studies the observable universe's origin, its large-scale structures and dynamics, and the ultimate fate of the universe, including the laws of science that govern it.

During the previous century, a great development was accomplished in the field of cosmology, a development that became a stepping stone for the scientific community in understanding the physical world. On the one side, Einstein with his famous theory of General Relativity (GR) described nature on large scales, featuring gravity as curvature, a property of space-time. Soon after his discovery Friedmann, Robertson, and Walker accomplished a model of the evolution of the universe. On the other side, for small scales, quantum mechanics developed by Dirac, Heisenberg, Bohr, Pauli, and more, in the same century, gives a descriptive picture of the fundamental particles and their interactions. With these two great theories in their hands, astrophysicists were able to understand the light emission of stars, which resulted in the measurability of the velocities of stars by the redshift.

Modern Cosmology of the 21st century is considered to be one of the two cornerstones of contemporary physics, the other one is quantum field theory (QFT). Technological progress brought, as it was obvious, progress in physical science and more specifically through the improvement of astrophysical observations of distant objects along with GR and the Friedmann-Robertson-Walker (FRW) cosmology Universe's modeling became possible. And lo and behold, the Big Bang theory was born [1–3], which most merely states that the reality with its principles and properties as we know it, started 13.8 billion years ago from an energy density singularity that inflated to the present day universe with us in it.

Some more historical comments we can make on this prologue is that originally, in the post-Word War II era, in the 40s, there were two distinct theories concerning Universe's initial conditions. On the one extreme Fred Hoyle, with his steady-state model supported the idea that new matter could flourish as the cosmos expanded. In his theory, the Universe is roughly the same at any point in time [4–7]. On the other extreme, the famous Big Bang theory, originated from Lemaitre [8, 9] and was developed further by Gamow, who introduced the Big Bang Nucleosyn-

thesis (BBN). Indeed, his colleagues Alpher and Herman predicted cosmic microwave background radiation (CMB) [10]. With a pinch of irony, the man who baptized Big Bang Lemaitre's theory was Hoyle in an attempt to reduce the importance of this model. But completely unexpectedly Penzias and Wilson in the year 1965 discovered by chance the CMB radiation[11] with an estimated calculation of its temperature to be around $3K$. This discovery was a huge confirmation step for Lemaitre's model.

1.2 Standard Cosmology

1.2.1 The standard ΛCDM model in brief

The standard Λ Cold Dark Matter (ΛCDM) model is an extremely predictive, explanatory, and observationally robust model, providing us with a substantial understanding of the formation of large-scale structure [12–15]. Let us define in brief the simple assumptions it is made of:

- Our Universe consists of ordinary matter (baryons and leptons), radiation (photons, neutrinos), cold (non-relativistic) dark matter briefly abbreviated as CDM [16–22] which is responsible for structure formation and a cosmological constant Λ [12][23] an enigmatic form of matter or energy that acts in opposition to gravity being responsible for the accelerating expansion of the Universe. This constant is considered by many physicists to be equivalent to dark energy or vacuum energy whose density remains constant even in an expanding background.

- General Relativity (GR) [24], the most famous theory in physics history, is considered to be the most suitable mathematical recipe so far to describe gravity on cosmological scales. The relevant action in these large scales is

$$S = \int d^4x\sqrt{-g}\left[\frac{1}{16\pi G}(R-2\Lambda)+\frac{1}{4\alpha}F_{\mu\nu}F^{\mu\nu}+\mathcal{L}_m(\psi,A)\right], \tag{1.1}$$

  where α is the fine structure constant, G is Newton's constant, $F_{\mu\nu}$ is the electromagnetic field strength tensor and $\mathcal{L}_m$ is the Lagrangian density for all matter fields ψ_m.

- The Cosmological Principle (CP) states the idea that the universe is essentially the same everywhere (statistically homogeneous and isotropic in space and matter) when viewed on a large scale above $100Mpc$.

- The universe is assumed to be flat. A description o a flat universe can be achieved through the Friedmann-Lemaître-Roberson-Walker (FLRW) metric

$$ds^2 = dt^2 - a(t)^2(dr^2 + r^2d\theta^2 + r^2\sin^2\theta d\phi^2). \tag{1.2}$$

  The above emerges from the cosmological principle. This metric accompanied by Einstein's field equations with a Λ-term can lead us to the Friedmann equations

$$H^2 \equiv \frac{\dot{a}^2}{a^2} = \frac{8\pi G\rho+\Lambda}{3} \tag{1.3}$$

  and

$$\frac{\ddot{a}}{a} = -\frac{4\pi G}{3}(\rho+3p)+\frac{\Lambda}{3}, \tag{1.4}$$

  where a is the scale factor.

- In order to address the horizon and flatness issues, it is also assumed that the early Universe experienced a cosmic exponential expansion of space, or simply inflation [25–28]. The Universe's great structures (galaxies, etc) are created from quantum fluctuations that are enlarged to cosmic size from the microscopic inflationary region.

- Its basic parameters are the following six: two energy densities $\omega_b = \Omega_b h^2$ and $\omega_c = \Omega_c h^2$ (for baryonic matter and cold dark matter separately, since they have distinct effects on the CMB power spectra), including a scaling of physical density with the dimensionless Hubble parameter, $h \equiv H_0/100\ km\ s^{-1}\ Mpc^{-1}$; a parameter θ_* that corresponds to the sound horizon divided by the angular diameter distance to the last scattering, the amplitude A_s of the initial power spectrum of density perturbations, defined at a particular scale, and often given as a logarithm; the slope n of the initial power spectrum as a function of wavenumber; and a parameter τ describing how much the primary CMB anisotropies are scattered by the reionized medium at low redshifts [29].

The standard model can be generalized by modification in the defining action of Eq.(1.1). This generalization can be accomplished by replacing the fundamental constants with dynamical variables in the action's expression, or by adding new terms. Some of these modifications are for example to allow Newton's constant to be dependent on a scalar field Φ as $G \to G(\Phi(r,t))$ promoting it to a dynamical degree of freedom, adding new terms in the action which may be functionally connected to the curvature scalar (Ricci scalar), allowing for a dynamical fine structure constant, quintessence of the cosmological constant, etc.

1.2.2 Observational hints and cosmos ingredients

The main observational pillars that support the standard model of cosmology are [30–39]:

- Homogeneity and isotropy: As it was referred previously, to scales larger than $\geq 100\,Mpc$ the Universe looks homogeneous and isotropic. This is confirmed by large-scale surveys and by the almost isotropy of the CMB.

- The Hubble expansion or otherwise the famous Hubble's law: Objects with a comoving distance d move away from one another with a velocity

$$u = Hd \tag{1.5}$$

  with $H \sim 70\,km\,sec^{-1}\,Mpc^{-1}$. The size of our causal horizon is determined by the Hubble expansion law. As a consequence of this statement, objects separated by a comoving distance

$$d_H = 3000h^{-1}\,Mpc \tag{1.6}$$

  are receding from each other at the speed of light and are therefore causally disconnected.

- The Cosmic Microwave Background radiation (CMB): a bath of thermal photons with an almost perfect Planck distribution at a temperature $T_0 = 2.725 \pm 0.001\,K$. In 1992 the COBE satellite [40–44] was the first to measure some temperature anisotropies $\Delta T/T_0 \sim 10^{-5}$. This finding represents a great triumph for Cosmology because this small anisotropy, whose existence is predicted by cosmological models, provides the clue to the origin of structure. It is an important confirmation of theories of the early Universe.

- The abundance of light elements: observations of the abundance of elements in low metallicity regions reveal that a percentage about 76% of ordinary matter is in the form of hydrogen, then a 24% is ^4He and trace abundances of ^3He ($\sim 10^{-5}$), deuterium ($\sim 10^{-10}$) and ^7Li ($\sim 10^{-15}$), all relative to hydrogen [45–49]. These elements formed during the first three minutes of the Universe. Much later, in the interior of the stars in astrophysical processes such as during supernovae explosions heavier elements (metals) are produced.

Let us also sum up the Universe's composition, and the materials that make it up according to GR:

- The chemical elements, which were mentioned above constitute ordinary matter, the first basic ingredient of the cosmos, which is composed of baryons (such as protons and neutrons). It comprises in general gas, dust, stars, planets, people, etc. Baryonic matter with Radiation, another ingredient i.e. particles with zeros mass such as photons, occupy a poor 4% of our Universe.

- Dark Matter (DM) which accounts for an estimated 22%. The motions of the galaxies relative to one another can give us some dynamical evidence [50–52] for its existence. Dark matter earned the nickname 'cold' because it is non-relativistic during the era of structure formation. Modern theories about this exotic element believe that it is composed of some kind of new elementary particle.

- The remaining 74% of the universe is filled with an unknown component called Dark Energy. We already referred to it in the previous subsection as a type of energy field repulsive to gravity, responsible for the accelerating expansion of the Universe.

1.3 Challenges for ΛCDM

1.3.1 ΛCDM in crisis?

The majority of the features of a large number of cosmological observations may be explained with excellent effectiveness using the conventional cosmological model. The accelerating expansion of the Universe [53][54], the spectrum and statistical characteristics of the cosmos' large structures [15][55], the power spectrum and statistical properties of the primordial CMB anisotropies, and the observed abundances of various light nuclei, including lithium, hydrogen, deuterium, and helium, are just a few of these achievements already been referred.

Despite its exceptional effectiveness in explaining cosmology in simple words, the validity of ΛCDM has recently come under scrutiny as the precision of cosmological observations has been improved [56–61]. All this "turmoil" in the Cosmology society and the questioning of the sovereignty of the concordance cosmological model is motivated by a variety of theoretical problems and observational difficulties of ΛCDM.

The most crucial theoretical issues faced by ΛCDM are the fine-tuning [62–64] and coincidence problems [65][66]. The fine-tuning or cosmological constant Λ problem is connected to the fact that there is a sizable gap between observations and predicted from the theory values of the cosmological constant which reaches at least 60 orders of magnitude [63][67–69]. The nature of the second problem is related to the coincidental, approximately equal values of observed energy densities Ω_Λ and Ω_m nowadays despite their totally different evolution properties. A possible solution in a philosophical prism to these theoretical difficulties could be the anthropic principle [70–72]. It simply states that we, observers, exist and we exist in this Universe or in a specific

section of it, and therefore the Universe exists in a way that allows observers to come into existence. Within the framework of a multiverse, which the Strong Anthropic Principle (SAP) includes, only a small ensemble of Universes with their physical laws, that may be like ours, can provide the properties, the "coincidences", for intelligent life to exist and grow [73][74].

Apart from the theoretical problems, there are some observational issues showing up in astrophysical and cosmological data. More specifically there are signals that appear to be in some tension with the standard model as specified by the Planck18 parameter values [75][76]. This tension could be equal to 2σ or larger.

1.3.2 List of important tensions

Some large scale tensions with great interest are the following [29][56] :

- **The growth tension $(2-3\sigma)$:** A lower growth rate indicated by direct measurements of cosmological perturbations (weak lensing, cluster counts, etc) than that indicated by the Planck/ΛCDM parameter values [77–79]. In contrast to what Planck/ΛCDM suggests, in a GR context, a lower growth rate could reflect a lower matter density and/or lower amplitude of the primordial fluctuation spectrum [80–83].

- **CMB anisotropy anomalies $(2-3\sigma)$:** These anomalies could be signs of a closed Universe, anomalies on super-horizon scales, cold spot anomalies, lensing anomalies, a predilection for odd parity correlations, rotation of the CMB linear polarization that violates parity, and more. For a review, someone can check [84][85].

- **Cosmic dipoles $(2-5\sigma)$:** The cosmological principle's applicability may need to be reevaluated in light of flow dipole with peculiar large-scale velocity [86][87], the variance of the Hubble flow in the cosmic rest frame [88], the dipole anisotropy in radio galaxy counts at various frequencies [89], the quasar density dipole [90] and the fine structure constant dipole (quasar spectra) [91][92].

- **Baryon Acoustic Oscillations (BAO) curiosities $(2.5-3\sigma)$:** Galaxy and Lyman-α (Lyα) BAO discrepancy at the effective redshift of $z \sim 2.34$ [93–95].

- **Parity violating rotation of CMB linear polarization (Cosmic Birefringence):** An important issue for the standard cosmological model arose based on late evidence of the non-zero value of birefringence. This may indicate a new ingredient beyond our ΛCDM model. A value other than zero of isotropic cosmic birefringence was recently detected in the Polarization Data of Planck18 at a 2.4σ [96–99].

- **Small-scale curiosities:** Galaxy-scale observations show that the ΛCDM model has a number of issues with describing structures at small scales, including the core-cusp problem, missing satellite problem, too big to fail problem, angular momentum catastrophe, satellite planes problem, baryonic Tully-Fisher relation problem, void phenomenon, etc [100][101].

- **Age of the Universe:** Our galaxy's oldest stars' ages suggest that the Universe is slightly older and in tension with the numbers obtained using CMB Planck18 data in the framework of ΛCDM cosmology [102].

- **The Lithium problem $(2-4\sigma)$:** The Big Bang Nucleosynthesis theory (BBN) predicts five times less lithium than the metal abundance measurements of old stars in Milky Way's halo [103].

- **Quasars Hubble diagram** ($\sim 4\sigma$)**:** Hints for phantom, late time expansion indicated because of the tension of the standard model with the distance modulus-redshift relation of 1598 quasars at higher redshift z between 0.5 and 5.5 [104–106].

- **Oscillating signals in short range gravity experiments:** Additional research on short-range gravity tests has revealed the presence of a sub-millimeter wavelength oscillating force signal.[107][108].

- **Anomalously low baryon temperature** ($\sim 3.8\sigma$)**:** The Experiment to Detect the Global Epoch of Reionization Signature (EDGES) collaboration [109] using global (sky-averaged) 21-cm absorption signal, reports anomalously low baryon temperature $T_b \approx 4K$ at $z \approx 17$, which is half of its expected value.

- **Colliding clusters with high velocity** ($\sim 6\sigma$)**:** The El Gordo (ACT-CL J0102-4915) galaxy cluster located at $z = 0.87$ is in process of formation occurring by a collision of two subclusters with mass ratio 3.6. These two subclusters merge at a velocity of $2500 km/s$, which is very high and extremely rare at such redshifts in the context of ΛCDM cosmology [110][111].

- **The Hubble tension** ($> 4\sigma$)**:** Last in this list, but the most relative for this thesis is the Hubble. We will emphasize this subject in Chapter 6.

1.3.3 Suggestions to address standard model's issues

In the effort to address the problems of the ΛCDM model, several alternative theories have been proposed, such as extra dimensions [112–114], quintessence models [115], $f(R)$ extended gravity theories [116–118], scalar-tensor quintessence models [119, 120], k-essence [121], Chaplygin gas [122–124] etc.

A great question asked by Paul Dirac in 1937 was if the fundamental constants of physics, such as the gravitational constant, are indeed constants or they are changing with time [125]. More specifically, in literature familiar to these subjects, it is assumed that the gravitational constant is time-dependent with a power law [126–128]

$$G(t) = G_0 \left(\frac{t_0}{t}\right)^{\beta}, \tag{1.7}$$

where $G_0 = (6.67408 \pm 0.00031) \times 10^{-8}\, g^{-1}\, cm^3\, s^{-2}$ is the current value of the gravitational constant by observation [129] and $t_0 = (13.799 \pm 0.021) \times 10^9\, yrs$ is the measured age of the Universe.

Via this time dependence, a connection can be found with astrophysical observable parameters such as the luminosity of the SnIa. The variation of the gravitational constant is supported by modified gravity theories, and an assumed variation of this kind could address some tensions of the standard model.

A way to resolve Hubble tension against the power law variance of G is if we assume a rapid transition of the gravitational constant at a low redshift ($z \sim 0.01$) via the false vacuum decay mechanism. In this work, in the final chapter, is being studied the possibility of a rapid transition of the gravitational constant G_{eff} [130], in the context of a $F(\phi)$ modified gravity theory, at late cosmological times as a resolution of the Hubble tension. Could a cosmological first-order phase transition, recently in terms of cosmic time, be indicated by observational data, or does some unknown systematic error exists in this data analysis?

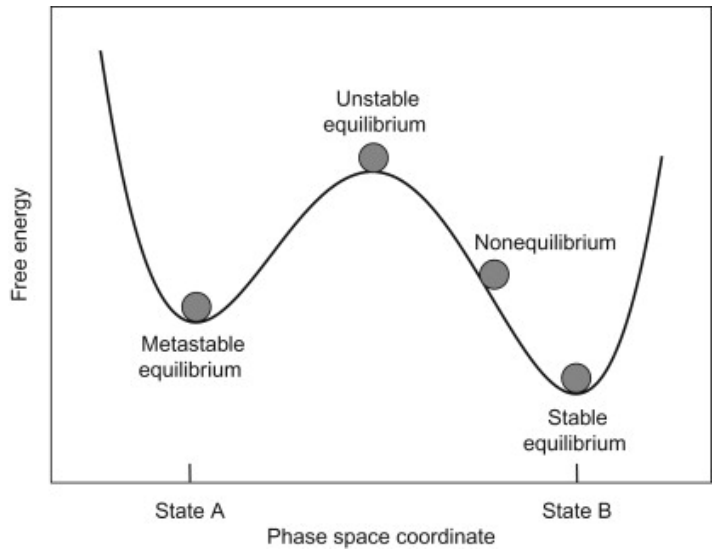

Figure 1.1: The three states of equilibrium: stable, metastable, and unstable.

1.4 False Vacuum decay: an overview

There could not be a more boring place in the Universe than vacuum, completely empty with no interesting events. This was an average person's notion living in the 19th century, a century before scientists achieve a respective understanding of quantum mechanics.

Over the last quarter of fifty years, we started discovering how fascinating and interesting this place is. In this previously doomed-to-boredom environment, all of a sudden a bubble is born. It grows and grows fast, almost with light speed and before we realize it we get engulfed by its fury. The vacuum gives birth to more bubbles, and new bubbles start to grow inside other bubbles and we end up with a universe full of universes, a multiverse. This sounds like a sci-fiction story but maybe it is not such much fiction but pure science.

But let us provide a clearer picture of the statements of the previous paragraph. We have already written that the one cornerstone of modern physics along with Cosmology is QFT. All the known particles that constitute the matter and interactions except for gravity can be very well described by the standard model (SM) of particle physics. It turns out that all the particles are excitations of some more fundamental objects that we call quantum fields. In QFT, a false vacuum is a hypothetical vacuum that is not in the most stable state possible in terms of energetics. This condition is called metastability and the vacuum metastable. To add a brief parenthesis, a stable state occurs when a particle is in its lowest energy state. A metastable state exists when the particle is in need of extra energy ΔG in order to reach its true stability. Finally, an unstable condition exists when for a transition to the stable or the metastable equilibrium $\Delta G = 0$ (check Fig.1.1). Although it might persist for a very long period, quantum tunneling might eventually cause it to decay into the true vacuum state, which is the most stable state. False vacuum decay is the name for this occurrence. The concept of bubble nucleation is frequently used to explain how such a decay might take place in the Universe. Therefore, this true vacuum bubble would expand in the false vacuum if a small area of our Universe was in its false vacuum condition and then suddenly reached a more stable vacuum (see Fig.1.2).

In the following chapters we will see a wide analysis of false vacuum decay, which is the main subject of this thesis, for now, let us say that if the potential of a field $U(\phi)$ has two or more minima, then quantum tunneling allows the particle or field to tunnel through the potential barriers

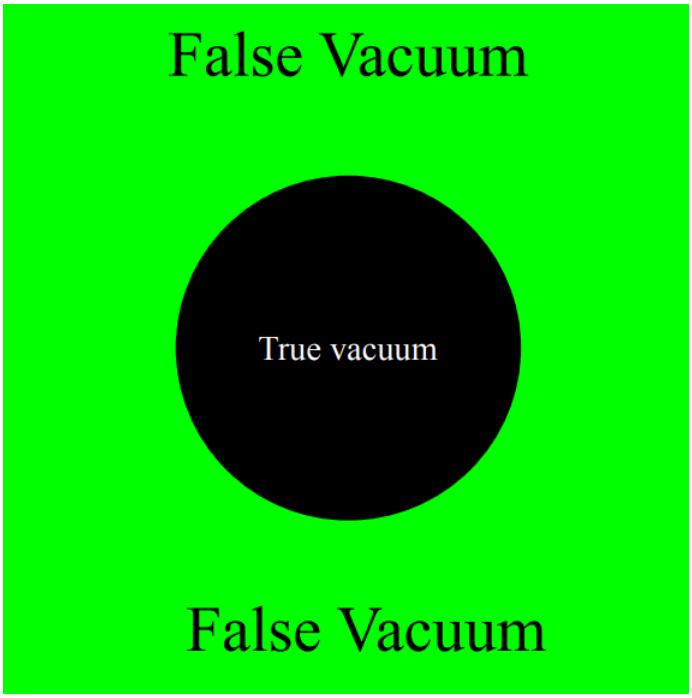

Figure 1.2: A true vacuum bubble surrounded by the false vacuum universe.

and move out of a metastable minimum. This means that if a field is not in its global minimum state of energy, it can switch there from the false vacuum through this quantum mechanism, something that is not allowed in classical mechanics. What happens in reality for quantum tunneling is that a bubble of the new phase is formed and expands. This is the familiar prescription for the first-order phase transitions we see in the everyday life. When we boil water, it does not evaporate all at once. Instead, small bubbles form near nucleation centers and then expand until the whole liquid phase disappears. The same thing will happen in a space vacuum decay and after a long enough time no trace of the old vacuum is left.

This whole situation sparks hordes of existential debates. The consequences of a false vacuum decay could be apocalyptically serious if our universe is actually in a false vacuum state. The implications of a new-physics bubble shallowing us could be as slight as a change in a few cosmic parameters, or they could result in the full cessation of all currently known fundamental forces, elementary particles, and structures that make them up.

1.5 Thesis synopsis

Some of the main questions we will try to answer in this thesis are the following: 1) Can we derive an analytic form for the decay rate of the false vacuum in finite and in zero temperature? 2) Can we derive an analytic form for the bubble's radius? 3) What are the differences between false vacuum decay in zero and in finite temperature? 4) What is the typical scale (size) of the produced true vacuum bubbles assuming that they form at the present cosmological time? 5) What is the required range of the scalar field mass so that the produced true vacuum bubbles expand and do not collapse? 6) How do these results change if the scalar field is non-minimally coupled to gravity and 7) what are the corresponding observational effects?

The thesis is organized as follows:

- In chapter 2 we make a review of the false vacuum decay at zero temperature in flat spacetime, as it was studied by Coleman, Callan, in their classical papers. We take a look at the decay rate coefficient, as it occurs from WKB approximation, and afterward, we try to calculate the two parameters, A and B, appearing in its expression, using the semi-classical approximation and path integral formulation. The bubble nucleated is assumed to be surrounded by a thin wall and this approach makes it possible for an analytical expression for B, or otherwise bounce action, to be derived. Some numerical solutions of the equation of motion for the rescaled potential are presented going a step further beyond the thin-wall approximation.

- In chapter 3 after the detailed derivation of the Euclidean field equations in the presence of gravity we come up with a new expression of the coefficient B in the thin-wall approach, always in the zero temperature case. Also, a numerical solution is presented in the Minkowski to Anti-de Sitter case transition.

- In chapter 4 we extend our calculations in the case of a non-minimally coupled scalar field theory, using the same methods as the second and third chapters. Numerical solutions are presented in the two cases of interest (de Sitter to Minkowski space transition and Minkowski to Anti-de Sitter transition).

- In chapter 5, the false vacuum decay is studied in finite temperature. Following Linde's work, we derive again analytical expressions for the bounce action, without and with gravitation. Also, we are including the calculations for the non-minimally coupled case in the thin-wall approximation.

- In chapter 6 the profile of a bubble nucleated at late cosmological times is studied, in the simple flat and in the non-minimally coupled case. We try to estimate a theoretical bubble scale for a rapid transition of G_{eff}, compare it with its value obtained by observational data if a phase transition in one of the parameters is allowed in the SH0ES analysis, and make a qualitative connection with the Hubble tension.

- In the final chapter we present a summary of this thesis, our conclusions, and future prospects.

Chapter 2

False vacuum decay at zero temperature

In this chapter, we take an analytic look at the background of the "false vacuum decay" issue, traveling through the concepts that have been discussed in the classic papers of the literature [131][132][133].

In order to understand deeper the object of our study it is useful to examine the problem through the semi-classical approach made in the papers by Coleman et al. Firstly, we will set the decay rate expression and discuss the two quantities (A and B) appearing on it. Then, as we will see, in the limit of vanishing energy density between the two ground states, it is possible to obtain an explicit expression for the coefficient B via a procedure called thin-wall approximation. Moreover, we will present some numerical solutions of the field equations in the flat spacetime studied in this chapter, obtained via shooting-method techniques. Later, using Feynman's path integral formulation we will try to get an explicit answer for the form of coefficient A.

The overall discussion in this chapter becomes at the background of the zero temperature limit (at flat spacetime), at Chapter 5 our subject will be examined in finite temperature.

2.1 The decay rate expression

In the first chapter, we discussed some of the properties of a first-order phase transition. We saw that a bubble of the new phase can grow in the sea of the old phase if it is energetically favorable for it.

A first-order phase transition is a good picture to describe the decay of the false vacuum in the new one. In our case, the bubble of the new phase is the bubble of the true vacuum. Once, a bubble of true vacuum forms large so that it is favorable to grow, it can spread throughout the cosmos converting false vacuum to true.

A helpful analogy that can be drawn comes from the point of view of nucleation processes in statistical physics. In a boiling superheated liquid, a similar phenomenon happens. As the liquid is heated, it settles in a metastable state of liquidity (instead of evaporating). To build the semantic correlation of what was already mentioned, the false and true vacua correspond, respectively, to the superheated liquid phase and to the vapor phase. In this case, small gas bubbles continuously materialize due to thermal fluctuations rather than quantum fluctuations in the liquid. Since the internal of the bubble is the location of the true vacuum, with lower energy density, its presence lowers the total energy of the system. However, the surface energy of the bubble increases the energy of the system as we will see in an upcoming section on the energetics of such a process. Eventually, a large enough bubble will materialize so that it is energetically

favorable for it to expand, in contrast, small bubbles tend to shrink and disappear. It will then convert the available liquid into vapor [134][135].

Thus, the thing to compute is the decay of the false vacuum per unit time per unit volume, Γ/V. From a cosmological aspect, an infinitely old universe must be in its true vacuum, no matter how slowly the false vacuum decays. However, our universe is not infinitely old. At the big bang time, the energy per unit volume was very high and the state of the universe was very far from any vacuum. As the universe expanded and cooled down, it might well have settled into a false vacuum instead of a true one. The relevant parameter for describing future events, as we shall see in Chapter 6, is that cosmic time for which the product of Γ/V and the four-volume of the past light cone becomes of order unity. If this time is on the order of milliseconds, the universe is still hot when the false vacuum decays, even on the scale of high-energy physics, and the zero-temperature computation of Γ/V is inapplicable. If this time is on the order of years, the decay of the false vacuum will lead to a sort of secondary big bang with interesting cosmological consequences. If the decay time is on the order of the current age of our universe, there is cause for concern. A false vacuum decay occurring at the present time might not bode well for the continuation of life, at least in the most pessimistic scenario akin to a horror film.

For a particle with total energy, E in a region with potential V the tunneling rate has the following form which is derived by the WKB approximation [1][136][137][138]

$$\Gamma(E) \approx e^{2\int_a^b \sqrt{2m(E-V)}\frac{dx}{\hbar}} \ . \tag{2.1}$$

In Appendix A tunneling rate formula is derived in detail.

In our case, using the WKB approximation, the probability of the decay of the false vacuum per unit time per unit volume is of the form [131][132]

$$\Gamma/V = Ae^{-B/\hbar}, \tag{2.2}$$

where A and B depend on the theory under study. In the next sections, we will try to derive explicit expressions for these two coefficients and give to the decay rate formula a compact form.

2.2 False vacuum decay in the absence of gravity

2.2.1 Barrier penetration in one dimension

First of all, we consider a particle of unit mass moving in one dimension with the Lagrangian,

$$L = \frac{1}{2}\dot{q}^2 - V(q). \tag{2.3}$$

The potential, V, is depicted in Fig.2.1. The point q_0 marks the classical stable equilibrium, but as we all know in quantum mechanics there is no quantum mechanical stable equilibrium state corresponding to the classical one. Note that the zero of the energy is chosen at the nullification of the potential.

In the semi-classical regime, which is a good approximation for a large B coefficient, our particle will penetrate the potential barrier (the classical forbidden area) through the well-known

[1] In the biggest part of this thesis (except for the appendices), we adopt the natural units system, where the reduced Planck constant ($\hbar$) and the speed of light (c) are both set to 1. This choice of units simplifies many equations allowing for a more streamlined analysis. It is important to note that when interpreting the results, one should convert the quantities back to standard units (e.g., SI units) for accurate physical interpretation.

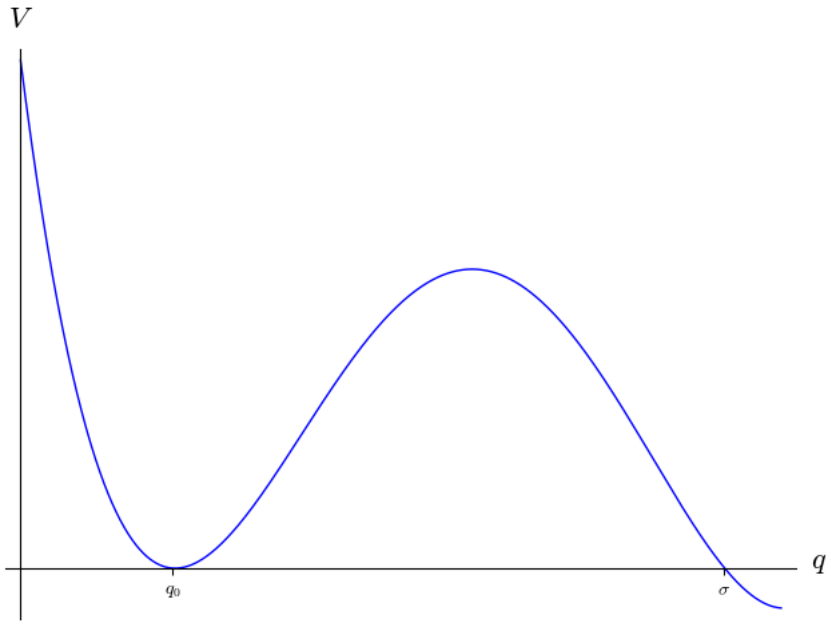

Figure 2.1: The potential of a theory with a false ground state.

process called "quantum tunneling" and will materialize at the escape point, σ, with zero kinetic energy. After this, it will propagate classically again in the new classical area.

Now, the width associated with this process is given by an expression of the form

$$\Gamma = Ae^{-B}. \tag{2.4}$$

Notice that Γ is not divided by the volume this time and it is making sense totally because we are examining the one-dimensional problem.

Now, let us state some information about the equilibrium points. Equilibrium points can be thought of as follows: If an object is placed at rest at an equilibrium point, it will stay there for all time. This is therefore a point where the force acting on the object is zero. Hence, this corresponds to a point where the slope of the potential energy curve is zero.

Now, returning again to the figure above, we can state that if the particle starts off at rest at the minimum, q_0, it will stay there. If it starts at rest away from it, it is pulled towards the minimum. Suppose it starts out from the left of the point q_0. It will start moving towards the minimum, transferring potential energy to kinetic energy. Since energy is conserved, the maximum potential energy is at the moment where the kinetic energy is zero. So, this is meaning that the particle cannot move up to a higher starting point above a certain amount of energy. Thus, the motion is bounded. We call this minimum, for obvious reasons, a stable equilibrium point [139][140].

The coefficient B is going to be

$$B = \int_{q_0}^{\sigma} (2V)^{1/2}\, dq\ . \tag{2.5}$$

In the next paragraph, we will try to explain the reason why this parameter, which throughout this thesis will be called bounce action, has this form.

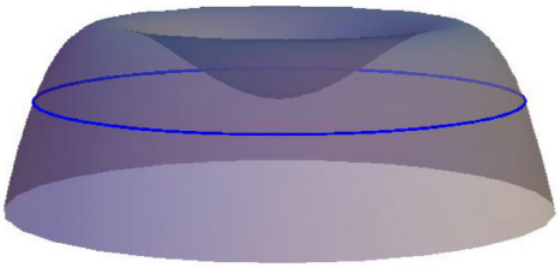

Figure 2.2: Probable escape points from the potential barrier in many dimensions (taken from [143]).

2.2.2 Barrier penetration in many dimensions

The generalization of the problem in many dimensions was first given by Banks, Bender, and Wu in a series of papers [141][142]. According to their work, the coordinates of the particle get concentrated into a vector, $\vec{q}$. The Lagrangian is

$$L = \frac{1}{2}\dot{\vec{q}} \cdot \dot{\vec{q}} - V(\vec{q}). \tag{2.6}$$

Just as in the one-dimensional case, the potential is assumed to have a local minimum at a point, $\vec{q_0}$ and the zero of the energy is chosen such that $V(\vec{q_0})$ vanishes. Of course, the single zero of potential, σ, from the previous subsection is replaced by a surface of zeros, Σ. In simpler words, in the one-dimensional problem, where the only quest was to calculate the possibility of the particle reaching the other side of the barrier, here, the starting point is surrounded by a lot of barriers, one for every degree of freedom. There are a lot of points with energy equal to the starting point, where the particle can be found (the blue line in Fig.2.2). Therefore, it is not enough to calculate the probability width of the passage through the barrier, but also the most probable reaching point must be computed. The method of generalizing the WKB approximation is based on founding the most probable escape path (MPEP). Eventually, the parameter of our interest is going to be

$$B = 2\int_{\vec{q_0}}^{\vec{\sigma}} (2V)^{1/2}\, ds \tag{2.7}$$

where every path P which overcomes the barrier can be represented by a trajectory $\vec{q}(s)$, where s the parameter defined as:

$$ds^2 = d\vec{q} \cdot d\vec{q}. \tag{2.8}$$

The vector $\vec{\sigma}$ is a point on the surface Σ. Also, the integral is over that path for which B is a minimum,

$$\delta B = \delta \int_{\vec{q_0}}^{\vec{\sigma}} (2V)^{1/2}\, ds \; = 0. \tag{2.9}$$

The above equation Eq.(2.9) definitely starts to remind us of the "principle of least action" from the mechanics' textbooks. The particle penetrates the potential barrier along the path of least resistance. After the penetration, the particle reaches the escape point, $\vec{\sigma}$, with zero kinetic energy and continues its classical propagation.

It is the right time to remind that in classical mechanics, Maupertuis's principle [144] asserts that a physical system takes the least-length path. It is a special case of the more generally stated

principle of least action. According to this principle, the true path of a system described by N generalized coordinates $\vec{q} = (q_1, q_2, \ldots, q_N)$ between two specified states $\vec{q}_1$ and $\vec{q}_2$ is a stationary point of the abbreviated action functional

$$S_0[\vec{q}(t)] = \int \vec{p} \cdot d\vec{q}, \tag{2.10}$$

where $\vec{p} = (p_1, p_2, \ldots, p_N)$ are the conjugate momenta of the generalized coordinates.

In Jacobi's formulation for such systems, the kinetic energy is related to the generalized momenta and the generalized velocities with a simple relation

$$2T = \vec{p} \cdot \dot{\vec{q}}. \tag{2.11}$$

Also, the kinetic energy term can be written as

$$T = \frac{1}{2}\left(\frac{ds}{dt}\right)^2, \tag{2.12}$$

it follows that,

$$2Tdt = \sqrt{2T}ds. \tag{2.13}$$

Therefore, the abbreviated action is going to be

$$S_0 = \int \vec{p} \cdot d\vec{q} = \int \vec{p} \cdot \frac{d\vec{q}}{dt}dt = \int 2Tdt = \int ds \left[2\left(E - V\right)\right]^{1/2}. \tag{2.14}$$

Let us now introduce the variational problem that arose from the above analysis:

$$\delta \int ds \left[2\left(E - V\right)\right]^{1/2} = 0. \tag{2.15}$$

This equation determines the shape of the particle's trajectory in the configuration space. These trajectories are solutions to the equations of motion derived by the Euler-Lagrange equations. For our Lagrangian which is described by Eq.(2.6) we get

$$\frac{\partial L}{\partial \vec{q}} = -V'(\vec{q}) \tag{2.16}$$

and

$$\frac{d}{dt}\left(\frac{\partial L}{\partial \dot{\vec{q}}}\right) = \frac{d^2\vec{q}}{dt^2}. \tag{2.17}$$

The Euler-Lagrange equation states the equality of the above two equations. So, we get the equation of motion (EoM)

$$\frac{d^2\vec{q}}{dt^2} = -V'(\vec{q}) \tag{2.18}$$

with energy

$$E = \frac{1}{2}\dot{q}^2 + V. \tag{2.19}$$

The intonation of V indicates derivation with respect to $\vec{q}$ and the dot on q suggests derivation with respect to time t.

Comparing Eq.(2.9) and Eq.(2.15) we notice that both variational principles differ in three aspects: in the first equation, $E = 0$ and the signs of the potential are flipped. In the second one,

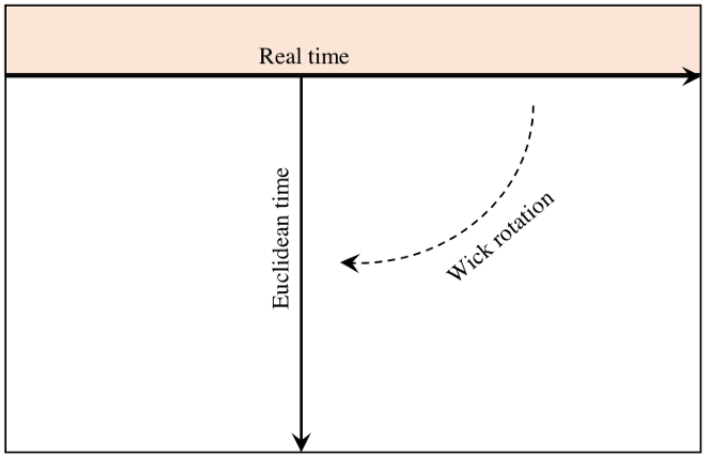

Figure 2.3: The imaginary/Euclidean time axis and a Wick rotation (taken from [145]).

the endpoints are not fixed but are free to vary along the surface Z, but let this last statement be ignored for the moment.

Equation (2.7) is derived by performing a Wick rotation at the Minkoswkian action of our problem [146][147][145]. This process is prompted by the realization that the metric signature $(+1,-1,-1,-1)$ of the Minkowski metric in natural units

$$ds^2 = dt^2 - dx^2 - dy^2 - dz^2 \tag{2.20}$$

and the four-dimensional Euclidean metric

$$ds^2 = -d\tau^2 - dx^2 - dy^2 - dz^2 \tag{2.21}$$

are equivalent if the coordinate t is allowed to have imaginary values. The Minkowski metric becomes Euclidean when t is restricted to the imaginary values, and vice versa. And as may one see in Fig.2.3 it is called a "rotation" because it rotates time values from the real axis to the imaginary one. Taking a problem expressed in Minkowski space with coordinates x, y, z, t and substituting $t \to -i\tau$ sometimes leads to a problem in real Euclidean coordinates x, y, z, τ which is easier to cope with. In a few words, the passage from real to imaginary time takes us from Minkowski space to Euclidean space as Coleman states.

The Minkoswkian action in our situation is

$$S_M = \int dt L = \int dt \left[\frac{1}{2}\dot{\vec{q}}\cdot\dot{\vec{q}} - V(\vec{q})\right], \tag{2.22}$$

if we perform the transformation $t \to -i\tau$ we will obtain

$$\begin{aligned} S_M &= \int \frac{d\tau}{i}\left[\frac{1}{2}\left(\frac{d\vec{q}}{-id\tau}\right)^2 - V\right] = \int \frac{d\tau}{i}\left[\frac{1}{2}\left(\frac{d\vec{q}}{d\tau}\right)^2 i^2 - V\right] = \int d\tau\left[\frac{i}{2}\left(\frac{d\vec{q}}{d\tau}\right)^2 - \frac{1}{i}V\right] \Rightarrow \\ &\Rightarrow S_M = i\int d\tau\left[\frac{1}{2}\left(\frac{d\vec{q}}{d\tau}\right)^2 + V\right] = iS_E. \end{aligned} \tag{2.23}$$

In equation (2.23), $S_E = \int d\tau \left[\frac{1}{2}\left(\frac{d\vec{q}}{d\tau}\right)^2 + V\right]$ is the Euclidean action. A Euclidean Lagrangian can also be defined as

$$L_E = \frac{1}{2}\frac{d\vec{q}}{d\tau}\cdot\frac{d\vec{q}}{d\tau} + V \tag{2.24}$$

and for the variational problem (2.9) we get the equations of motion

$$\frac{d^2\vec{q}}{d\tau^2} = \frac{\partial V}{\partial \vec{q}}, \tag{2.25}$$

which is the imaginary-time version of Eq.(2.18) obtained by using the Euler-Lagrange equation on the Euclidean Lagrangian, with zero total energy

$$\frac{1}{2}\frac{d\vec{q}}{d\tau}\cdot\frac{d\vec{q}}{d\tau} - V = 0. \tag{2.26}$$

By the above equation, a condition arises and states that the system can reach the classical equilibrium point only asymptotically, q_0, as τ goes to minus infinity, this condition is the following

$$\lim_{\tau\to-\infty}\vec{q} = \vec{q}_0. \tag{2.27}$$

From the equation (2.26) again we get a second condition. The system is time-translation invariant, as may one see there is no explicit dependence on the imaginary time, hence we can choose $\tau = 0$, the Euclidean time at which the particle reaches the point $\vec{\sigma}$. If the particle at this time is at the escaping point where $V = 0$, we get from (2.26):

$$\left.\frac{d\vec{q}}{d\tau}\right|_{\tau=0} = 0. \tag{2.28}$$

Yet again by Eq.(2.26)

$$\frac{1}{2}\frac{d\vec{q}}{d\tau}\cdot\frac{d\vec{q}}{d\tau} = V \Rightarrow dq^2 = ds^2 = 2d\tau^2 V \Rightarrow d\tau = ds(2V)^{-1/2}, \tag{2.29}$$

putting this result at Euclidean action integral, using the two conditions and $E = 0$ we get

$$\begin{aligned} S_E &= \int_{-\infty}^{0} d\tau L_E = \int_{-\infty}^{0} d\tau\left[\frac{1}{2}\frac{d\vec{q}}{d\tau}\cdot\frac{d\vec{q}}{d\tau} + V\right] \\ &= \int_{\vec{q_0}}^{\vec{\sigma}} ds(2V)^{-1/2}2V \Rightarrow S_E = \int_{\vec{q_0}}^{\vec{\sigma}} ds(2V)^{1/2} \end{aligned} \tag{2.30}$$

This result looks almost the same with Eq.(2.9) which means we are close to understanding what coefficient B represents at the decay rate expression. Equation (2.28) is telling us that the motion of the particle for positive τ is just the time reversal of its motion for negative τ; the particle begins its motion at $\tau = -\infty$ from $\vec{q}_0$, simply bounces off Σ at $V = 0$ and returns to $\vec{q}_0$, at $\tau = +\infty$. The coefficient B is the Euclidean action for the bounce. In conclusion we can write

$$B = \int_{-\infty}^{+\infty} L_E = S_E. \tag{2.31}$$

Therefore, to find B we must find the bounce, which is the solution of the imaginary-time equations of motion with the boundary conditions described at equations (2.27) and (2.28). For the mechanism of this motion, namely, particle bouncing back at its starting point $\vec{q}_0$ as imaginary time goes to infinity, someone understands that the zero energy statement is a consequence of the first boundary condition.

2.2.3 Barrier penetration in field theory

In this section, the prescription of the previous calculations is going to be extended in field theory. Consider a field theory of a scalar field in the four-dimensional space-time described of the Lagrangian density [131][133]

$$\mathcal{L} = \frac{1}{2}\partial_\mu\phi\partial^\mu\phi - U(\phi). \tag{2.32}$$

with the action at Minkowski space to be

$$S_M = \int d^4x\mathcal{L} = \int d^4x \left[\frac{1}{2}\partial_\mu\phi\partial^\mu\phi - U(\phi)\right]. \tag{2.33}$$

Let the potential U hold two relative minima, $\phi_\pm$. One of them, let us say ϕ_-, is the absolute minimum (see Fig.2.4).The state of the classical field theory for which $\phi = \phi_-$ is the unique classical state of lowest energy. This minima in perturbation theory correspond to the unique vacuum state of the quantum theory. The state of the classical field theory for which $\phi = \phi_+$, is a stable classical equilibrium state. However, it is rendered unstable by quantum effects, in particular, by barrier penetration. This state is called a false vacuum, and this false vacuum state can decay in the true one ϕ_- with catastrophic consequences for the universe's existence. It is a good idea to finish this nihilistic paragraph with the saying of the famous theoretic physicist who studied this issue. Well, as Sidney Coleman said: *"In the true vacuum, the constants of nature, the masses, and couplings of the elementary particles, are all different from what they were in the false vacuum, and thus the observer is no longer capable of functioning biologically, or even chemically."*

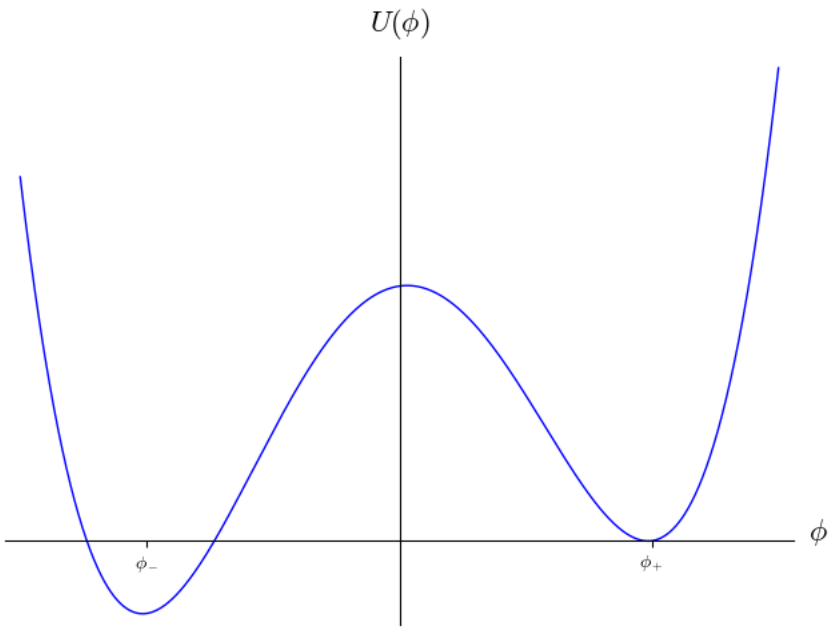

Figure 2.4: The potential in a theory with a false vacuum.

But, let us forget for the moment the decay of the false vacuum and remember some basic concepts from the field theory. As we know, the Lagrangian can be a function of ϕ and $\partial_\mu\phi$

$$\mathcal{L} = \mathcal{L}(\phi, \partial_\mu\phi). \tag{2.34}$$

In this way the action in Minkowski space is

$$S_M = \int d^4x \mathcal{L}(\phi, \partial_\mu \phi), \tag{2.35}$$

where the Lorentz invariant space-time volume element is used

$$d^4x = dt d^3x. \tag{2.36}$$

We now wish to vary the action in Eq.(2.35) in order to find the extremal solutions and obtain the equations of motion. Here we get

$$\delta S_M = \int d^4 \delta \mathcal{L} = \int d^4x \left\{ \frac{\partial \mathcal{L}}{\partial \phi} \delta\phi + \frac{\partial \mathcal{L}}{\partial(\partial_\mu \phi)} \delta(\partial_\mu \phi) \right\}. \tag{2.37}$$

But the variation of the partial derivatives of the field can be written as

$$\delta(\partial_\mu \phi) = \partial_\mu(\delta\phi) \tag{2.38}$$

and the action will be

$$\begin{aligned} \delta S_M &= \int d^4x \left\{ \frac{\partial \mathcal{L}}{\partial \phi} \delta\phi + \frac{\partial \mathcal{L}}{\partial(\partial_\mu \phi)} \partial_\mu(\delta\phi) \right\} \\ &= \int d^4x \left\{ \partial_\mu \left(\frac{\partial \mathcal{L}}{\partial(\partial_\mu \phi)} \delta\phi \right) - \partial_\mu \left(\frac{\partial \mathcal{L}}{\partial(\partial_\mu \phi)} \right) \delta\phi + \frac{\partial \mathcal{L}}{\partial \phi} \delta\phi \right\} \\ &= \int d^4x \partial_\mu \left(\frac{\partial \mathcal{L}}{\partial(\partial_\mu \phi)} \delta\phi \right) + \int d^4x \left\{ \frac{\partial \mathcal{L}}{\partial \phi} - \partial_\mu \left(\frac{\partial \mathcal{L}}{\partial(\partial_\mu \phi)} \right) \right\} \delta\phi. \end{aligned} \tag{2.39}$$

In the second line of the above equation, we have the product rules of the derivatives. The first term in the third line is a four-divergence, i.e. a total derivative. Since the integral is over the volume of all of space-time, the resulting hyper-surface term must be evaluated at infinity. The value of the field variation at these extremes is $\delta\phi = 0$. Thus, the hyper-surface term in Eq.(2.39) does not contribute.

Then imposing Hamilton's principle $\delta S = 0$, the first term, in the third line in Eq.(2.39) multiplying $\delta\phi$ must vanish for all possible values of $\delta\phi$. We obtain

$$\frac{\partial \mathcal{L}}{\partial \phi} - \partial_\mu \left(\frac{\partial \mathcal{L}}{\partial(\partial_\mu \phi)} \right) = 0, \tag{2.40}$$

which are the Euler-Lagrange equations. Making usage of Eq.(2.40) in our field theory of Eq.(2.32) in a background with the characteristic metric signature $\eta^{\mu\nu} = (+1, -1, -1, -1)$ giving rise to the results below:

$$\begin{aligned} &\frac{\partial \mathcal{L}}{\partial \phi} = -\frac{\partial U}{\partial \phi} = -U'(\phi), \\ &\partial_\mu \left(\frac{\partial \mathcal{L}}{\partial(\partial_\mu \phi)} \right) = \partial_\mu \left[\partial_{\partial_\mu \phi} \left(\frac{1}{2} \partial_\mu \phi \partial^\mu \phi \right) \right] = \partial_\mu \left[\partial_{\partial_\mu \phi} \left(\frac{1}{2} \partial_\mu \phi \eta^{\alpha\mu} \partial_\alpha \phi \right) \right] = \\ &= \partial_\mu \left[\eta^{\alpha\mu} \partial_{\partial_\mu \phi} \left(\frac{1}{2} \partial_\mu \phi \partial_\alpha \phi \right) \right] = \partial_\mu \left[\eta^{\mu\mu} \partial_{\partial_\mu \phi} \left(\frac{1}{2} (\partial_\mu \phi)^2 \right) \right] = \partial_\mu (\eta^{\mu\mu} \partial_\mu \phi) \Rightarrow \\ &\Rightarrow \partial_\mu \left(\frac{\partial \mathcal{L}}{\partial(\partial_\mu \phi)} \right) = \eta^{\mu\mu} \partial_\mu^2 \phi = \left(\nabla^2 - \frac{\partial^2}{\partial t^2} \right) \phi, \end{aligned} \tag{2.41}$$

where in the third line, in the middle term, we used the fact that the metric is a diagonal matrix (the only nonzero components are these with the same indices). As a consequence of the above results, the equation of motion becomes

$$\left(\nabla^2 - \frac{\partial^2}{\partial t^2}\right)\phi = -U'(\phi). \tag{2.42}$$

Performing a Wick rotation [148] ($t \to -i\tau$), as in the previous section, the Euclidean action of our theory is transforming as $S_M \to iS_E$.

$$\begin{aligned} S_M &= \int d^4x\mathcal{L} = \int d^3x dt\mathcal{L} = \int d^3x dt \left[\frac{1}{2}\partial_\mu\phi\partial^\mu\phi - U(\phi)\right] \\ &= \int d^3x dt \left[\frac{1}{2}(\partial_t\phi)^2 - \frac{1}{2}(\vec{\nabla}\phi)^2 - U(\phi)\right] \\ &\overset{t\to -i\tau}{=} \int d^3x d(-i\tau) \left[\frac{1}{2}(\partial_{(-i\tau)}\phi)^2 - \frac{1}{2}(\vec{\nabla}\phi)^2 - U(\phi)\right] \\ &= -i\int d^3x d\tau \left[-\frac{1}{2}(\partial_\tau\phi)^2 - \frac{1}{2}(\vec{\nabla}\phi)^2 - U(\phi)\right] \\ &= \int d^3x d\tau \left[\frac{1}{2}(\partial_\tau\phi)^2 + \frac{1}{2}(\vec{\nabla}\phi)^2 + U(\phi)\right] = iS_E. \end{aligned} \tag{2.43}$$

In Euclidean space we have similar to the previous pages:

$$S_E = \int d^4x\mathcal{L}_E = \int d^4x \left[\frac{1}{2}(\partial_\tau\phi)^2 + \frac{1}{2}(\vec{\nabla}\phi)^2 + U(\phi)\right]. \tag{2.44}$$

Where now d^4x is defined at the Euclidean space with signature $\delta_{\mu\nu} = (-,-,-,-)$. The indices μ, ν, when we are working in Euclidean space, change values from 1 to 4 unlike the "0−3" variation in Minkowsky space. This is a comfortable way to distinguish one space from the other, and this convention will be used in the next sections.

Back to our work now, performing Euler-Lagrange equations in Euclidean Lagrangian someone gets the imaginary-time equation of motion

$$\left(\nabla^2 + \frac{\partial^2}{\partial \tau^2}\right)\phi = U'(\phi). \tag{2.45}$$

There are three bounce boundary conditions similar to the previous section case. The first condition states that the bounce solution goes from the false vacuum ϕ_+ at $-\infty$ back to the false vacuum at $+\infty$

$$\lim_{\tau\to\pm\infty}\phi(\tau,\vec{x}) = \phi_+, \tag{2.46}$$

the second condition is necessary for the Euclidean action (or equivalently, the coefficient B)

$$B = S_E = \int d^4x \left[\frac{1}{2}(\partial_\tau\phi)^2 + \frac{1}{2}(\vec{\nabla}\phi)^2 + U(\phi)\right], \tag{2.47}$$

to remain finite. It reads:

$$\lim_{|\vec{x}|\to\infty}\phi(\tau,\vec{x}) = \phi_+. \tag{2.48}$$

The last one

$$\frac{\partial\phi}{\partial\tau}(0,\vec{x}) = 0, \tag{2.49}$$

which corresponds to the second condition in Eq.(2.28).

The equations discussed, describe the formation of bubbles of true vacuum. The second condition (2.48) states that a bubble may appear somewhere, someplace, due to quantum fluctuations, but far from it the system will be in its false vacuum. These equations have no nontrivial solution invariant under spatial translations. So, any spatial translation of a solution is also a solution with the same Euclidean action. To obtain the total bounce action appearing at the false vacuum decay rate we must integrate over the group of spatial translations. An attempt to illustrate the last sentences is shown in the figure below (Fig.2.5).

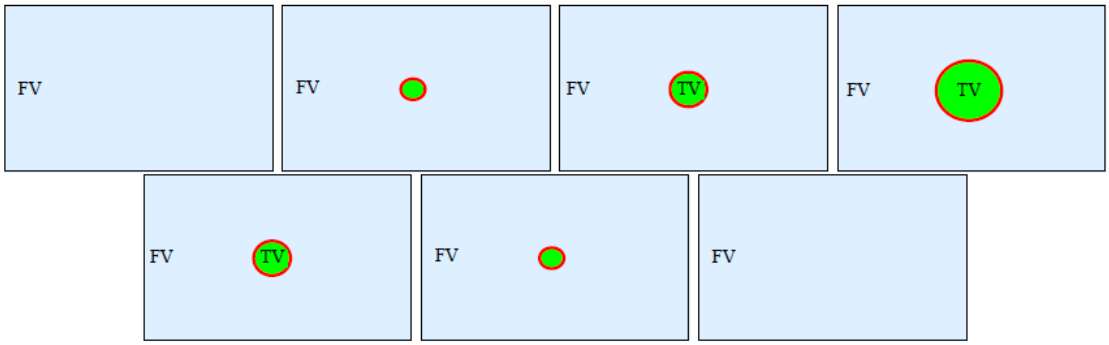

Figure 2.5: Illustration of bubble nucleation in field theory as seen in Euclidean time. The order of the pictures is from top left to bottom right.

We referred a quite amount of times to the formation of bubbles and it is not difficult for someone to imagine these bubbles as 4-spheres being invariant under four-dimensional Euclidean rotations. The assumption that the system always admits an $\mathcal{O}(4)$ invariant bounce has been proven by Coleman et al. [149] and it will be discussed in Appendix B. If there are non-invariant bounces, they have higher Euclidean action than the $\mathcal{O}(4)$ invariant bounce and can be safely ignored because they do not contribute at the exponential at the Γ/V expression.

To be precise, if we define ρ by

$$\rho = \sqrt{\tau^2 + |\vec{x}|^2}, \tag{2.50}$$

the Euclidean distance from an appropriately chosen center of coordinates, then we can assume that ϕ is a function only of ρ. Let us examine how (2.47) will transform after this statement. First, we have

$$\frac{\partial \rho}{\partial \tau} = \frac{\tau}{\sqrt{\tau^2 + |\vec{x}|^2}} = \frac{\tau}{\rho}, \qquad \frac{\partial \phi(\rho)}{\partial \tau} = \frac{\partial \phi}{\partial \rho}\frac{\partial \rho}{\partial \tau} = \phi'(\rho)\frac{\tau}{\rho}. \tag{2.51}$$

So, for the second term of Eq.(2.45) we get

$$\begin{aligned} &\frac{\partial^2 \phi}{\partial \tau^2} = \frac{\partial(\frac{\partial \phi}{\partial \tau})}{\partial \tau} = \frac{\partial}{\partial \tau}\left(\frac{\partial \phi}{\partial \rho}\frac{\partial \rho}{\partial \tau}\right) = \frac{\partial}{\partial \tau}\left(\phi'(\rho)\frac{\tau}{\rho}\right) = \\ &\frac{\partial}{\partial \tau}(\phi'(\rho))\frac{\tau}{\rho} + \phi'(\rho)\frac{\partial(\frac{\tau}{\rho})}{\partial \tau} = \frac{\partial}{\partial \tau}(\phi'(\rho))\frac{\tau}{\rho} + \phi'(\rho)\left(\frac{1}{\rho} - \frac{\tau^2}{\rho^3}\right) = \\ &\frac{\partial \phi'}{\partial \rho}\frac{\partial \rho}{\partial \tau}\frac{\tau}{\rho} + \phi'(\rho)\left(\frac{1}{\rho} - \frac{\tau^2}{\rho^3}\right) \Rightarrow \frac{\partial^2 \phi}{\partial \tau^2} = \phi''(\rho)\left(\frac{\tau}{\rho}\right)^2 + \phi'(\rho)\left(\frac{\rho^2 - \tau^2}{\rho^3}\right). \end{aligned} \tag{2.52}$$

In a similar way, someone gets for the first term,

$$\nabla^2\phi(\rho) = \phi''(\rho)\left(\frac{|\vec{x}|}{\rho}\right)^2 + \phi'(\rho)\left(\frac{3\rho^2 - |\vec{x}|^2}{\rho^3}\right). \tag{2.53}$$

Plugging equations (2.52) and (2.53) in Eq.(2.45) we get,

$$\begin{aligned}
&\left(\nabla^2 + \frac{\partial^2}{\partial\tau^2}\right)\phi = U'(\phi) \Rightarrow \\
&\Rightarrow \phi''(\rho)\left[\left(\frac{|\vec{x}|}{\rho}\right)^2 + \left(\frac{\tau}{\rho}\right)^2\right] + \phi'(\rho)\left[\left(\frac{3\rho^2 - |\vec{x}|^2}{\rho^3}\right) + \left(\frac{\rho^2 - \tau^2}{\rho^3}\right)\right] = U'(\phi) \overset{(2.50)}{\Rightarrow} \\
&\Rightarrow \frac{\mathrm{d}^2\phi}{\mathrm{d}\rho^2} + \frac{3}{\rho}\frac{\mathrm{d}\phi}{\mathrm{d}\rho} = U'(\phi).
\end{aligned}$$

Hence,

$$\frac{\mathrm{d}^2\phi}{\mathrm{d}\rho^2} + \frac{3}{\rho}\frac{\mathrm{d}\phi}{\mathrm{d}\rho} = U'(\phi) \tag{2.54}$$

is the new equation of motion of the problem. The boundary conditions of Eq.(2.46) and Eq.(2.48) now become a single equation,

$$\lim_{\rho\to\infty}\phi(\rho) = \phi_+, \tag{2.55}$$

The term in the integral of the coefficient B (2.47) will be

$$\begin{aligned}
&\frac{1}{2}(\partial_\tau\phi)^2 + \frac{1}{2}(\vec{\nabla}\phi)^2 + U(\phi) = \frac{1}{2}\left[\phi'(\rho)\frac{\tau^2}{\rho^2} + \phi'(\rho)\frac{|\vec{x}|^2}{\rho^2}\right] + U(\phi) = \\
&= \frac{1}{2}\phi'(\rho)\left(\frac{\tau^2}{\rho^2} + \frac{|\vec{x}|^2}{\rho^2}\right) + U(\phi) = \frac{1}{2}\left(\frac{\partial\phi}{\partial\rho}\right)^2 + U(\phi),
\end{aligned} \tag{2.56}$$

where in the first line, at the LHS of Eq.(2.56) we have used Eq.(2.51) and at the second line, at the RHS we used Eq.(2.50). The 4-volume term of the integral, d^4x, will be [150]

$$d^4x = \rho^3 d\rho\Omega_n = \rho^3 d\rho\frac{2\pi^{n/2}}{\Gamma(n/2)}\bigg|_{n=4} = 2\pi^2\rho^3 d\rho, \tag{2.57}$$

where $\Gamma(n)$ is the Gamma function and $\Gamma(2) = 1$. After this procedure, equation (2.47) becomes

$$B = 2\pi^2\int_0^\infty \rho^3 d\rho\left[\frac{1}{2}\left(\frac{\partial\phi}{\partial\rho}\right)^2 + U(\phi)\right]. \tag{2.58}$$

Also, the condition in (2.49) becomes

$$\frac{\mathrm{d}\phi}{\mathrm{d}\rho}\bigg|_{\rho=0} = 0, \tag{2.59}$$

in order to avoid a singularity at the origin of the coordinates. As noted by Coleman [134], this method is extremely powerful since it reduces the problem of barrier penetration in a system with infinite degrees of freedom to the study of the properties of a single classical differential equation. Note that if the solution to Eq.(2.54) is interpreted as a particle position and ρ as time,

the equations of motion are identical to mechanical equations for a particle moving in a potential with flipped sign $U \to -U$ (Fig.2.6) subject to a viscous force (v.f.) inversely proportional to time (the $3/\rho$ term at the EoM). According to the boundary condition of Eq.(2.59), the particle is released at rest (zero speed) at time $\rho = 0$. If its initial position is appropriately chosen, the particle will come to rest at $\rho = \infty$ at $\phi = \phi_+$, the false vacuum. With that mechanical description, the boundary conditions described in the previous pages acquire a virtual representation easily understandable.

If the particle is sufficiently close to the true vacuum hill and released to the right then it will overshoots and pass the false vacuum hill. On the other hand, if the particle is released far from ϕ_- then it will undershoot and will never reach the false vacuum. For example, If the particle is released at the right of the point ϕ_1 (Fig.2.7a), then it will not have enough energy to reach ϕ_+. This argument is not affected by the viscous damping force, because it decreases the energy. Let it be checked from the EoM (2.54),

$$\frac{\mathrm{d}^2\phi}{\mathrm{d}\rho^2} + \frac{3}{\rho}\frac{\mathrm{d}\phi}{\mathrm{d}\rho} = U'(\phi) \Rightarrow \frac{d}{d\rho}\left(\frac{1}{2}\left(\frac{\mathrm{d}^2\phi}{\mathrm{d}\rho^2}\right) - U\right) = -\frac{3}{\rho}\left(\frac{\mathrm{d}\phi}{\mathrm{d}\rho}\right)^2 \leq 0. \tag{2.60}$$

If it starts too close to the true vacuum, it will stay there for a long time. This suppresses the v.f. term so due to the difference between the potentials and lack of enough friction (v.f. $\approx \rho^{-1}$) will pass ϕ_+ in a finite time (Fig.2.7b). To demonstrate overshoot [151] we must linearize Eq.(2.54) for ϕ very close to ϕ_-. To do it a Taylor approximation around ϕ_- must be performed to the RHS of the EoM,

$$U'(\phi) = U'(\phi_-) + \frac{\mathrm{d}U'}{\mathrm{d}\phi}\cdot(\phi - \phi_-) + ... = m^2(\phi - \phi_-), \tag{2.61}$$

where terms until the first order were kept. Also, it is used the fact that $U'(\phi_-) = 0$, because it is a minimum and

$$m^2 = U''(\phi_-). \tag{2.62}$$

Eq.(2.54) becomes

$$\left(\frac{\mathrm{d}^2}{\mathrm{d}\rho^2} + \frac{3}{\rho}\frac{\mathrm{d}}{\mathrm{d}\rho} - m^2\right)(\phi - \phi_-) = 0. \tag{2.63}$$

This equation has a solution, which is not a subject of study in this thesis so we will demonstrate only the answer here taken from [131]:

$$\phi(\rho) - \phi_- = 2[\phi(\rho) - \phi_-]I_1(m\rho)/m\rho. \tag{2.64}$$

On the above solution, we have that $I_1(x) = -iJ_1(ix)$, with the J_1 to be the first order Bessel function which gives a solution to the following equation

$$J_1''(x) + \frac{J_1'(x)}{x} + \left(1 - \frac{1}{x^2}\right)J_1(x) = 0. \tag{2.65}$$

Therefore, there must be some point in between for which the particle does not overshoot or undershoot and reaches the false vacuum at infinity [131][134]. This proves that the Euclidean equations of motion always admit a solution. A closed form solution can be obtained via the thin-wall approximation at the $\epsilon = U(\phi_+) - U(\phi_-) \to 0$ limit. This procedure will be examined at the next section. For more information on the overshoot-undershoot technique the reader should take a look at [152].

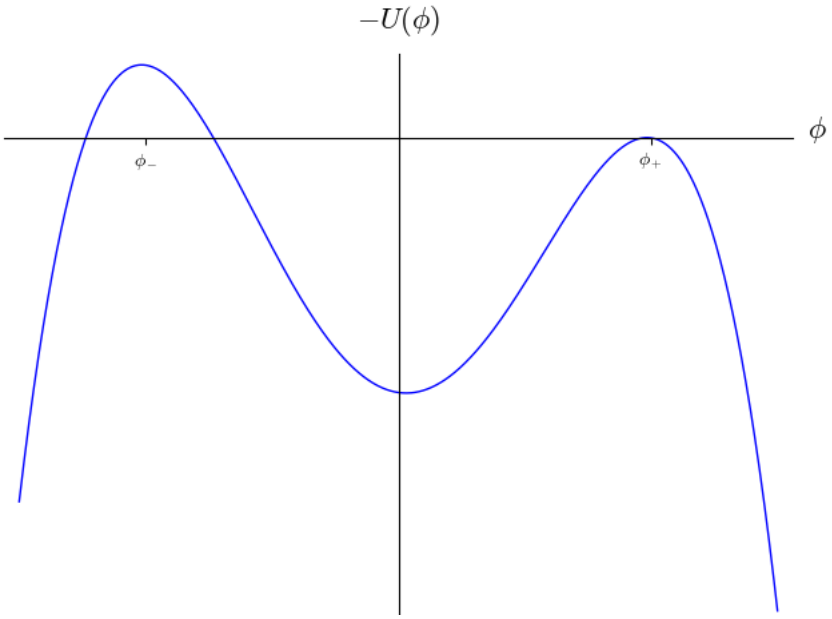

Figure 2.6: The reversed potential in Euclidean space

2.2.4 The thin-wall approximation

In this section, we will try to give a compact form to the coefficient B. Starting with the consideration of a symmetric potential U_0, function of ϕ

$$U_0(\phi) = U_0(-\phi), \tag{2.66}$$

with minima at points $\pm\alpha$,

$$U'(\pm\alpha) = 0. \tag{2.67}$$

An example of such a potential is the function below,

$$U_0 = \frac{\lambda}{8}\left(\phi^2 - \frac{m^2}{\lambda}\right)^2, \tag{2.68}$$

where λ is a dimensionless coupling constant of our theory and

$$m^2 = U''(\pm\alpha), \tag{2.69}$$

this is the negative mass term in the potential because of which a spontaneous symmetry breaking occurs at the system [146] and gives rise to a duo of minima. The existence of this negative mass term in a theory is responsible of the spontaneous symmetry breaking and as a consequence of this cosmological first-order phase transitions could occur. Also, from Eq.(2.67) and Eq.(2.68),

$$U_0' = 0 \Rightarrow \frac{\lambda}{2}\phi\left(\phi^2 - \frac{m^2}{\lambda}\right) = 0 \Rightarrow \alpha^2 = \frac{m^2}{\lambda}. \tag{2.70}$$

Let us add to our potential a small term $\mathcal{O}(\epsilon)$ that breaks the symmetry, where

$$\epsilon = U(\phi_+) - U(\phi_-), \tag{2.71}$$

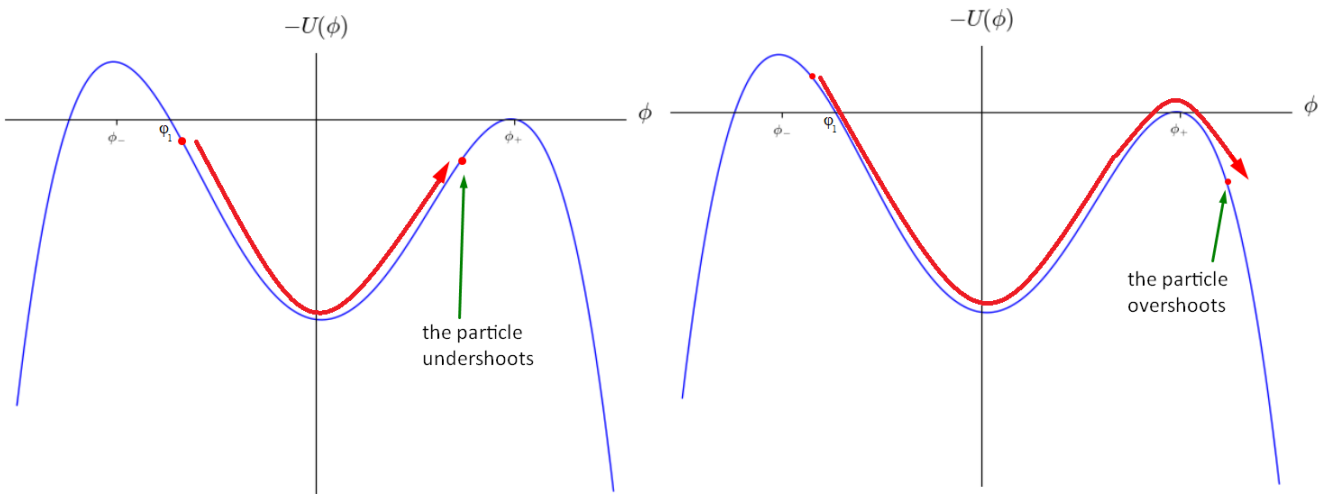

(a) Undershoot (b) Overshoot

Figure 2.7: In the left picture (a) the particle starts right to point ϕ_1 and it has not the sufficient energy to climb over the false vacuum hill, in this case, we have an undershoot. In the right picture, the particle starts near the true vacuum, it rolls down and surpasses the false vacuum hill. It is an overshoot. It will be a starting point, the bounce solution, where the particle arrives at ϕ_+ at time $\rho \to \infty$.

is a positive number, the energy difference between the vacua states, then we can write

$$U = U_0 + \frac{\epsilon}{2\alpha}(\phi - \alpha), \tag{2.72}$$

and to lowest non-trivial order to ϵ

$$\phi_\pm = \pm\alpha. \tag{2.73}$$

As has been already stated in the final paragraph of the previous section, it can be shown that in the limit of small ϵ it is possible to get a closed-form result for B. From our mechanical analogy at Subsection 2.2.3, we can understand the form of the bounce. In order not to lose too much energy, $\phi(0)$, the starting point of the particle is chosen to be very close to ϕ_-. Suppose it stays there for a very long time until $\rho \equiv \bar{\rho}$. When ρ is close to $\bar{\rho}$ it rolls quickly across the valley of Fig.2.6 and slowly comes to rest at ϕ_+ at time infinity. In the field-theoretic language, this mechanical analogy for the bounce corresponds to a four-dimensional spherical bubble of large radius $\bar{\rho}$ with a thin wall separating the false vacuum inside the bubble from the false vacuum outside it.

Close to the boundary $\rho = \bar{\rho}$, the viscous damping force term is $3/\bar{\rho} \approx 0$ and we can drop it from the equation of motion. Let us also set $\epsilon \to 0$ to Eq.(2.54) to simplify it to,

$$\frac{\mathrm{d}^2\phi}{\mathrm{d}\rho^2} = U_0'(\phi). \tag{2.74}$$

This familiar to physicists equation, which is the classical equation of motion for a particle in a symmetric double well, has solutions called solitons (one-dimensional instantons) [134][153–155]. Solitons and instantons have been studied widely in field theory literature. The properties of Eq.(2.74) have been extensively discussed in Appendix C. Here, the results will be summarized in order to get to the point of our study.

Before we continue our calculation of B, we will use for convenience from now on the definition Coleman and De Lucia gave to the bounce action in their famous paper written in 1980 [133]. First, let ϕ be a solution of the Euclidean equation of motion associated with S_E such that (1) ϕ approaches the false vacuum, ϕ_+ at Euclidean infinity, (2) ϕ is not a constant, and (3) ϕ has Euclidean action less than or equal to that of any other solution obeying (1) and (2). Then the coefficient B at the vacuum decay amplitude is given by

$$B = S_E(\phi) - S_E(\phi_+), \tag{2.75}$$

which is slightly different from the original definition, it is more general (we just used $U(\phi_+) = 0$ before which is a convention), and it is convenient for the process to be shown.

As ρ traverses the real line, ϕ goes monotonically from ϕ_- to ϕ_+. Equation (2.74) gets a solution of the form,

$$\int_{(\phi_-+\phi_+)/2}^{\phi} d\phi[2(U_0(\phi) - U_0(\phi_\pm))]^{-1/2} = \rho - \bar{\rho}, \tag{2.76}$$

where we chose $\bar{\rho}$ the point at which ϕ is the average of its two extreme values. For our theory of Eq.(2.68) we get

$$\phi = \alpha \tanh\left[\frac{1}{2}m(\rho - \bar{\rho})\right]. \tag{2.77}$$

Now, we will divide the region of integration into three parts and write that

$$B = B_{in} + B_{wall} + B_{out} \tag{2.78}$$

Outside the wall, where $\phi = \phi_+$, we get from Eq.(2.75)

$$B_{out} = S_E(\phi_+) - S_E(\phi_+) = 0. \tag{2.79}$$

Inside the wall, $\phi = \phi_-$. Hence,

$$\begin{aligned} B_{in} = S_E(\phi_-) - S_E(\phi_+) = 2\pi^2 \int_0^{\bar{\rho}} \rho^3 d\rho \left[\frac{1}{2}\left(\frac{\mathrm{d}\phi_-}{\mathrm{d}\rho}\right)^2 + U_0(\phi_-) - \frac{1}{2}\left(\frac{\mathrm{d}\phi_+}{\mathrm{d}\rho}\right)^2 - U_0(\phi_+)\right] = \\ 2\pi^2 \int_0^{\bar{\rho}} \rho^3 d\rho[U_0(\phi_-) - U_0(\phi_+)] \overset{(2.71)}{=} 2\pi^2(-\epsilon)\int_0^{\bar{\rho}} \rho^3 d\rho = -2\pi^2\epsilon\frac{\bar{\rho}^4}{4} = -\pi^2\epsilon\frac{\bar{\rho}^4}{2}. \end{aligned} \tag{2.80}$$

Finally, within the wall, $\rho = \bar{\rho}$

$$\begin{aligned} B_{wall} &= 2\pi^2\bar{\rho}^3 \int_{wall} d\rho \left[\frac{1}{2}\left(\frac{\mathrm{d}\phi}{\mathrm{d}\rho}\right)^2 + U(\phi) - U(\phi_+)\right] \\ &\approx 2\pi^2\bar{\rho}^3 \int_{wall} d\rho \left[\frac{1}{2}\left(\frac{\mathrm{d}\phi}{\mathrm{d}\rho}\right)^2 + U_0(\phi) - U_0(\phi_+)\right] = 2\pi^2\bar{\rho}^3 S_1. \end{aligned} \tag{2.81}$$

From the soliton equation (2.74)

$$\begin{aligned} &\frac{\mathrm{d}^2\phi}{\mathrm{d}\rho^2} = \frac{\mathrm{d}U_0}{\mathrm{d}\phi} \Rightarrow d\phi\frac{\mathrm{d}^2\phi}{\mathrm{d}\rho^2} = dU_0 \Rightarrow d\phi\frac{\mathrm{d}\left(\frac{\mathrm{d}\phi}{\mathrm{d}\rho}\right)}{\mathrm{d}\rho} = dU_0 \Rightarrow \\ &\frac{\mathrm{d}\phi}{\mathrm{d}\rho}d\left(\frac{\mathrm{d}\phi}{\mathrm{d}\rho}\right) = dU_0 \Rightarrow \int \frac{\mathrm{d}\phi}{\mathrm{d}\rho}d\left(\frac{\mathrm{d}\phi}{\mathrm{d}\rho}\right) = \int dU_0 \Rightarrow \frac{1}{2}\left(\frac{\mathrm{d}\phi}{\mathrm{d}\rho}\right)^2 - U_0 = const. \end{aligned} \tag{2.82}$$

From the boundary condition that demands $\phi(\infty) = \phi_+$ we get that

$$\frac{1}{2}\left(\frac{\mathrm{d}\phi}{\mathrm{d}\rho}\right)^2 - U_0 = -U_0(\phi_+). \tag{2.83}$$

Using Eq.(2.83) we can write for S_1,

$$\begin{aligned} S_1 = \int_{wall} d\rho \left[\frac{1}{2}\left(\frac{\mathrm{d}\phi}{\mathrm{d}\rho}\right)^2 + U_0(\phi) - U_0(\phi_+)\right] = \int_{wall} d\rho 2[(U_0(\phi) - U_0(\phi_+)] \Rightarrow \\ \Rightarrow S_1 = 2\int \frac{\mathrm{d}\phi}{\mathrm{d}\rho} d\rho[(U_0(\phi) - U_0(\phi_+)]d\phi = \int_{\phi_-}^{\phi_+} d\phi\{2[(U_0(\phi) - U_0(\phi_+)]\}^{1/2}. \end{aligned} \tag{2.84}$$

In the second line, we used again equation (2.83) which leads to a usual result

$$d\phi = d\rho\sqrt{2[U_0 - U_0(\phi_+)]} \Rightarrow d\rho = d\phi[2(U_0 - U_0(\phi_+))]^{-1/2}. \tag{2.85}$$

Summing the contribution of the "inside" and the "wall" term,

$$B = -\frac{1}{2}\pi^2\epsilon\rho^4 + 2\pi^2\rho^3 S_1. \tag{2.86}$$

Varying with respect to $\bar{\rho}$, we obtain

$$\frac{\mathrm{d}B}{\mathrm{d}\bar{\rho}} = 0 \Rightarrow -2\pi^2\epsilon\bar{\rho}^3 + 6\pi^2\bar{\rho}^2 S_1 = 0. \tag{2.87}$$

Hence,

$$\bar{\rho} = 3S_1/\epsilon. \tag{2.88}$$

An important observation can be made here. Check that if $\epsilon \to 0$, ρ goes to infinity. This result is consistent with the qualitative picture built in this chapter. Recall the words written a few pages before, in the small ϵ limit, our particle will remain to the true vacuum hill for $\rho \to \infty$ and then it will roll over the false vacuum at Euclidean infinity.

In a future section dedicated to instantons, we will see that these pseudo-particles have a width around $1/\omega$, where $\omega^2 = |V''(\alpha)|$. Respectively, the width of the bounce will be around $1/m$. From the soliton equation results the bubble wall thickness is

$$\Delta\rho = \frac{1}{m} \sim \frac{\Delta\phi}{\sqrt{U}} \tag{2.89}$$

Equation (2.88) can be used to give a more precise condition of validity of the thin-wall approximation:

$$m\bar{\rho} = 3mS_1/\epsilon \gg 1. \tag{2.90}$$

We can also use it to compute

$$B = -\frac{1}{2}\pi^2\epsilon\bar{\rho}^4 + 2\pi^2\bar{\rho}^3 S_1 \overset{(2.88)}{=} -\frac{1}{2}\pi^2\epsilon\bar{\rho}^4 + 2\pi^2\bar{\rho}^3\frac{\epsilon\bar{\rho}}{3} \Rightarrow B = 27\pi^2 S_1^4/2\epsilon^3, \tag{2.91}$$

this is the the closed-form expression for the coefficient B in the $\epsilon \ll 1$ limit. For the theory under consideration described by Eq.(2.68) we have,

$$\begin{aligned} S_1 &= \int_{\phi_-}^{\phi_+} d\phi\{2[(U_0(\phi) - U_0(\phi_+)]\}^{1/2} \\ &= \int_{\phi_-}^{\phi_+} d\phi[2U_0(\phi)]^{1/2} \\ &= \int_{-m/\sqrt{\lambda}}^{m/\sqrt{\lambda}} d\phi \frac{\sqrt{\lambda}}{2}\left(\phi^2 - \frac{m^2}{\lambda}\right) \\ &\sim m^3/3\lambda. \end{aligned} \tag{2.92}$$

So, the validity of the approximation condition becomes

$$m^4/\epsilon\lambda \gg 1, \tag{2.93}$$

and Eq.(2.91),

$$B = \frac{\pi^2 m^{12}}{6\epsilon^3\lambda^4}. \tag{2.94}$$

2.2.5 Bubble growth

We have used the bounce to compute a coefficient that enters into the probability for the quantum materialization of a bubble of true vacuum within the false vacuum ($\Gamma/V \approx e^{-B}$). The bounce can be used to describe the classical growth of the true vacuum bubble after its materialization, too.

As in the particle case, the field ϕ makes a quantum jump to the state

$$\begin{aligned} &\phi(\tau = 0, \vec{x}) = \phi(t = 0, \vec{x}), \\ &\frac{\partial}{\partial t}\phi(t = 0, \vec{x}) = 0. \end{aligned} \tag{2.95}$$

These two expressions describe in brief everything that was written about the classical particle's quantum jump in the previous section. In the same way, the field makes the quantum jump from the local minimum of the potential to the escape point at $t = 0$, where its momentum is zero. Afterward, it propagates classically, according to the classical field equation

$$-\frac{\partial^2\phi}{\partial t^2} + \nabla^2\phi = U'(\phi). \tag{2.96}$$

The first of these equations states that the same function, $\phi(\rho)$, that gives the bounce's shape in the 4-dimensional Euclidean space also shapes the bubble at the moment of its materialization at the escape point in ordinary three-space. In addition, Eq.(2.95) does more. The Minkowskian Eq.(2.96) is simply the analytic continuation of the Euclidean equation Eq.(2.45), back to the real time. Note that this equation is obtained merely by Wick rotating τ, exactly in the same way done in the previous paragraphs. The solution to this is simply the analytic continuation of the bounce.

$$\phi(t, \vec{x}) = \phi(\rho = \sqrt{\vec{x}^2 - t^2}). \tag{2.97}$$

Some conclusions can be made of Eq.(2.96) are the following. The $\mathcal{O}(4)$ invariance of the bounce now becomes an $\mathcal{O}(3,1)$ invariance of the classical field equations. This means that the growth

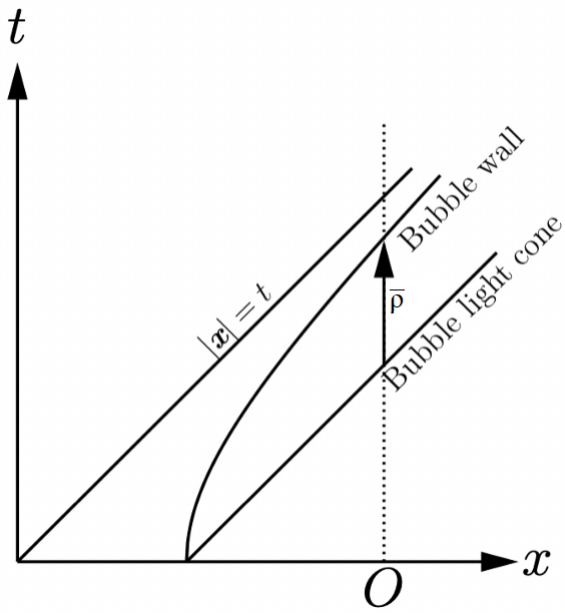

Figure 2.8: Classical growth of the bubble of true vacuum after its materialization. The hyperboloid is the path traced out by the bubble wall. The observer receives a warning about the bubble's expansion toward him when he crosses the light cone.

of the bubble looks the same to any Lorentz observer. Secondly, in the $\epsilon \to 0$ case there is a thin wall separating the true vacuum from the false one located at $\rho = \bar{\rho}$. As the bubble expands, its wall evolves as a hyperboloid:

$$|\vec{x}|^2 - t^2 = \bar{\rho}^2. \tag{2.98}$$

The bubble radius $\bar{\rho}$ is determined by the potential as described in the previous pages. It should be of the same order as the energy scales of the scalar field and therefore a relatively short length compared to macroscopic lengths. This means that immediately after the nucleation of the bubble, the wall spreads almost with a light speed and starts eating away more and more of the false vacuum. The wall's speed is

$$u = \frac{\mathrm{d}|\vec{x}|}{\mathrm{d}t} = \frac{\mathrm{d}\sqrt{t^2 + \bar{\rho}^2}}{\mathrm{d}t} = \frac{2t}{2\sqrt{t^2 + \bar{\rho}^2}} = \frac{t}{\sqrt{x^2}} = \frac{\sqrt{|\vec{x}|^2 - \bar{\rho}^2}}{|\vec{x}|} \sim 1. \tag{2.99}$$

The Lorentz factor of the wall (for $c = 1$) with the help of (2.98) will be

$$\gamma = (1 - u^2)^{-1/2} = \left(1 - \frac{t^2}{|\vec{x}|^2}\right)^{-1/2} = \left(\frac{|\vec{x}|^2 - t^2}{|\vec{x}|^2}\right)^{-1/2} = \left(\frac{\bar{\rho}^2}{|\vec{x}|^2}\right)^{-1/2} = \frac{x}{\bar{\rho}}. \tag{2.100}$$

The observer O only notices the bubble when he crosses the bubble's light cone. After time $\bar{\rho}$ the observer is inside the bubble (Fig.2.8).

2.2.6 Energetics

Let us make a recapitulation of first-order transition dynamics combined with the analogy made in the first section of the chapter. In the situation of the liquid-gas phase transition, for

example in water, the thermodynamic state of the system is trapped in an "unwanted" metastable state, locally stable under small thermodynamic perturbations, but with higher free energy than the global minimum. This metastable state shows stability under small amplitude perturbations but it can decay via spontaneous large amplitude fluctuations. These fluctuations correspond to bubbles of the stable phase trying to blur, immersed in the metastable hosting container.

Consider, a spherical bubble of radius, $\bar{\rho}$. Inside it is stated a globality of the stable phase and outside is the metastable ocean. Since the globally stable state has a lower free energy than the metastable state, there is a gain in the free energy given by $-4\pi\bar{\rho}^3\epsilon/3$, where ϵ, as usual, is the difference in the effective potential between the stable and the metastable state. Because the order parameter is inhomogeneous in this configuration there is an elastic contribution to the free energy from the gradients of the order parameter field which is proportional to the surface of the bubble. The reason for this is that the wall surface constitutes the region in which the spatial derivatives of the order parameter are non-vanishing [156]. This elastic contribution is a positive number summed to the total energy and given by $4\pi\bar{\rho}^2 S_1$ where S_1 is the surface tension. Consequently, the total change in the free energy for such a bubble configuration is going to be

$$E = 4\pi\bar{\rho}^2 S_1 - 4\pi\bar{\rho}^3\epsilon/3. \tag{2.101}$$

In our situation, where a bubble of the true universe is emerging in the sea of the false one, the basic concept of thinking does not change. The rapidly expanding bubble carries a great amount of energy. The total energy consists here of the two same terms, the negative volume term and the positive surface tension contribution.

Let us make a complementary comment about the bubble's wall energy. The energy released during the transition of the false vacuum to the true is converted to the kinetic energy of the wall. At rest, a section of the wall the moment that appears at $t = \tau = 0$ carries energy:

$$\begin{aligned}
E_{wall} &= \int_{\rho_M \approx \bar{\rho}} d^3x \left[-\frac{1}{2}\left(\frac{\partial\phi_M}{\partial t}\right)^2 + \frac{1}{2}(\nabla\phi_M)^2 + U(\phi_M) - U_+ \right] \\
&= \int_{\rho_M \approx \bar{\rho}} d^3x \left[\frac{1}{2}(\vec{\nabla}\phi_M)^2 + U(\phi_M) - U_+ \right] \\
&= 4\pi \int_{\bar{\rho}-\Delta\rho/2}^{\bar{\rho}+\Delta\rho/2} d\rho_M \rho_M^2 \left[\frac{1}{2}(\vec{\nabla}\phi_M)^2 + U(\phi_M) - U_+ \right] \\
&= 4\pi\bar{\rho}^2 \int_{\bar{\rho}-\Delta\rho/2}^{\bar{\rho}+\Delta\rho/2} d\rho \left[\frac{1}{2}(\vec{\nabla}\phi)^2 + U(\phi) - U_+ \right] \\
&= 4\pi\bar{\rho}^2 \int_{\bar{\rho}-\Delta\rho/2}^{\bar{\rho}+\Delta\rho/2} d\rho \left[\frac{1}{2}\left(\frac{\mathrm{d}\phi}{\mathrm{d}\rho}\right)^2 + U(\phi) - U_+ \right] \\
&= 4\pi\bar{\rho}^2 S_1.
\end{aligned} \tag{2.102}$$

Any part of the wall is connected with a Lorentz transformation from any other part. A part of the wall at a time when the radius is $|\vec{x}|$ moving with speed u carries energy:

$$E'_{wall} = \gamma E_{wall} = 4\pi\bar{\rho}^2 S_1 (1-u^2)^{-1/2}. \tag{2.103}$$

Then, from (2.99)

$$E'_{wall} = 4\pi\bar{\rho}^3 S_1/\bar{\rho} = 4\pi\epsilon\bar{\rho}^3/3. \tag{2.104}$$

Now, we have a big picture for the terms appearing in the energy expression. The "′" here suggests the Lorentz transformation.

2.2.7 Numerical Computations for the vacuum decay

In this subsection will be presented the solution to the following boundary value problem[2]:

$$-\Phi_{cl}'' - \frac{3}{r}\Phi_{cl} + \Phi_{cl} - \frac{3}{2}\Phi_{cl}^2 + \frac{k}{2}\Phi_{cl}^3 = 0, \tag{2.105}$$

with the boundary conditions given by

$$\Phi_{cl}'(0) = 0, \qquad \Phi_{cl}(\infty) = \Phi_+. \tag{2.106}$$

This is the equation of motion of the classical bounce resulting from the rescaling of the potential of Eq.(2.72). The rescaled-dimensionless potential is given in the below equation

$$U(\Phi) = \frac{1}{2}\Phi^2 - \frac{1}{2}\Phi^3 + \frac{k}{8}\Phi^4. \tag{2.107}$$

The parameter k is dimensionless and $0 < k < 1$. In Fig.2.9 are depicted some bubble profiles for different values of k. One observation that can be made is that as k is getting bigger the scalar field fulfills the second boundary condition at a bigger bubble radius. Also, a second observation is that the bounce profiles have a form that can be described by $\Phi_{cl} \propto \tanh(-r)$ exactly as it was expected from the soliton-instanton solutions. A full analysis of the potential rescaling and the numerical procedure with the complete *Mathematica* coding steps can be found in Appendix I.

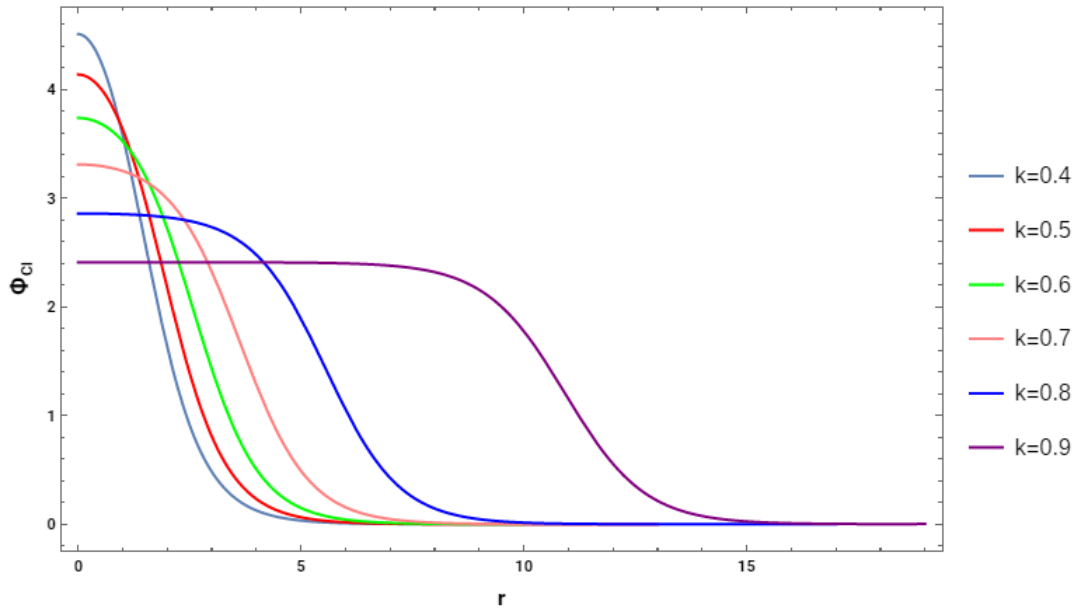

Figure 2.9: Various bounce solutions $\Phi_{cl}(r)$ plotted for $k = 0.4$, 0.5 0.6, 0.7, 0.8, 0.9.

A final comment that can be made here is that, while $k \to 1$, the potential reaches the double-well potential (check Appendix I for the potential). The vacua become degenerate. As k gets lower, ϵ (the energy density between the vacua) is getting bigger, and from the figure above we can see that the bubble radius is getting lower too. The physical reason for this is that bigger ϵ means more energy available for the false vacuum to true vacuum conversion. Hence, less volume is necessary to compensate the wall energy cost and the radius is getting lower in agreement with our results in the 'Energetics' section. Also, as ϵ becomes smaller we can say that the thin-wall approach validity becomes weaker.

[2]In this subsection the formulation of [157] is followed.

2.3 Path integral approach

2.3.1 Summary

In this section, we will try to export a mathematical expression for the second coefficient in the tunneling rate formula of Eq.(2.2), which is coefficient A. Coleman and Callan in the late 70's [132][153] used the famous Feynman's path integral formulation adapted in Euclidean spacetime to calculate the tunneling exponent and prefactor for the decay of metastable vacua. We will follow their calculations through these pages.

2.3.2 Computing the path integral

Let us try to keep it as simple as possible and begin our mathematical procedure from a particle of unit mass moving in one dimension under the influence of a potential $V(x)$. The amplitude for a particle to move from position x_i at time $-T/2$ to x_f at time $T/2$ is [158][159]

$$\langle x_f | \, e^{-H\tau} \, | x_i \rangle = \int [dx] e^{-S_E}, \tag{2.108}$$

where H is the Hamiltonian and S_E is our familiar Euclidean action, here integrated from $-T/2$ to $T/2$ and $[dx]$ denotes that the integration is over all the paths that satisfy the boundary conditions $x(-T/2) = x_i$ and $x(T/2) = x_f$. This so-called Euclidean path integral results after an analytic continuation to imaginary time, our familiar Wick rotation, to the real-time Feynman one.

$$\langle x_f | \, e^{-iHt} \, | x_i \rangle = \int [dx(t)] e^{iS_M}. \tag{2.109}$$

If we expand into a complete set of eigenstates,

$$H \, | n \rangle = E_n \, | n \rangle \, , \tag{2.110}$$

and focus on the left-hand side of Eq.(2.108) we can write

$$\begin{aligned} \langle x_f | \, e^{-H\tau} \, | x_i \rangle &= \sum_n | n \rangle \, \langle n | \, \langle x_f | \, e^{-H\tau} \, | x_i \rangle \Rightarrow \\ \Rightarrow \langle x_f | \, e^{-H\tau} \, | x_i \rangle &= \sum_n e^{-E_n \tau} \, \langle x_f | n \rangle \, \langle n | x_i \rangle \, , \end{aligned} \tag{2.111}$$

where we used Eq.(2.110) to bring the exponential term outside the brakets. From the leading term at the RHS of Eq.(2.111), in the $\tau \to \infty$, we can say that the ground state is the major contributor to the whole expression. Recall that we are interested in the case where the time goes to infinity, similar to our previous analysis. With that given Eq.(2.111) will be,

$$\langle x_f | \, e^{-H\tau} \, | x_i \rangle = e^{-E_0 \tau} \, \langle x_f | 0 \rangle \, \langle 0 | x_i \rangle \, . \tag{2.112}$$

This gives a simple expression for the ground state energy E_0.

The right-hand side of equation (2.108) is of interest to us, because in the semi-classical limit ($S_E \to \infty$), the path integral can be calculated. As it has been discussed the exponential term on the integral will be dominated by the least value of the action. Therefore, only the stationary

points of S_E will be taken into account. For simplicity, it will be assumed that there is only one such stationary point, $\bar{x}$, then we have,

$$\begin{aligned} S_E &= \int_{-T/2}^{T/2} d\tau' \left[\frac{1}{2} \left(\frac{\mathrm{d}x}{\mathrm{d}\tau'} \right)^2 + V(x) \right] \Rightarrow \frac{\delta S_E}{\delta \bar{x}(\tau)} = 0 \\ \Rightarrow \frac{\delta}{\delta \bar{x}(\tau)} \int_{-T/2}^{T/2} d\tau' L_E &= \int_{-T/2}^{T/2} d\tau' \left[\frac{\partial L_E}{\partial x} \frac{\delta x(\tau')}{\delta \bar{x}(\tau)} + \frac{\partial L_E}{\partial \dot{x}} \frac{\delta \dot{x}(\tau')}{\delta \bar{x}(\tau)} \right], \end{aligned} \tag{2.113}$$

now using the fact that $\frac{\delta \dot{x}(\tau')}{\delta \bar{x}(\tau)} = \frac{\mathrm{d}}{\mathrm{d}\tau'} \frac{\delta x(\tau')}{\delta \bar{x}(\tau)}$ and integrating by parts with respect to τ',

$$\begin{aligned} \Rightarrow \frac{\delta S_E}{\delta \bar{x}(\tau)} &= \int_{-T/2}^{T/2} d\tau' \left[\frac{\partial L_E}{\partial x} - \frac{\mathrm{d}}{\mathrm{d}\tau'} \frac{\partial L}{\partial \dot{x}} \right] \frac{\delta x(\tau')}{\delta \bar{x}(\tau)} = \\ = \int_{-T/2}^{T/2} d\tau' \left[\frac{\partial L_E}{\partial x} - \frac{\mathrm{d}}{\mathrm{d}\tau'} \frac{\partial L_E}{\partial \dot{x}} \right] \delta(\tau' - \tau) &= \frac{\partial L_E}{\partial x} - \frac{\mathrm{d}}{\mathrm{d}\tau} \frac{\partial L_E}{\partial \dot{x}} = 0, \end{aligned} \tag{2.114}$$

where we used that

$$\frac{\delta x(\tau')}{\delta \bar{x}(\tau)} = \delta(\tau' - \tau), \tag{2.115}$$

in Eq.(2.114) and $\delta(\tau' - \tau)$ is the Dirac delta "function". Dot is denoting differentiation with respect to imaginary time. Some steps in Eq.(2.113) were ignored because the same procedure as Eq.(2.39) was followed.

As someone can observe if we set to zero the first variational derivative of our Euclidean action, this corresponds to the Euler-Lagrange equations. Consequently, someone gets,

$$\frac{\delta S_E}{\delta \bar{x}} = -\frac{\mathrm{d}^2 \bar{x}}{\mathrm{d}\tau^2} + V'(\bar{x}) = 0, \tag{2.116}$$

with the prime denoting differentiation with respect to $\bar{x}$. This is the familiar equation of motion of a classical particle moving in an upside-down potential, $-V$.

We will use the method of steepest descent [160] to evaluate the path integral in a neighborhood of the classical path and we will expand our paths in terms of weak variations around paths that are stationary with respect to the Euclidean action. We assume currently that there is only one such path, this is of course not generally true but we can always sum the contributions from other such stationary paths. We will express any path $x(\tau)$ as

$$x(\tau) = \bar{x}(\tau) + \Delta x(\tau), \tag{2.117}$$

with $\bar{x}(\tau)$ the stationary point of the Euclidean action and $\Delta x(\tau)$ is a small correction to the classical trajectory. The next step is the expansion of the action around a classical trajectory, $\bar{x}(\tau)$:

$$\begin{aligned} S_E[x(\tau)] &= S_E[\bar{x}(\tau) + \Delta x(\tau)] = S_E[\bar{x}] + \delta S_E[\bar{x}, \Delta x] + \frac{1}{2!} \delta^2 S_E[\bar{x}, \Delta x] + ... \\ &= S_E[\bar{x}] + \frac{1}{2!} \int \int \frac{\delta^2 S_E}{\delta x(\tau_1) \delta x(\tau_2)} \Delta x(\tau_1) \Delta x(\tau_2) d\tau_1 d\tau_2 + ..., \end{aligned} \tag{2.118}$$

where we used the fact that the first functional derivative is zero at the stationary point. Now, it is the moment to calculate the second functional derivative of the action. First, we express the

RHS of Eq.(2.116) with Dirac's deltas. For the first term, we get

$$\begin{aligned}\ddot{x}(\tau') &= \int_{-\infty}^{\infty} \ddot{x}(s)\delta(s-\tau')ds \\ &= \dot{x}\delta(s-\tau')\Big|_{-\infty}^{\infty} - \dot{x}\dot{\delta}(s-\tau')\Big|_{-\infty}^{\infty} + \int_{-\infty}^{\infty} x\ddot{\delta}(s-\tau')ds \\ &= \int_{-\infty}^{\infty} x(s)\ddot{\delta}(s-\tau')ds,\end{aligned} \tag{2.119}$$

where the boundary conditions obviously vanish. So, if we take another functional derivative we get,

$$\int \frac{\delta x(s)}{\delta x(\tau)}\ddot{\delta}(s-\tau')ds = \int \delta(\tau-s)\ddot{\delta}(s-\tau')ds = \ddot{\delta}(\tau-\tau'). \tag{2.120}$$

For the second part also,

$$V'(x(\tau')) = \int V'(x(s))\delta(s-\tau')ds \tag{2.121}$$

and

$$\int \frac{\delta V'(x(s))}{\delta x(\tau)}\delta(s-\tau')ds = \int V''(x(s))\delta(s-\tau)\delta(s-\tau')ds = V''(x(\tau))\delta(\tau-\tau'). \tag{2.122}$$

Equation (2.115) was used at (2.120) and (2.122). The second functional derivative of the Euclidean action is

$$\frac{\delta^2 S_E}{\delta x(\tau_1)\delta x(\tau_2)} = -\ddot{\delta}(\tau_1-\tau_2) + V''(x(\tau))\delta(\tau_1-\tau_2). \tag{2.123}$$

The second variation is

$$\begin{aligned}\frac{1}{2!}\delta^2 S_E &= \frac{1}{2!}\int\int \frac{\delta^2 S_E}{\delta x(\tau_1)\delta x(\tau_2)}\Delta x(\tau_1)\Delta x(\tau_2)d\tau_1 d\tau_2 \\ &= \frac{1}{2}\int\int \Big[-\ddot{\delta}(\tau_1-\tau_2) + V''(x(\tau))\delta(\tau_1-\tau_2)\Big]\Delta x(\tau_1)\Delta x(\tau_2)d\tau_1 d\tau_2 \\ &= \frac{1}{2}\Big\{\int\int -\ddot{\delta}(\tau_1-\tau_2)\Delta x(\tau_1)\Delta x(\tau_2)d\tau_1 d\tau_2 + \int\int V''(x(\tau))\delta(\tau_1-\tau_2)\Delta x(\tau_1)\Delta x(\tau_2)d\tau_1 d\tau_2\Big\} \\ &= \frac{1}{2}\Big\{\int\int \Big[-\Delta x(\tau_2)\delta(\tau_1-\tau_2)\frac{\mathrm{d}^2\Delta x(\tau_1)}{\mathrm{d}\tau_1^2}\Big]d\tau_1 d\tau_2 + \int V''(\bar{x}(\tau_1))\Delta x(\tau_1)^2 d\tau_1\Big\} \\ &= \frac{1}{2}\int\Big[-\Delta x(\tau_1)\frac{\mathrm{d}^2\Delta x(\tau_1)}{\mathrm{d}\tau_1^2} + V''(\bar{x}(\tau_1))\Delta x(\tau_1)^2\Big]d\tau_1 \\ &= \frac{1}{2}\int\Delta x(\tau_1)\Big[-\frac{\mathrm{d}^2\Delta x(\tau_1)}{\mathrm{d}\tau_1^2} + V''(\bar{x}(\tau_1))\Delta x(\tau_1)\Big]d\tau_1.\end{aligned} \tag{2.124}$$

In the third and the fourth line of Eq.(2.124) the integral with respect to τ_2 is performed in order to collapse the delta "functions". Also, with the aid of Eq.(2.120) we integrate by parts delta's second derivative (double dotted) of the first term. Let us now turn our attention to the last line, the term in the brackets is an operator of the Sturm-Liouville form [161]

$$-\frac{\mathrm{d}}{\mathrm{d}t}\Big[p(t)\frac{\mathrm{d}x}{\mathrm{d}t}\Big] + q(t)y = \lambda w(t)x, \tag{2.125}$$

which, in general, has an infinity of eigenvalues and eigenvectors. Let us call this operator $S''(\tau)$ and write

$$S''(\tau) = -\frac{\mathrm{d}^2}{\mathrm{d}\tau^2} + V''(\bar{x}). \tag{2.126}$$

To proceed the usual procedure we will look for eigenvalues of S''

$$\left(-\frac{\mathrm{d}^2}{\mathrm{d}\tau^2} + V''(\bar{x})\right) x_n = \lambda_n x_n(\tau). \tag{2.127}$$

This indicates that when the x_n's are normalized properly, they will form a total orthonormal basis for the Lebesgue space $L^2\left([-T/2, T/2], 1dx\right)$ and hence we can express our Δx terms in an infinite sum of x_n's.

A general function obeying the boundary conditions can be written as

$$x(\tau) = \bar{x}(\tau) + \sum_n c_n x_n(\tau), \tag{2.128}$$

if, of course, $\bar{x}$ is obeying the boundary conditions, and for the x_n's, a complete set of orthonormal functions it holds that

$$\begin{aligned} &x_n(-T/2) = x_n(T/2) = 0, \\ &\int_{-T/2}^{T/2} d\tau x_n(\tau) x_m(t) = \delta_{nm}, \end{aligned} \tag{2.129}$$

which makes perfect sense, for a general function obeying the boundary conditions. Then, in the semi-classical limit, the integral transforms into a product of Gaussians. Now, it is the right moment to gather everything and check how the path integral becomes:

$$\begin{aligned} \langle x_f | \, e^{-H\tau} \, | x_i \rangle &= \int [dx] e^{-S_E[x(\tau)]} \\ &= \int [d(\bar{x}(\tau) + \Delta x)] e^{-S_E[\bar{x} + \Delta x]} \\ &\approx e^{-S_E[\bar{x}]} \int [\Delta x] e^{-S_E^{fl}[\Delta x]} \\ &= e^{-S_E[\bar{x}]} \mathcal{F}. \end{aligned} \tag{2.130}$$

We used the fact that the action has been factorized into the contribution from the classical path and the contribution from quadratic fluctuations $\mathcal{F}$ around that path. For the fluctuating term, we can write,

$$\begin{aligned} S_E^{fl} &= \frac{1}{2} \int \Delta x(\tau_1) \left[-\frac{\mathrm{d}^2}{\mathrm{d}\tau_1^2} + V''(\bar{x})\right] \Delta x(\tau_1) d\tau_1 \\ &\overset{(2.128)}{=} \frac{1}{2} \int \sum_n c_n x_n \left[-\frac{\mathrm{d}^2}{\mathrm{d}\tau_1^2} + V''(\bar{x})\right] \sum_m c_m x_m d\tau_1 \\ &\overset{(2.127)}{=} \frac{1}{2} \int \sum_n c_n x_n \sum_m c_m x_m \lambda_n d\tau_1 \\ &= \frac{1}{2} \sum_n c_n^2 \lambda_n, \end{aligned} \tag{2.131}$$

in the fourth line it used the orthonormality of x_n Eq.(2.129). Eventually,

$$\begin{aligned}\mathcal{F} &= \int [\Delta x(\tau)] e^{-S_E^{fl}[\Delta x(\tau)]} \\ &= N \prod_n \left[\int_{-\infty}^{\infty} \frac{dc_n}{\sqrt{2\pi}} \right] \exp\left\{ -\frac{1}{2} \sum_n c_n^2 \lambda_n \right\} \\ &= N \prod_n \int_{-\infty}^{\infty} \frac{dc_n}{\sqrt{2\pi}} \exp\left\{ -\frac{1}{2} \sum_n c_n^2 \lambda_n \right\} \\ &\approx \frac{N}{\sqrt{\prod_n \lambda_n}},\end{aligned} \tag{2.132}$$

where N is a normalization factor that needs to be dealt with by some regularization procedure. So, the summation over the trajectories on the first line of Eq.(2.132) has been reduced, because of Eq.(2.131), to integrations over c_n's. More to the point, the expansion is actually a parametrization of the possible paths in terms of a set of orthonormal functions, and it can be used to define the integration measure to be,

$$[\Delta x] = \prod_n (2\pi)^{-1/2} dc_n. \tag{2.133}$$

The original path integral has now been reduced to

$$\langle x_f | \, e^{-H\tau} \, | x_i \rangle = e^{-S_E[\bar{x}]} \frac{N}{\sqrt{\prod_n \lambda_n}}. \tag{2.134}$$

For the final step, recall that the determinant of an operator is equal to the product of its eigenvalues. For our Sturm-Luvville differential operator defined at (2.126) we get

$$\det S'' = \det\left[-\partial_\tau^2 + V''(\bar{x}) \right] = \prod_n \lambda_n, \tag{2.135}$$

from the latest equation, (2.134) takes its final form

$$\langle x_f | \, e^{-H\tau} \, | x_i \rangle = N e^{-S_E[\bar{x}]} \det\left[-\partial_\tau^2 + V''(\bar{x}) \right]^{-1/2}. \tag{2.136}$$

Of course, we are tacitly assuming here that all the eigenvalues are positive, otherwise, the integrals would diverge. If there are more than one stationary points, in general, someone has to sum all over them.

2.3.3 The case of potential with one minimum

As it was stated a few pages earlier (and in previous sections), Eq.(2.116) is the equation of motion for a particle of unit mass moving in a turned upside down potential, $-V$. Therefore,

$$E = \frac{1}{2} \left(\frac{\mathrm{d}\bar{x}}{\mathrm{d}\tau} \right)^2 - V(\bar{x}) \tag{2.137}$$

is a constant of its motion. This can be used to specify some qualitative characteristics of the solutions of the equation of motion. Let us consider a simple example for investigation, the potential in Fig.2.10.a, by the selection of $x_i = x_f = 0$. Figure 2.10.b shows the inverted potential

case. It is clear from the figures that the only solution of EoM which obeys the boundary conditions selected is

$$\bar{x} = 0. \tag{2.138}$$

For this solution, it is also clear that

$$S_E = 0. \tag{2.139}$$

Therefore, going back to Eq.(2.136) we will take the following result

$$\langle 0|\, e^{-H\tau}\, |0\rangle = N\{\det \partial_\tau^2 + \omega^2]\}^{-1/2}, \tag{2.140}$$

where

$$\omega^2 = V''(0). \tag{2.141}$$

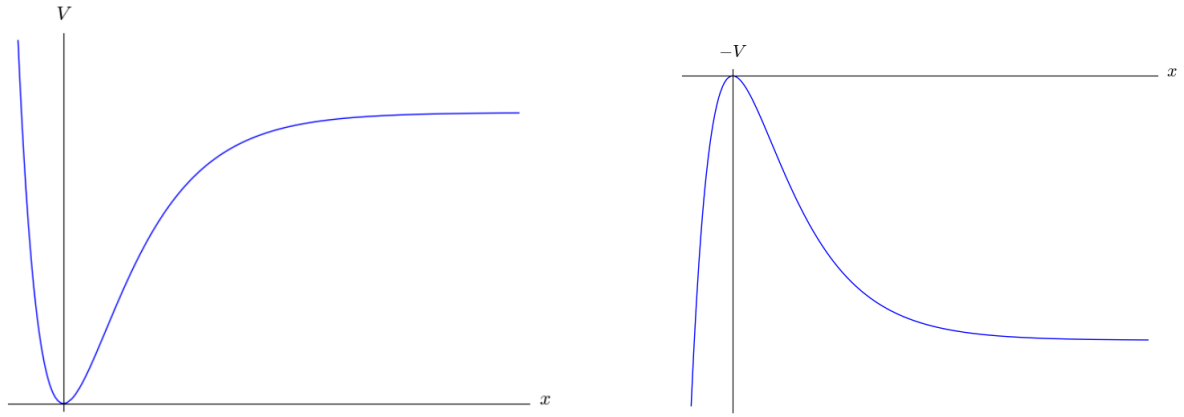

(a) (b)

Figure 2.10: a) Potential energy as a function of position, for a particle problem with a true ground state. b) Same case with the inverted potential.

In Appendix D the functional determinant for this case, for large $\tau = T$ is computed. It is shown that

$$N\{\det\left[-\partial_\tau^2 + \omega^2\right]\}^{-1/2} = \left(\frac{\omega}{\pi}\right)^{1/2} e^{-\omega T/2}. \tag{2.142}$$

At $T \to \infty$, from Eq.(2.112) and Eq.(2.142)

$$\langle 0|\, e^{-H\tau}\, |0\rangle = e^{-E_0\tau}\, \langle 0|0\rangle\, \langle 0|0\rangle = \left(\frac{\omega}{\pi}\right)^{1/2} e^{-\omega T/2}. \tag{2.143}$$

So, the ground state energy will be

$$E_0 = \frac{1}{2}\omega, \tag{2.144}$$

which is the familiar zero energy of a harmonic oscillator (we use $\hbar = 1$).

2.3.4 Instantons and the double-well potential

In the previous example, we reproduced in the path integral language a fundamental problem of physics - a system oscillating between an equilibrium point. The results obtained are accurate for the harmonic oscillator case but also for potentials that diverge from the harmonic oscillator potential on a small scale, for example, $V(x) = \frac{1}{2}\omega^2 x^2 + \lambda x^4$. Specifically, we took into account small perturbations and make a step for a classical perturbation theory.

However, there are systems that cannot be described by a classical perturbation theory. The simplest example of such a system is the double-well potential, with two minima at points $x = \pm\alpha$. Also, we assume that the potential is symmetric and we set $V''(\pm\alpha) = \omega^2$ (Fig.2.11).

As we have pointed out, the main contribution to the path integral is given by the classical Euclidean solutions. The mechanical analogue EoM is corresponding to a particle moving in the negative potential from one hill to the other. The equation of motion is (2.116) with boundary conditions $x_i = x(-T/2) = -\alpha$, $x_f = x(T/2) = \alpha$. Furthermore, in order to take the limit $T \to \infty$, we will consider that the particle is starting his motion with $\dot{x}(-T/2) = \dot{x}(-\alpha) = 0$ and when it reaches the other minimum $\dot{x}(T/2) = \dot{x}(\alpha) = 0$. As a result of this, we can have solutions of finite action, for non-finite time to obtain zero energy.

It is obvious that two solutions are existing under our boundary conditions. In one of them, the particle starts from rest at $-\alpha$ and reaches α in rest. The other solution is vice versa. We can observe that under analytic continuation in real time these solutions represent a motion in the classical forbidden area, so they describe the quantum tunneling.

The conservation of energy gives:

$$\frac{1}{2}\left(\frac{\mathrm{d}\bar{x}}{\mathrm{d}\tau}\right)^2 = V(\bar{x}) \Rightarrow \frac{\mathrm{d}\bar{x}}{\mathrm{d}\tau} = \sqrt{2V(\bar{x})}. \tag{2.145}$$

If we Taylor expand the potential $V(\bar{x})$ around $\bar{x} = \alpha$ and take into account that $V(\alpha) = V'(\alpha) = 0$ we take that

$$\frac{\mathrm{d}\bar{x}}{\mathrm{d}\tau} = \left[2V(\alpha) + 2V'(\alpha)(\bar{x}-\alpha) + V''(\alpha)(\bar{x}-\alpha)^2\right]^{1/2} = \omega(\alpha - \bar{x}) \tag{2.146}$$

from the above

$$(\alpha - \bar{x}) \propto e^{-\omega\tau}. \tag{2.147}$$

This relation, makes us conclude that the solution has a characteristic width in the imaginary time $\tau \sim 1/\omega$. That is to say, it is time located. Someone could say, that this is not right, because the particle is located in two different spots as $\tau \to \pm\infty$. However, these spots, although different, they are physically equivalent ground states. So, the solution describes a disposition interposed between two ground states. The system is in one ground state, except for a moment (instant), a tiny period of time. This is the reason, these pseudo-particle solutions are called "instantons". In Fig.2.12 we have sketched an instanton solution.

If we solve the soliton (one-dimensional instanton) equation, for a potential with the specific usual form $V(x) = \lambda(x^2 - \alpha^2)^2$ (Appendix C) we will find

$$x_I = \bar{x} = \pm\alpha \tanh\left[\frac{\omega}{2}(\tau - \tau_c)\right], \tag{2.148}$$

which for time goes to infinity gives $x_I = \pm\alpha$. The plus sign represents an instanton and the minus is an anti-instanton.

For the transition matrix element for one instanton we have that

$$\begin{aligned} I_1 &= \langle\alpha|\, e^{-HT}\, |-\alpha\rangle = e^{-E_0 T}\psi_0(\alpha)\psi_0^*(-\alpha) \\ &= N e^{-S_I}[\det\left(-\partial_\tau^2 + V''(x_I)\right)]^{-1/2}, \end{aligned} \tag{2.149}$$

where the instanton x_I is the stationary point of the action.

Now, we must go back to Eq.(2.127) , at the stationary point $\bar{x}$. In order to perform the Gaussian integrals in the path integral, we had to assume that all the eigenvalues were positive

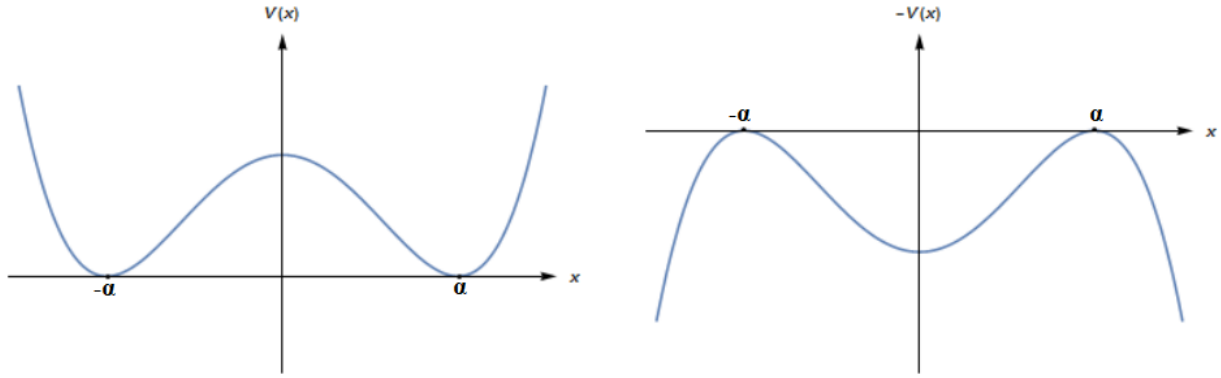

Figure 2.11: The double-well potential and the reversed double-well potential.

numbers to avoid the integral's divergence. Due to the time translation invariance of the equations of motion, except the positive eigenvalues if we act on the EoM of Eq.(2.116) with the operator ∂_τ we have

$$\begin{aligned}
&\partial_\tau\left(-\partial_\tau^2\bar{x}+V'(\bar{x})\right)=0\Rightarrow-\partial_\tau(\partial_\tau^2\bar{x})+\partial_\tau V'=0\\
&\Rightarrow-\partial_\tau^3\bar{x}+V''\partial_\tau\bar{x}=0\Rightarrow\left(-\partial_\tau^2+V''\right)\partial_\tau\bar{x}=0\\
&\Rightarrow\lambda\partial_\tau\bar{x}=0\Rightarrow\lambda=0,
\end{aligned}\tag{2.150}$$

this means that our Sturm–Liouville operator has a zero eigenvalue (a zero mode), $\lambda_1=0$, too.

We can write:

$$x(\tau)=x_I(\tau+d\tau)=x_I(\tau)+x_I(\tau+d\tau)-x_I(\tau)=x_I(\tau)+\frac{\mathrm{d}x_I}{\mathrm{d}\tau}d\tau+\cdots.\tag{2.151}$$

In addition, if we go to Eq.(2.128) for $n=1$ it becomes

$$x(\tau)=x_I(\tau)+c_1x_1(\tau).\tag{2.152}$$

From the above, this corresponds to an eigenfunction of the form,

$$x_1=c_1\partial_\tau\bar{x},\tag{2.153}$$

with x_1 as a normalization factor. Hence the action will be

$$S_I=\int_{-\infty}^{\infty}d\tau(d\bar{x}/d\tau)^2=\int_{-\infty}^{\infty}d\tau\frac{x_1^2}{c_1^2}\Rightarrow c_1^2S_I=1\Rightarrow c_1=S_I^{1/2}.\tag{2.154}$$

So, the -zero eigenvalue- eigenfunction is

$$x_1=S_I^{-1/2}\frac{\mathrm{d}\bar{x}}{\mathrm{d}\tau}.\tag{2.155}$$

This zero mode is the Goldstone mode from the SSB of the time-translation symmetry [163]. Let c_1 be the Fourier coefficient in Eq.(2.128) corresponding to the Goldstone mode. Actually, for a given instanton solution $\bar{x}$, one can obtain another one by shifting the instanton center to $-\tau_c$, due to time translation invariance, i.e.,

$$\bar{x}(\tau)\to\bar{x}(\tau+\tau_c)\tag{2.156}$$

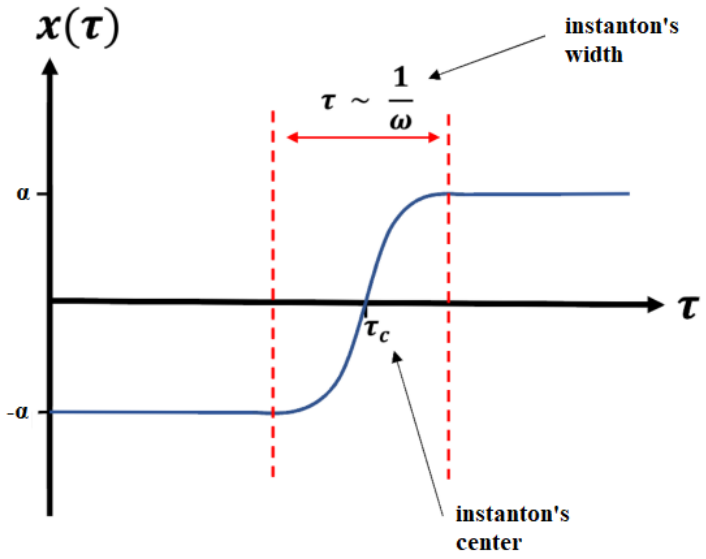

Figure 2.12: The instanton solution in one dimension (taken from [162]).

Here τ_c appears as a free parameter. The integral over the zero mode can be traded for an integral over the collective coordinate τ_c [164]. Change in x corresponding to some small change in c_1 is

$$dx = x_1 dc_1. \tag{2.157}$$

On the other hand, the change dx under a shift $d\tau_c$ of the instanton center is

$$dx = \partial_\tau \bar{x} d\tau_c = \sqrt{S_I} x_1 d\tau_c, \tag{2.158}$$

where in the last equality we used the expression for the zero mode, Eq.(2.155). Comparing the relations of Eq.(2.157) and Eq.(2.158) to each other, one obtains

$$x_1 dc_1 = \sqrt{S_I} x_1 d\tau_c \Rightarrow dc_1 = \sqrt{S_I} d\tau_c. \tag{2.159}$$

Thus, the integral over c_1 has been traded for that over the collective coordinate τ_c which with the help of Eq.(2.133) gives us,

$$(2\pi)^{-1/2} dc_1 = (S_I/2\pi)^{1/2} d\tau_c. \tag{2.160}$$

Now, we return to the transition matrix element, with the help of Eq.(2.134), we isolate the zero mode and integrate over the new variable of the above equation and we have

$$\begin{aligned} I_1 = \langle \alpha | \, e^{-HT} \, | -\alpha \rangle &= N e^{-S_I} \sqrt{\frac{S_I}{2\pi}} [\det'(-\partial_\tau^2 + V''(x_I))]^{-1/2} \int_{-T/2}^{T/2} d\tau_c \\ &= N e^{-S_I} T \sqrt{\frac{S_I}{2\pi}} [\det'(-\partial_\tau^2 + V''(x_I))]^{-1/2} \\ &= N e^{-S_I} [\det S''(x_{SHO})]^{-1/2} K T, \end{aligned} \tag{2.161}$$

where $\det' S''(x_I)$ is the determinant with the contribution of non-zero eigenvalues and

$$K = \sqrt{\frac{S_I}{2\pi}} \left[\frac{\det' S''(x_I)}{\det S''(x_{SHO})} \right]^{-1/2}. \tag{2.162}$$

In the last step, we multiplied and divide with the determinant of the operator of the harmonic oscillator. The reason we expressed the transition instanton matrix element in this way is that we want the parameter K to be identified by a corrective term from the harmonic oscillator case.

It is obvious that the solution from the previous section will contribute to the path integral, because as it was stated instanton is a pseudo-particle between two minima, indeed it spends the longest period of time in these spots. To explain this in different words, the harmonic oscillator contribution describes the contribution of the solution $x_I = \pm\alpha$, in which the particle is located in one of the two minima, like the one minimum potential case.

According to the above, in the limit $T \to \infty$ the harmonic oscillator contribution is going to be

$$\begin{aligned} I_0 &= \langle \pm\alpha | \, e^{-HT} \, | \pm\alpha \rangle \\ &= N[\det S''(x_{SHO})]^{-1/2} = N[\det S''(\pm\alpha)]^{-1/2} = N[\det\left(\partial_\tau^2 + \omega^2\right)]^{-1/2} \\ &= \sqrt{\frac{\omega}{\pi}} e^{-\omega T/2}. \end{aligned} \tag{2.163}$$

Finally, the transition matrix element for one instanton will be

$$I_1 = \sqrt{\frac{\omega}{\pi}} e^{-\omega T/2} e^{-S_I} K T. \tag{2.164}$$

We have one last step to make in order to calculate the transition matrix element for the double well potential. If we process this problem a little further we will see that the contribution of one instanton is not the only one. In fact, there is a series of instantons and anti-instantons traveling from one minimum to the other, because of the time translation invariance under translations of the center τ_c. For time periods bigger than the instanton's width, we have to take into account the instantons located in each intermediate time interval. The only restriction is that one instanton from $-\alpha$ to α must be followed by an anti-instanton from α to $-\alpha$.

We consider a dilute gas of n instantons [165] clearly separated in imaginary time τ. In Fig.2.13 we demonstrate a chain of these pseudo-particles, each vertical line corresponds to one specific instanton as the horizontal lines (the distance between two particles) are very larger than their width.

Under this perspective, we can treat this dilute instanton gas as one classical solution which is an approximate stationary point of the Euclidean action. The action of this gas will be

$$S = n S_I. \tag{2.165}$$

Obviously, the gas will obtain n zero modes corresponding to n independent time translations of the instantons' centers τ_n. But, as we found earlier these zero eigenvalues are the reason for the integrals' divergence, thus we have to separate them from the positive eigenvalues. Following the same method, we transform the integration over the c_n parameters of the zero modes to integration over the instantons' centers. So, we take

$$\int_{-T/2}^{T/2} d\tau_1 \int_{-T/2}^{\tau_1} d\tau_2 \cdots \int_{-T/2}^{t_{n-1}} d\tau_n = T^n/n!. \tag{2.166}$$

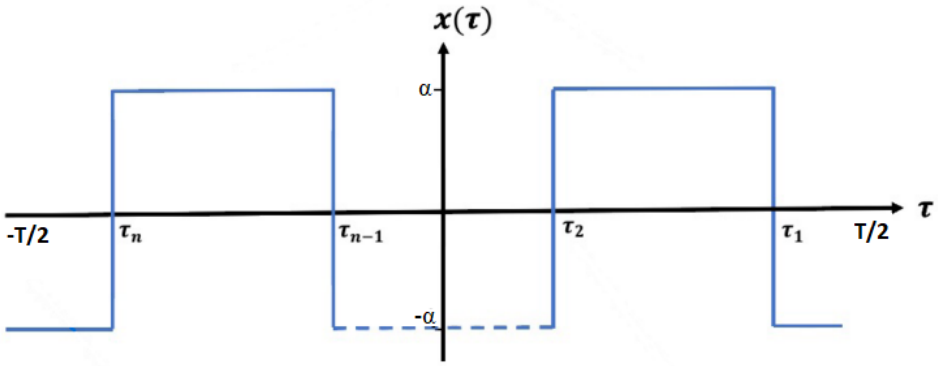

Figure 2.13: The approximation of the dilute instanton gas (taken from [162]) .

Under the condition that $T/2 > \tau_1 > \tau_2 ... > \tau_n > -T/2$. From the last two relations and the I_1 matrix element, we conclude that the contribution of n instantons and anti-instantons is

$$I_n = \sqrt{\frac{\omega}{\pi}} e^{-\omega T/2} e^{-nS_I} K^n \frac{T^n}{n!}. \tag{2.167}$$

Finally, we have to sum the contribution over all the possible instanton chains. In order for a particle to begin from $\pm\alpha$ and arrive at the same point, we need an even number of instanton chains, while to end up at the other vacuum state we need an odd number. Therefore, we can write

$$\begin{aligned} \langle \pm\alpha | \, e^{-HT} \, | \pm\alpha \rangle &= \sum_{\text{even n}} I_n \\ &= \sqrt{\frac{\omega}{\pi}} e^{-\omega T/2} \sum_{\text{even n}} \frac{(Ke^{-S_I T})^n}{n!} \\ &= \sqrt{\frac{\omega}{\pi}} e^{-\omega T/2} \cosh\left(Ke^{-S_I T}\right), \end{aligned} \tag{2.168}$$

$$\begin{aligned} \langle \pm\alpha | \, e^{-HT} \, | \mp\alpha \rangle &= \sum_{\text{odd n}} I_n \\ &= \sqrt{\frac{\omega}{\pi}} e^{-\omega T/2} \sum_{\text{even n}} \frac{(Ke^{-S_I T})^n}{n!} \\ &= \sqrt{\frac{\omega}{\pi}} e^{-\omega T/2} \sinh\left(Ke^{-S_I T}\right). \end{aligned} \tag{2.169}$$

The above can be expressed as follows

$$\langle \pm\alpha | \, e^{-HT} \, | -\alpha \rangle = \sqrt{\frac{\omega}{\pi}} e^{-\omega T/2} \frac{1}{2} \left[e^{Ke^{-S_I T}} \mp e^{-Ke^{-S_I T}} \right]. \tag{2.170}$$

In the $T \to \infty$ limit, the LHS of Eq.(2.170) can be written on the frame of the two eigenstates of the least energy $|+\rangle$ and $|-\rangle$:

$$\langle \pm\alpha | \, e^{-HT} \, | -\alpha \rangle = e^{-E_- T} \langle \pm\alpha | - \rangle \langle - | -\alpha \rangle + e^{-E_+ T} \langle \pm\alpha | + \rangle \langle + | -\alpha \rangle . \tag{2.171}$$

Where, after comparison with (2.170) someone can find the energies and the eigenfunctions of these two eigenstates:

$$E_{\pm} = \frac{1}{2}\omega \pm Ke^{-S_I} \tag{2.172}$$

and

$$\begin{aligned}\Psi_-(-\alpha)\Psi_-^*(+\alpha) &= -\Psi_+(-\alpha)\Psi_+^*(+\alpha) = \Psi_-(-\alpha)\Psi_-^*(-\alpha) \\ &= \Psi_+(-\alpha)\Psi_+^*(-\alpha) = \frac{1}{2}\sqrt{\frac{\omega}{\pi}}.\end{aligned} \tag{2.173}$$

Our analysis shows that the solution derived here depicts a series of transitions through the classical forbidden area, between $|\alpha\rangle$ and $|-\alpha\rangle$.

From the eigenfunctions' relations results that

$$\Psi_-(-\alpha) = \Psi_-(+\alpha), \qquad \Psi_+(-\alpha) = -\Psi(+\alpha). \tag{2.174}$$

This means that $|-\rangle$ is an even superposition of $|\pm\alpha\rangle$, while $|+\rangle$ is an odd function. These two are the well-known eigenfunctions of the lowest energy appearing in traditional quantum mechanics and they are responsible for the energy separation between $|\alpha\rangle$ and $|-\alpha\rangle$.

A final comment to be made here is that our calculation concern the energy difference, and not the energy corrections. Indeed, there are existing perturbative corrections in energy that are very greater than the non-perturbative correction derived here. However, these perturbative corrections cannot predict the quantum tunneling, instead, our calculation achieves that. In summary, the energy separation, can be shown only through the path integral formulation and not through perturbation theory [166].

2.3.5 Path integral approach for bounce solutions

We now turn to a less trivial problem and recall the one-dimensional case choosing $x_i = x_f = 0$. We can see from the figure below that there are no trivial solutions to the EoM like the double-well potential. As we have repeatedly analyzed in the previous paragraphs, the particle can begin its motion at the top of the hill at $x = 0$, bounce off the potential wall at its right side, and return back to its starting point. At the limit of interest, when imaginary time goes to infinity we call this limiting form "the bounce" as we know.

The bounce has $E = 0$, because of our descriptions, at the time $T \to -\infty$ and $T \to \infty$ the particle attains at the top of the hill, and it was declared that its Euclidean action will be

$$S_E = B = \int_{-\infty}^{\infty} d\tau (d\bar{x}/d\tau)^2 = \int_0^{\sigma} dx [2V(x)]^{1/2}, \tag{2.175}$$

where σ is the turning point of the particle. Very good so far with our brief review of the bounce, but allow us to introduce some new stuff in our path integral approach, and make the connection with the instanton analysis made. We define the "center of the bounce" as the point where $dx/d\tau = 0$. In our figure is the point σ where for an instance the particle stops its motions and begins the turning back to the starting point. Because of time translation invariance, this point can be placed everywhere at the τ axis. In the $T \to \infty$ limit, a randomly centered bounce in the interval of integration is an approximate stationary point of the action functional, as in the previous non-bounce case. Stationary points also will be n widely separated bounces in a multi-bounce configuration, centered at $\tau_1, \tau_2, ...\tau_n$ with $T/2 > \tau_1 > \tau_2 ... > \tau_n > -T/2$. In

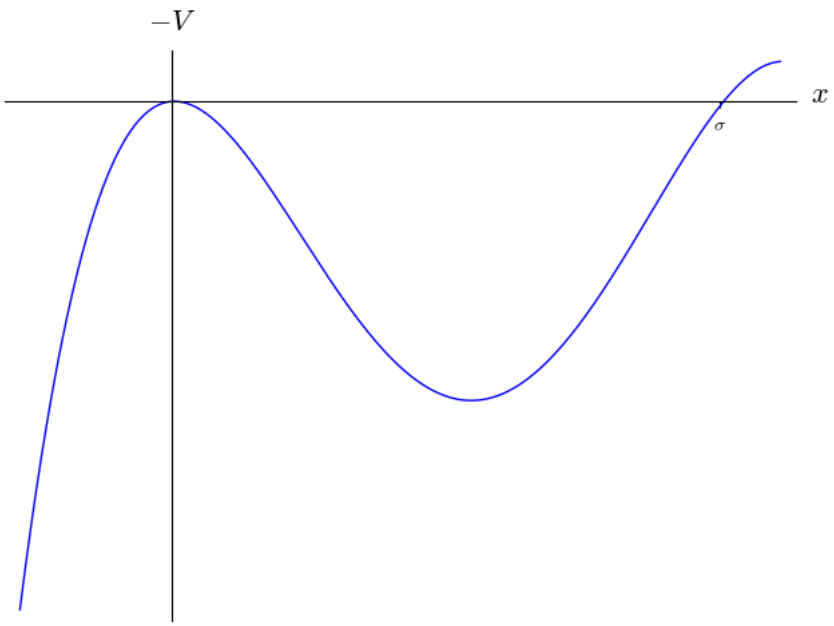

Figure 2.14: An upside down potential, for the one-dimensional problem.

this situation, we have to sum over the location of all of them as we did with the instanton gas approximation.

For n bounces the Euclidean action S_E will be nB. This multi-bounce term takes place at the exponential. From the description of the bounce in Fig.2.14, it is understandable that the particle will remain at the starting point $x = 0$ at very large T after its return to it. So, the bounces are separated by vast vacant regions. As a result of this, the determinant $\det[\partial_\tau^2 + V''(\bar{x})]$ is the product of the determinant of n single bounces which are separated by large time intervals surrounding the bounces and even larger time intervals containing the regions with $x = 0$ separating them. Under this perception, in accordance with that happened in the multi-instanton case, the determinant is

$$\left(\frac{\omega}{\pi}\right)^{1/2} e^{-\omega T/2} K^n. \tag{2.176}$$

Here, again K is a factor chosen so that this expression is correct for a single bounce ($n = 1$). It will be evaluated later in this section. The last step is to integrate over the locations of the centers, with the same result of Eq.(2.166).

Now we can sum over all the contributions from bounces to compute the transition matrix element between $x_i = 0$ and $x_f = 0$ at large T:

$$\begin{aligned}
\langle 0|\, e^{-H\tau}\, |0\rangle &= e^{-E_0\tau}\, \langle 0|0\rangle\, \langle 0|0\rangle \\
&= \sum_{n=0}^{\infty} \left(\frac{\omega}{\pi}\right)^{1/2} e^{-\omega T/2} \frac{(Ke^{-B}T)^n}{n!} \\
&= \left(\frac{\omega}{\pi}\right)^{1/2} e^{-\omega T/2} \sum_{n=0}^{\infty} \frac{(Ke^{-B}T)^n}{n!} \\
&\approx \left(\frac{\omega}{\pi}\right)^{1/2} e^{-\omega T/2} e^{Ke^{-B}T} \\
&= \left(\frac{\omega}{\pi}\right)^{1/2} \exp\!\left(-\omega T/2 + Ke^{-B}T\right),
\end{aligned} \tag{2.177}$$

where in the third line we used the Taylor expansion for an exponential function which is

$$e^{f(x)} \approx \sum_{n=0}^{\infty} \frac{f^n(x)}{n!}. \tag{2.178}$$

The ground energy eigenvalue from Eq.(2.177) is given by

$$E_0 = \frac{1}{2}\omega - Ke^{-B} \tag{2.179}$$

In conclusion, including a multi-bounce configuration makes a small modification in the functional integral estimation for the ground state of the energy similar to the previous. The added term to Eq.(2.179) is very small in magnitude for the semi-classical approximation limit. However, as we will see shortly, K is imaginary and this term is in fact, the first nonzero contribution to the imaginary part of the energy.

Now, we will turn our interest to the evaluation of K. We must go back to Eq.(2.127) with a single bounce, at the stationary point $\bar{x}$. In order to perform the Gaussian integrals in the path integral, we had to assume that all the eigenvalues were positive numbers to avoid the integral's divergence. Similar to the double-well case due to the time translation invariance of the equations of motion, except the positive eigenvalues if we act on the EoM of Eq.(2.116) with the operator ∂_τ. The zero eigenvalue appears again, and now we get

$$x_1 = B^{-1/2}\frac{\mathrm{d}\bar{x}}{\mathrm{d}\tau}. \tag{2.180}$$

In the same way, for a given bounce solution $\bar{x}$, one can obtain another one by shifting the bounce center to $-\tau_c$, due to time translation invariance, i.e., Here τ_c appears as a free parameter. The integral over the zero mode can be traded for an integral over the collective coordinate τ_c etc. This procedure lead to the following result

$$(2\pi)^{-1/2} dc_1 = (B/2\pi)^{1/2} d\tau_c. \tag{2.181}$$

To summarize, in evaluating the determinant, we should not include the zero eigenvalue, but we should include in K a factor of $(B/2\pi)^{1/2}$.

The classical EoM has a solution in which the particle begins at the top of the hill at $x = 0$, bounces off the classical turning point σ and returns at the top of the hill. The bounce has a maximum at σ, where the particle's velocity goes to zero ($\frac{\mathrm{d}\bar{x}}{\mathrm{d}\tau} = 0$) (Fig.2.15). So, the zero eigenfunction, $x_1 \propto \frac{\mathrm{d}\bar{x}}{\mathrm{d}\tau}$, has a node. A node occurs at points where the eigenfunction is zero and changes signs. The ground state eigenfunction must have not nodes. As a consequence of this, there must be another lower eigenvalue in the spectrum of these variations. The nodeless eigenfunction, x_0, must have a negative eigenvalue. Thus, the bounce is not the minimum of the action, but a saddle point, and due to the negative eigenvalue the product of the eigenvalues (except the zero one) is negative. This leads the Gaussian integral over the expansion coefficient c_0 to be divergent.

In brief, eigenvalues can be used to determine whether a fixed point (also known as an equilibrium point) is stable or unstable. A system has a stable fixed point when it can be initially disturbed in the area around it and eventually return to and remain there. Any fixed point that is not stable is unstable. Imagine our particle as a round ball sandwiched between two hills to help you visualize this idea, the ball will not move if left alone, hence its location is regarded as a fixed point. The ball will return back to its original location between the two hills if we disrupt it by slightly pushing it up the hill. This is a stable fixed point. Now, illustrate the ball standing

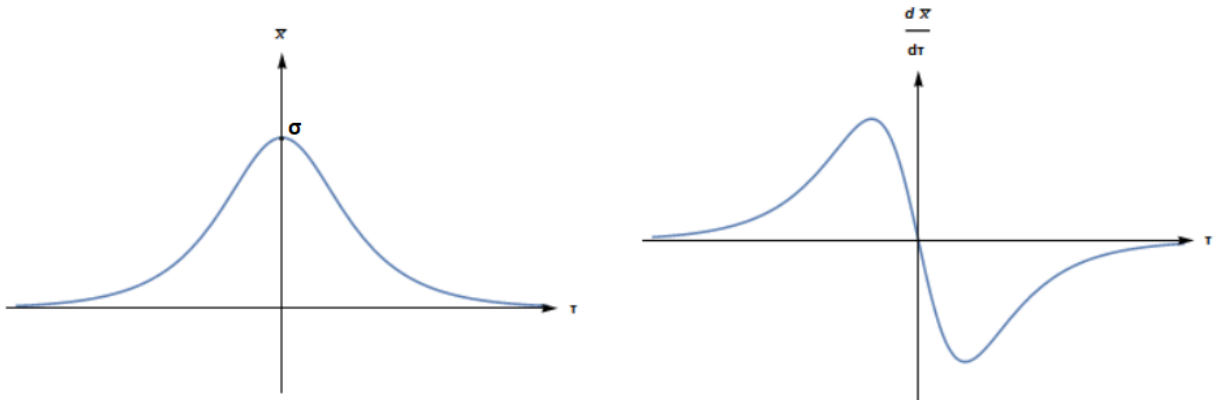

Figure 2.15: The bounce solution and its derivative.

at the peak of one of the hills. If left undisturbed, the ball will still remain at the peak, so this is also considered a fixed point. The ball will, however, start to roll away from the top of the hill if there is a disturbance in any direction. Similar to the starting point of our particle, the hilltop is seen as an unstable fixed point.

The fixed point is an unstable saddle point if the system's set of eigenvalues contains both positive and negative eigenvalues, as it does in our case. A saddle point is a point where a series of minimum and maximum points converge at one area in a gradient field, without hitting the point. Because the function in a three-dimensional surface plot resembles a saddle, the point is known as a saddle point.

This is worrisome and puts us in trouble because now the path integral diverges. But also, this should not be very surprising, because from the beginning we were trying to calculate the energy of a state localized near the true vacuum. We knew that such a state should not be stable and therefore it should not be part of the spectrum of the Hamiltonian. The correct way to treat this problem and save the computation is by analytic continuation.

To make this situation as simple as possible, we restrict ourselves to a subspace of paths parametrized by a real parameter z and not an integral over all function space. The integral will be of the form,

$$J = \int dz (2\pi)^{-1/2} e^{-S(z)}, \tag{2.182}$$

where $S(z)$ is the action along the path. These paths are shown in Fig.2.16. The $z = 0$ path is the constant path $\bar{x} = 0$ (the τ axis), that stays at the false vacuum and therefore has zero action. The $z = 1$ path is the bounce (the bold line), as we can see it has a maximum, and this is where the turning point σ is. We know that these two solutions are action's extreme points, and for the trivial solution, the action goes to zero, so as z gets bigger, the action gets bigger monotonically and this is the reason the bounce is a maximum. Furthermore, the paths were chosen in a way that the tangent vector to the $z = 1$ path is the negative mode x_0 and therefore we are sampling the divergent region of the path integral. The bounce is a maximum of $S(z)$ as is shown in Fig.2.17.a. The action goes to minus infinity as z goes to infinity, because for $z > 1$, the functions spend more time in the region beyond σ, where the potential is negative (check again Fig.2.10).

To correctly make use of the method of steepest descent, one needs to complexify the paths $x(\tau)$ and then perform the path integral on a deformed middle-dimensional contour. Such a procedure can be very generically carried out with the help of Picard-Lefschetz theory [168][169],

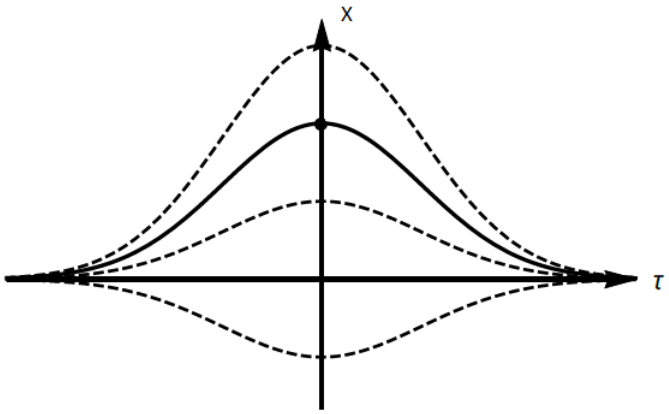

Figure 2.16: A class of paths parametrized by a real variable z. The bold line is for $z = 1$, the bounce (taken from [167]).

but this is a subject beyond the interests of this thesis.

We are following the Coleman-Callan analysis, so it is sufficient to take only care of the particular negative mode whose eigenvalue is x_0. Now, if $x = 0$, was the absolute minimum of V, such as in the Fig.2.10.a, we would have for the same path a different situation, depicted in Fig.2.17.b. The reason behind this is that in this situation the potential is non-negative so the functions will not spend time in regions where the action as a function of the potential will take more and more negative values, here instead the action goes to plus-infinity. In this case, we would have no divergence in the integral of Eq.(2.182). Let us suppose that somehow the potential is analytically changed in a way such that it goes from the situation of Fig.2.17.b back to 2.17.a. To keep the integral convergent, we must distort the right-hand portion of the contour of integration into the complex plane. How we distort it depends on the details of the analytic passage from one potential to the other.

Before we go to the distortion of the integral's contour it is a good time to remember in brief some important things. If an energy state is unstable, the energy possesses an imaginary part[153], which causes the system's exponential decay. Here, the state is rendered unstable by barrier penetration. Recall,

$$|\Psi(t)\rangle = e^{-iEt}\,|\Psi_n\rangle \tag{2.183}$$

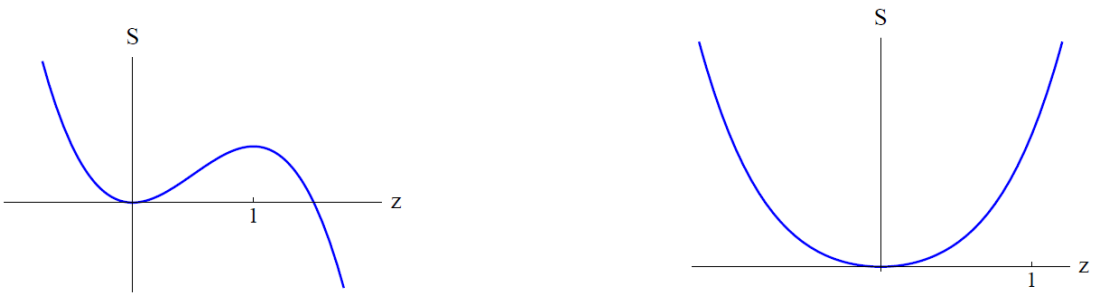

(a) (b)

Figure 2.17: a) Euclidean action as a function of the path parameter z, for the paths in Fig.2.16 and for the potential shown in Fig.2.1. b) The same procedure for the potential shown in Fig.2.10.

and the probability of finding the system at time t in the state $|\Psi_n\rangle$ is

$$P_n = |\langle\Psi_n|\Psi(t)\rangle|^2 = 1. \tag{2.184}$$

If the energy contains an imaginary part,

$$E = \mathrm{Re}(E) + i\,\mathrm{Im}(E) = E_R - iE_I \tag{2.185}$$

then the exponential term in equation (2.183) is going to be

$$e^{-Et} = e^{-i(E_R - E_I)t} = e^{-iE_Rt}e^{-E_It}. \tag{2.186}$$

We then have

$$P_n = \left|e^{-2E_It}\right|. \tag{2.187}$$

This imaginary part causes to an unstable state exponential decay. We can therefore take into account phenomenologically the instability of a state $|\Psi_n\rangle$ by adding an imaginary part to its energy. From Eq.(2.179) we conclude that K should be imaginary,

$$\mathrm{Im}\, E_0 = -|K|e^{-B}. \tag{2.188}$$

Now, let us turn our attention to the saddle point approximation. In the simplest form, the saddle point method is used to approximate integrals of the form

$$I \equiv \int_{-\infty}^{\infty} dx e^{-f(x)}. \tag{2.189}$$

The idea is that the negative exponential function is so rapidly decreasing that we only need to look at the contribution from where $f(x)$ is at its minimum. Let us say $f(x)$ is at its minimum at x_0. Then we could approximate $f(x)$ the first terms of its Taylor expansion,

$$f(x) \approx f(x_0) + \frac{1}{2}(x - x_0)^2 f''(x_0) + \cdots. \tag{2.190}$$

There is no linear term because x_0 is a minimum. Plugging this into our integral gives

$$I \approx \int_{-\infty}^{+\infty} dx\, e^{-f(x_0) - \frac{1}{2}(x-x_0)^2 f''(x_0)} = e^{-f(x_0)} \int_{-\infty}^{\infty} dx\, e^{-\frac{1}{2}(x-x_0)^2 f''(x_0)}. \tag{2.191}$$

The crucial point now is that the saddle point method works only if $f''(t_0)$ is positive. The Gaussian integral can be evaluated to give

$$I = e^{-f(x_0)}\sqrt{\frac{2\pi}{f''(x_0)}}. \tag{2.192}$$

It is time to return to our problem. To keep our J integral convergent, the right-hand portion of the contour of integration must be distorted into the complex plane. How it is distorted depends on the details of the analytic passage from one potential to the other as we have said. In their work Coleman and Callan argued that this contour extends from $-\infty$ along the positive z axis to the saddle point at $z = 1$ and distorts to the upper half plane along a line of the constant imaginary part of S. This distortion of the contour is depicted in Fig.2.18. The main contribution comes

from the region near $z = 1$, from the bounce action. The integral there acquires an imaginary part, and using the standard steepest decent procedure someone gets,

$$\begin{aligned} \mathrm{Im}\, J &= \mathrm{Im} \int_1^{1+i\infty} dz (2\pi)^{-1/2} e^{-S(z)} \\ &\approx \mathrm{Im} \int_1^{1+i\infty} dz (2\pi)^{-1/2} e^{[-S(1) - \frac{1}{2}(z-1)^2 S''(1)]} \\ &= \mathrm{Im} \int_1^{1+i\infty} dz (2\pi)^{-1/2} e^{-S(1)} e^{-\frac{1}{2}(z-1)^2 S''(1)} \\ &\overset{(2.192)}{\approx} e^{-S(1)} \frac{1}{2\sqrt{|S''(1)|}}. \end{aligned} \tag{2.193}$$

Because the integration took a path only half-way, $\mathrm{Im}\, z \in [0, \infty)$, around the saddle point, a factor of $\frac{1}{2}$ appeared here.

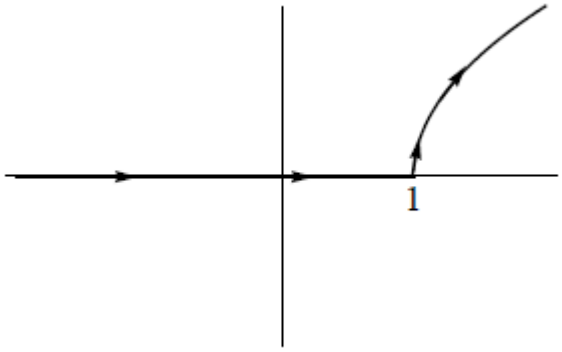

Figure 2.18: The contour of integration chosen for the path integral along z which continues from $-\infty$ on the real axis and extends to the saddle point at $z = 1$ where the bounce is located. Then it distorts to the complex upper half plane where the Euclidean action is again positive. (taken from [167])

By generalizing this analysis from the one-dimensional integral to the path integral over the whole function space, we find that the one-bounce contribution to the functional integral is given by

$$\begin{aligned} \mathrm{Im} \left(N \int [dx] e^{-S_E} \right)_{\textit{one bounce}} &= \mathrm{Im} \left(N \prod_n \int_{-\infty}^{\infty} (2\pi)^{-1/2} dc_n e^{-S_E} \right) \\ &= \frac{1}{2} N e^{-B} (B/2\pi)^{1/2} T \left| \det{}' [-\partial_\tau^2 + V''(\bar{x})] \right|^{-1/2}. \end{aligned} \tag{2.194}$$

In Eq.(2.194) $\det'$ means that in the evaluation of the determinant the zero mode must be ignored. Recall that in the zero mode situation the integral has been traded for that over the collective coordinate τ_c. Integrating Eq.(2.181) gives us a factor

$$T \left(\frac{B}{2\pi} \right)^{1/2}, \tag{2.195}$$

that it should be included instead of zero eigenvalues in the K factor. For $n = 1$ bounce at Eq.(2.177) we have

$$\begin{aligned}\langle 0|\, e^{-H\tau}\, |0\rangle &= \left(\frac{\omega}{\pi}\right)^{1/2} e^{-\omega T/2} \sum_{n=1}^{\infty} \frac{(Ke^{-B}T)^n}{n!} \\ &\overset{n=1}{=} \left(\frac{\omega}{\pi}\right)^{1/2} e^{-\omega T/2} K e^{-B} T \\ &\overset{(2.142)}{=} N\{\det\left[-\partial_\tau^2 + \omega^2\right]\}^{-1/2} K e^{-B} T.\end{aligned} \tag{2.196}$$

By comparing Eq.(2.194) to the definition of K, we get for its imaginary part

$$\operatorname{Im} K = \frac{1}{2}(B/2\pi)^{1/2} \left| \frac{\det'[-\partial_\tau^2 + V''(\bar{x})]}{\det[-\partial_\tau^2 + \omega^2]} \right|^{-1/2}. \tag{2.197}$$

Hence the decay probability per unit time, Γ, of the unstable state is going to be, with the help of Eq.(2.188),

$$\Gamma = -2\operatorname{Im}\{E_0\} = e^{-B}(B/2\pi)^{1/2} \left| \frac{\det'[-\partial_\tau^2 + V''(\bar{x})]}{\det[-\partial_\tau^2 + \omega^2]} \right|^{-1/2}. \tag{2.198}$$

2.3.6 Generalisation to field theory

The generalization to field theory is very straightforward. First, we consider the familiar theory of a single scalar field ϕ, from Section 2.2.3 in four-dimensional space-time with a Euclidean action of the form of (2.44). We need to notice that there are four zero modes, corresponding to four translations in spacetime. Besides the time-translation symmetry, we have space-translation symmetries in the field theory. In four dimensions, there are four such eigenfunctions, ϕ_μ, proportional to $\partial_\mu \bar{\phi}$. This causes four factors of $\left(\frac{B}{2\pi}\right)^{1/2}$ in the equation (2.198) of the decay rate. Integrating over the center of the bounce, we pick up a factor of VT, where V is the volume of three-space, instead of just a factor of T. The decay (nucleation) rate, in this case, is per unit volume and we get our familiar

$$\frac{\Gamma}{V} = e^{-B}(B/2\pi)^2 \left| \frac{\det'[-\partial^2 + U(\bar{\phi})]}{\det[-\partial^2 + U''(\phi_+)]} \right|^{-1/2}, \tag{2.199}$$

where, as before, $\det'$, denotes the determinant computed with the zero eigenvalues omitted. Also, $\partial^2 = \partial_\mu \partial_\mu$ is the four-dimensional Laplacian. Comparing to Eq.(2.1) we can understand which terms of Eq.(2.199) are matching to coefficient A and get

$$A = (B/2\pi)^2 \left| \frac{\det'[-\partial^2 + U(\bar{\phi})]}{\det[-\partial^2 + U''(\phi_+)]} \right|^{-1/2}. \tag{2.200}$$

As someone may observe, Eq.(2.200) is a very complicated expression.

Let us remind the reader once again that in the zero-temperature case, we moved to the Euclidean space via a Wick rotation and the equation of motion got a simpler form

$$\frac{\mathrm{d}^2\phi}{\mathrm{d}\rho^2} + \frac{3}{\rho}\frac{\mathrm{d}\phi}{\mathrm{d}\rho} = U'(\phi) \tag{2.201}$$

with the simplest $\mathcal{O}(4)$-symmetric solution $\phi(\rho^2 + \tau^2)$. We have dealt with this equation to a large extent in this chapter.

Unfortunately, the above equation can seldom be solved analytically, so both the solution and the associated value of the Euclidean action must often be computed numerically. Under this condition, determinants can only be calculated in certain special cases. It turns out, however, that in most practical problems in literature, just a rough dimensional estimation of A can be enough. Such an estimate for A can be done by observing that it has dimensionality m^4, and its value is determined by three different quantities with dimensionality m. These are $\phi(0)$, $\sqrt{U''(\phi}$ and ρ^{-1}, the radius of the bubble [170][171]. In the theories that we are interested in most, these three quantities lie within an order of magnitude of one another, so for a rough estimate one may assume that

$$\frac{\det'[-\partial^2 + U(\bar{\phi})]}{\det[-\partial^2 + U''(\phi_+)^2]} = \mathcal{O}(\rho^{-4}, \phi^4(0), (U'')^2). \tag{2.202}$$

These Linde results agree with Coleman and Callan's consistency check for the right dimensions in SI units. To summarise in SI units, both B and $\hbar$ have the dimensions of action. The differential operators have the dimensions of $1/\text{length}^2$, as do their eigenvalues. Since the four zero modes are omitted from $\det'$, the quotient $\det' / \det$ has the dimensions of $(\text{length})^8$. Thus, the total expression of Γ/V has the dimensions of $1/\text{length}^4$, which is what it is supposed to be for a decay rate per unit time per unit volume. We mention all these because in natural units

$$[\text{mass}] \approx 1/[\text{length}]. \tag{2.203}$$

Chapter 3

Gravitational effects in zero temperature false vacuum decay

In this chapter, the analysis of Section 2.2 will be extended by a theory of a scalar field interacting with gravity. The Minkowskian action of such a theory is

$$S_M = \int d^4x\sqrt{-g}\left[\frac{1}{2}g^{\mu\nu}\partial_\mu\phi\partial_\nu\phi - U(\phi) - (16\pi G)^{-1}R\right], \tag{3.1}$$

where R is the Ricci scalar, the curvature scalar. The only change made was to add the Einstein-Hilbert term [172] to the action of the free scalar theory. The $-g$ term is the determinant of the matrix form of the Minkowskian metric tensor. As in the non-gravity situation, we will try to construct a bounce obeying some appropriate boundary conditions. This time we have to be more careful because now we have to keep track of the ten components of the metric tensor, $g_{\mu\nu}$, except the scalar field.

As it has been discussed, $\mathcal{O}(4)$ symmetry bubbles have the minimum Euclidean action in the absence of gravity, but this result has not been proved in the presence of gravity case yet. Assuredly, there is no specific reason for gravitation to break the symmetries of the purely scalar problem. So, a reasonable assumption that can be made is that the inclusion of gravity in our calculations keeps the bounce invariant under four-dimensional rotations.

Along this the chapter, we will first introduce the most general rotationally invariant Euclidean metric of our problem, then we will derive the Friedman-like equations and construct the Euclidean action. Furthermore, via the thin-wall approximation again we will get a result for B. Finally, a numerical bounce solution is presented. In this extreme mathematical path we use as the main guide the famous paper of Coleman and De Luccia (CDL) [133].

In general, we can say that gravity plays an important role when the field mass is close to the Planck scale. But its effects must be considered in fields with smaller masses if the nucleation radius of the bubble D is big enough in order to be sensitive in spacetime curvature. To obtain an estimation of the order of magnitude of this radius we can consider the following. A bubble of radius D and energy density ϵ has a Schwarzschild radius $R_S = 2GE = 2G\epsilon\frac{4\pi D^3}{3}$. The radius D will be equal to R_S for:

$$D = \left(\frac{8\pi G\epsilon}{3}\right)^{-1/2}. \tag{3.2}$$

For an ϵ around $(1\,GeV)^4$, we get $D = 0.8\,km$. Therefore, the gravitational effects become important in false vacuum decay in scales neither subnuclear nor astronomical. Moreover, even if gravitation inclusion is negligible in the bubble nucleation, it becomes important in the bubble's evolution.

3.1 The metric tensor of the problem

According to conventional cosmology, let us consider a homogeneous, isotropic, and spatially flat Universe, known as the Friedmann-Robertson-Walker (FRW) Universe. This model can be described by the non-flat element [2][172][173]

$$ds^2 = -dt^2 + a^2(t)\left[\frac{dr^2}{1-kr^2} + r^2(d\theta^2 + \sin^2\theta d\phi^2)\right]. \tag{3.3}$$

In the above expression and all the way through this paragraph was used $c = \hbar = 1$ again for convenience, $a(t)$ is the scale factor that measures the universal expansion rate, it is a function of time alone and it describes how physical separations are growing with time. The parameter k, named the scalar curvature, is a dimensionless number that can take the values $+1, 0, -1$. The scalar curvature describes an open, a flat, and a closed universe respectively. The topological geometry of each case is depicted in Fig.3.1.

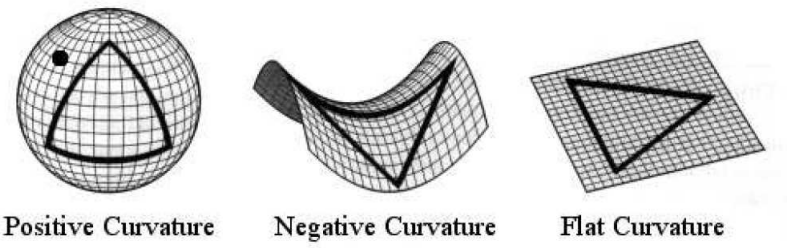

Figure 3.1: The universes described by k for $+1, -1, 0$ respectively (taken from [173]).

Taking CDL's assumption for $\mathcal{O}(4)$ symmetry into consideration, the perfect choice for the value of the scalar curvature is $k = +1$, a closed universe. Its topology becomes more conceivable if we introduce a new coordinate through the relation $r = \sin\chi$. Then,

$$dr = \cos\chi d\chi = \sqrt{1-r^2}d\chi, \tag{3.4}$$

and the three-dimensional length element can be written as

$$d\Omega_3^2 = d\chi^2 + \sin^2\chi(d\theta^2 + \sin^2\theta d\phi^2). \tag{3.5}$$

Therefore, the non-flat element now will be

$$ds^2 = -dt^2 + a^2(t)d\Omega_3^2 = -dt^2 + a^2(t)\left[d\chi^2 + \sin^2\chi(d\theta^2 + \sin^2\theta d\phi^2)\right]. \tag{3.6}$$

Turning the system to Euclidean space by a Wick rotation, we can write the most general rotationally invariant Euclidean metric as

$$ds^2 = d\eta^2 + \rho^2(\eta)\left[d\chi^2 + \sin^2\chi(d\theta^2 + \sin^2\theta d\phi^2)\right], \tag{3.7}$$

where ρ corresponds to the scale factor in this Euclidean description. Note that rotational invariance has made its usual enormous simplification; ten unknown functions of four variables have been reduced to one unknown function of one variable.

Also, for the line element, we can write the general expression

$$ds^2 = g_{\mu\nu}dx^\mu dx^\nu, \tag{3.8}$$

from Eq.(3.8) the components of the metric tensor can be produced

$$g_{11} = 1 \qquad g_{22} = \rho^2$$
$$g_{33} = \rho^2 \sin^2\chi \qquad g_{44} = \rho^2 \sin^2\chi \sin^2\theta$$

or equivalently for the inverse metric tensor

$$g^{11} = 1 \qquad g^{22} = \rho^{-2}$$
$$g^{33} = \rho^{-2} \sin^{-2}\chi \qquad g^{44} = \rho^{-2} \sin^{-2}\chi \sin^{-2}\theta.$$

As may one observes the indices in the Euclidean space are taking values from 1 to 4. The metric can be written in a matrix form such as

$$g_{\mu\nu} = \begin{pmatrix} 1 & 0 & 0 & 0 \\ 0 & \rho^2 & 0 & 0 \\ 0 & 0 & \rho^2 \sin^2\chi & 0 \\ 0 & 0 & 0 & \rho^2 \sin^2\chi \sin^2\theta \end{pmatrix} \tag{3.9}$$

3.2 Christoffel's Symbols

Afterward, we compute the Christoffel symbols for the metric described in Eq.(3.9). The definition used is [173][174]

$$\Gamma^{\rho}_{\mu\nu} = \frac{1}{2} g^{\rho\sigma}(g_{\sigma\nu,\mu} + g_{\mu\sigma,\nu} - g_{\mu\nu,\sigma}). \tag{3.10}$$

The non-zero Christoffel symbols are displayed below:

- $$\Gamma^1_{22} = \frac{1}{2} g^{1\sigma}(g_{\sigma 2,2} + g_{2\sigma,2} - g_{22,\sigma}) = \frac{1}{2} g^{11}(\cancel{g_{12,2}} + \cancel{g_{21,2}} - g_{22,1}) =$$
$$= -\frac{1}{2} \cdot 1 \cdot \partial_\eta \rho^2 = -\rho\dot{\rho}$$

- $$\Gamma^1_{33} = \frac{1}{2} g^{1\sigma}(g_{\sigma 3,3} + g_{3\sigma,3} - g_{33,\sigma}) = \frac{1}{2} g^{11}(\cancel{g_{13,3}} + \cancel{g_{31,3}} - g_{33,1}) =$$
$$= -\frac{1}{2} \cdot 1 \cdot \partial_\eta(\rho^2 \sin^2\chi) = -\rho\dot{\rho}\sin^2\chi$$

- $$\Gamma^1_{44} = \frac{1}{2} g^{1\sigma}(g_{\sigma 4,4} + g_{4\sigma,4} - g_{44,\sigma}) = \frac{1}{2} g^{11}(\cancel{g_{14,4}} + \cancel{g_{41,4}} - g_{44,1}) =$$
$$= -\frac{1}{2} \cdot 1 \cdot \partial_\eta(\rho^2 \sin^2\chi \sin^2\theta) = -\rho\dot{\rho}\sin^2\chi \sin^2\theta$$

- $$\Gamma^2_{12} = \frac{1}{2} g^{2\sigma}(g_{\sigma 2,1} + g_{1\sigma,2} - g_{12,\sigma}) = \frac{1}{2} g^{22}(g_{22,1} + \cancel{g_{12,2}} - \cancel{g_{12,2}}) =$$
$$= \frac{1}{2}\rho^{-2}\partial_\eta \rho^2 = \frac{1}{\cancel{2}}\rho^{-\cancel{2}}\cancel{2}\rho\dot{\rho} = \frac{\dot{\rho}}{\rho}$$

- $$\Gamma^3_{13} = \frac{1}{2}g^{3\sigma}(g_{\sigma 3,1} + g_{1\sigma,3} - g_{13,\sigma}) = \frac{1}{2}g^{33}(g_{33,1} + \cancel{g_{13,3}} - \cancel{g_{13,3}}) =$$
$$= \frac{1}{2}\rho^{-2}\sin^{-2}\chi\partial_\eta(\rho^2\sin^2\chi) = \frac{\dot\rho}{\rho}$$

- $$\Gamma^4_{14} = \frac{1}{2}g^{4\sigma}(g_{\sigma 4,1} + g_{1\sigma,4} - g_{14,\sigma}) = \frac{1}{2}g^{44}(g_{44,1} + \cancel{g_{14,4}} - \cancel{g_{14,4}}) =$$
$$= \frac{1}{2}\rho^{-2}\sin^{-2}\chi\sin^{-2}\theta\partial_\eta(\rho^2\sin^2\chi\sin^2\theta) = \frac{\dot\rho}{\rho}$$

- $$\Gamma^2_{33} = \frac{1}{2}g^{2\sigma}(g_{\sigma 3,3} + g_{3\sigma,3} - g_{33,\sigma}) = \frac{1}{2}g^{22}(\cancel{g_{23,3}} + \cancel{g_{32,3}} - g_{33,2}) =$$
$$= -\frac{1}{2}\rho^{-2}\partial_\chi(\rho^2\sin^2\chi) = -\sin\chi\cos\chi$$

- $$\Gamma^2_{44} = \frac{1}{2}g^{2\sigma}(g_{\sigma 4,4} + g_{4\sigma,3} - g_{44,\sigma}) = \frac{1}{2}g^{22}(\cancel{g_{24,4}} + \cancel{g_{42,4}} - g_{44,2}) =$$
$$= -\frac{1}{2}\rho^{-2}\partial_\chi(\rho^2\sin^2\chi\sin^2\theta) = -\sin\chi\cos\chi\sin^2\theta$$

- $$\Gamma^3_{44} = \frac{1}{2}g^{3\sigma}(g_{\sigma 4,4} + g_{4\sigma,3} - g_{44,\sigma}) = \frac{1}{2}g^{33}(\cancel{g_{34,4}} + \cancel{g_{43,4}} - g_{44,3}) =$$
$$= -\frac{1}{2}\rho^{-2}\sin^{-2}\chi\partial_\theta(\rho^2\sin^2\chi\sin^2\theta) = -\sin\theta\cos\theta$$

- $$\Gamma^3_{23} = \frac{1}{2}g^{3\sigma}(g_{\sigma 3,2} + g_{2\sigma,3} - g_{23,\sigma}) = \frac{1}{2}g^{33}(g_{33,2} + \cancel{g_{23,3}} - \cancel{g_{23,3}}) =$$
$$= \frac{1}{2}\rho^{-2}\sin^{-2}\chi\partial_\chi(\rho^2\sin^2\chi) = \sin^{-1}\chi\cos\chi$$

- $$\Gamma^4_{24} = \frac{1}{2}g^{4\sigma}(g_{\sigma 4,2} + g_{2\sigma,4} - g_{24,\sigma}) = \frac{1}{2}g^{44}(g_{44,2} + \cancel{g_{24,4}} - \cancel{g_{24,4}}) =$$
$$= \frac{1}{2}\rho^{-2}\sin^{-2}\chi\sin^{-2}\theta\partial_\chi(\rho^2\sin^2\chi\sin^2\theta) = \sin^{-1}\chi\cos\chi$$

- $$\Gamma^4_{34} = \frac{1}{2}g^{4\sigma}(g_{\sigma 4,3} + g_{3\sigma,4} - g_{34,\sigma}) = \frac{1}{2}g^{44}(g_{44,3} + \cancel{g_{34,4}} - \cancel{g_{34,4}}) =$$
$$= \frac{1}{2}\rho^{-2}\sin^{-2}\chi\sin^{-2}\theta\partial_\theta(\rho^2\sin^2\chi\sin^2\theta) = \sin^{-1}\theta\cos\theta$$

the non-zero Christoffel symbols are summarised in the following Table

Table 3.1: Christoffel Symbols

$\Gamma^1_{22} = -\rho\dot{\rho}$	$\Gamma^2_{12} = \frac{\dot{\rho}}{\rho}$	$\Gamma^3_{13} = \frac{\dot{\rho}}{\rho}$	$\Gamma^4_{14} = \frac{\dot{\rho}}{\rho}$
$\Gamma^1_{33} = -\rho\dot{\rho}\sin^2\chi$	$\Gamma^2_{33} = -\sin\chi\cos\chi$	$\Gamma^3_{23} = \sin^{-1}\chi\cos\chi$	$\Gamma^4_{24} = \sin^{-1}\chi\cos\chi$
$\Gamma^1_{44} = -\rho\dot{\rho}\sin^2\chi\sin^2\theta$	$\Gamma^2_{44} = -\sin\chi\cos\chi\sin^2\theta$	$\Gamma^3_{44} = -\sin\theta\cos\theta$	$\Gamma^4_{34} = \sin^{-1}\theta\cos\theta$

3.3 Ricci Scalar

In the action of Eq.(3.1) the Ricci scalar appears, therefore it must be calculated. In order to do it, we will use the non-zero Christoffel's symbols along with the definition [173][174]

$$R_{\mu\nu} = R^{\rho}_{\mu\rho\nu} = \Gamma^{\rho}_{\mu\nu,\rho} - \Gamma^{\rho}_{\mu\rho,\nu} + \Gamma^{\rho}_{\sigma\rho}\Gamma^{\sigma}_{\mu\nu} - \Gamma^{\rho}_{\sigma\nu}\Gamma^{\sigma}_{\mu\rho}. \tag{3.11}$$

The Ricci scalar is written

$$R = g^{\mu\nu}R_{\mu\nu} = g^{11}R_{11} + g^{22}R_{22} + g^{33}R_{33} + g^{44}R_{44}. \tag{3.12}$$

Hence, we must obtain all the components of the Ricci tensor via (3.11) and plug them in (3.12). We may have for them:

- $$\begin{aligned} R_{11} &= \cancel{\Gamma^{\rho}_{11,\rho}} - \Gamma^{\rho}_{1\rho,1} + \Gamma^{\rho}_{\sigma\rho}\Gamma^{\sigma}_{11} - \Gamma^{\rho}_{\sigma 1}\Gamma^{\sigma}_{1\rho} \\ &= -\partial_1\Gamma^{\rho}_{1\rho} + \cancel{\Gamma^{\rho}_{\sigma\rho}} - \Gamma^{\rho}_{\sigma 1}\Gamma^{\sigma}_{1\rho} \\ &= -\partial_1\Gamma^2_{12} - \partial_1\Gamma^3_{13} - \partial_1\Gamma^4_{14} - \Gamma^2_{21}\Gamma^2_{12} - \Gamma^3_{31}\Gamma^3_{13} - \Gamma^4_{41}\Gamma^4_{14} \\ &= -3\left(\frac{\ddot{\rho}}{\rho} - \frac{\dot{\rho}^2}{\rho^2}\right) - 3\frac{\dot{\rho}^2}{\rho^2} = -3\frac{\ddot{\rho}}{\rho} \Rightarrow R_{11} = -3\frac{\ddot{\rho}}{\rho} \end{aligned}$$

- $$\begin{aligned} R_{22} &= \Gamma^{\rho}_{22,\rho} - \Gamma^{\rho}_{2\rho,2} + \Gamma^{\rho}_{\sigma\rho}\Gamma^{\sigma}_{22} - \Gamma^{\rho}_{\sigma 2}\Gamma^{\sigma}_{2\rho} \\ &= \partial_1\Gamma^1_{22} - \partial_2\Gamma^{\rho}_{2\rho} + \Gamma^{\rho}_{\sigma\rho}\Gamma^{\sigma}_{22} - \Gamma^{\rho}_{\sigma 2}\Gamma^{\sigma}_{2\rho} \\ &= \partial_1(-\rho\dot{\rho}) - \partial_2\Gamma^3_{23} - \partial_2\Gamma^4_{24} + 3\frac{\dot{\rho}}{\rho}(-\rho\dot{\rho}) - \Gamma^2_{12}\Gamma^1_{22} - \Gamma^3_{23}\Gamma^3_{32} - \Gamma^2_{12}\Gamma^1_{22} - \Gamma^4_{42}\Gamma^4_{24} \\ &= -\dot{\rho}^2 - \rho\ddot{\rho} + \cancel{2\sin^{-2}\chi\cos^2\chi} + 2 - 3\dot{\rho}^2 + 2\dot{\rho}^2\cancel{-2\sin^{-2}\chi\cos^2\chi} \\ &= -2\dot{\rho}^2 - \rho\ddot{\rho} + 2 \Rightarrow R_{22} = -2\dot{\rho}^2 - \rho\ddot{\rho} + 2 \end{aligned}$$

- $$\begin{aligned} R_{33} &= \Gamma^{\rho}_{33,\rho} - \Gamma^{\rho}_{3\rho,3} + \Gamma^{\rho}_{\sigma\rho}\Gamma^{\sigma}_{33} - \Gamma^{\rho}_{\sigma 3}\Gamma^{\sigma}_{3\rho} \\ &= \partial_1\Gamma^1_{33} + \partial_2\Gamma^2_{33} - \partial_3\Gamma^4_{34} + \Gamma^{\rho}_{1\rho}\Gamma^1_{33} + \Gamma^{\rho}_{2\rho}\Gamma^2_{33} - \\ &- \Gamma^3_{13}\Gamma^1_{33} - \Gamma^3_{23}\Gamma^2_{33} - \Gamma^1_{33}\Gamma^3_{31} - \Gamma^2_{33}\Gamma^3_{32} - \Gamma^4_{43}\Gamma^4_{34} \\ &= \partial_1\Gamma^1_{33} + \partial_2\Gamma^2_{33} - \partial_3\Gamma^4_{34} + \Gamma^2_{12}\Gamma^1_{33} + \cancel{\Gamma^3_{13}\Gamma^1_{33}} + \Gamma^4_{14}\Gamma^1_{33} + \\ &+ \cancel{\Gamma^3_{23}\Gamma^2_{33}} - \cancel{\Gamma^3_{13}\Gamma^1_{33}} - \cancel{\Gamma^3_{23}\Gamma^2_{33}} - \Gamma^1_{33}\Gamma^3_{13} - \Gamma^2_{33}\Gamma^3_{32} - \Gamma^4_{43}\Gamma^4_{34} + \Gamma^4_{24}\Gamma^2_{33} \\ &= -\dot{\rho}^2\sin^2\chi - \rho\ddot{\rho}\sin^2\chi - \cancel{\cos^2\chi} + \sin^2\chi + \cancel{\sin^{-2}\theta\cos^2\theta} + 1 - \\ &\cancel{-\dot{\rho}^2\sin^2\chi} + \cancel{\dot{\rho}^2\sin^2\chi} + \cancel{\cos^2\chi} - \cancel{\sin^{-2}\theta\cos^2\theta} - \cos^2\chi - \dot{\rho}^2\sin^2\chi \Rightarrow \\ &\Rightarrow R_{33} = \sin^2\chi(-2\dot{\rho}^2 - \rho\ddot{\rho} + 2) \end{aligned}$$

•

$$
\begin{aligned}
R_{44} &= \Gamma^{\rho}_{44,\rho} - \cancel{\Gamma^{\rho}_{4\rho,4}} + \Gamma^{\rho}_{\sigma\rho}\Gamma^{\sigma}_{44} - \Gamma^{\rho}_{\sigma 4}\Gamma^{\sigma}_{4\rho} \\
&= \partial_1\Gamma^1_{44} + \partial_2\Gamma^2_{44} + \partial_3\Gamma^3_{44} + \Gamma^2_{12}\Gamma^1_{44} + \Gamma^3_{13}\Gamma^1_{44} + \cancel{\Gamma^4_{14}\Gamma^1_{44}} + \\
&+ \Gamma^3_{23}\Gamma^2_{44} + \cancel{\Gamma^4_{24}\Gamma^2_{44}} + \cancel{\Gamma^4_{34}\Gamma^3_{44}} - \cancel{\Gamma^4_{14}\Gamma^1_{44}} - \cancel{\Gamma^4_{24}\Gamma^2_{44}} - \cancel{\Gamma^4_{34}\Gamma^3_{44}} - \\
&- \Gamma^1_{44}\Gamma^4_{41} - \Gamma^2_{44}\Gamma^4_{42} - \Gamma^3_{44}\Gamma^4_{43} \\
&= \cancel{\dot\rho^2\sin^2\chi\sin^2\theta} - \rho\ddot\rho\sin^2\chi\sin^2\theta - \cos^2\chi\sin^2\theta + \sin^2\chi\sin^2\theta - \\
&- \cancel{\cos^2\theta} + \sin^2\theta - 2\dot\rho^2\sin^2\chi\sin^2\theta - \cancel{\cos^2\chi\sin^2\theta} + \\
&+ \cancel{\dot\rho^2\sin^2\chi\sin^2\theta} + \cancel{\cos^2\chi\sin^2\theta} + \cancel{\cos^2\theta} \Rightarrow \\
&\Rightarrow R_{44} = \sin^2\theta(-2\ddot\rho^2\sin^2\chi - \rho\ddot\rho\sin^2\chi + 2\sin^2\chi)
\end{aligned}
$$

Then Eq.(3.12) is going to be

$$
\begin{aligned}
R =& g^{\mu\nu}R_{\mu\nu} = g^{11}R_{11} + g^{22}R_{22} + g^{33}R_{33} + g^{44}R_{44} = \\
&= -3\frac{\ddot\rho}{\rho} + \rho^{-2}(-2\dot\rho^2 - \rho\ddot\rho + 2) + \rho^{-2}\sin^{-2}\chi\sin^2\chi(-2\dot\rho^2 - \rho\ddot\rho + 2) + \\
&+ \rho^{-2}\sin^{-2}\chi\sin^{-2}\theta\sin^2\theta(2\dot\rho^2\sin^2\chi - \rho\ddot\rho\sin^2\chi + 2\sin^2\chi) = \\
&= -3\frac{\ddot\rho}{\rho} + 3\left(-2\frac{\dot\rho^2}{\rho} - \frac{\ddot\rho}{\rho} + \frac{2}{\rho^2}\right) = -6\left(\frac{\ddot\rho}{\rho} - \frac{\dot\rho^2}{\rho^2} + \frac{1}{\rho^2}\right) \Rightarrow \\
&\Rightarrow R = \frac{-6(\ddot\rho\rho + \dot\rho^2 - 1)}{\rho^2},
\end{aligned}
\tag{3.13}
$$

where the dot denotes $\frac{\mathrm{d}}{\mathrm{d}\eta}$.

3.4 The Euclidean field equations

In order to derive the equations of motion we will vary the action. Firstly, we will vary the Euclidean action with respect to the ϕ field, in order to derive the Klein-Gordon equation in our case. Once again the action principle tells us that the variation of this action is zero.

$$
\begin{aligned}
&\delta S_E = 0 \Rightarrow \delta\int d^4x\sqrt{g_E}\left[\frac{1}{2}g^{\mu\nu}\nabla_\mu\phi\nabla_\nu\phi + U(\phi) - (16\pi G)^{-1}R\right] = 0 \\
&\Rightarrow \int d^4x\sqrt{g_E}\left[\frac{1}{2}\delta(g^{\mu\nu}\nabla_\mu\phi\nabla_\nu\phi) + \delta U(\phi) - \cancel{\delta(16\pi G)^{-1}R}\right] = 0 \\
&\Rightarrow \int d^4x\sqrt{g_E}\left[-\frac{\cancel{2}}{\cancel{2}}g^{\mu\nu}\nabla_\mu\nabla_\nu\phi\delta\phi + \delta U(\phi)\right] = 0 \\
&\Rightarrow \int d^4x\sqrt{g_E}\left[-\nabla_\mu\nabla^\mu\phi + \frac{\mathrm{d}U(\phi)}{\mathrm{d}\phi}\right]\delta\phi = 0 \Rightarrow \nabla_\mu\nabla^\mu\phi - \frac{\mathrm{d}U(\phi)}{\mathrm{d}\phi} = 0 \\
&\Rightarrow \nabla_\mu\nabla^\mu\phi = \frac{\mathrm{d}U(\phi)}{\mathrm{d}\phi}.
\end{aligned}
\tag{3.14}
$$

This is an interesting result, let us extend it a little more. We know that for a scalar field the covariant derivative is identical to the partial derivative [172]. The definition of the covariant derivative for a general four-vector field, V^μ, is the below,

$$
\nabla_\mu V^\nu = \partial_\mu V^\nu + \Gamma^\nu_{\mu\sigma}V^\sigma, \tag{3.15}
$$

for our scalar field $\phi(\eta)$ in the above we get

$$\begin{aligned}\nabla_\mu\nabla^\mu\phi &= \nabla_\mu(\partial^\mu\phi) = \partial_\mu\partial^\mu\phi + \Gamma^\mu_{\mu\sigma}\partial^\sigma\phi \\ &= \partial_\eta\partial^\eta\phi + \Gamma^\mu_{\mu\eta}\partial^\eta\phi \\ &= \ddot{\phi} + \cancel{\Gamma^\eta_{\eta\eta}\partial_\eta\phi} + \Gamma^\chi_{\chi\eta}\partial_\eta\phi + \Gamma^\theta_{\theta\eta}\partial_\eta\phi + \Gamma^\phi_{\phi\eta}\partial_\eta\phi \\ &= \ddot{\phi} + 3\frac{\dot{\rho}}{\rho}\dot{\phi} = U'(\phi).\end{aligned} \tag{3.16}$$

So, from Eq.(3.16) we take

$$\ddot{\phi} + 3\frac{\dot{\rho}}{\rho}\dot{\phi} = U'(\phi), \tag{3.17}$$

where the prime denotes differentiation with respect to the field ϕ. We will return to this important result later, in the thin-wall approximation section.

We derived our first equation relatively easily, but we did not finish our job yet. We must derive one more equation for $\dot{\rho}$. Now, the Euclidean action must be varied with respect to the inverse metric too. In order to calculate the dynamical equations we will use some identities proved in Appendix E. These are

$$\delta R = R_{\mu\nu}\delta g^{\mu\nu} + \nabla_\sigma(g^{\mu\nu}\delta\Gamma^\sigma_{\mu\nu} - g^{\mu\sigma}\delta\Gamma^\rho_{\rho\mu}) \tag{3.18}$$

and

$$\delta\sqrt{g_E} = -\frac{1}{2}\sqrt{g_E}g_{\mu\nu}\delta g^{\mu\nu}. \tag{3.19}$$

Next, from these two it can be proved that

$$\begin{aligned}\delta R &= R_{\mu\nu}\delta g^{\mu\nu} - \nabla_\sigma\nabla_\alpha\delta g^{\alpha\sigma} + g_{\alpha\beta}\nabla_\sigma\nabla^\sigma\delta g^{\sigma\beta} \\ &= R_{\mu\nu}\delta g^{\mu\nu} - \nabla_\mu\nabla_\nu\delta g^{\mu\nu} + g_{\mu\nu}\nabla_\sigma\nabla^\sigma\delta g^{\mu\nu}.\end{aligned} \tag{3.20}$$

Returning to the variation of the action, using the above identities and setting $\kappa = 8\pi G$, one can reproduce the following algebraic steps to obtain the Einstein field equation:

$$\delta S_E = 0 \Rightarrow \delta\int d^4x\sqrt{g_E}\left[-\frac{R}{2\kappa} + \frac{1}{2}g^{\mu\nu}\partial_\mu\phi\partial_\nu\phi + U(\phi)\right] = 0 \Rightarrow$$

$$\Rightarrow \int d^4x\delta\sqrt{g_E}\left[-\frac{R}{2\kappa} + \frac{1}{2}g^{\mu\nu}\partial_\mu\phi\partial_\nu\phi + U(\phi)\right] + \int d^4x\sqrt{g_E}\left[-\frac{1}{2\kappa}\delta R + \frac{1}{2}\delta g^{\mu\nu}\partial_\mu\phi\partial_\nu\phi\right] = 0 \Rightarrow$$

$$\Rightarrow \int d^4x\sqrt{g_E}\Bigg[-\frac{1}{2}g_{\mu\nu}\left(-\frac{1}{2\kappa}R + \frac{1}{2}g^{\alpha\beta}\partial_\alpha\phi\partial_\beta\phi + U(\phi)\right) - \frac{1}{2\kappa}R_{\mu\nu} +$$

$$+\nabla_\mu\nabla_\nu\frac{1}{2\kappa} - g_{\mu\nu}\nabla_\sigma\nabla^\sigma\frac{1}{2\kappa} + \frac{1}{2}\partial_\mu\phi\partial_\nu\phi\Bigg]\delta g^{\mu\nu} = 0 \Rightarrow$$

$$\Rightarrow +\frac{1}{2}\frac{1}{2\kappa}g_{\mu\nu}R - \frac{1}{4}g_{\mu\nu}g^{\alpha\beta}\partial_\alpha\phi\partial_\beta\phi + \frac{U(\phi)}{2}g_{\mu\nu} - \frac{1}{2\kappa}R_{\mu\nu} + \nabla_\mu\nabla_\nu\frac{1}{2\kappa} + g_{\mu\nu}\nabla_\sigma\nabla^\sigma\frac{1}{2\kappa} - \frac{1}{2}\partial_\mu\phi\partial_\nu\phi = 0 \Rightarrow$$

$$\overset{\times 2\kappa}{\Rightarrow} +\frac{1}{2}g_{\mu\nu}R - \frac{\kappa}{2}g_{\mu\nu}g^{\alpha\beta}\partial_\alpha\phi\partial_\beta\phi - \kappa U(\phi)g_{\mu\nu} - R_{\mu\nu} + \kappa\nabla_\mu\nabla_\nu\frac{1}{\kappa} - g_{\mu\nu}\kappa\nabla_\sigma\nabla^\sigma\frac{1}{\kappa} + \kappa\partial_\mu\phi\partial_\nu\phi = 0 \Rightarrow$$

$$\Rightarrow R_{\mu\nu} - \frac{1}{2}g_{\mu\nu}R = -\frac{\kappa}{2}g_{\mu\nu}g^{\alpha\beta}\partial_\alpha\phi\partial_\beta\phi - \kappa U(\phi)g_{\mu\nu} + \cancel{\kappa\nabla_\mu\nabla_\nu\frac{1}{\kappa}} - \cancel{g_{\mu\nu}\kappa\nabla_\sigma\nabla^\sigma\frac{1}{\kappa}} + \kappa\partial_\mu\phi\partial_\nu\phi. \tag{3.21}$$

The left-hand side in the last line is that of the Einstein field equation which is [173][174]

$$R_{\mu\nu} - \frac{1}{2}g_{\mu\nu}R = G_{\mu\nu} \tag{3.22}$$

and

$$G_{\mu\nu} = \kappa T_{\mu\nu}, \tag{3.23}$$

is the equation which connects the Einstein tensor, $G_{\mu\nu}$, with the energy-momentum tensor, $T_{\mu\nu}$. Therefore,

$$\begin{aligned} T_{\mu\nu} &= -\frac{1}{2} g_{\mu\nu} g^{\alpha\beta} \partial_\alpha \phi \partial_\beta \phi - U(\phi) g_{\mu\nu} + \partial_\mu \phi \partial_\nu \phi \\ &= \partial_\mu \phi \partial_\nu \phi - g_{\mu\nu} \left[\frac{1}{2} g^{\alpha\beta} \partial_\alpha \phi \partial_\beta \phi + U(\phi) \right]. \end{aligned} \tag{3.24}$$

Our final step is to take the Einstein equation for the component η and use the previous results for R and the Ricci tensor

$$\begin{aligned} &R_{\eta\eta} - \frac{1}{2} g_{\eta\eta} R = \kappa T_{\eta\eta} \Rightarrow \\ &\Rightarrow -3\frac{\ddot{\rho}}{\rho} + \frac{3(\ddot{\rho}\rho + \dot{\rho}^2 - 1)}{\rho^2} = \kappa T_{\eta\eta}, \end{aligned} \tag{3.25}$$

from Eq.(3.24) $T_{\eta\eta}$ will be

$$\begin{aligned} T_{\eta\eta} &= \dot{\phi}^2 - \frac{1}{2} g^{\alpha\beta} \partial_\alpha \phi \partial_\beta \phi - U(\phi) = \dot{\phi}^2 - \frac{1}{2} g^{\alpha\alpha} (\partial_\alpha \phi)^2 - U(\phi) \\ &= \dot{\phi}^2 - \frac{1}{2} g^{\eta\eta} (\partial_\alpha \phi)^2 - U(\phi) = \frac{1}{2} \dot{\phi}^2 - U(\phi). \end{aligned} \tag{3.26}$$

Let us plug Eq.(3.26) in Eq.(3.25) and get

$$\dot{\rho}^2 = 1 + \frac{\kappa}{3} \rho^2 \left(\frac{1}{2} \dot{\phi}^2 - U \right), \tag{3.27}$$

the other Einstein equations are either identities or trivial consequences of these equations. If we differentiate one more time the equation for $\dot{\rho}$ it is easy to obtain an expression for $\ddot{\rho}$ (2nd Friedmann-like equation):

$$\ddot{\rho} = -\frac{\kappa}{3} \rho (\dot{\phi}^2 + U). \tag{3.28}$$

3.5 The Euclidean action

As we already did, to obtain Euclidean action we will add the Einstein-Hilbert term to the S_E's expression in the absence of gravity. Hence, we will get

$$S_E = \int d^4x \sqrt{g_E} \left[-\frac{R}{16\pi G} + \frac{1}{2} g^{\mu\nu} \partial_\mu \phi \partial_\nu \phi + U(\phi) \right], \tag{3.29}$$

where now g_E is the Euclidean determinant of the metric. For this term, we have that

$$g_E = \begin{vmatrix} 1 & 0 & 0 & 0 \\ 0 & \rho^2 & 0 & 0 \\ 0 & 0 & \rho^2 \sin^2 \chi & 0 \\ 0 & 0 & 0 & \rho^2 \sin^2 \chi \sin^2 \theta \end{vmatrix} = \rho^6 \sin^4 \chi \sin^2 \theta. \tag{3.30}$$

Therefore, in Eq.(3.14) the $d^4x\sqrt{g_E}$ becomes

$$\begin{aligned} d^4x\sqrt{g_E} &= d\eta d\chi d\theta d\phi \sqrt{\rho^6 \sin^4\chi \sin^2\theta} \\ &= \rho^3 \sin^2\chi \sin\theta d\eta d\chi d\theta d\phi \\ &= \rho^3 d\eta d\Omega_3, \end{aligned} \tag{3.31}$$

and

$$\rho^3 d\eta d\Omega_3 = \rho^3 d\eta \frac{2\pi^{n/2}}{\Gamma(n/2)}\Big|_{n=4} = \rho^3 d\eta 2\pi^2. \tag{3.32}$$

The $\mathcal{O}(4)$ invariance states that ϕ is a function of η only. Subsequently, the action can get a new form

$$\begin{aligned} S_E &= \int d^4x\sqrt{g_E}\left[-\frac{R}{2\kappa} + \frac{1}{2}g^{\mu\nu}\partial_\mu\phi\partial_\nu\phi + U(\phi)\right] \\ &= 2\pi^2 \int d\eta\rho^3 \left[\frac{6(\rho\ddot{\rho}+\dot{\rho}^2-1)}{2\kappa\rho^2} + \frac{1}{2}\dot{\phi}^2 + U(\phi)\right] \\ &= 2\pi^2 \int d\eta \left[\rho^3\left(\frac{1}{2}\dot{\phi}^2 + U(\phi)\right) + \frac{3}{\kappa}(\rho^2\ddot{\rho} + \rho\dot{\rho}^2 - \rho)\right], \end{aligned} \tag{3.33}$$

where in the second line of Eq.(3.33), Eq.(3.3) was used, as well the fact that $\phi \equiv \phi(\eta)$.

In the thin-wall approximation, the construction of the bounce action from Eq.(3.17) and Eq.(3.27) is astonishingly simple. The first one differs from the EoM of the free scalar case, Eq.(2.54), in only two respects. First of all, the independent variable is η rather than ρ. Of course, this is a trivial change. Secondly, the coefficient of $\dot{\phi}$ is a factor of $\dot{\rho}/\rho$ rather than a $1/\rho$. But this is also a trivial change, since in the thin-wall approximation, as it has been discussed, we neglect this term anyway. Thus, in our approximation, the only thing we have to do is to revive Eq.(2.76) again,

$$\int_{(\phi_-+\phi_+)/2}^{\phi} d\phi[2(U_0(\phi) - U_0(\phi_\pm))]^{-1/2} = \eta - \bar{\eta}, \tag{3.34}$$

here $\bar{\eta}$ is an integration constant, it is a convention with no independent meaning.

If ϕ is known, then Eq.(3.27) can be solved for ρ, which is a first-order differential equation. In order to get its solution specified, we need one integration constant. Let our choice be

$$\bar{\rho} = \rho(\bar{\eta}), \tag{3.35}$$

this is the radius of curvature of the wall separating the false from the true vacuum. The main task of our work again is to find $\bar{\rho}$, which is the same quantity from the "free scalar thin-wall approximation" process.

Before we begin our standard computational procedure, we will first eliminate the second-derivative term from the action in Eq.(3.33). Let us act with integration by parts; the surface term from the parts-integration must be somehow canceled because as we will see in an open manifold η_{max} goes to infinity so the action diverges. The surface term added in order to get rid of the parts-integration term is known as the Gibbons-Hawking surface term [175]. It can be proved that if we add or not this term it changes the bounce and the false vacuum action in a way that $B = S_E - S_E(\phi_+)$ to not diverge [176]. Here we will include the surface term in the trivial solutions of the next subsections and we will erase it with the Gibbons-Hawking term in the thin-wall approach. Hence, from the integration by parts

$$\int d\eta\rho^2\ddot{\rho} = \dot{\rho}\rho^2 - \int d\eta 2\rho\dot{\rho}^2 \tag{3.36}$$

we can get from the Euclidean action

$$\begin{aligned} S_E &= 2\pi^2 \int d\eta \left[\rho^3 \left(\frac{1}{2}\dot{\phi}^2 + U(\phi)\right) + \frac{3}{\kappa}(\rho^2\ddot{\rho} + \rho\dot{\rho}^2 - \rho)\right] \\ &= 2\pi^2 \int d\eta \left[\rho^3 \left(\frac{1}{2}\dot{\phi}^2 + U(\phi)\right) - \frac{3}{\kappa}(\rho\dot{\rho}^2 + \rho)\right] + \frac{6\pi^2}{\kappa}\rho^2\dot{\rho}\Big|_{\eta_{min}}^{\eta_{max}}, \end{aligned} \tag{3.37}$$

then we can eliminate $\dot{\rho}$, using its equation. We find

$$\begin{aligned} S_E &= 2\pi^2 \int d\eta \left[\rho^3 \left(\frac{1}{2}\dot{\phi}^2 + U(\phi)\right) - \frac{3}{\kappa}(\rho\dot{\rho}^2 + \rho)\right] + \frac{6\pi^2}{\kappa}\rho^2\dot{\rho}\Big|_{\eta_{min}}^{\eta_{max}} \\ &= 2\pi^2 \int d\eta \left[\rho^3 \left(\frac{1}{2}\dot{\phi}^2 + U\right) - \frac{3}{\kappa}\left(\rho + \frac{\rho^3}{3}\kappa(\frac{1}{2}\dot{\phi}^2 - U) + \rho\right)\right] + \frac{6\pi^2}{\kappa}\rho^2\dot{\rho}\Big|_{\eta_{min}}^{\eta_{max}} \\ &= 2\pi^2 \int d\eta \left[\rho^3 \left(\frac{1}{2}\dot{\phi}^2 + U\right) - \frac{6\rho}{\kappa} - \rho^3\left(\frac{1}{2}\dot{\phi}^2 - U\right)\right] \Rightarrow + \frac{6\pi^2}{\kappa}\rho^2\dot{\rho}\Big|_{\eta_{min}}^{\eta_{max}} \\ &\Rightarrow S_E = 4\pi^2 \int d\eta \left(\rho^3 U - \frac{3\rho}{\kappa}\right) + \frac{6\pi^2}{\kappa}\rho^2\dot{\rho}\Big|_{\eta_{min}}^{\eta_{max}}. \end{aligned} \tag{3.38}$$

An alternate form for the Euclidean action can easily be obtained if Eqs.(3.27) and (3.28) are substituted in the first line of Eq.(3.37). This procedure gives

$$S_E = -2\pi^2 \int d\eta \rho^3 U(\phi) + \text{surface terms}. \tag{3.39}$$

3.6 Trivial solutions

The most trivial solution of the Euclidean field equations is that in which the field is constant everywhere:

$$\dot{\phi} = 0, \quad \frac{\partial U}{\partial \phi} = 0, \tag{3.40}$$

that is stable particle in one of the two minima U_s, $\phi = \phi_s$. Eq.(3.27) gives:

$$\rho(\eta) = \begin{cases} D_s \sin\left(\frac{\eta}{D_s}\right), & U_s > 0 \\ D_s \sinh\left(\frac{\eta}{D_s}\right), & U_s < 0 \\ \eta, & U_s = 0, \end{cases} \tag{3.41}$$

where $D_s^2 = 3/\kappa|U_s|$. If U_s is positive, the scale ρ has a sinusoidal behavior. As a result of this ρ has two null points and the domain of η is $[0, \pi D_s]$. The manifold, in this case, has the shape of a Euclidean de Sitter (dS) space. For $U_s \leq 0$, ρ is an increasing function and there is no second null point. These cases are corresponding to open manifolds and specifically, the geometry for $U_s < 0$ is a Euclidean Anti-de Sitter (AdS) space, while for $U_s = 0$ the space is flat.

If we use the relation (3.38) we can calculate the Euclidean action in these cases. For $U_s > 0$:

$$\begin{aligned} S_{dS} &= 4\pi^2 \int_0^s d\eta \left[D_s^3 \sin^3\left(\frac{\eta}{D_s}\right) U_s - \frac{3}{\kappa}\sin\left(\frac{\eta}{D_s}\right)\right] \\ &= -\frac{24\pi^2}{\kappa U_s} = -\frac{8\pi^2}{\kappa} D_s. \end{aligned} \tag{3.42}$$

For $U_s < 0$:

$$\begin{aligned} S_{AdS} &= \pi^2 \int_0^\infty d\eta \left[D_s^3 \sinh^3\left(\frac{\eta}{D_s}\right) U_s - \frac{3}{\kappa} \sinh\left(\frac{\eta}{D_s}\right) \right] + \frac{6\pi^2}{\kappa} \rho^2 \dot{\rho} \Big|_0^\infty \\ &= \lim_{\rho_{max}\to\infty} \left\{ -\frac{12\pi^2}{\kappa^2 U_s} \left[1 - \left(1 - \frac{\kappa}{3} \rho_{max}^2 U_S \right)^{3/2} \right] \right\} + \frac{6\pi^2}{\kappa} \rho^2 \dot{\rho} \Big|_0^\infty \\ &= \lim_{\rho_{max}\to\infty} \left\{ -\frac{4\pi^2}{\kappa} D_s \left[\left(1 + \frac{\rho_{max}^2}{D_s^2})^{3/2} - 1 \right] \right\} + \frac{6\pi^2}{\kappa} \rho^2 \dot{\rho} \Big|_0^\infty \end{aligned} \tag{3.43}$$

and for $U_s = 0$:

$$S_{ME} = -4\pi^2 \int_0^\infty d\eta \frac{3\eta}{\kappa} + \frac{6\pi^2}{\kappa} \eta^2 \Big|_0^\infty \kappa = 0 \tag{3.44}$$

3.7 The thin-wall approximation

Now, in order to find analytical expressions for the decay rate let us review the thin-wall approach one more time. First, we will evaluate B, the difference in action between the bounce and the false vacuum. Then, we will find $\bar{\rho}$ by demanding that B will be stationary at it. As in the free scalar situation, we separate B into three regions.

$$B = B_{out} + B_{in} + B_{wall}. \tag{3.45}$$

In the outer area, the bounce and the false vacuum are the same thus, as before,

$$B_{out} = 0. \tag{3.46}$$

On the wall, we will replace ρ by $\bar{\rho}$ and U by U_0,

$$\begin{aligned} B_{wall} &= S(\phi) - S(\phi_+) \\ &= 4\pi^2 \int d\eta \left(\rho^3 U - \frac{3\rho}{\kappa} \right) - 4\pi^2 \int d\eta \left(\rho_+^3 - \frac{3\rho_+}{\kappa_+} \right) \\ &= 4\pi^2 \bar{\rho}^3 \int d\eta \Big(U_0(\phi) - U_0(\phi_+) \Big) \\ &= 2\pi^2 \bar{\rho}^3 \int d\eta 2 \Big(U_0(\phi) - U_0(\phi_+) \Big) \\ &= 2\pi^2 \bar{\rho}^3 S_1, \end{aligned} \tag{3.47}$$

where, S_1 has been defined at Eq.(2.84), also we applied our calculations for the potential of Eq.(2.72), we used Eq.(2.75) for B and the approximation

$$\rho \approx \bar{\rho} = \rho(\eta) \approx \rho_+(\eta). \tag{3.48}$$

At the last region, inside the wall, the field ϕ is constant. Thus, (3.27) becomes

$$\dot{\rho}^2 = 1 - \frac{1}{3}\kappa\rho^2 U \Rightarrow d\eta = d\rho (1 - \frac{1}{3}\kappa\rho^2 U)^{-1/2} \tag{3.49}$$

and

$$\begin{aligned}
B_{in} &= S(\phi_-) - S(\phi_+) \\
&= 4\pi^2 \int_0^{\bar{\rho}} d\eta \left(\rho_-^3 U_- \frac{3\rho_-}{\kappa}\right) - 4\pi^2 \int_0^{\bar{\rho}} d\eta \left(\rho_+^3 U_+ - \frac{3\rho_+}{\kappa}\right) \\
&= 4\pi^2 \int_0^{\bar{\rho}} d\rho_- \left(1 - \frac{1}{3}\kappa\rho_-^2 U_-\right)^{-1/2} \left(\rho_-^3 U_- - \frac{3\rho_-}{\kappa}\right) - 4\pi^2 \int_0^{\bar{\rho}} (- \to +) \\
&= -4\pi^2 \int_0^{\bar{\rho}} d\rho_- \left(1 - \frac{1}{3}\kappa\rho_-^2 U_-\right)^{-1/2} \frac{3\rho_-}{\kappa} \left(1 - \frac{\rho^2 U\kappa}{3}\right) - (- \to +) \\
&= -4\pi^2 \int_0^{\bar{\rho}} d\rho_- \frac{3\rho_-}{\kappa} \left(1 - \frac{1}{3}\kappa\rho_-^2 U_-\right)^{1/2} - (- \to +) \\
&= \frac{12\pi^2}{\kappa^2} \left\{ U_-^{-1} \left[\left(1 - \frac{1}{2}\kappa\bar{\rho}^2 U_-^{3/2}\right) - 1 \right] - (- \to +) \right\}.
\end{aligned} \tag{3.50}$$

The last line of the above result is true for non-zero values of $U_\pm$, either for open or closed manifold (in the open-manifold case we have to replace D^2 with $-D^2$ because $U < 0$. We have that

$$\dot{\rho} = \cos\left(\frac{\eta}{D}\right) = \left(1 - \sin^2\left(\frac{\eta}{D}\right)\right)^{1/2} = \left(1 - \frac{\rho^2}{D^2}\right)^{1/2}, \quad \text{closed manifold} \tag{3.51}$$

$$\dot{\rho} = \cosh\left(\frac{\eta}{D}\right) = \left(1 + \sinh^2\left(\frac{\eta}{D}\right)\right)^{1/2} = \left(1 + \frac{\rho^2}{D^2}\right)^{1/2}, \quad \text{open manifold} \tag{3.52}$$

In the limit $\kappa \to 0$, B_{in} goes to the free scalar theory value. The result of (3.50) is definitely an ugly and complicated expression, and in order to avoid monstrous algebraic calculations our attention will be restricted to two special cases.

The first one, the post-apocalyptic case, is a universe resulting from a decay of positive energy density into zero energy density (going from de-Sitter space to flat space, Fig.3.2). In this situation

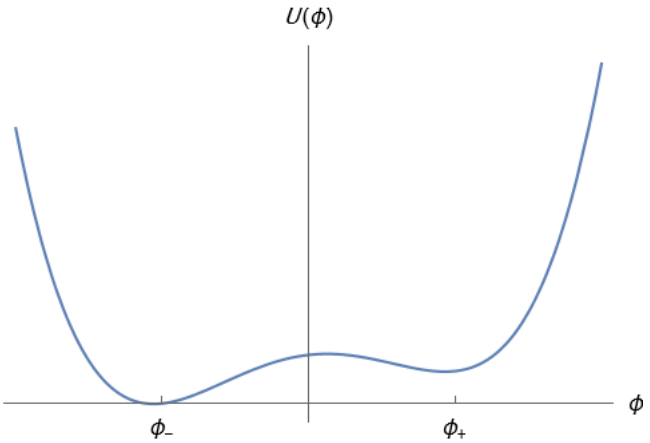

Figure 3.2: A $dS \to M$ transition (first case).

$$U(\phi_+) = \epsilon, \qquad U(\phi_-) = 0. \tag{3.53}$$

Now, we will find where B is stationary. First of all,

$$B' = B'_{wall} + B'_{in}, \tag{3.54}$$

with

$$B'_{wall} = 6\pi^2 \bar{\rho}^2 S_1 \tag{3.55}$$

and

$$\begin{aligned} B'_{in} &= \left\{ \frac{12\pi^2}{\kappa^2} \left\{ U_-^{-1} \left[\left(1 - \frac{1}{2}\kappa\bar{\rho}^2 U_-^{3/2} \right) - 1 \right] - (- \to +) \right\} \right\}' \\ &= -\frac{12\pi^2\bar{\rho}}{\kappa} \left(1 - \frac{1}{2}\kappa\bar{\rho}^2 U_-^{3/2} \right)^{1/2} - (- \to +) \\ &\overset{(3.53)}{=} -\frac{12\pi^2\bar{\rho}}{\kappa} + \frac{12\pi^2\bar{\rho}}{\kappa} \left(1 - \frac{\epsilon\kappa\bar{\rho}^2}{3} \right)^{1/2} \\ &= \frac{12\pi^2\bar{\rho}}{\kappa} \left[\left(1 - \frac{\epsilon\kappa\bar{\rho}^2}{3} \right)^{1/2} - 1 \right]. \end{aligned} \tag{3.56}$$

For the coefficient B to be stationary, it must

$$\begin{aligned} &B' = 0 \Rightarrow \cancel{6}\cancel{\pi^2}\bar{\rho}^{\cancel{2}} S_1 + \frac{\cancel{12^6}\cancel{\pi^2}\bar{\rho}}{\kappa} \left[\left(1 - \frac{\epsilon\kappa\bar{\rho}^2}{3} \right)^{1/2} - 1 \right] = 0 \Rightarrow \\ &\Rightarrow \bar{\rho} S_1 + \frac{2}{\kappa} \left[\left(1 - \frac{\epsilon\kappa\bar{\rho}^2}{3} \right)^{1/2} - 1 \right] = 0 \Rightarrow \\ &\Rightarrow \bar{\rho} \left(\kappa\frac{S_1}{4} + \frac{\epsilon}{3} \right) = S_1 \Rightarrow \bar{\rho} = \frac{12 S_1}{4\epsilon + 3\kappa S_1^2} = \frac{\bar{\rho}_0}{1 + (\bar{\rho}_0/2D)^2} = \bar{\rho}_{cr}, \end{aligned} \tag{3.57}$$

where $\bar{\rho}_0 = 3S_1/\epsilon$, is the bubble radius in the absence of gravity, a familiar result. Also, $D = (\kappa\epsilon/3)^{-1/2}$. At this critical radius, we get the interior bounce action from (3.39) which is:

$$\begin{aligned} B_{in} &= -2\pi^2 \int_0^{\bar{\rho}_{cr}} d\eta \rho^3 U \\ &= 2\pi^2\epsilon \int_0^{\bar{\rho}_{cr}} d\rho \rho^3 \left[1 - \left(\frac{\rho}{D} \right)^2 \right]^{-1/2} \\ &= 2\pi^2\epsilon \left[\frac{D}{3} \left[D^2 - \bar{\rho}_{cr}^2 \right]^{3/2} - D^3 \left[D^2 - \bar{\rho}_{cr}^2 \right]^{1/2} + \frac{2}{3} D^4 \right] \\ &= \frac{6\pi^2}{\kappa^2\epsilon} \left[\left(\frac{4\epsilon - 3S_1^2\kappa}{4\epsilon + 3S_1^2\kappa} \right)^3 - 3 \left(\frac{4\epsilon - 3S_1^2\kappa}{4\epsilon + 3S_1^2\kappa} \right) + 2 \right] \\ &= \frac{6^3}{2\epsilon} \frac{S_1^4\pi^2}{(4\epsilon + 3S_1^2\kappa)^3} (12\epsilon + 3S_1^2\kappa). \end{aligned} \tag{3.58}$$

From the same relation, the wall contribution will be

$$B_{wall} = -\pi^2 S_1 \bar{\rho}_{cr}^3 = -\frac{12^3\pi^2 S_1^4}{(4\epsilon + 3S_1^2\kappa)^3}, \tag{3.59}$$

and the total bounce action

$$\begin{aligned} B[\bar{\rho}_{crit}] &= B_{wall}[\bar{\rho}_{crit}] + B_{in}[\bar{\rho}_{crit}] \\ &= -\frac{12^3\pi^2 S_1^4}{4\epsilon + 3S_1^2\kappa}^3 + \frac{6^3}{2\epsilon}\frac{S_1^4\pi^2}{4\epsilon + 3S_1^2\kappa}^3 (12\epsilon + 3S_1^2\kappa) \\ &= \frac{3 \times 6 \times 12\pi^2 S_1^4 \cancel{(4\epsilon + 3S_1^2\kappa)}}{\epsilon(4\epsilon + 3S_1^2\kappa)^{\cancel{3^2}}} \\ &= \frac{6 \times 3 \times 9\pi^2 S_1^4}{12\epsilon[1 + (\rho_0/2D)^2)]^2} \\ &\Rightarrow B = \frac{B_0}{[1 + (\rho_0/2D)^2)]^2} \end{aligned} \tag{3.60}$$

where $B_0 = 27\pi^2 S_1^4/2\epsilon^3$, the free scalar theory result.

The second special case, the pre-apocalyptic one (a transition from flat space to Anti-de Sitter space, Fig.3.3), is caused by decay from a space of zero energy density into a space of negative energy density. In this case

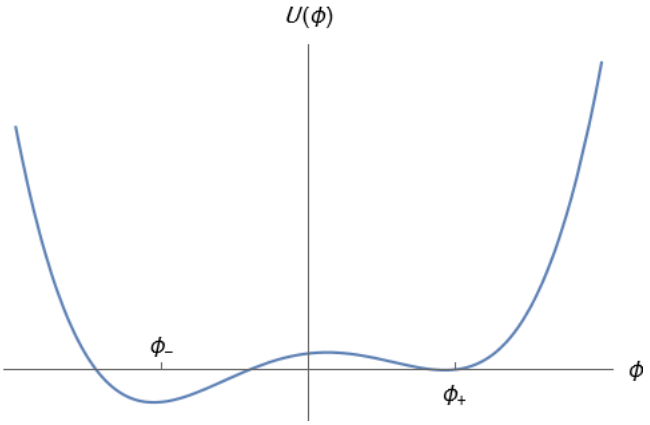

Figure 3.3: A $M \to AdS$ transition (second case).

$$U(\phi_+) = 0, \qquad U(\phi_-) = -\epsilon. \tag{3.61}$$

In a similar way, with trivial algebra, someone will get

$$\bar{\rho} = \frac{\bar{\rho}_0}{1 - (\bar{\rho}_0/2D)^2} \tag{3.62}$$

and

$$B = \frac{B_0}{[1 - (\bar{\rho}_0/2D)^2]^2}. \tag{3.63}$$

The modification of these results will also concern us in Chapter 5.

In the first case, we observe that in the presence of gravitation, the probability of bubble nucleation is getting bigger in contrast to the flat case, because now B gets bigger. In the second case, the opposite happens. More specifically, if we define the critical value κ_{cr} as

$$\kappa_{cr} = \frac{4\epsilon}{3S_1^2}, \tag{3.64}$$

the above relations become

$$\bar{\rho} = \frac{\bar{\rho}_0}{1 - \kappa/\kappa_{cr}} \tag{3.65}$$

and

$$B = \frac{\bar{\rho}_0}{(1 - \kappa/\kappa_{cr})^2}. \tag{3.66}$$

From these expressions, someone can conclude that the gravitation vanishes the false vacuum decay possibility for $\kappa \geq \kappa_{cr}$ or equivalently $\bar{\rho}_0 \geq 2D_-$, where $D_- = (\kappa U_-/3)^{-1/2}$.

The bubble wall thickness in this case will be

$$\Delta\rho = \rho(\bar{\eta} + \Delta\eta/2) - \rho(\eta - \Delta\eta/2) \approx \dot{\rho}\Delta\eta \tag{3.67}$$

where the area from $\bar{\eta} - \Delta\eta/2$ to $\bar{\eta} + \Delta\eta/2$ is the thin-wall area.

In the flat case, the TWA was valid if the radius $\bar{\rho}$ was large in comparison to the characteristic range of the field ϕ variation. In the EoM the friction term $1/\rho$ should be small at the wall to get the soliton equation. In the curved case, this term is replaced by $\dot{\rho}/\rho$, thus this time this is going to be the term that must be tiny at the wall. The equation of ρ can be written as

$$\frac{\dot{\rho}^2}{\rho^2} = \frac{1}{\rho^2} + \frac{\kappa}{3}\left(\frac{1}{2}\dot{\phi}^2 - U\right). \tag{3.68}$$

The LHS of this relation is small if the two terms of the RHS are small too. The $(1/\rho)^2$ term is the same flat case term. For the other term, we can say that the parentheses content is in good approximation constant over the bubble wall, it gets zero on the one side of it, and it has a magnitude equal to ϵ on the other side. So, it could be a good approximation if we replace this quantity by ϵ everywhere and the second term will turn into $(1/D)^2$.

Thus, the TWA can be justified if D and $\bar{\rho}$ are very larger than the characteristic range of the field variation. This is no restriction of the ratio $\bar{\rho}_0/D$, which measures how important is the gravitation in the decay rate, but in this thesis we will work on the case where this ratio is a small number and the gravitation is insignificant.

3.8 Bubble growth

As in the flat space case, in order to study the bubble growth after its materialization we have to make the analytic continuation of the scalar field from the $\mathcal{O}(4)$ invariant Euclidean manifold to the $\mathcal{O}(3,1)$ Minkowskian one. To give a more precise picture of this, the analytic continuation was just a reinterpretation of the Euclidean distance χ as spacelike separation in Minkoskian space r_M, this under the choice of the center of coordinates to be the bubble center at the materialization moment. In addition to this, in the gravitational case, the metric has to be continued to the invariant Minkowskian manifold too.

Space-like region, outside the light cone, $r_M > t$:

If we choose the coordinates (τ, r_M)[177] with:

$$\tau = f(\eta)\cos r, \qquad r_M = f(\eta)\sin r \tag{3.69}$$

where $f(\eta)$ is a function which satisfies $f' = f/\rho$ with $f(0) = 0$ and $f'(0) > 0$, then the metric (3.7) becomes conformally flat as follows

$$ds_M^2 = \frac{\rho^2}{f^2}(-d\tau^2 - dr_M^2 - r_M^2 d\Omega_2^2), \tag{3.70}$$

where, the minus sign is due to the $(+,-,-,-)$ metric signature. With analytic continuation $t=-i\tau$ the above metric becomes Lorentzian with time coordinate $t=-i\tau$

$$ds_M^2=\frac{\rho}{f^2}(dt^2-dr_M^2-r_M^2d\Omega_2^2). \tag{3.71}$$

It can be shown easily that this analytical continuation is identical to

$$t=f(\eta)\sinh\psi_+, \qquad r_M=f(\eta)cosh\psi_+ \tag{3.72}$$

where $\psi_+=-i(\pi/2-\chi)$ in the metric (3.7). These relations are for the space-like region only.

Consequently, the analytic continuation

$$\chi\to\pi/2-i\psi_+ \tag{3.73}$$

in the metric (3.7) gives the $\mathcal{O}(3,1)$ space-like metric:

$$\begin{aligned} ds_M^2&=-d\eta^2-\rho^2(\eta)(-d\psi_+^2+\cosh^2\psi_+d\Omega_2^2)\\ &=-d\eta^2-\rho^2(\eta)d\Omega_S^2. \end{aligned} \tag{3.74}$$

Here, the minus sign is due to the $(+,-,-,-)$ metric signature as before.

The surface $\tau=t=0$ that represents the bubble at its time of nucleation is corresponding to the surface $\chi=\pi/2$ at the system (η,χ) and with the surface $\psi_+=0$ at the system (χ,ψ_+). Since η does not be affected by the analytic continuation and f^{-1} exists ($f'=f/\rho>0$) from Eq.(3.72) we get

$$\eta=f^{-1}\left[(r_M^2-t^2)^{1/2}\right]. \tag{3.75}$$

Consequently, the scalar field ϕ and the scale factor ρ will satisfy the same equations as bounce did Eqs.(3.17) and (3.27) but with the dots now to denote differentiation with respect to η described by Eq.(3.75). Thereafter, in the same frame with the flat space-time, the form of ϕ and ρ in the space-like zone is identical to their Euclidean shape.

The coordinate system expands through the light cone and defines the initial conditions $\eta=0$ and $\rho=0$ for the bubble growth in the time-like region.

Time-like region, inside the light cone, $r_M<t$:

For the description inside the light-cone we chose the coordinates $(\tilde{t},\psi_-)$:

$$t=f(\tilde{t})\cosh\psi_-, \qquad r_M=f(\tilde{t})\sinh\psi_-, \tag{3.76}$$

with $\tilde{t}=-i\eta$, $\psi_-=-i\chi$ and $a(\tilde{t})=-i\rho(\eta)=-i\rho(i\tilde{t})$. This system responds only to the time-like region. The metric (3.7) now becomes $\mathcal{O}(3,1)$ and conformally flat with the form above

$$ds_M^2=\frac{a^2(\tilde{t})}{f^2}(dt^2-dr_M^2-r_M^2d\Omega_2^2). \tag{3.77}$$

Therefore, the analytical continuation

$$\begin{aligned} \eta&\to i\tilde{t}\\ r&\to i\psi_-\\ \rho(\eta)&\to ia(\tilde{t}) \end{aligned} \tag{3.78}$$

in the Euclidean metric will give the time-like metric:

$$\begin{aligned} ds_M^2 &= d\tilde{t}^2 - a^2(\tilde{t})(d\psi_-^2 + \sinh^2\psi_- d\Omega_2^2) \\ &= d\tilde{t}^2 - a^2(\tilde{t}) d\Omega_T^2, \end{aligned} \tag{3.79}$$

with the same reason for the minus sign.

Now, the interior of the bubble is an open FRW universe. The scale factor a can be described by the Friedmann equation

$$\dot{a}^2 = 1 + \frac{\kappa}{3} a^2 \left(\frac{1}{2}\dot{\phi}^2 + U \right) \tag{3.80}$$

and the field by

$$\ddot{\phi} + 3\frac{\dot{a}}{a}\dot{\phi} = -\frac{\mathrm{d}U}{\mathrm{d}\phi} \tag{3.81}$$

with initial conditions $\eta = \tilde{t} = 0$. The dots now mean differentiation with respect to $\tilde{t}$.

As in the flat case, the wall is in the space-like region and its trajectory asymptotically reaches the light cone. Contrary to Minkowski space, where every pair of cones intersect, in de Sitter space the presence of the horizon prevents the collision of two expanding bubbles nucleated far far away from each other. As a consequence, if the decay rate is very small compared to cosmic inflation, the bubbles do not merge to create a universal true vacuum region. Thus, the bubbles stay restricted alone or in bubble clusters [2].

Now, we will apply the prescription made in the previous pages for the two special cases. In the TWA, the scalar field does not require analytic continuation, because it is ϕ_+ outside the bubble and ϕ_- indide it. If we solve Eq.(3.27) we obtain the metric outside the bubble:

$$\dot{\rho}^2 = 1 - \frac{\kappa\rho^2}{3} U_+. \tag{3.82}$$

In a similar way, we get the metric inside if we solve with the replacement of ϕ_+ with ϕ_-. These metrics come together at the wall at the same scale $\rho = \bar{\rho}$.

In the first special case, the potential vanishes in the bubble interior. Thus the metric inside is $\rho = \eta$, an ordinary Minkowski space. In the region outside Eq.(3.82) gives

$$\dot{\rho}^2 = 1 - \rho^2/D^2. \tag{3.83}$$

The solution to the above is

$$\rho = D\sin(\eta/D). \tag{3.84}$$

It will be shown that we have a de Sitter space (dS) outside. First, let us define de Sitter space. Consider a 5d flat space with an invariant $\mathcal{O}(4,1)$ metric described by

$$ds^2 = -dw^2 + dt^2 - dx^2 - dy^2 - dz^2. \tag{3.85}$$

Now, in this space let us consider the hyperboloid defined by

$$D^2 = w^2 - t^2 + x^2 + y^2 + z^2, \tag{3.86}$$

where D has a positive value. So, we now have a 4d manifold and a Minkowskian metric; this is de Sitter space. A good comment to be made here is that dS space is homogeneous exactly like the flat space and we can transform from one point to another by making $\mathcal{O}(4,1)$ transformations.

In order to bring the dS metric into the standard form, we chose the bubble center location at the materialization moment to be at $(D,0,0,0,0)$. The $\mathcal{O}(3,1)$ symmetry of the decay event is

the Lorentz group taking action on the coordinates after w. We can replace them with "angular" coordinates exactly as we did before and take

$$ds^2 = -dw^2 - d\rho^2 - \rho^2 d\Omega_S^2. \tag{3.87}$$

The equation for the manifold now is

$$D^2 = w^2 + \rho^2 \tag{3.88}$$

We can define η by the following expressions

$$w = D\cos(\eta/\lambda), \qquad \rho = D\sin(\eta/D). \tag{3.89}$$

In a metric like this, the scale factor is bounded from above by the scale D and this can be obvious from (3.86). A space-like de Sitter space slice (for example the hypersurface $t = 0$) is a D radius hypersphere. On a hypersphere, no circle can have a circumference bigger than the great circle that divides the hypersphere into two equal parts. From this, we can explain a feature appearing in the $\bar{\rho}$ expression

$$\bar{\rho} = \frac{\bar{\rho}_0}{1 + (\bar{\rho}_0/2D)^2}.$$

No matter the choice of $\bar{\rho}_0$, the radius $\bar{\rho}$ is in every case equal to or smaller than D. The reason is clear; the bubble nucleating in the dS false vacuum space cannot be larger than this because it could not fit in it.

In the second case, the pre-apocalyptic one, the potential is zero outside the bubble, here the exterior is a flat space. For the interior, we have that

$$\dot{\rho}^2 = 1 + \rho^2/D^2. \tag{3.90}$$

From this we get

$$\rho = D\sinh(\eta/D). \tag{3.91}$$

Since in this situation, we are in the bubble, we will need the analytic continuation to the time-like region; from Eq.(3.78) we take

$$ds^2 = d\tilde{t}^2 - D^2\sin^2(\tilde{t}/D)d\Omega_T^2. \tag{3.92}$$

This metric describes an open and expanding universe. As far as we can see, this metric has singularities for $\tilde{t}$ be a $n\pi D$ with n integral. But these singularities are a result of coordinate artifacts not physical pathologies.

As before, we take a 5d $\mathcal{O}(3,2)$ invariant metric in a Minkowski space of the following form

$$ds^2 = dw^2 + dt^2 - dx^2 - dy^2 - dz^2, \tag{3.93}$$

and the 4d manifold with a Minkowski metric described by

$$D^2 = w^2 + t^2 - x^2 - y^2 - z^2, \tag{3.94}$$

with D to be positive again. With the same analysis done on the dS case, someone can obtain the metric defined by Eqs.(3.91) and (3.92).

As we can see the hyperboloid is singularity free, but it has some pathologies. For example, it contains circles in the (w,t) plane. The hyperboloid is homeomorphic by $\mathbb{R}_3 \times S^1$, which means that if we freely take x, y, and z then w and t must lie on a circle. The hyperboloid is not simply

connected and we must replace it with its simply connected covering space. In this covering space, there is no singularity or pathologies. This space is the familiar Anti-de Sitter space (AdS) and it is the interior universe of the bubble. From Eq.(3.80), for a $M \to AdS$ transition we can get

$$\dot{a}^2 = 1 - \frac{a^2}{D^2} \tag{3.95}$$

with solution:

$$a = \sin(\eta/D) \tag{3.96}$$

We explained that a can vanish due to coordinates anomalies. However, Eq.(3.81) shows that a real anomaly exists if $\dot{\phi} \neq 0$ when $a = 0$. The TWA corrections, although exponentially small, give ϕ a time dependence in order to $\dot{\phi} \neq 0$ when $a = 0$. Even not in the twin-wall approximation, if a starts to get smaller and become less than D, then it is going to vanish again, as we can see from the following expression

$$\dot{a}^2 \geq 1 - \frac{a^2}{D^2}. \tag{3.97}$$

Apart from very specific values of $\phi(0)$, $\dot{\phi}$ does not go to zero at the second zeroing point of a and then the bubble ends up collapsing after a finite time after its formation [133].

3.9 Energetics

In the dS $\to$ M transition, gravity's presence increases the nucleation probability as B and $\bar{\rho}$ gets smaller. In the second case (M $\to$ AdS), the opposite happens. Let us have a look at the bubble's energy in order to have a better picture of what is happening.

In the absence of gravity, as we know from the previous chapter energy obtains one negative volume term and one surface term:

$$E = -\frac{4}{3}\pi\epsilon\bar{\rho}^3 + 4\pi S_1\bar{\rho}^2 = \frac{4}{3}\pi\epsilon\bar{\rho}^2(\bar{\rho}_0 - \bar{\rho}). \tag{3.98}$$

It is obvious that for $\bar{\rho} = \bar{\rho}_0$, energy vanishes as it is supposed to happen. Also, someone can notice that if the gravitational correction is positive, the bubble radius will become bigger in order to balance this energy gain and the energy be zero again. If the correction is negative, the bubble will shrink.

There are two gravitational terms that contribute to the total energy. The first one is the usual Newtonian term which comes up from the bubble's gravitational potential and can be easily computed by Gauss's law, it is

$$E_{Newton} = -\frac{\epsilon\pi\bar{\rho}_0^5}{15D^2}. \tag{3.99}$$

this term is negative, as it should be. The second term is a consequence of geometry distortion because of the nonzero energy in the bubble's interior. From Eq.(3.49)

$$\begin{aligned} 4\pi\eta^2 &= 4\pi\rho^2 d\rho\left(1 + \frac{\kappa}{3}\rho^2\epsilon\right)^{-1/2} \\ &\approx 4\pi\rho^2 d\rho\left(1 - \frac{1}{2}\frac{8\pi G}{3}\rho^2\epsilon\right) + \mathcal{O}(G^2) \\ &= 4\pi\rho^2 d\rho\left(1 - \frac{1}{2}\frac{\rho^2}{D^2}\right) + \mathcal{O}(G^2). \end{aligned} \tag{3.100}$$

So, the additional correction due to geometry distortion is

$$E_{geom} = -\int_0^{\bar{\rho}_0} 4\pi\rho^2 d\rho \frac{1}{2}\frac{\rho^2}{D^2}(-\epsilon) = \frac{2\pi\epsilon\bar{\rho}_0^5}{5D^2}. \tag{3.101}$$

Consequently, the total correction will be

$$E_{grav} = E_{Newton} + E_{geom} = \frac{\pi\epsilon\bar{\rho}_0^5}{3D^2} \tag{3.102}$$

which is positive, hence the bubble is going to be larger when gravity is present than absent. Something that fits with the second special case [133].

3.10 A general transition

Before the last two sections of our chapter, we will give in brief the results for the general case (not post-apocalyptic nor pre-apocalyptic universe) derived by Parke [178] at 1982. For this general case, the extremum is given by

$$\bar{\rho}^2 = \frac{\bar{\rho}_0^2}{1 + 2(\bar{\rho}_0/2d)^2 + (\bar{\rho}_0/2D)^4}, \tag{3.103}$$

where now $\bar{\rho}_0 = \frac{3S_1}{U_+ - U_-}$, the coefficient λ is

$$d = [\kappa(U_+ + U_-)/3]^{-1/2} \tag{3.104}$$

and

$$D = [\kappa(U_+ - U_-)/3]^{-1/2}. \tag{3.105}$$

Parke found with a computation similar to the previous cases that the bounce action for the critical size bubble is

$$B = B_0 r[(\bar{\rho}_0/2D)^2, D^2/d^2] \tag{3.106}$$

where now the "gravity-free" coefficient is

$$B_0 = 27\pi^2 S_1^4/2(U_+ - U_-)^3 \tag{3.107}$$

and the function r is given by

$$r(x,y) = \frac{2[(1+xy) - (1+2xy+x^2)^{1/2}]}{x^2(y^2-1)(1+2xy+x^2)^{1/2}}. \tag{3.108}$$

The Coleman-De Luccia calculations are the limits D^2/d^2 go to ± 1. Let us check if this statement is true. At this limit

$$\bar{\rho}^2 = \frac{\bar{\rho}_0^2}{1 \pm 2(\bar{\rho}_0/2D)^2 + (\bar{\rho}_0/2D)^4} = \frac{\bar{\rho}_0^2}{(1 \pm (\bar{\rho}_0/2D)^2)^2} \tag{3.109}$$

and

$$\begin{aligned}\lim_{y\to\pm1} r(x,y) &= \lim_{y\to\pm1} \frac{2[(1+xy)-(1+2xy+x^2)^{1/2}]}{x^2(y^2-1)(1+2xy+x^2)^{1/2}} \\ &= \lim_{y\to\pm1} \frac{\left(2[(1+xy)-(1+2xy+x^2)^{1/2}]\right)'}{\left(x^2(y^2-1)(1+2xy+x^2)^{1/2}\right)'} \\ &= \lim_{y\to\pm1} \frac{2[x-(1+2xy+x^2)^{-1/2}x]}{2yx^2(1+2xy+x^2)^{1/2}+x^2(y^2-1)(1+2xy+x^2)^{-1/2}x} \\ &= \frac{x-x(1\pm x)^{-1}}{x^2(1\pm x)} = \frac{1}{(1\pm x)^2}\end{aligned} \tag{3.110}$$

which are obviously the CDL results.

In Fig.3.4, $r(x,y)$ (B/B_0) is plotted for several values of the quantity D^2/d^2 (y). Let us discuss some limits of interest. For $d^2>0$, first:

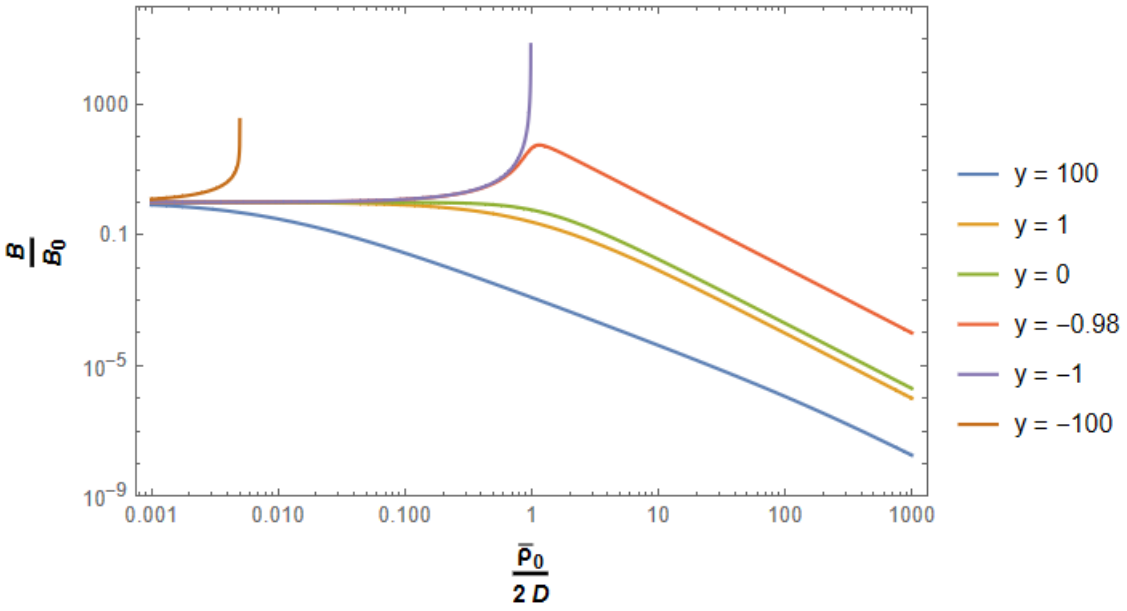

Figure 3.4: The function $B/B_0(x)=r(x)$, plotted for several values of $y=D^2/d^2$.

1. For $d^2/D^2 \ll (\bar\rho_0/2D)^2 \ll D^2/d^2$, then

$$r[(\bar\rho_0/2D)^2, D^2/d^2] = (2^{1/2}d^3/D^3)(\bar\rho_0/2D)^{-3}. \tag{3.111}$$

2. For $(\bar\rho_0/2D)^2 \gg 1$ and $(\bar\rho_0/2D)^2 \gg D^2/d^2$, we have that

$$r[(\bar\rho_0/2D)^2, D^2/d^2] = [2d^2/(d^2+D^2)](\bar\rho_0/2D)^{-4}. \tag{3.112}$$

So, for $D^2/d^2>1$, the function's falloff going from a cubic to a quartic power around

$$(\bar\rho_0/2D)\cdot d/D = 1. \tag{3.113}$$

Moreover, for $d^2 > 0$, $B \leq B_0$.

For negative d^2, if $D^2/d^2 \leq -1$, that means $U_+ \leq 0$, then the gravitational effects are lowering the nucleation rate of the bubble. Here, we have a stabilizing effect on the false vacuum which is completed when

$$(\bar{\rho}_0/2D)^2 \geq -D^2/d^2 - (D^4/d^4 - 1)^{1/2}, \tag{3.114}$$

this happens when

$$S_1\sqrt{6\pi G} \leq \sqrt{-U_-} - \sqrt{-U_+}, \tag{3.115}$$

and the stability of the false vacuum is achieved.

If, $-1 < D^2/d^2 < 0$, that is $0 < U_+ < |U_-|$, this is the region between $d^2 > 0$ in which gravitational presence stimulates the false vacuum decay and the region $d^2 \leq -D^2$, where gravity makes the false vacuum stable. In this specific region ($y = -0.98$, in the figure) as gravity becomes important, firstly the false vacuum becomes more stable, but as long as gravity becomes stronger and stronger the decay is stimulated.

For $U_+ > 0$,

$$\bar{\rho}^2 \leq 2d^2D^2/(d^2 + D^2) = [\kappa U_+/3]^{-1}. \tag{3.116}$$

This means that the critical scale of the bubble with gravitational presence is smaller or equal to the background de Sitter space regardless of the critical bubble size in the flat universe. This makes the CDL bounce solution to fit inside the Euclidean old phase de Sitter space.

3.11 Numerical computation for the Minkowski to Anti-de Sitter transition

Here, with a slightly different method which is explained in great detail in Appendix I too, we will show the results for the system of the coupled equations (3.17) and (3.27). After an appropriate rescaling, these equations become

$$\ddot{\tilde{\phi}} = -3\frac{\dot{\tilde{\rho}}}{\tilde{\rho}}\dot{\tilde{\phi}} + \frac{\mathrm{d}\tilde{U}}{\mathrm{d}\tilde{\phi}}, \tag{3.117}$$

$$\ddot{\tilde{\rho}} = -\frac{8\pi}{3}M\tilde{\rho}\left(\dot{\tilde{\phi}}^2 + \tilde{U}\right), \tag{3.118}$$

where $M = m/m_{Pl}$. The equation of $\ddot{\tilde{\rho}}$ resulted after differentiation with respect to η of $\dot{\tilde{\rho}}$ equation.

The boundary conditions for this system read

$$\lim_{x\to\infty}\tilde{\phi}(x) = \frac{\phi_+}{m}, \tag{3.119}$$

$$\left.\frac{\mathrm{d}\tilde{\phi}(x)}{\mathrm{d}x}\right|_{x=0} = 0, \tag{3.120}$$

$$\tilde{\rho}(0) = 0, \tag{3.121}$$

$$\dot{\tilde{\rho}}(0) = 1. \tag{3.122}$$

And the rescaled potential is given by

$$\tilde{U}(\tilde{\phi}) = \frac{1}{8}(\tilde{\phi}^2 - 1)^2 + \frac{\tilde{\epsilon}}{2}(\tilde{\phi} - 1). \tag{3.123}$$

Applying a shooting method to this boundary value problem (BVP), with the precious aid of *Mathematica* we achieved to get an instanton solution depicted in Fig.3.5. For more information about this problem's solution check the appendix.

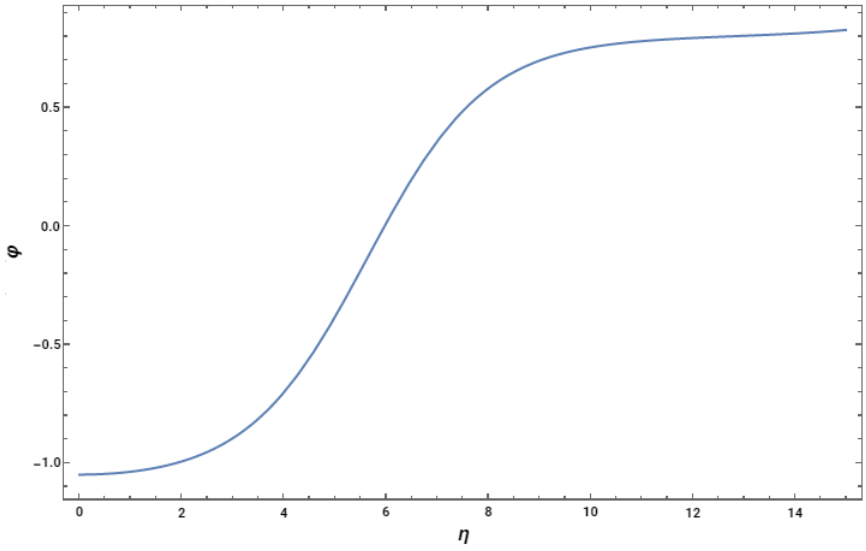

Figure 3.5: The bounce solution in the presence of gravity ($M \to AdS$ case).

3.12 The Hawking-Moss bounce

Even if the potential become flat enough so that CDL bounce does not exist, there is always another trivial solution proposed by Hawking and Moss in the early 1980s [179]. In the so-called Hawking-Moss (HM) bounce the field is stable at the top of the barrier: $\phi = \phi_{top}$, for every point of the space, and then it classically rolls down in one of the two vacua.

In a flat space, a solution of this type is not possible. The volume of the flat space is infinite, hence it is impossible for the field to fluctuate everywhere in the space in order to be placed at the top of the barrier. This would cost an infinite amount of energy. The Euclidean action of this solution is infinite and the decay rate is zero. The same is true about Anti-de Sitter space.

However, the closed de Sitter space has a horizon with radius $\rho = D$ and finite volume. As a result of this, the Hawking-Moss solution is possible only for de-Sitter background. The scale factor will be:

$$\rho = D_{top} \sin\left(\frac{\eta}{D_{top}}\right) \tag{3.124}$$

and the Euclidean action

$$S_{HM} = S_E(\phi_{top}) = -\frac{24\pi^2}{\kappa^2} U_{top} = -\frac{8\pi^2}{\kappa} D_{top}^2, \tag{3.125}$$

where D_{top}, the horizon radius of de-Sitter space with energy U_{top}. The decay rate exponential

will be

$$\begin{aligned} B_{HM} &= S_{HM} - S_E(\phi_f) \\ &= \frac{24\pi^2}{\kappa^2}\left(\frac{1}{U_f} - \frac{1}{U_{top}}\right) \\ &= \frac{8\pi^2}{\kappa}(D_f^2 - D_{top}^2). \end{aligned} \tag{3.126}$$

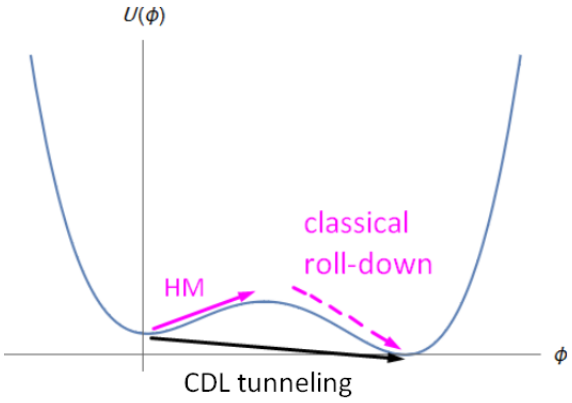

Figure 3.6: A comparison between the CDL and the HM solutions.

The HM solution gives birth to the question of how it is possible for a static solution to describe a vacuum decay process. The answer is related to the thermal nature of de-Sitter space. In the limit $(U_{top} - U_f)/U_f \ll 1$, the two extremes, have in first order a common horizon of radius D. The above equation becomes

$$B_{HM} \approx \frac{\frac{4\pi}{3}D^3}{T_{dS}}(U_{top} - U_f), \tag{3.127}$$

with $T_{dS} = 2\pi/D$, the temperature of the de Sitter horizon. The numerator expresses the energy cost that is needed for a horizon volume with ϕ_f to make a transition to ϕ_{top}. Therefore

$$B_{HM} \approx \frac{\Delta U_{hor}}{T_{dS}}, \tag{3.128}$$

where ΔU_{hor} is the energy difference between a volume of horizon with ϕ_{top} and one with ϕ_f. This relation is valid in the limit where the potential difference, as well as the difference in the geometry of the two extrema is very very small. Conclusively, there is no contribution of gravitational energy and the above result indicates the thermal nature of the HM bounce. To sum up, the explanation that can be given for the HM bounce is that a region, with a volume equal to the de Sitter horizon, due to thermal fluctuations, makes a transition from the false vacuum to the top of the barrier and from there it rolls down classically to reach the true vacuum [180] (Fig.3.6).

Chapter 4

False vacuum decay in a non-minimally coupled scalar field theory

In this brief chapter, our study will be extended to Einstein theories of gravity with non-minimally coupled scalar field [181–183]. Firstly, the new Lagrangian with the coupling term will be introduced. Next, similarly to Chapter 3, using the same assumptions about the $\mathcal{O}(4)$ symmetry we will derive the field equations from the variation of the action. Finally, the thin-wall approximation will be used to compute false vacuum decay rates and the bubbles' radii analytically in the post (M background) and pre-apocalyptic cases (dS background). Some numerical computations for theses cases will be presented too. In this journey, a very useful guide is the work of Lee and Lee [181][182].

4.1 The action of the theory

The non-minimal coupling of the scalar field to the Ricci scalar is an issue of discussion in many scenarios which concern modern cosmology in topics such as inflation and extended quintessence [184–186]. As already has been mentioned here it will be studied the process of bubble nucleation in a theory containing a coupling term between the scalar field ϕ and the Ricci curvature. The Lagrangian density for Einstein's gravity theory with a non-minimally coupled scalar field can be of the form

$$\mathcal{L} = \frac{R}{2\kappa} - \frac{1}{2}g^{\mu\nu}\partial_\mu\phi\partial_\nu\phi - \frac{1}{2}\xi R\phi^2 - U(\phi), \tag{4.1}$$

where again $\kappa = 8\pi G$, $U(\phi)$ is the scalar field potential, R denotes the familiar Ricci curvature of the spacetime, and the term $-\xi R\phi^2/2$ is the non-minimal coupling of the field to the Ricci scalar. The field obeys the Klein-Gordon equation

$$\frac{1}{\sqrt{-g}}\partial_\mu[\sqrt{-g}g^{\mu\nu}\partial_\nu\phi] - \xi R\phi - U'(\phi) = 0, \tag{4.2}$$

the above result includes a coupling term $\xi R\phi$. The prime denotes differentiation with respect to ϕ. Eq.(4.2) is easily obtained from the Euler-Lagrange equations as usual.

The Minkowskian action of the theory under study, with the help of Eq.(4.1), will be

$$S_M = \int d^4x\sqrt{-g}\left[\frac{R}{2\kappa} - \frac{1}{2}g^{\mu\nu}\partial_\mu\phi\partial_\nu\phi - \frac{1}{2}\xi R\phi^2 - U(\phi)\right]. \tag{4.3}$$

Our action looks like a general action of a modified gravity theory involving gravity non-minimally coupled with one scalar field in four dimensions [187][188],

$$S_M = \int d^4x\sqrt{-g}\left[\frac{F(\phi)}{2}R - \frac{1}{2}g^{\mu\nu}\partial_\mu\phi\partial_\nu\phi - U(\phi)\right], \tag{4.4}$$

but here we have:

$$F(\phi) = \frac{1}{\kappa} - \xi\phi^2. \tag{4.5}$$

4.2 Modification of the curved space-time results

Let us consider again the case where the potential $U(\phi)$ has the form

$$U(\phi) = \frac{\lambda}{8}(\phi^2 - \alpha^2)^2 \pm \frac{\epsilon}{2\alpha}(\phi \pm \alpha). \tag{4.6}$$

The potential has two minima, $U(\phi_-)$ corresponding to the true vacuum which is the absolute minimum of the potential and, $U(\phi_+)$, as we are used to, is the false vacuum which is a local minimum of the function. Parameter $a^2 = m^2/\lambda$, has been defined in Chapter 2 and ϵ is the difference between the minima. In our work, the non-minimal coupling parameter ξ is considered to be both positive and negative constant.

In this chapter, we consider the cases where $\frac{m^2\kappa}{8\pi}$ and $\frac{\epsilon}{m^4}$ are small quantities. With that in mind, we approximate arising quantities to the first order of these parameters.

As in the CDL case of Chapter 3, we assume that the bubbles are subject to an $\mathcal{O}(4)$ symmetry and due to this have the minimum Euclidean action, something that has not been proved in the presence of gravity, but it is a reasonable assumption as it has been discussed. We assume the $\mathcal{O}(4)$ symmetry for both the field ϕ and the spacetime metric, so as before the most general rotationally invariant Euclidean metric is

$$ds^2 = d\eta^2 + \rho^2(\eta)\left[d\chi^2 + \sin^2\chi(d\theta^2 + \sin^2\theta d\phi^2)\right]. \tag{4.7}$$

Then ϕ is a function of η only and by treating the Christoffel symbols in the same way as in the last section of the previous chapter someone has

$$R = \frac{-6(\ddot{\rho}\rho + \dot{\rho}^2 - 1)}{\rho^2}. \tag{4.8}$$

In this case, according to the above equation and Eq.(4.1) , the Euclidean Lagrangian density becomes

$$\mathcal{L}_E = \frac{1}{2}\dot{\phi}^2 + \frac{1}{2}\xi R\phi^2 + U(\phi) + \frac{3}{\kappa}\left(\frac{\ddot{\rho}}{\rho} + \frac{\dot{\rho}^2}{\rho^2} - \frac{1}{\rho^2}\right), \tag{4.9}$$

where the dots denote the differentiation with respect to η.

Now, let us find the Euclidean field equations for ϕ and ρ. Like before from the variation of the action with respect to the scalar field we can get

$$\ddot{\phi} + 3\frac{\dot{\rho}}{\rho}\dot{\phi} - \xi R\phi = U'(\phi), \tag{4.10}$$

where we can observe only a little difference with the CDL result (3.17), this is the coupling term $-\xi R\phi$.

Following, it is the turn of the variation of the action with respect to the metric. From this procedure, we can get the energy-momentum tensor

$$T_{\mu\nu} = \frac{1}{1-\xi\phi^2\kappa}\left[\partial_\mu\phi\partial_\nu\phi - g_{\mu\nu}\left(\frac{1}{2}g^{\alpha\beta}\partial_\alpha\phi\partial_\beta\phi + U(\phi)\right)\right]. \tag{4.11}$$

Here we adopt the notations and sign conventions of Misner, Thorne, and Wheeler [189] as Lee and Lee did in their work. From the $\eta\eta$ component of Eq.(4.11) we can get the equation of $\dot{\rho}$ which is

$$\begin{aligned}\dot{\rho}^2 &= 1 + \frac{\kappa\rho^2}{3(1-\xi\phi^2\kappa)}\left(\frac{1}{2}\dot{\phi}^2 - U + 6\xi\dot{\phi}\phi\frac{\dot{\rho}}{\rho}\right)\\ &= 1 + \frac{\kappa_{\text{eff}}\rho^2}{3}\left(\frac{1}{2}\dot{\phi}^2 - U + 6\xi\dot{\phi}\phi\frac{\dot{\rho}}{\rho}\right),\end{aligned} \tag{4.12}$$

with

$$\kappa_{\text{eff}}(\phi) = \frac{\kappa}{1-\xi\phi^2\kappa}, \tag{4.13}$$

our equation can be written in a more elegant and compact form. The other components of Eq.(4.11) reproduce trivial results. We are familiar with the boundary conditions for the bounce which are

$$\lim_{\eta\to\infty}\phi(\eta) = \phi_+, \qquad \left.\frac{\mathrm{d}\phi}{\mathrm{d}\eta}\right|_{\eta=0} = 0. \tag{4.14}$$

If we multiply Eq.(4.10) by $\frac{\mathrm{d}\phi}{\mathrm{d}\eta} = \dot{\phi}$ we will get

$$\begin{aligned}&\dot{\phi}\ddot{\phi} + 3\dot{\phi}\frac{\dot{\rho}}{\rho}\dot{\phi} - \dot{\phi}\xi R\phi = \dot{\phi}U'(\phi) \Rightarrow \frac{\mathrm{d}}{\mathrm{d}\eta}\left(\frac{1}{2}\dot{\phi}^2\right) + 3\frac{\dot{\rho}}{\rho}\dot{\phi}^2 - \xi R\phi\dot{\phi} = \frac{\mathrm{d}\phi}{\mathrm{d}\eta}\frac{\mathrm{d}U}{\mathrm{d}\phi} \Rightarrow\\ &\Rightarrow \frac{\mathrm{d}}{\mathrm{d}\eta}\left[\frac{1}{2}\dot{\phi}^2 - U\right] = -3\frac{\dot{\rho}}{\rho}\dot{\phi}^2 + \xi R\phi\dot{\phi}.\end{aligned} \tag{4.15}$$

Here the quantity in the square parentheses can be interpreted as the total energy of the particle with the potential energy to be $-U$. On the right-hand side, the first term can be interpreted as the dissipation rate of the total energy, and the second one is the extra source of the power.

Once again, we point out that the nucleation rate can be obtained from Eq.(2.2), and the bounce is a solution of the Euclidean field equation satisfying appropriate boundary conditions of Eq.(4.14). If we have a multi-bounce configuration the main contribution comes from the one with the minimum Euclidean action. The effects of the rest of the bounces can be absorbed in coefficient A [181].

Before we go through our familiar procedure of thin-wall approximation let us have a glare at the effects of Eq.(4.8) at the Euclidean action. First from Eq.(4.9) we get for the action

$$\begin{aligned}S_E &= \int d^4x\sqrt{g_E}\left[\frac{1}{2}\dot{\phi}^2 + \frac{1}{2}\xi R\phi^2 + U(\phi) + \frac{3}{\kappa}\left(\frac{\ddot{\rho}}{\rho} + \frac{\dot{\rho}^2}{\rho^2} - \frac{1}{\rho^2}\right)\right]\\ &= 2\pi^2\int_0^{+\infty} d\eta\left[\rho^3\left(\frac{1}{2}\dot{\phi}^2 + U\right) + \frac{3}{\kappa}(\rho\dot{\rho}^2 + \rho^2\ddot{\rho} - \rho) - 3\xi\phi^2(\rho\dot{\rho}^2 + \rho^2\ddot{\rho} - \rho)\right]\\ &= 4\pi^2\int_0^{+\infty} d\eta\left[\rho^3 U - \frac{3\rho}{\kappa} + 3\rho\xi\phi^2 + 3\xi\rho^2\dot{\rho}\phi\dot{\phi}\right].\end{aligned} \tag{4.16}$$

Here, as in the CDL situation, we eliminate the second derivative term, $\ddot{\rho}$ by integration by parts. We also use the Euclidean field equation of $\dot{\rho}$, Eq.(4.12), to lighten the action from the first derivative term. The third term in the final line will vanish because $\dot{\rho}$ in the wall is going to zero and the field is a constant both outside and inside the wall in our approximation.

It is the right moment to return to the thin-wall approximation scheme to evaluate B. Recall that B is the difference between the Euclidean action of the bounce and that of the false vacuum state

$$B = S_E(\phi) - S_E(\phi_+), \tag{4.17}$$

then we divide B in three regions. Outside the wall, we can write

$$B_{out} = S_E(\phi_+) - S_E(\phi_+) = 0. \tag{4.18}$$

On the wall, ρ can be replaced by $\bar{\rho}$. This action modifies Eq.(4.10) because $\dot{\bar{\rho}}$ goes to zero in the specific region.

$$\ddot{\phi} + 3\cancel{\frac{\dot{\bar{\rho}}}{\bar{\rho}}}\dot{\phi} - \xi R\phi = U'(\phi) \Rightarrow \frac{\mathrm{d}^2\phi}{\mathrm{d}\eta^2} \simeq \xi R\phi + U'(\phi). \tag{4.19}$$

Integrating Eq.(4.15) over η someone gets

$$\begin{aligned} &\frac{\mathrm{d}}{\mathrm{d}\eta}\left[\frac{1}{2}\dot{\phi}^2 - U\right] = -\cancel{\frac{\dot{\rho}}{\rho}}\dot{\phi}^2 + \xi R\phi\dot{\phi} \Rightarrow d\left[\frac{1}{2}\dot{\phi}^2 - U\right] = d\eta\xi R\phi\dot{\phi} \Rightarrow \\ &\Rightarrow \left(\frac{\mathrm{d}\phi}{\mathrm{d}\eta}\right)^2 = 2[U(\phi) - U(\phi_+)] + \xi R(\phi^2 - \phi_+^2). \end{aligned} \tag{4.20}$$

Remember that the curvature scalar is a function of ρ only and ϕ is a function of η due to the $\mathcal{O}(4)$ symmetry. Then, the wall term is

$$\begin{aligned} B_{wall} &= S_E(\phi) - S_E(\phi_+) \\ &= 4\pi^2 \int d\eta \left\{ \bar{\rho}^3[U(\phi) - U(\phi_+)] + 3\xi\bar{\rho}(\phi^2 - \phi_+^2) \right\} \\ &= 4\pi^2\bar{\rho}^3 \int d\eta \left\{ [U(\phi) - U(\phi_+)] + \frac{3}{\bar{\rho}^2}\xi(\phi^2 - \phi_+^2) \right\}. \end{aligned} \tag{4.21}$$

Now, from Eq.(4.20) we can write

$$d\phi = \sqrt{2[U(\phi) - U(\phi_+)] + \xi R(\phi^2 - \phi_+^2)}d\eta, \tag{4.22}$$

also, on the wall $\dot{\bar{\rho}} = 0$ and $\ddot{\bar{\rho}} = 0$. As a consequence of this Eq.(4.8) becomes

$$R = -\frac{6}{\bar{\rho}^2}. \tag{4.23}$$

Returning to the evaluation of B_{wall} and making use of the above results

$$\begin{aligned} B_{wall} &= 4\pi^2\bar{\rho}^3 \int d\eta \left\{ [U(\phi) - U(\phi_+)] + \frac{3}{\bar{\rho}^2}\xi(\phi^2 - \phi_+^2) \right\} \\ &= 2\pi^2\bar{\rho}^3 \int d\eta \left\{ 2[U(\phi) - U(\phi_+)] + \frac{6}{\bar{\rho}^2}\xi(\phi^2 - \phi_+^2) \right\} \\ &= 2\pi^2\bar{\rho}^3 \int_{\phi_-}^{\phi_+} d\phi \sqrt{2[U(\phi) - U(\phi_+)] + \frac{6}{\bar{\rho}^2}\xi(\phi^2 - \phi_+^2)} \\ &\simeq 2\pi^2\bar{\rho}^3 \left[\int_{\phi_-}^{\phi_+} d\phi \sqrt{2[U(\phi) - U(\phi_+)]} - C\xi \right] \\ &= 2\pi^2\bar{\rho}^3 S, \end{aligned} \tag{4.24}$$

where $S = S_1 - C\xi$, S_1 the surface tension has been defined in the previous chapters as

$$S_1 = \int_{\phi_-}^{\phi_+} d\phi \sqrt{2[U(\phi) - U(\phi_+)]}. \tag{4.25}$$

In the third line, the quantity in the square root approximated to the first order of the small quantities,

$$\sqrt{1 + \frac{6\xi}{\bar{\rho}^2}\frac{\phi^2 - \phi_+^2}{2[U(\phi) - U(\phi_+)]}} \approx 1 + \frac{3\xi}{\bar{\rho}^2}\frac{\phi^2 - \phi_+^2}{2[U(\phi) - U(\phi_+)]}. \tag{4.26}$$

So

$$C = \frac{3}{\bar{\rho}^2}\int_{\phi_-}^{\phi_+} \frac{\phi^2 - \phi_+^2}{2[U(\phi) - U(\phi_+)]} d\phi = \frac{12\alpha}{\sqrt{\lambda}\bar{\rho}^2}. \tag{4.27}$$

Under the condition that $U \sim U_0$. Recall that the potential is a sum of two terms $U = U_0 + O(\epsilon)$ and in the thin-wall case, this ϵ term is a small number. Also due to the symmetry we have $\phi_\pm \sim \alpha^2$. This C parameter reflects the small correction of surface energy density due to the coupling of the field with gravity.

Finally, we left with the last region of B. Inside the wall, we have $\phi = const$ and $\dot{\phi} = 0$. From Eq.(4.12) we can take

$$d\rho = d\eta \left[1 - \frac{\kappa\rho^2 U(\phi_\mp)}{3(1 - \xi\phi_\mp^2\kappa)} \right]^{1/2}, \tag{4.28}$$

and proceed to the evaluation of B_{in}:

$$\begin{aligned}
B_{in} &= S_E(\phi_-) - S_E(\phi_+) \\
&= 4\pi^2 \int_0^\infty d\eta \left[\rho^3 U(\phi_-) - \frac{3\rho}{\kappa} + 3\rho\xi\phi_-^2\right] - (\phi_- \to \phi_+) \\
&= 4\pi^2 \int_0^{\bar\rho} d\rho \left[1 - \frac{\kappa\rho^2 U(\phi_-)}{3(1-\xi\phi_-^2\kappa)}\right]^{-1/2} \left(\rho^3 U(\phi_-) - \frac{3\rho}{\kappa} + 3\rho\xi\phi_-^2\right) - (\phi_- \to \phi_+) \\
&= 4\pi^2 \int_0^{\bar\rho} d\rho \left[1 - \frac{\kappa\rho^2 U(\phi_-)}{3(1-\xi\phi_-^2\kappa)}\right]^{-1/2} \left(\frac{-3\rho}{\kappa}\right)(1-\kappa\xi\phi_-^2) \left[1 - \frac{\kappa\rho^2 U(\phi_-)}{3(1-\xi\phi_-^2\kappa)}\right] - (\phi_- \to \phi_+) \\
&= -\frac{12\pi^2}{\kappa} \int_0^{\bar\rho} d\rho \left[1 - \frac{\kappa\rho^2 U(\phi_-)}{3(1-\xi\phi_-^2\kappa)}\right]^{1/2} \rho(1-\kappa\xi\phi_-^2) - (\phi_- \to \phi_+) \\
&= \frac{12\pi^2}{\kappa^2} \left[(1-\xi\phi_-^2\kappa)^2 U^{-1}(\phi_-) \left\{ \left(1 - \frac{\kappa\bar\rho^2 U(\phi_-)}{3(1-\xi\phi_-^2\kappa)}\right)^{3/2} - 1 \right\} - (\phi_- \to \phi_+)\right].
\end{aligned} \tag{4.29}$$

The total value of B is then given by

$$B = B_{in} + B_{wall} + B_{out}. \tag{4.30}$$

We consider again the two simple cases from Chapter 3. In the first one, a scalar field originally in the false vacuum state of a positive energy density decays into the true vacuum state of zero energy density (post-apocalyptic case), and in the second the false vacuum state with zero energy density decays into the true vacuum state with negative energy density (pre-apocalyptic case). The values of the potentials in the true and the false vacuum state of these two cases are described in Eq.(3.53) and Eq.(3.61) respectively.

To find the critical bubble size, B has to be extremized with respect to $\bar\rho$,

$$\frac{\mathrm{d}B}{\mathrm{d}\bar\rho} = 12\pi^2\bar\rho \left[\left(\frac{1-\xi\phi_+^2\kappa}{\kappa}\right)\left(1 - \frac{\kappa\bar\rho^2 U(\phi_+)}{3(1-\xi\phi_+^2\kappa)}\right)^{1/2} - (\phi_+ \to \phi_-)\right] + 6\pi^2\bar\rho^2 S_1 - 2\pi^2\bar\rho^2 C\xi = 0. \tag{4.31}$$

In the post-apocalyptic case, the above equation is going to be:

$$\begin{aligned}
&6\left[\left(1 - \frac{\kappa_+\bar\rho^2\epsilon}{3}\right)^{1/2} - 1\right] + 3\bar\rho S_1\kappa_+ - C\xi\bar\rho\kappa_+ = 0 \\
&\Rightarrow [\bar\rho\kappa_+(C\xi - 3S_1) + 6]^2 = 36\left[\left(1 - \frac{\kappa_+\bar\rho^2\epsilon}{3}\right)^{1/2} - 1\right] \\
&\Rightarrow \bar\rho^{\cancel{2}}\kappa_+^{\cancel{2}}(C\xi - 3S_1)^2 + 12\cancel{\bar\rho\kappa_+}(C\xi - 3S_1) + \cancel{36} = \cancel{36} - 12\cancel{\kappa_+}\bar\rho_+^{\cancel{2}}\epsilon \\
&\Rightarrow \bar\rho = \frac{12(3S_1 - C\xi)}{12\epsilon + \kappa_+(C\xi - 3S_1)^2}
\end{aligned} \tag{4.32}$$

where $\kappa_+ = \kappa/(1-\xi\alpha^2\kappa)$. Now, a Taylor expansion will be performed with respect to ξ around zero

$$\bar\rho(\xi) \approx \bar\rho(0) + \bar\rho'(0)\xi. \tag{4.33}$$

With

$$\bar{\rho}(0) = \frac{12S_1}{4\epsilon + 3\kappa S_1^2} = \bar{\rho}_{CDL} \tag{4.34}$$

and

$$\bar{\rho}'(0) = -\frac{36\alpha^2 S_1^3 \kappa^2}{(3S_1^2\kappa + 4\epsilon)^2} + \mathcal{O}(C). \tag{4.35}$$

The first term will give us:

$$-\frac{36\alpha^2 S_1^3 \kappa^2}{(3S_1^2\kappa + 4\epsilon)^2} \approx -\alpha^2 \kappa \bar{\rho}_0 \left(\frac{\bar{\rho}_0}{2D}\right)^2 \tag{4.36}$$

and the second:

$$\mathcal{O}(C) = \frac{12S_1^2\kappa C - 16\epsilon C}{[(3S_1^2\kappa + 4\epsilon)^2]^2} \approx -\frac{3C}{\epsilon[1 + (\bar{\rho}_0/2D)^2]}. \tag{4.37}$$

Finally,

$$\bar{\rho} = \frac{\bar{\rho}_0}{[1 + (\bar{\rho}_0/2D)^2]} - \bar{\rho}_0 \xi \left[\frac{3C}{\bar{\rho}_0 \epsilon \left[1 + (\bar{\rho}_0/2D)^2\right]} + \alpha^2 \kappa \left(\frac{\bar{\rho}_0}{2D}\right)^2\right], \tag{4.38}$$

where as before $\bar{\rho}_0 = 3S_1/\epsilon$ is the bubble radius in the absence of gravity and $D = (\kappa\epsilon/3)^{-1/2}$. Here, $\frac{\phi_+^2 \kappa}{8\pi}$ and $\frac{\phi_-^2 \kappa}{8\pi}$ are approximated to $\frac{\alpha^2\kappa}{8\pi}$, which is the first order term. At this point, with the same approach

$$B(\xi) \approx B(0) + B'(0)\xi \tag{4.39}$$

after some trivial algebra, someone can find

$$B = \frac{B_0}{\left[1 + (\rho_0/2D)^2\right]^2} - 2B_0 \xi \left[\frac{6C}{\rho_0 \epsilon \left[1 + (\rho_0/2D)^2\right]^2} + \alpha^2 \kappa \left(\frac{\bar{\rho}_0}{2D}\right)^2\right], \tag{4.40}$$

where, as we know, $B_0 = 27\pi^2 S_1^4/2\epsilon^3$ is the decay coefficient in the free-of-gravity case.

In the pre-apocalyptic hypothesis, we obtain after variational computation

$$\bar{\rho} = \frac{\bar{\rho}_0}{[1 - (\bar{\rho}_0/2D)^2]} - \bar{\rho}_0 \xi \left[\frac{3C}{\bar{\rho}_0 \epsilon \left[1 - (\bar{\rho}_0/2D)^2\right]} - \alpha^2 \kappa \left(\frac{\bar{\rho}_0}{2D}\right)^2\right] \tag{4.41}$$

and

$$B = \frac{B_0}{\left[1 - (\rho_0/2D)^2\right]^2} - 2B_0 \xi \left[\frac{6C}{\rho_0 \epsilon \left[1 - (\rho_0/2D)^2\right]^2} - \alpha^2 \kappa \left(\frac{\bar{\rho}_0}{2D}\right)^2\right]. \tag{4.42}$$

In both cases, we can observe that the first term is the standard CDL result derived in the previous chapter. Also, we can see that if the non-minimal coupling constant ξ is positive then the materialization of the bubble becomes more likely because it diminishes B and makes the radius of the bubble when it materializes smaller. On the other hand, when ξ is negative we get the opposite results, the materialization becomes less likely and the radius of the bubble at the moment of materialization gets bigger.

For the final step, let us see how the coupling constant modifies the results obtained by Parke. He considered that both the false and true vacuum have arbitrary constants and his calculation is performed at the zero temperature limit. To obtain an analytic result, the potential for the scalar field is assumed to allow the use of the thin-wall approximation. The modified results are

$$\bar{\rho} = \frac{\bar{\rho}_0}{\triangle} - \rho_0 \xi \left[\frac{CD^2\kappa}{\bar{\rho}_0 \triangle} + \left(\alpha^2\kappa - \frac{2CD^2\kappa}{\bar{\rho}_0}\right)\left(\left(\frac{\bar{\rho}_0}{2d}\right)^2 + \left(\frac{\bar{\rho}_0}{2D}\right)^4\right)\right], \tag{4.43}$$

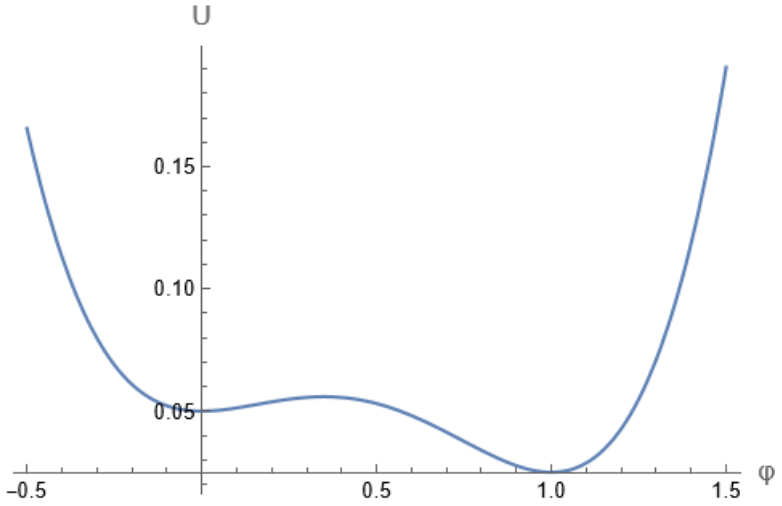

Figure 4.1: The toy model potential for a $dS \to M$ transition with $a = 1$, $b = 0.1$ and $c = 0.05$.

where now $\bar{\rho}_0 = 3S_1/(U(\phi_+) - U(\phi_-))$, the bubble size in the free scalar theory, $d = [3/\kappa(U(\phi_+) + U(\phi_-))]^{1/2}$ and $D = [3/\kappa(U(\phi_+) - U(\phi_-))]^{1/2}$. Therefore, at this point

$$B = \frac{2B_0\left[\left\{1+(\bar{\rho}_0/2d)^2\right\}-\triangle\right]}{\left[(\bar{\rho}_0/2D)^4\left\{(D/d)^2-1\right\}\triangle\right]} - 2B_0\xi\left[\frac{4CD^2\kappa\left[\left\{1+(\bar{\rho}_0/2d)^2\right\}-\triangle\right]}{\bar{\rho}_0\left[(\bar{\rho}_0/2D)^4\left\{(D/d)^2-1\right\}\triangle\right]}\right] - 2B_0\xi\frac{\left(\alpha^2\kappa-\frac{2CD^2\kappa}{\bar{\rho}_0}\right)\left((\bar{\rho}_0/2d)^2+(\bar{\rho}_0/2D)^4\right)\left[\left\{1+(\bar{\rho}_0/2d)^2\right\}-\triangle\right]}{\left[(\bar{\rho}_0/2D)^4\left\{(D/d)^2-1\right\}\right]}. \tag{4.44}$$

This is an extremely complicated and enormous expression and is stated for the sole purpose of providing supplementary information on the subject under study. Therefore, this mathematical relation will not be used throughout this thesis. In these two equations, $\triangle = \left[1 + 2\left(\frac{\bar{\rho}_0}{2d}\right)^2 + \left(\frac{\bar{\rho}_0}{2D}\right)^4\right]$ and the first term at each one is the result obtained by Parke, whose results have been discussed briefly in Section 3.10.

In a slightly different approach [183], where correction due to the coupling in the B_{wall} term defined as

$$C_1 = \frac{12\alpha}{\sqrt{\lambda}} \tag{4.45}$$

the thin-wall approximation leads to

$$B_{TW} = 2\pi^2\left[\bar{\rho}^3 S_1 + \xi\bar{\rho}C_1 - \frac{2}{3}\frac{(1-\bar{\rho}^2\kappa_+U_+)^{3/2}-1}{\kappa_+^2U_+} + \frac{2}{3}\frac{(1-\bar{\rho}^2\kappa_-U_-)^{3/2-}-1}{\kappa_-^2U_-}\right] \tag{4.46}$$

where $\kappa_\pm = \kappa/(1-\kappa\xi\phi_\pm^2)$. If we differentiate B_{TW} we will take

$$\frac{dB_{TW}}{d\bar{\rho}} = 2\pi^2\left(3\bar{\rho}^2S_1 - \frac{2\bar{\rho}\sqrt{1-\kappa_-\bar{\rho}^2U_-}}{\kappa_-} + \frac{2\bar{\rho}\sqrt{1-\kappa_+\bar{\rho}^2U_+}}{\kappa_+} + C_1\xi\right). \tag{4.47}$$

Rearranging the terms of $\frac{dB_{TW}}{d\bar{\rho}} = 0$ we can find

$$\left((\kappa_+\kappa_-)^2(9\bar{\rho}^4S_1^2 + 6\bar{\rho}^2S_1C_1\xi + C_1^2\xi^2) - 4\bar{\rho}^4(\kappa_+U_+ - \kappa_-U_-)\right)^2 = 64\bar{\rho}^4(1-\kappa_-\bar{\rho}^2U_-)(1-\kappa_+\bar{\rho}^2U_+). \tag{4.48}$$

Finally, if we Taylor expand to linear order in coupling ξ, after some algebra we will obtain a bi-quadratic equation

$$\left[\left(\frac{1}{\kappa_+^2}-\frac{1}{\kappa_-^2}\right)^2 - 3\xi S_1C_1\left(\frac{1}{\kappa_+^2}+\frac{1}{\kappa_-^2}\right)\right] + \bar{\rho}^4\left[\frac{9}{2}S_1^2\left(\frac{U_+}{\kappa_+}+\frac{U_-}{\kappa_-}\right) + \left(\frac{U_-}{\kappa_-}-\frac{U_+}{\kappa_+}\right)^2 + \frac{81S_1^4}{16}\right] +$$
$$\bar{\rho}^2\left[-2\left(\frac{U_+}{\kappa_+^3}+\frac{U_-}{\kappa_-^3}\right) - \frac{9}{2}S_1^2\left(\frac{1}{\kappa_+^2}+\frac{1}{k_-^2}\right) + \frac{2}{\kappa_+\kappa_-}\left(\frac{U_+}{\kappa_-}+\frac{U_-}{\kappa_+}\right) + 3\xi S_1C_1\left(\frac{U_+}{\kappa_+}+\frac{U_-}{\kappa_-}+\frac{9}{4}S_1^2\right)\right] = 0. \tag{4.49}$$

This equation can be solved analytically (with *Mathematica*) but it gives four long enough solutions. To keep it simple we will demonstrate the solutions for the pre-apocalyptic case scenario (dS background transition). In this case, the bi-quadratic equation will be simplified to

$$\begin{aligned}\left(\frac{1}{\kappa_+^2}-\frac{1}{\kappa_-^2}\right)^2 - 3\xi S_1C_1\left(\frac{1}{\kappa_+^2}+\frac{1}{\kappa_-^2}\right) + \bar{\rho}^4\left(\frac{9}{2}S_1^2\frac{\epsilon}{\kappa_+} + \frac{\epsilon^2}{\kappa_+^2} + \frac{81S_1^4}{16}\right) + \\ \bar{\rho}^2\left(-2\frac{\epsilon}{\kappa_+^3} - \frac{9}{2}S_1^2\left(\frac{1}{\kappa_+^2}+\frac{1}{\kappa_-^2}\right) + \frac{2\epsilon}{\kappa_+\kappa_-^2} + 3\xi S_1C_1\left(\frac{\epsilon}{\kappa_+}+\frac{9}{4}S_1^2\right)\right) = 0.\end{aligned} \tag{4.50}$$

The solutions will be the following

$$\bar{\rho}_1^2 = \frac{72S_1^2}{\kappa_\alpha^2H_1} - \frac{24\epsilon S_1C_1\xi}{\kappa_\alpha H_1} - \frac{54S_1^3C_1\xi}{H_1} - \frac{\sqrt{D_1^2+4H_1E_1^2}}{2H_1} \tag{4.51}$$

and

$$\bar{\rho}_2^2 = \frac{72S_1^2}{\kappa_\alpha^2H_1} - \frac{24\epsilon S_1C_1\xi}{\kappa_\alpha H_1} - \frac{54S_1^3C_1\xi}{H_1} + \frac{\sqrt{D_1^2+4H_1E_1^2}}{2H_1} \tag{4.52}$$

with

$$H_1 = \left(\frac{16\epsilon^2}{\kappa_\alpha^2} + \frac{72\epsilon S_1^2}{\kappa_\alpha} + 81S_1^4\right), \tag{4.53}$$

$$D_1 = \frac{384\epsilon S_1H_1C_1\xi}{\kappa_\alpha^2} \tag{4.54}$$

and

$$E_1 = -\frac{144S_1^2}{\kappa_\alpha^2} + \frac{48\epsilon S_1^3C_1\xi}{\kappa_\alpha} + 108S_1^4C_1\xi. \tag{4.55}$$

Here, in order to simplify our results the following approximation was made $\kappa_\alpha = \kappa/(1-\kappa\xi\alpha^2)$ in the first order of α.

4.3 Numerical Calculations

In this section, we are going to solve the field equations with the shooting method described in the final appendix of this thesis, similar to the curved case. We will use a slightly different but very informative toy model potential which is the following

$$U = -\frac{1}{4}a^2(3b-1)\phi^2 + \frac{1}{2}a(b-1)\phi^3 + \frac{1}{4}\phi^4 + a^4c. \tag{4.56}$$

This potential has two minima located at $\phi_f = 0$ which is the false vacuum and the true vacuum at $\phi_t = a$. We set $a = 1$, this is a dimensionful quantity, and the usual choice of unity means that the ϕ_t is at the Planck scale where $M_{Pl} = 1$, (natural units). Parameter c is corresponding to the vacuum energy. For a transition in a dS background $c > 0$ (Fig.4.1), while for a transition in a Minkowski background, we have $c = 0$ (Fig.4.2). Last but not least b, which is the controller of the vacua degeneration, is chosen to be 0.1 for the equations' solution. The system of equations

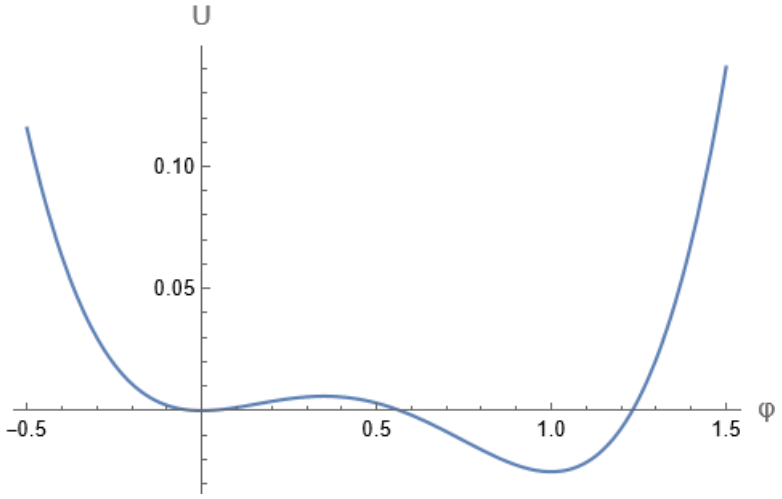

Figure 4.2: The toy model potential for a $M \to AdS$ transition with $a = 1$, $b = 0.1$ and $c = 0$.

to be solved is the EOM of the scalar field

$$\ddot{\phi} + 3\frac{\dot{\rho}}{\rho}\dot{\phi} - \xi R\phi = \frac{\partial U}{\partial \phi} \tag{4.57}$$

and the second Friedman-like equation which easily can be derived from the modified Einstein equation with energy-momentum tensor given in (4.11) is

$$\ddot{\rho} = \frac{\kappa\rho}{3(1-\kappa\xi\phi^2)}\left[-\dot{\phi}^2 - U + 3\xi\left(\dot{\phi}^2 + \ddot{\phi}\phi + \dot{\phi}\phi\frac{\dot{\rho}}{\rho}\right)\right], \tag{4.58}$$

with the usual boundary conditions of Eq.(4.14). In our definition of Ricci scalar, the denominator has a ρ^2 term, so this is a dangerous spot for divergence. For our convenience in these numerical calculations, we will express R with the help of the Friedman equations. It is trivial to show

$$R = \frac{\kappa}{(1-\kappa\xi\phi^2)}\left[\dot{\phi}^2 + 4U - 6\xi\left(\dot{\phi}^2 + \phi\ddot{\phi} + 3\dot{\phi}\phi\frac{\dot{\rho}}{\rho}\right)\right]. \tag{4.59}$$

In this form, the curvature scalar contains only the friction term $\dot{\rho}/\rho$ term which appears in the EOM too. Thus, it now must be numerically stable. In the figures below, bubble profiles and bubble radii are depicted for a $dS \to M$ transition and a $M \to AdS$ transition respectively.

For the first case, $c = 0.05$ was chosen, and the solutions are shown in Fig.4.3 and Fig.4.4. For the post-apocalyptic case, where $c = 0$ the results can be seen in Fig.4.5 and in Fig.4.6 for the bubble profiles and the bubble radius respectively.

Something we can observe directly from the scale factor behavior of a decay in a dS false vacuum space is that it obtains a second zero. This has been shown in [190]. In order to keep it simple let us visit the $\xi = 0$ case. We are in a dS background, thus $U > 0$ and by convention

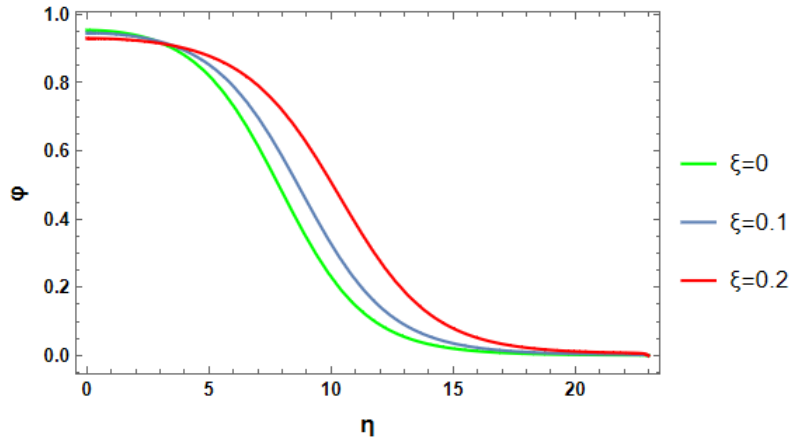

Figure 4.3: The bubble profiles for a $dS \to M$ transition for several of the coupling ξ.

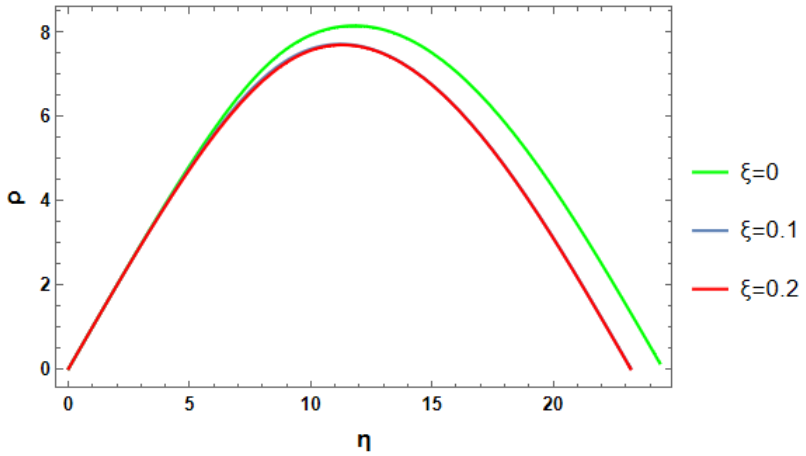

Figure 4.4: The bubble radius for a $dS \to M$ transition for several values of the coupling ξ.

$\rho \geq 0$. Then Eq.(4.58) implies that the second derivative $\ddot{\rho} \leq 0$. For $\rho \neq 0$, the only way for the second derivative to be equal to zero is to have $\phi = \phi_t$ and $\dot{\phi} = 0$. With these initial conditions of one value of η the Euclidean field equations give the unique solution

$$\phi(\eta) = \phi_t \tag{4.60}$$

and

$$\rho(\eta) = \eta + \text{constant}. \tag{4.61}$$

This solution gives one zero point to the scale factor and for all the other solutions $\ddot{\rho} < 0$. From the last sentence can be implied that ρ must obtain at least one zero. We can take one zero of the scale factor to be at the beginning $\eta = 0$ as we did in our numerical computation, thus $\dot{\rho}(0) = 1$ (due to the η translation symmetry we chose 1 without loss of generality). For the second derivative of the field at $\eta = 0$ not to be singular from the EOM someone has $\dot{\phi}(0) = 0$. We define from the equation of $\dot{\rho}$:

$$Z(\eta) = \frac{\kappa}{3}(U - \frac{1}{2}\dot{\phi}^2). \tag{4.62}$$

It is trivial to show that from the Euclidean equations of the system

$$\dot{Z} = \frac{\kappa}{3}(\dot{\rho}/\rho)\dot{\phi}^2, \tag{4.63}$$

and

$$\dot{\rho} = \pm(1 - Z\rho^2)^{1/2}. \tag{4.64}$$

To be noted that $Z_0 \equiv Z(0) \geq 0$, the zero case is the trivial solution of the true vacuum. Now, if $Z_0 > 0$, we will show that $\dot{\rho}(\eta)$ gets a zero in the region $0 < \eta \leq \pi/(2Z_0^{1/2})$. It will be proved by contradiction. If our assumption is wrong then $\dot{\rho}$ is positive in this interval and $\dot{Z} \geq 0$ in this area. We will define

$$\rho(\eta) = Z^{-1/2}(\eta)\sin\theta(\eta) \tag{4.65}$$

with $\theta(0) = 0$. From (4.64), $\dot{\rho} = \cos\theta$ and

$$\dot{\theta} = Z^{1/2} + \frac{1}{2}(\dot{Z}/Z)\tan\theta. \tag{4.66}$$

If the scale factor derivative $\dot{\rho}$ is not zero in the interval of interest, then θ is in $0 \leq \theta \leq \pi/2$. So $\tan\theta \geq 0$, and Eq.(4.66) says $\dot{\theta} \geq Z^{1/2} \geq Z_0^{1/2}$. Thus θ will go to $\pi/2$ by $\eta = \pi/(2Z_0^{1/2})$, this results $\dot{\rho} = 0$.

We will denote this zero by η_1, and $Z(\eta_1) \equiv Z_1 \geq Z_0$. We stated before that $\ddot{\rho} < 0$ which implies that $\dot{\rho} < 0$ for $\eta > \eta_1$ and (4.63) states that $\dot{Z} \leq 0$. This time define

$$\rho(\eta) = Z_1^{-1/2}\cos\Theta(\eta) \tag{4.67}$$

with $\Theta(\eta_1) = 0$. Similar to the previous proof, we will show by contradiction that ρ must have a zero value in the region $\eta_1 \leq \eta \leq \eta_1 + \pi/(2Z_0^{1/2})$. A false hypothesis implies that Θ is confined to $0 \leq \Theta \leq \pi/2$. With the aid of (4.64) and (4.67)

$$\begin{aligned} -\dot{\rho} = Z_1^{1/2}(\sin\Theta)\dot{\Theta} &= (1 - Z\rho^2)^{1/2} \\ &\geq (1 - Z_1\rho^2)^{1/2}\sin\Theta. \end{aligned} \tag{4.68}$$

As a result

$$\dot{\Theta} \geq Z_1^{1/2} \geq Z_0^{1/2} \tag{4.69}$$

and Θ must reach $\pi/2$ within the interval, resulting a point where $\rho(\eta) = 0$.

Unlike, the dS background case in the flat universe background the scale factor goes asymptotically to a linear $\rho = \eta$ function, instead of going to zero for a second time. For more information about bubble growth in the presence of gravity, after the analytic continuation, you should visit Chapter 3. As, we know in the first case we will have a bubble growing in the de-Sitter hypersphere. In the second case, the anti-de Sitter bubble is unstable and collapses after a certain time. As we see and expected the presence of the coupling ξ, in the order of magnitude chosen in this work, does not affect the physics of the solutions.

In both cases, the bubble radius maximum value is larger as we decrease the coupling ξ. This is a visible effect of the coupling ξ to our numerical solutions.

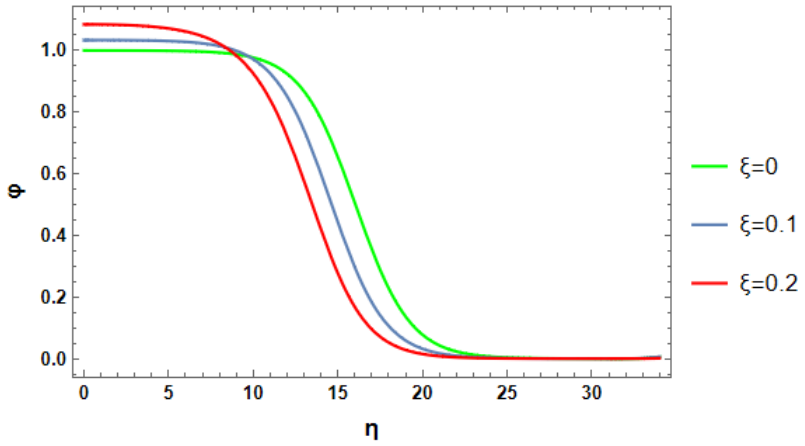

Figure 4.5: The bubble profiles for a $M \to AdS$ transition for several values of the coupling ξ.

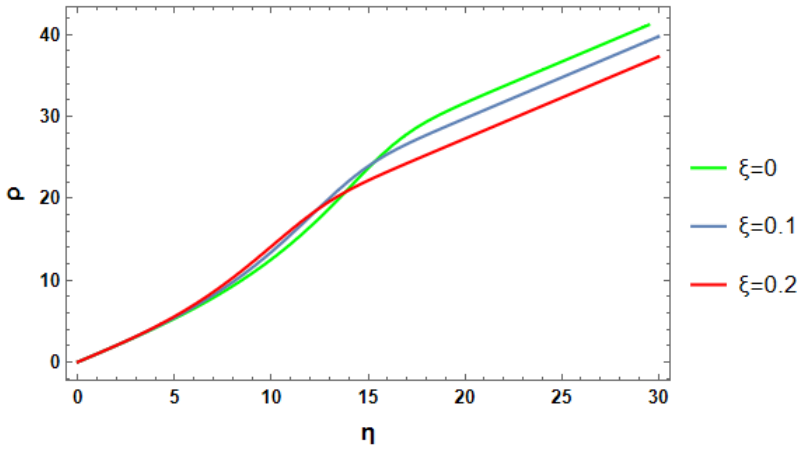

Figure 4.6: The bubble radius for a $M \to AdS$ transition for several values of the coupling ξ.

Chapter 5

False vacuum decay at finite temperature

Apart from the research of the false vacuum decay in extremely low temperatures (zero temperature false vacuum decay), the natural aftermath is a generalization to the case of finite temperature. Vacuum transitions at finite temperatures are perhaps more compatible with cosmological phase transitions, which may occur at very extreme temperatures in the early Universe such as the electroweak and the QCD transition [191].

In this chapter, we will make the jump to the finite temperature vacuum decay, giving emphasis on the high-temperature case. Examples of bounce solutions in the high-temperature limit will be presented. Furthermore, an effort to give a detailed modified answer to the CDL case and the non-minimally coupling case of the scalar field with gravity in high temperature will be attempted.

5.1 Extension to the non-zero temperature case

Let us begin our discussion of the $T \neq 0$ case based on the following literature references[170, 171, 192]. It is important to remember that quantum statistical physics of bosons and fermions at finite temperatures is equivalent to quantum field theory in the Euclidean space-time, periodic and anti-periodic respectively at the "time" direction β with period T^{-1}. To be specific, at finite temperature, where the thermal fluctuations dominate over the quantum fluctuations, one instead considers the following partition function under the assumption of a canonical ensemble

$$Z = \mathrm{Tr}\left[e^{-\beta H}\right], \tag{5.1}$$

where $\beta = 1/T$ is the thermodynamical beta. The partition function can be rewritten as a path integral

$$\begin{aligned} Z &= \mathrm{Tr}\left[e^{-\beta H}\right] \\ &= \int [d\phi] \left\langle \phi \right| e^{-\beta H} \left| \phi \right\rangle \\ &= \int [d\phi] \int_{\Phi(0,\vec{x})=\phi}^{\Phi(\beta,\vec{x})=\phi} [d\Phi] e^{-\int_0^\beta d\tau \int d^3\vec{x} L_E}, \end{aligned} \tag{5.2}$$

where, as usual, L_E is the Lagrangian in the Euclidean space. The path integral is a sum over all the trajectories, in this case with the same starting and ending point ϕ at time β. Therefore, the integral over ϕ can be simply eliminated, making our life easier, by imposing a periodic condition

to the quantum field Φ [193][194]. This leads as to

$$Z = \int_{\Phi(0,\vec{x})=\Phi(\beta,\vec{x})} [d\Phi] e^{-\int_0^\beta d\tau \int d^3\vec{x} L_E}. \tag{5.3}$$

In conclusion, the thermal field theory is equivalent to a Euclidean field theory with periodicity to Euclidean time (anti-periodic for fermionic fields). For more information on thermal field theory, someone can check the work of Laine and Vuorinen [195].

In the finite temperature case, we will use the effective potential $V_{\text{eff}}(\phi, T)$ instead of the zero temperature potential marked as $U(\phi) \equiv V_{\text{eff}}(\phi, 0)$. Here, we will act in complete analogy with the calculations performed in the $T \to 0$ situation with a significant modification. At the zero temperature false vacuum decay we were looking for an $\mathcal{O}(4)$ symmetric solution of the Euclidean equation of motion Eq.(2.45), now one should search for an $\mathcal{O}(3)$ symmetric solution periodic in the "time" direction $1/\beta$ with period T^{-1} [170, 171, 192]. At $T = 0$ the solution of the equation of motion is the $\mathcal{O}(4)$ symmetric bubble studied in Chapter 2. This spherical bubble-solution is corresponding to the minimal value of the four-dimensional Euclidean action noted as S_E obtaining a radius $\rho \equiv r(0)$[1]. Such a solution is said to describe quantum tunneling, this can be shown at Fig.5.1.a. At $T \ll r^{-1}(0)$ the solution will be a series of such bubbles placed at distance T^{-1} from one another in the "time" direction β, this situation is shown at Fig.5.1.b. If the temperature increases and β decreases, the four-volume becomes "squeezed" and this affects the form of the solution, the bubbles start to overlap (Fig.5.1.c). This happens at $T \sim r^{-1}(0)$ and we can say that "quantum tunneling" and "thermal tunneling" both play a role. Finally, at $T \gg r^{-1}(0)$, the squeezing of the space becomes more and more and we expect the solution to be a cylinder, depicted at Fig.5.1.d, with $\mathcal{O}(3)$ spatial symmetry. Then, an $\mathcal{O}(3)$ symmetric bubble arises with a radius $r(T)$.

5.2 The high-temperature case

5.2.1 The action and the decay rate

The previous paragraph ended with the saying that when the temperature is much larger than the reversed radius then the bounce solution becomes essentially a cylinder. At this high-temperature limit, the mechanism for bubble creation is, instead of quantum tunneling, thermal over-barrier nucleation. The four-dimensional action can be approximated with the three-dimensional one. In this situation, like in dimensional reduction, we can factorize and perform the integration over the τ-coordinate, and the four-dimensional Euclidean action becomes [170][171][196][197]

$$S_E = \int_0^\beta d\tau \int d^3\vec{x} L_E = \frac{1}{T} S_3, \tag{5.4}$$

where S_3 is the three-dimensional Euclidean action corresponding to the $\mathcal{O}(3)$-symmetric bubble

$$S_3 = \int d^3\vec{x} \left[\frac{1}{2} (\nabla\phi)^2 + V_{\text{eff}}(\phi, T) \right], \tag{5.5}$$

[1] In chapters 2,3 and 4 we used the letter ρ to describe radius, in this chapter we will use the notation $r(T)$ to separate the two cases (zero and high T) and to demonstrate the temperature dependence of the radius.

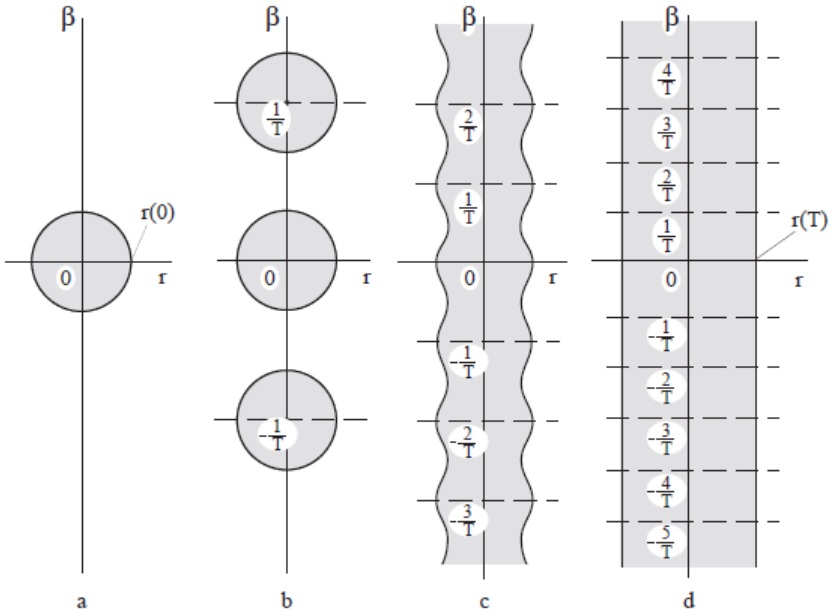

Figure 5.1: The form taken by solving the classical equation of motion for the field in Euclidean space at various temperatures: a) $T = 0$; b) $T << r^{-1}(0)$; c) $T \sim r^{-1}(0)$; d) $T >> r^{-1}(0)$. The shaded regions contain the classical field $\phi \neq 0$. For simplicity, we have drawn bubbles for those cases in which the thickness of their walls is much less than their radii (taken from [170]).

in order to calculate S_E we must solve the equation of motion resulting from the nullification of the variational derivative of the three-dimensional action

$$\left.\frac{\delta S_3}{\delta \phi}\right|_{\bar{\phi}} = -\nabla^2\phi + V'_{\text{eff}} = 0, \tag{5.6}$$

where the prime means derivative with respect to ϕ. The boundary conditions are the following: the derivative of the solution must vanish at the center of the bubble, chosen to be at the origin, and at infinity, the solution must be in the metastable vacuum, similar to the zero temperature case,

$$\bar{\phi}(\infty) = 0, \tag{5.7}$$

and

$$\left.\frac{\mathrm{d}\bar{\phi}}{\mathrm{d}r}\right|_{r=0} = 0. \tag{5.8}$$

Assuming spherical symmetry, the EoM can be written as

$$\frac{\mathrm{d}^2\phi}{\mathrm{d}r^2} + \frac{2}{r}\frac{\mathrm{d}\phi}{\mathrm{d}r} = V'_{\text{eff}}. \tag{5.9}$$

The probability of tunneling per unit time per unit volume in the high-temperature limit can be derived in complete analogy with the method followed by Coleman and Calan [132]. We will here write down, in brief, some important parts of the derivation which became in complete analysis at Section 2.3.

Consider a system at zero temperature and suppose boundary conditions at spatial infinity of the form, $\phi(\infty) = 0$, in order to define metastable energy eigenstates. The vacuum fluctuations

taking place in this system cause the time evolution of these would-be states to look like

$$\begin{aligned} |\phi(t)\rangle &= e^{-iEt}\,|\phi(0)\rangle = e^{-i[\mathrm{Re}(E)+i\,\mathrm{Im}(E)]}\,|\phi(0)\rangle \\ \Rightarrow \langle\phi(t)|\phi(t)\rangle &= e^{2\,\mathrm{Im}(E)}\,\langle\phi(0)|\phi(0)\rangle\,. \end{aligned} \tag{5.10}$$

Thereby, it could be said that such a metastable state possesses a decay rate, Γ/V, given by

$$\Gamma/V \cong -2\,\mathrm{Im}(E). \tag{5.11}$$

Analogously, to a thermal ensemble, it could be expected that

$$\Gamma_{\mathrm{therm}}/V \cong -2\,\mathrm{Im}(F), \tag{5.12}$$

where F is the free energy of the system, defined in the usual way

$$F = -T\ln Z. \tag{5.13}$$

It must be pointed out that this generalization is just a guess because it is a little bit strange if a real-time observable, the decay rate, could be determined exactly from a Euclidean observable, the free energy.

It is important to impose the question, of whether the free energy could indeed develop an imaginary part similar to the energy at the zero limit. It turns out that the answer to this is positive, as can be seen via the following argument [132]. Consider the path integral expression for the partition function and write for the free energy

$$F = -T\ln\left\{\int_{\mathrm{b.c}}\exp(-S_E)\right\}, \tag{5.14}$$

where b.c. refers to the periodic boundary conditions. Now, let us assume that at least two different saddle points $\bar{\phi}$ exist, satisfying

$$\left.\frac{\delta S_E}{\delta\phi}\right|_{\bar{\phi}} = 0, \qquad \bar{\phi}(0,\vec{x}) = \bar{\phi}(\beta,\vec{x}), \qquad \bar{\phi}(\tau,\infty) = 0. \tag{5.15}$$

Also, we will make the assumption that one of them is the trivial $\bar{\phi}=0$, whereas the other is a non-trivial solution denoted by $\bar{\phi}(\tau,\vec{x})$.

For the next step, let us consider fluctuations imposed around the non-trivial saddle point with an unstable direction. As it has been done already in the second chapter, suppose the fluctuation operator around the solution possesses a negative eigenmode

$$\left.\frac{\delta^2 S_E}{\delta\phi^2}\right|_{\bar{\phi}}\phi_-(\tau,\vec{x}) = -\lambda_-^2,\phi_-(\tau,\vec{x}) \tag{5.16}$$

as well, for the non-negative eigenfunctions, we write

$$\left.\frac{\delta^2 S_E}{\delta\phi^2}\right|_{\bar{\phi}}\phi_n(\tau,\vec{x}) = \lambda_n^2,\phi_n(\tau,\vec{x}), \tag{5.17}$$

with $n\geq 0$. Writing now a generic deviation of the field ϕ from the saddle point solution in the form

$$\delta\phi = \phi - \bar{\phi} = \sum_n c_n\phi_n, \tag{5.18}$$

where c_n is assumed to be real coefficients and taking the eigenfunctions to be orthonormal the integration measure of the path integral over the fluctuations can be written as a product

$$\int [d\phi] = \prod_n \frac{dc_n}{\sqrt{2\pi}}. \tag{5.19}$$

In the vicinity of the saddle point, the action with the help of a Taylor expansion gives

$$S_E[\phi] \approx S_E[\bar{\phi}] + \int_X \frac{1}{2}\delta\phi \frac{\delta^2 S_E}{\delta\phi^2}\delta\phi = S_E[\bar{\phi}] - \frac{1}{2}\lambda_-^2 c_-^2 + \sum_n \lambda_n^2 c_n^2. \tag{5.20}$$

We can use the semi-classical approximation to write the free energy in a form separating the saddle points,

$$F \sim -T \ln \left\{ Z_0 + e^{-S_E[\bar{\phi}]} \int \frac{dc_-}{\sqrt{2\pi}} e^{\frac{1}{2}\lambda_-^2 c_-^2} \prod_n \frac{dc_n}{\sqrt{2\pi}} e^{-\frac{1}{2}\lambda_n^2 c_n^2} \right\}, \tag{5.21}$$

where with Z_0 we denote the partition function of the trivial solution. The Gaussian integral over the negative mode confirms our initial intuitive hypothesis giving an imaginary part to the partition function and as result to the free energy

$$\int \frac{dc_-}{\sqrt{2\pi}} e^{\frac{1}{2}\lambda_-^2 c_-^2} \sim \frac{1}{\sqrt{2\pi}} \sqrt{\frac{2\pi}{-\lambda_-^2}} \sim i\sqrt{\frac{1}{\lambda_-^2}}. \tag{5.22}$$

Finally, assuming furthermore that the contribution from the trivial saddle point is much larger in absolute magnitude than that originating from the non-trivial one, with the help of Eq.(5.12) we get

$$\Gamma/V \sim \frac{T}{Z_0} \exp\big(-S_E[\bar{\phi}]\big) \big|\det\big(\delta^2 S_E[\bar{\phi}]/\delta\phi^2\big)\big|^{-1/2}, \tag{5.23}$$

where the determinant is simply the product of all eigenvalues.

All these are a brief recap of the analysis that took place in the second chapter extended in a thermal ensemble. As someone can see so far we used the same procedure, but it was considered necessary for this synopsis to be made here as a helpful reminder and guide in order to evaluate the "thermal" probability of the bubble nucleation.

We have already shown that the integral over τ in the high-temperature limit is simply reduced to multiplication by β in Eq.(5.4). Since the solution has no dependence on imaginary time, it does not break the τ-translation symmetry and consequently, we get only three zero modes. Thereby by comparing with Eq.(2.199) we can write

$$-2\,\mathrm{Im}(F) \cong TV \left(\frac{\bar{S}_3(\phi,T)}{2\pi T}\right)^{3/2} \left|\frac{\det'[-\partial^2 + V''_{\text{eff}}(\bar{\phi},T)]}{\det[-\partial^2 + V''_{\text{eff}}(0,T)]}\right|^{-1/2} e^{-S_3/T}. \tag{5.24}$$

Moreover, it turns out that our initial guess of $\Gamma_{\text{therm}}/V \sim -2\,\mathrm{Im}(F)$ must be slightly corrected into [196]

$$\Gamma_{\text{therm}}/V \cong -\frac{\beta\lambda_-}{\pi}\,\mathrm{Im}(F), \tag{5.25}$$

leading to a conjectured result

$$\Gamma_{\text{therm}}/V \cong \left(\frac{\lambda_-}{2\pi}\right) \left(\frac{\bar{S}_3(\phi,T)}{2\pi T}\right)^{3/2} \left|\frac{\det'[-\partial^2 + V''_{\text{eff}}(\bar{\phi},T)]}{\det[-\partial^2 + V''_{\text{eff}}(0,T)]}\right|^{-1/2} e^{-S_3/T}, \tag{5.26}$$

or according to the approximation made by Linde [171] someone can write

$$\Gamma_{\rm therm}/V \cong T\left(\frac{\bar{S}_3(\phi,T)}{2\pi T}\right)^{3/2}\left|\frac{\det'[-\partial^2+V''_{\rm eff}(\bar{\phi},T)]}{\det[-\partial^2+V''_{\rm eff}(0,T)]}\right|^{-1/2}e^{-S_3/T}. \tag{5.27}$$

Here, as before $\det'$ implies that the three zero modes of the operator will be omitted from the computation. Therefore, compared to the zero-temperature case we can easily guess that the contribution from the zero eigenmodes gives us the factor $\left(\bar{S}_3(\phi,T)/2\pi T\right)^{3/2}$, in front of the determinants. The factor T arises when we take into account the periodicity in the β direction.

Comparing Eq.(5.12) and Eq.(5.25), someone may expect the high-temperature result of (5.26) to be more accurate than the low-temperature result of (2.199) above the regime in which the prefactors cross each other [195], i.e. for

$$T \geq \frac{\lambda_-}{2\pi}. \tag{5.28}$$

We will close this section with one last comment. Likewise the $T=0$ case, it is usually an extremely difficult task to compute the determinants at the nucleation rate expression. However, a dimensional estimation may be of great usefulness. The dominant factors in the thermal nucleation rate are the exponential part and the dimensional part of the prefactor. The expression $\left|\det'[-\partial^2+V''_{\rm eff}(\bar{\phi},T)]/\det[-\partial^2+V''_{\rm eff}(0,T)^2]\right|^{-1/2}$, has the dimension m^3. The order of this expression may be

$$\left|\frac{\det'[-\partial^2+V''_{\rm eff}(\bar{\phi},T)]}{\det[-\partial^2+V''_{\rm eff}(0,T)]}\right|^{-1/2} \sim O(\phi^3,(V''_{\rm eff})^{3/2},r^{-3}(T),T^3), \tag{5.29}$$

in our case where $T \gg r^{-1}(0)$, the quantities $\phi,(V''_{\rm eff})^{1/2},r^{-1}(T)$ turn out to be of the same order of magnitude [170][171], as a result, the expression of interest is expected to be of the order of T^3 making us rewrite Eq.(5.27)

$$\Gamma_{\rm therm}/V \cong T^4\left(\frac{\bar{S}_3(\phi,T)}{2\pi T}\right)^{3/2}e^{-S_3/T}. \tag{5.30}$$

5.2.2 The thin-wall approximation

In this section, we will examine the high-temperature limit in a case via the thin-wall approximation. We are going to extend the results obtained by Coleman [131] in our occasion.

First of all, we have considered an $\mathcal{O}(3)$ spherical symmetry and that the field is a function of radius only. As a result of these, we can write for the three-dimensional action

$$\begin{aligned} S_3 &= \int d^3\vec{x}\left[\frac{1}{2}(\nabla\phi)^2+V_{\rm eff}(\phi,T)\right] \\ &= \int_0^\infty\int_0^\pi\int_0^{2\pi} r^2\sin\theta dr d\theta d\phi\left[\frac{1}{2}\left(\frac{{\rm d}\phi}{{\rm d}r}\right)^2+V_{\rm eff}(\phi,T)\right] \\ &= 4\pi\int_0^\infty r^2 dr\left[\frac{1}{2}\left(\frac{{\rm d}\phi}{{\rm d}r}\right)^2+V_{\rm eff}(\phi,T)\right]. \end{aligned} \tag{5.31}$$

Before proceeding, recall the mechanical analog of the "particle in a valley" problem with friction. If we replace the radius with the time, the field with the position of the particle and we reverse the potential, the situation is the same as it is in the second chapter.

Similar to Coleman's method we can separate the action in contributions from three regions. Outside the bubble where the false vacuum state exists we get the usual zero contribution. Inside the bubble where $r \ll \bar{r}$ the field is in the true vacuum in a constant state. Thus, the derivative with respect to the radius will be zero and the potential will get its value at this state

$$\frac{\mathrm{d}\bar{\phi}}{\mathrm{d}r} = 0 \tag{5.32}$$

and

$$V_{\text{eff}}(\bar{\phi}, T) \equiv V_{\text{eff}}(\phi_-, T), \tag{5.33}$$

inside the bubble, where ϕ_- is the field value at the true vacuum state. The contribution from the bubble's volume at the action will be

$$\begin{aligned} S_{3,in} &= 4\pi \int_0^{\bar{r}} r^2 dr \left[\frac{1}{2} \left(\frac{\mathrm{d}\bar{\phi}}{\mathrm{d}r} \right)^2 + V_{\text{eff}}(\bar{\phi}, T) \right] \\ &= 4\pi \int_0^{\bar{r}} r^2 dr \left[V_{\text{eff}}(\phi_-, T) - V_{\text{eff}}(\phi_+, T) \right] \\ &= 4\pi(-\epsilon) \int_0^{\bar{r}} r^2 dr \\ &= -\frac{4\pi}{3} \bar{r}^3 \epsilon, \end{aligned} \tag{5.34}$$

a volume term as expected. To be noted that we used Eqs.(5.32-5.33). Finally, let us inspect the region at $r \simeq \bar{r}$ where from our experience so far we are expecting a surface term. If $\bar{r}$ is very large, then the first derivative term at the equation of motion, Eq.(5.9), is very small and it can be neglected. Thereby

$$\frac{\mathrm{d}^2\bar{\phi}}{\mathrm{d}r^2} \cong V'_{\text{eff}} \tag{5.35}$$

which through multiplication with $d\bar{\phi}/dr$ can be integrated into

$$\frac{1}{2} \left(\frac{\mathrm{d}\bar{\phi}}{\mathrm{d}r} \right)^2 \cong V_{\text{eff}}, \tag{5.36}$$

again the soliton equation. The contribution of the wall is

$$\begin{aligned} S_{3,wall} &= 4\pi\bar{r}^2 \int_{wall} dr \left[\frac{1}{2} \left(\frac{\mathrm{d}\bar{\phi}}{\mathrm{d}r} \right)^2 + V_{\text{eff}}(\bar{\phi}, T) \right] \\ &= 4\pi\bar{r}^2 \int_{wall} dr \left(\frac{\mathrm{d}\bar{\phi}}{\mathrm{d}r} \right)^2 \\ &= 4\pi\bar{r}^2 \int_{\phi_-}^{\phi_+} d\bar{\phi} \frac{\mathrm{d}\bar{\phi}}{\mathrm{d}r} \\ &= 4\pi\bar{r}^2 \int_{\phi_-}^{\phi_+} d\bar{\phi} \sqrt{2V_{\text{eff}}} = 4\pi\bar{r}^2 S_1(T), \end{aligned} \tag{5.37}$$

where $S_1(T)$ is the surface tension term which represents the energy density of a planar surface and it is

$$S_1(T) \equiv \int_{wall} dr \left[\frac{1}{2} \left(\frac{\mathrm{d}\bar{\phi}}{\mathrm{d}r} \right)^2 + V_{\text{eff}}(\bar{\phi}, T) \right] \cong \int_{\phi_-}^{\phi_+} d\bar{\phi} \sqrt{2V_{\text{eff}}}. \tag{5.38}$$

Summing up the contributions, we get

$$S_3 = -\frac{4}{3}\pi\bar{r}^3\epsilon + 4\pi\bar{r}^2 S_1(T), \tag{5.39}$$

and the variational computation leads to

$$\bar{r}(T) = \frac{2S_1(T)}{\epsilon}, \tag{5.40}$$

plugging this result in Eq.(5.39)

$$S_3 = \frac{16\pi S_1^3(T)}{3\epsilon^2}. \tag{5.41}$$

The expression thus obtained for the probability of bubble formation is

$$\frac{\Gamma_{\text{therm}}}{V} \approx \exp\left(-\frac{16\pi S_1^3(T)}{3\epsilon^2 T}\right). \tag{5.42}$$

This coincides with the well-known expression from textbooks on statistical mechanics [198]. In a similar way to Coleman's condition of applicability of the thin-wall approximation here we have

$$\frac{2S_1(T)}{\epsilon} \gg (d^2V_{\text{eff}}(\phi_-, T)/d\phi^2)^{-1/2}, \tag{5.43}$$

where $(d^2V_{\text{eff}}(\phi_-, T)/d\phi^2)^{-1/2}$, is the order of magnitude of the bubble wall thickness at high temperature.

5.2.3 Examples

In this subsection, we will try to derive exact solutions for the quantities of interest in some special cases. First of all, let us consider the case presented in Linde's work [170][171] and state that the effective potential shown in Fig.5.2 can be approximated by the expression

$$V(\phi) = \frac{1}{2}M(T)\phi^2 - \frac{1}{3}\delta(T)\phi^3 + \frac{1}{4}\lambda\phi^4. \tag{5.44}$$

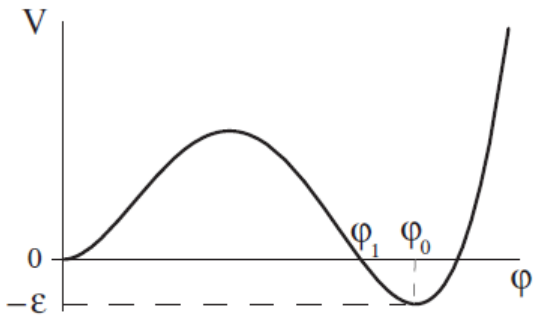

Figure 5.2: Potential in the case of slight supercooling of the phase $\phi = 0$ (the quantity $\epsilon \to 0$) (taken from [170]).

For this potential, the surface tension can be calculated exactly, and thus this result can lead us to analytic expressions for S_3 and $\bar{r}(T)$. At the limit of interest ($\epsilon \to 0$), the depths of the minima at $\phi = 0$ and $\phi = \phi_0(T)$ become equal, so we can write

$$\begin{aligned} V(0) = V(\phi_0) \Rightarrow \frac{M}{2}\phi_0^2 - \frac{\delta}{3}\phi_0^3 + \frac{\lambda}{4}\phi_0^4 = 0 \Rightarrow \\ \Rightarrow \frac{\lambda}{4}\phi_0^2 - \frac{\delta}{3}\phi_0 + \frac{M}{2} = 0, \end{aligned} \tag{5.45}$$

where the solution $\phi_0 = 0$ is trivial. Now, if we demand a zero discriminant at the quadratic equation of Eq.(5.45) we will take a relation for M, λ and δ,

$$2\delta^2 = 9\lambda M \tag{5.46}$$

and

$$\phi_0 = \frac{2\delta}{3\lambda}. \tag{5.47}$$

Under this limit the potential transforms to

$$V(\phi) = \frac{\lambda}{4}\phi^2(\phi - \phi_0)^2. \tag{5.48}$$

In the above equation we have just replaced $\delta = 3\lambda\phi_0/2$ and $M^2 = \lambda\phi_0^2/2$ from the Eqs.(5.46-5.47) and plugged them in Eq.(5.44).

The surface tension, using Eq.(5.38), will be

$$\begin{aligned} S_1 &= \int_0^{\phi_0} d\phi\sqrt{2V(\phi)} = \int_0^{\phi_0} d\phi\sqrt{\frac{\lambda}{2}\phi^2(\phi-\phi_0)^2} \\ &= \int_0^{\phi_0} d\phi\sqrt{\frac{\lambda}{2}}|\phi(\phi-\phi_0)| = \int_0^{\phi_0} d\phi\sqrt{\frac{\lambda}{2}}\phi(\phi_0-\phi) \\ &= \int_0^{\phi_0} d\phi\sqrt{\frac{\lambda}{2}}(\phi_0\phi-\phi^2) = \sqrt{\frac{\lambda}{2}}\left(\phi_0\frac{\phi^2}{2} - \frac{1}{3}\phi^3\right)\Bigg|_0^{\phi_0} \Rightarrow \\ &\Rightarrow S_1 = \frac{\sqrt{\lambda}\phi_0^3}{6\sqrt{2}} = \frac{2\sqrt{2}\delta^3}{3^4\lambda^{5/2}}, \end{aligned} \tag{5.49}$$

where in the last line the relation between ϕ_0 and δ was used. In the high temperature case, the three-dimensional action from Eq.(5.41) will be

$$S_3 = \frac{16\pi S_1^3}{3\epsilon^2} \overset{(5.49)}{\Rightarrow} S_3 = \frac{\pi\lambda^{3/2}\phi_0^9}{2^{1/2}3^4\epsilon^2} = \frac{2^{17/2}\pi\delta^9}{3^{13}\lambda^{15/2}\epsilon^2} \tag{5.50}$$

and the radius of the bubble from Eq.(5.40) will become

$$\bar{r} = \frac{2S_1}{\epsilon} \overset{(5.49)}{\Rightarrow} \bar{r} = \frac{2^{5/2}\delta^3}{3^4\lambda^{5/2}\epsilon}. \tag{5.51}$$

For a second paradigm, we will examine phase transitions in gauge theories at high temperatures. In this case, a typical expression for the one-loop effective potential is [199][200]

$$V_{\text{eff}}(\phi, T) = \frac{1}{2}\gamma(T^2 - T_c^2)\phi^2 - \frac{1}{3}aT\phi^3 + \frac{1}{4}\lambda\phi^4, \tag{5.52}$$

here only the contribution of W and Z bosons, and the top quark to radiative corrections were considered. Notice that in this potential appears a cubic term that can be provided by the contribution to the effective potential of bosonic fields. For more information about the computation of effective potentials in scalar field theories, fermionic and gauge bosonic fields someone can take a look at the work of Mariano Quiros [200]. In Eq.(5.52) T_c is the critical temperature above which the symmetric phase $\phi = 0$ is metastable, γ and α are some numerical coefficients [201–205]. The temperature T_0, at which the potential for $\phi = 0$ and $\phi = \phi_0(T)$ have the same value is given after a quick process similar to the previous example,

$$\begin{aligned} &V_{\text{eff}}(0,T_0) = V_{\text{eff}}(\phi_0,T_0) \Rightarrow \phi_0^2\left[\frac{1}{2}\gamma(T_0^2-T_c^2) - \frac{1}{3}\alpha T_0\phi_0 + \frac{1}{4}\lambda\phi_0^2\right] = 0 \Rightarrow \\ &\Rightarrow \frac{1}{2}\gamma(T_0^2-T_c^2) - \frac{1}{3}\alpha T_0\phi_0 + \frac{1}{4}\lambda\phi_0^2 = 0, \end{aligned} \tag{5.53}$$

then the nullification of the discriminant at the quadratic equation leads to the desired result

$$\begin{aligned} &\Delta = b^2 - 4abc = 0 \Rightarrow \frac{1}{9}\alpha^2 T_0^2 - \cancel{4}\frac{1}{\cancel{4}}\lambda\frac{1}{2}\gamma(T_0^2-T_c^2) = 0 \Rightarrow \\ &\Rightarrow T_0^2\left(\frac{1}{9}\alpha^2 - \frac{1}{2}\lambda\gamma\right) = \frac{1}{2}\lambda\gamma T_c^2 \Rightarrow T_0^2\left(1 - \frac{2\alpha^2}{9\lambda\gamma}\right) = T_c^2. \end{aligned} \tag{5.54}$$

Then the unique solution for the field is going to be

$$\phi_0 = \frac{b}{2a} = -\frac{2}{3}\frac{aT_0}{\lambda}, \tag{5.55}$$

which is of course T_0 dependent. One can readily determine the quantity ϵ as a function of the deviation of the temperature T_c from T_0 at the $\epsilon \to 0$ limit:

$$\begin{aligned} \epsilon &= V_{\text{eff}}(0,T_0) - V_{\text{eff}}(\phi_0,T_0) = -V_{\text{eff}}(\phi_0,T_0) \\ &= -\frac{1}{2}\gamma(T_0^2-T_c^2)\phi_0^2 + \frac{1}{3}aT_0\phi_0^3 - \frac{1}{4}\lambda\phi_0^4 \\ &= -\frac{1}{2}\gamma(T_0^2-T_c^2)\phi_0^2 + \cancel{O(T_0^4)} - \cancel{O(T_0^4)} \\ &\overset{(5.55)}{=} -\frac{1}{2}\gamma(T_0^2-T_c^2)\frac{4\alpha^2T_0^2}{9\lambda^2} \\ &= \frac{\gamma}{2}(T_c-T_0)(T_c+T_0)\frac{4\alpha^2T_0^2}{9\lambda^2} \Rightarrow \\ &\Rightarrow \epsilon = \frac{2T_cT_0^2\alpha^2\gamma}{9\lambda^2}\Delta T, \end{aligned} \tag{5.56}$$

where $\Delta T = T_0 - T_c$. We can get exact results for the quantities of interest with the aid of the relations obtained from both examples. We will extract these quantities at the limit $(T_0 - T_c)/T_c \ll 1$. By comparing Eq.(5.44) with Eq.(5.52) we can make the following match

$$\begin{aligned} &M^2(T) \to \gamma(T^2 - T_c^2), \\ &\delta(T) \to \alpha T. \end{aligned} \tag{5.57}$$

Thus, we can take advantage of the expressions obtained for the first potential. Using Eq.(5.49), the surface tension can be written as

$$S_1 = \frac{2\sqrt{2}\delta^3}{3^4\lambda^{5/2}} = \frac{2\sqrt{2}\alpha^3}{3^4\lambda^{5/2}}T_c^3, \tag{5.58}$$

in the second equality, the aforementioned match was made. Next, the three-dimensional action is to be calculated in a similar way,

$$\begin{aligned}\frac{S_3}{T_0} &= \frac{2^{17/2}\pi\delta^9}{3^{13}\lambda^{15/2}\epsilon^2 T_0} = \frac{2^{17/2}\pi\alpha^9 T_0^9}{3^{13}\lambda^{15/2}T_0}\frac{3^4\lambda^4}{2^2T_0^2T_c^4a^4\gamma^2}\frac{1}{DT^2} \Rightarrow \\ \Rightarrow \frac{S_3}{T_0} &= \frac{2^{13/2}\pi\alpha^5}{3^9\gamma^2\lambda^{7/2}}\frac{1}{x^2},\end{aligned} \tag{5.59}$$

where the equation for ϵ and the temperature's condition were used. The parameter x is defined as $x = \Delta T/T_c$. In closing, the radius will be

$$\bar{r} = \frac{2^{5/2}\delta^3}{3^4\lambda^{5/2}\epsilon} = \sqrt{\frac{8}{\lambda}}\frac{\alpha}{9\gamma T_c}\frac{1}{x}. \tag{5.60}$$

Conclusively, the thin-wall approximation makes it possible to compute analytically S_1, S_3, and $\bar{r}$ in the high-temperature limit in a very important class of theories. It is obvious that this works in the zero temperature case in the same way exactly regardless of whether it was not presented in this thesis.

5.2.4 Applicability of the method

Let us now investigate the question of the applicability of this method to the gauge theory studied. As we know the solution of the soliton equation is of the form

$$r = \int_{\phi}^{\phi_0} \frac{d\phi}{\sqrt{2V_{\text{eff}(\phi,T)}}}. \tag{5.61}$$

For this case, the integral can be calculated exactly [154] leading us to the bubble wall thickness which is

$$\Delta r \approx \sqrt{\frac{2}{\lambda}}\frac{2}{\phi_0} = \frac{3\sqrt{\lambda}}{\sqrt{2}\alpha T_c}. \tag{5.62}$$

Now let us write the conditions of applicability of the thin-wall approximation in the form

$$r > N\Delta r, \tag{5.63}$$

for $N \gg 1$. From Eqs.(5.59-5.60) it follows that

$$x < \frac{\alpha^2}{3N\gamma\lambda} \tag{5.64}$$

and

$$\frac{S_3}{T} > N^2\frac{2^{13/2}\pi\alpha}{3^3\lambda^{3/2}}. \tag{5.65}$$

For $N = 2$ we get

$$x = \frac{\Delta T}{T_c} < 2\cdot 10^{-2}\frac{\alpha^2}{\gamma\lambda}, \tag{5.66}$$

$$\frac{S_3}{T} > 40\frac{\alpha}{\lambda^{3/2}}. \tag{5.67}$$

Some other inequalities can be derived from the condition $T \gg \bar{r}^{-1}(T)$. One easily can find that

$$x \ll \sqrt{\frac{2}{\lambda}}\frac{\alpha}{9\gamma} \tag{5.68}$$

and

$$\frac{S_3}{T} \gg \frac{2^{11/2}\pi\alpha^3}{3^5\lambda^{5/2}}. \tag{5.69}$$

As a consequence of these restrictions, the thin-wall approximation is applicable only to processes proceeding with a comparatively small supercooling x. The decay rate of these processes is completely dominated by the exponential factor $e^{-S_3/T}$. These conditions can only be applied to relatively slow phase transitions. The restrictions such as that of the Eq.(5.67)[170] are not satisfied in many cases of interest, forcing us to seek ways of proceeding beyond the scope of the thin-wall approximation such as the numerical study of the equations of motion. Nevertheless, the method itself and its results turn out to be useful and aid us to obtain useful conclusions about the development of the theory of the metastable phase decay. In the final appendix of this thesis a numerical bounce solution is presented for the thermal case.

5.3 Effects of gravity at high-temperature vacuum decay

5.3.1 Calculation of the bounce action

Let us turn now our attention in evaluating the gravitational effects of the decay of the false vacuum at high temperatures. We will follow the standard techniques used by Coleman and De Luccia [133] and will derive some of the results obtained by Loveridge [206].

First of all, we begin with the action for a scalar field including the Einstein-Hilbert term

$$S_M = \int d^4x\sqrt{-g}\left[\frac{1}{2}g^{\mu\nu}\partial_\mu\phi\partial_\nu\phi - V_{\text{eff}}(\phi,T) - (16\pi G)^{-1}R\right], \tag{5.70}$$

where the effective potential took the place of the zero temperature potential in order to be in agreement with our work so far in the present chapter. This time will be used the metric of the below form

$$ds^2 = d\tau^2 + d\eta^2 + r^2(\eta)(d\theta^2 + \sin^2\theta d\phi^2), \tag{5.71}$$

which is not the same with Eq.(3.7) and Eq.(4.7). Recall, the cylindrical symmetry of the problem at high temperature, in this situation the solution to the bounce is a 4-cylinder (spherically symmetric in three orthogonal dimensions), or write it down in a more elegant and comprehensive way,

$$ds^2 = d\tau^2 + d\eta^2 + r^2(\eta)d\Omega^2, \tag{5.72}$$

where $d\Omega^2$ is the line element of a two-sphere.

The metric can be written in a matrix form as

$$g_{\mu\nu} = \begin{pmatrix} 1 & 0 & 0 & 0 \\ 0 & 1 & 0 & 0 \\ 0 & 0 & r^2(\eta) & 0 \\ 0 & 0 & 0 & r^2(\eta)\sin^2\theta \end{pmatrix}. \tag{5.73}$$

Using Eq.(3.10) someone can calculate the non-zero Christoffel's symbols. The six surviving

symbols are the following

$$\begin{aligned}
\Gamma^2_{33} &= -r\dot{r}, \\
\Gamma^2_{44} &= -r\dot{r}\sin^2\theta, \\
\Gamma^3_{23} &= \frac{\dot{r}}{r}, \\
\Gamma^3_{44} &= -\sin\theta\cos\theta, \\
\Gamma^4_{24} &= \frac{\dot{r}}{r}, \\
\Gamma^4_{34} &= \sin^{-1}\theta\cos\theta.
\end{aligned} \tag{5.74}$$

Then, we can find the Ricci tensor components needed in order to calculate the curvature scalar. These can be expressed as a function of Christoffel's symbols and their derivatives and they are

$$\begin{aligned}
R_{11} &= 0, \\
R_{22} &= -2\frac{\ddot{r}}{r}, \\
R_{33} &= -\dot{r}^2 - r\ddot{r} + 1, \\
R_{44} &= \sin^2\theta(-\dot{r}^2 - r\ddot{r} + 1).
\end{aligned} \tag{5.75}$$

Finally, we can find the curvature scalar from the below equation

$$R = g^{11}R_{11} + g^{22}R_{22} + g^{33}R_{33} + g^{44}R_{44}. \tag{5.76}$$

This is leading to

$$R = -\frac{2}{r^2}(2r\ddot{r} + \dot{r}^2 - 1). \tag{5.77}$$

Computing the Euclidean equations of motion is now a straightforward process completed in previous chapters, here the results will be presented following the familiar recipe. By varying the action with respect to ϕ we find the equation

$$\ddot{\phi} + 2\frac{\dot{r}}{r}\dot{\phi} = V'_{\text{eff}}, \tag{5.78}$$

the dots denote $d/d\eta$ and the prime denotes $d/d\phi$. Varying with respect to the metric yields the Einstein Equation

$$G_{\mu\nu} = \kappa T_{\mu\nu}, \tag{5.79}$$

the $\eta\eta$ component of this becomes the second important equation of interest

$$\dot{r}^2 = 1 + \kappa r^2\left(\frac{1}{2}\dot{\phi}^2 - V_{\text{eff}}\right), \tag{5.80}$$

with $\kappa = 8\pi G$. These two equations have minor differences from the equations obtained by Coleman and De Luccia in the early eighties. Using these results, imposing the field to be a

function of η only and making a Wick rotation the Euclidean action can be written as

$$\begin{aligned} S_E &= \int d^4x\sqrt{g_E}\left(\frac{1}{2}g^{\mu\nu}\partial_\mu\phi\partial_\nu\phi + V_{\text{eff}} - \frac{R}{2\kappa}\right) \\ &= \int_0^\beta\int_0^{2\pi}\int_0^\pi\int d\tau d\eta d\theta d\phi\sqrt{r^4\sin^2\theta}\left(\frac{1}{2}\dot{\phi}^2 + V_{\text{eff}} - \frac{R}{2\kappa}\right) \\ &= \frac{4\pi}{T}\int d\eta\left[r^2\left(\frac{1}{2}\dot{\phi}^2 + V_{\text{eff}}\right) - r^2\frac{R}{2\kappa}\right] \\ &= \frac{4\pi}{T}\int d\eta\left[r^2\left(\frac{1}{2}\dot{\phi}^2 + V_{\text{eff}}\right) - \frac{\cancel{r^2}2}{\cancel{2}\kappa\cancel{r^2}}(2r\ddot{r} + \dot{r}^2 - 1)\right] \Rightarrow \\ \Rightarrow S_E &= \frac{4\pi}{T}\int d\eta\left[r^2\left(\frac{1}{2}\dot{\phi}^2 + V_{\text{eff}}\right) + \frac{1}{\kappa}(2\ddot{r}r + \dot{r}^2 - 1)\right] = \frac{S_3}{T}. \end{aligned} \tag{5.81}$$

Here, as we have already seen, if the temperature is much higher so that β is very small compared with the radius of the nucleating bubble, then the bounce solution is cylindrical. That is to say a three-sphere in the spatial directions and constant in time. Then, the integration over τ becomes simply a multiplicative factor $\beta = 1/T$.

The action of Eq.(5.81) can be simplified by using integration by parts to eliminate the second derivative term and Eq.(5.80) to make the first derivative term vanish which yields

$$S_E = \frac{8\pi}{T}\int d\eta\left(r^2V_{\text{eff}} - \frac{1}{\kappa}\right) + \text{surface terms}. \tag{5.82}$$

The bounce action is

$$B = S_E(\phi) - S_E(\phi_+) \tag{5.83}$$

and we divide it into three parts, outside the wall, the wall itself, and inside the wall where the first part does not contribute to the total B. At the wall, it is useful to define $V_{0,\text{eff}}$ such that

$$V_{\text{eff}}(\phi, T) = V_{0,\text{eff}}(\phi, T) + \mathcal{O}(V_{+,\text{eff}} - V_{-,\text{eff}}), \tag{5.84}$$

and $dV_{0,\text{eff}}/d\phi = 0$ at both ϕ_+ and ϕ_-. We will also make the approximation $r \to \bar{r}$ and $V_{\text{eff}}(\phi, T) \to V_{0,\text{eff}}(\phi, T)$ to get

$$B_{wall} = \frac{8\pi}{T}\bar{r}^2\int d\eta[V_{0,\text{eff}}(\phi, T) - V_{0,\text{eff}}(\phi_+, T)] = \frac{4\pi}{T}\bar{r}^2S_1. \tag{5.85}$$

Finally, inside the wall, the universe is in its new true vacuum phase and ϕ is constant so that from Eq.(5.80) someone can extort

$$d\eta = dr(1 - \kappa r^2V_{\text{eff}})^{-1/2}, \tag{5.86}$$

so that the bounce action inside the bubble to be

$$\begin{aligned} B_{in} &= -\frac{8\pi}{T\kappa}\int_0^{\bar{r}} dr\Big\{[1 - \kappa r^2V_{\text{eff}}(\phi_-)]^{1/2} - (\phi_- \to \phi_+)\Big\} \\ &= -\frac{4\pi}{T\kappa}\left\{\left[\frac{\arcsin\sqrt{\kappa|V_{-,\text{eff}}|}\bar{r}}{\sqrt{\kappa|V_{-,\text{eff}}|}} + \bar{r}\sqrt{1 - \kappa V_{-,\text{eff}}\bar{r}^2}\right] - (\phi_- \to \phi_+)\right\}. \end{aligned} \tag{5.87}$$

This is a prettily complicated integral whose some more steps to calculate it are depicted in Appendix F. It should be noted that when the potential is less than zero the arcsine must be changed to an inverse hyperbolic sine. We can accomplish that by dropping the absolute values, too. Otherwise, the equation does not change.

5.3.2 Curved space-time results modification

Let us now extend in our finite temperature approach the cases studied by Coleman and De Luccia in [133]. We begin with the case that is relevant if we are now in a post-apocalyptic age, or as Loveridge [206] called it the "null true vacuum". Here, the true vacuum is zero (null) and the false vacuum is small and positive,

$$V_{\text{eff}}(\phi_+, T) = \epsilon, \qquad V_{\text{eff}}(\phi_-, T) = 0. \tag{5.88}$$

We must find the value of $\bar{r}$ where the bounce action is stationary. The derivative with respect to the radius for the wall contribution is

$$B'_{wall} = \frac{8\pi}{T}\bar{r}S_1. \tag{5.89}$$

The derivative for the part inside the wall is a little bit more complicated but after some trivial algebra someone can find

$$B'_{in} = -\frac{8\pi}{T\kappa}\left(1 + \frac{\epsilon\kappa\bar{r}^2}{\sqrt{1-\epsilon\kappa\bar{r}^2}}\right). \tag{5.90}$$

Then, we must solve the resultant equation with respect to $\bar{r}$,

$$\begin{aligned}
&B' = B'_{wall} + B'_{in} = 0 \Rightarrow \\
&\Rightarrow \frac{8\pi}{T}\left(\bar{r}S_1 - \frac{1}{\kappa} - + \frac{\epsilon\kappa\bar{r}^2}{\kappa\sqrt{1-\epsilon\kappa\bar{r}^2}}\right) = 0 \\
&\Rightarrow \bar{r}S_1 - \frac{1}{\kappa} - + \frac{\epsilon\kappa\bar{r}^2}{\kappa\sqrt{1-\epsilon\kappa\bar{r}^2}} = 0 \\
&\Rightarrow (1-\epsilon\kappa\bar{r}^2)(\bar{r}S_1\kappa - 1)^2 = (\epsilon\kappa\bar{r}^2 - 1)^2 \\
&\Rightarrow (\bar{r}S_1\kappa - 1)^2 = -(\epsilon\kappa\bar{r}^2 - 1) \\
&\Rightarrow \cancel{\bar{r}^2}S_1^2\cancel{\kappa^2} - 2\cancel{\bar{r}}S_1\cancel{\kappa} + \cancel{1} = -\epsilon\cancel{\kappa}\cancel{\bar{r}^2} + \cancel{1} \\
&\Rightarrow \bar{r}(S_1^2\kappa + \epsilon) = 2S_1,
\end{aligned} \tag{5.91}$$

after all this procedure we find the following result

$$\bar{r} = \frac{2S_1}{\epsilon + \kappa S_1^2} = \frac{\bar{r}_L}{1 + (\bar{r}_L/2D)^2}, \tag{5.92}$$

where $\bar{r}_L = 2S_1/\epsilon$, is Linde's result obtained at Eq.(5.40) and $D = (\kappa\epsilon)^{-1/2}$.

The bounce action can not be put in quite as simple a form as in Coleman's paper. Let us look at the terms one by one, if we insert Eq.(5.92) in the wall term we get

$$\begin{aligned}
B_{wall} &= \frac{4\pi}{T}\bar{r}^2 S_1 = \frac{4\pi}{T}\frac{\bar{r}_L^2}{(1+b^2)^2}S_1 \\
&= \frac{4\pi}{T}\frac{\bar{r}_L^2}{(1+b^2)^2}\frac{\epsilon\bar{r}_L}{2} \\
&= \frac{2\pi}{T}\frac{\bar{r}_L^3}{(1+b^2)^2}\epsilon,
\end{aligned} \tag{5.93}$$

where we set $b = \bar{r}_L/2D$ and Linde's solution was used in the second line, too. Thereafter, let us take a look and see what happens at the contribution inside the wall if we act with the stationary

point. In the null true vacuum case then we have

$$\begin{aligned} B_{in} &= -\frac{8\pi}{T\kappa}\bar{r} + \frac{4\pi}{T\kappa}\left[\frac{\arcsin(\sqrt{\kappa\epsilon}\bar{r})}{\sqrt{\kappa\epsilon}} + \bar{r}\sqrt{1-\kappa\epsilon\bar{r}^2}\right] \\ &= -\frac{8\pi}{T}D^2\epsilon\frac{\bar{r}_L}{1+b^2} + \frac{4\pi}{T}D^2\epsilon\left[D\arcsin\left(D^{-1}\frac{\bar{r}_L}{1+b^2}\right) + \frac{\bar{r}_L}{1+b^2}\sqrt{1-\frac{1}{D^2}\frac{\bar{r}_L^2}{(1+b^2)^2}}\right] \\ &= -\frac{8\pi}{T}D^2\epsilon\frac{\bar{r}_L}{1+b^2} + \frac{4\pi}{T}D^3\epsilon\left[\arcsin\left(\frac{2b}{1+b^2}\right) + \frac{2b}{1+b^2}\sqrt{1-\frac{4b^2}{(1+b^2)^2}}\right]. \end{aligned} \tag{5.94}$$

Then let us add the two terms:

$$\begin{aligned} B &= B_{wall} + B_{in} \\ &= \frac{2\pi}{T}\frac{\bar{r}_L^3}{(1+b^2)^2}\epsilon - \frac{8\pi}{T}D^2\epsilon\frac{\bar{r}_L}{1+b^2} + \frac{4\pi}{T}D^3\epsilon\left[\arcsin\left(\frac{2b}{1+b^2}\right) + \frac{2b}{1+b^2}\sqrt{1-\frac{4b^2}{(1+b^2)^2}}\right] \\ &= \frac{4\pi}{T}D^3\epsilon\left[\frac{1}{2D^3}\frac{\bar{r}_L^3}{(1+b^2)^2} - \frac{2}{D}\frac{\bar{r}_L}{1+b^2}\right] + \frac{4\pi}{T}D^3\epsilon\left[\arcsin\left(\frac{2b}{1+b^2}\right) + \frac{2b}{1+b^2}\sqrt{1-\frac{4b^2}{(1+b^2)^2}}\right] \\ &= \frac{4\pi}{T}D^3\epsilon\left[\frac{4b^3}{(1+b^2)^2} - \frac{4b}{1+b^2}\right] + \frac{4\pi}{T}D^3\epsilon\left[\arcsin\left(\frac{2b}{1+b^2}\right) + \frac{2b}{1+b^2}\sqrt{1-\frac{4b^2}{(1+b^2)^2}}\right] \\ &= \frac{4\pi}{T}D^3\epsilon\left[\frac{4b^3}{(1+b^2)^2} - \frac{4b}{1+b^2} + \arcsin\left(\frac{2b}{1+b^2}\right) + \frac{2b}{1+b^2}\sqrt{1-\frac{4b^2}{(1+b^2)^2}}\right] \\ &\approx \frac{4\pi}{T}D^3\epsilon\left[\arcsin\left(\frac{2b}{1+b^2}\right) - \frac{4b}{1+b^2} + \frac{4b^3}{(1+b^2)^2} + \frac{2b}{1+b^2}\left(1-\frac{2b^2}{(1+b^2)^2}\right)\right] \\ &= \frac{4\pi}{T}D^3\epsilon\left[\arcsin\left(\frac{2b}{1+b^2}\right) - \frac{2b}{1+b^2} + O(b^3)\right], \end{aligned} \tag{5.95}$$

we will keep only linear terms for b, so we can write for the bounce action from Eq.(5.95)

$$\begin{aligned} B &= \frac{4\pi}{T}D^3\epsilon\left[\arcsin\left(\frac{2b}{1+b^2}\right) - \frac{2b}{1+b^2}\right] \\ &= \frac{4\pi}{T}D^3\epsilon\left[\arccos\left(\frac{1-b^2}{1+b^2}\right) - \frac{2b}{1+b^2}\right]. \end{aligned} \tag{5.96}$$

The last expression gives Linde's result at the limit $D \to \infty$. Let us check if this is true for a moment. As D goes to infinity, b goes to zero and we get

$$\begin{aligned} B_L &= \lim_{b\to 0^+}\frac{4\pi}{T}\frac{\bar{r}_L^3}{8b^3}\epsilon\left[\arccos\left(\frac{1-b^2}{1+b^2}\right) - \frac{2b}{1+b^2}\right] \\ &= \frac{4\pi}{T}\epsilon\frac{\bar{r}_L^3}{8}\frac{4}{3} = \frac{16\pi}{3T}\frac{S_1^3}{\epsilon^2}, \end{aligned} \tag{5.97}$$

the limit in the brackets divided by b^3 gives a factor equal to $4/3$, the final result is the expression obtained at Eq.(5.41). Recall that $B = S_3/T$. The change to the inverse cosine was made because the first form traces both the domain and range of the inverse sine twice yielding incorrect results. The second form gives the correct results.

The other case we studied in the zero temperature limit was the opposite one where now the false vacuum is null and the true vacuum is a very small and negative number. In the finite temperature, this is described by

$$V_{\text{eff}}(\phi_+, T) = 0, \qquad V_{\text{eff}}(\phi_-, T) = -\epsilon. \tag{5.98}$$

Here we find that

$$\bar{r} = \frac{2S_1}{\epsilon - \kappa S_1^2} = \frac{\bar{r}_L}{1 - (\bar{r}_L/2D)^2}, \tag{5.99}$$

and the exponential term B is

$$\begin{aligned} B &= \frac{4\pi}{T} D^3 \epsilon \left[\frac{2b}{1-b^2} - \sinh^{-1}\left(\frac{2b}{1-b^2} \right) \right] \\ &= \frac{4\pi}{T} D^3 \epsilon \left[\frac{2b}{1-b^2} - \cosh^{-1}\left(\frac{1+b^2}{1-b^2} \right) \right]. \end{aligned} \tag{5.100}$$

Closing this, let us make one final remark if $(\bar{r}_L/2D)^2 > 1$ then the new vacuum state is not going sizeable enough to withstand the bubble nucleation and the decay never flourishes. This stabilizing effect is present at the zero-temperature vacuum decay too.

5.3.3 The general case

Proceeding now to the general case, neither the greater vacuum $V_{+,\text{eff}}$ nor the true is null. In this situation, we have to cope with more complicated equations though still reasonably tractable. Let us derive first the radius for which the bounce action is stationary. The derivative of wall contribution is the same again as in Eq.(5.89). For the interior someone gets

$$\begin{aligned} B'_{in} &= \left(-\frac{4\pi}{T\kappa} \left\{ \left[\frac{\arcsin \sqrt{\kappa |V_{-,\text{eff}}|}\bar{r}}{\sqrt{\kappa |V_{-,\text{eff}}|}} + \bar{r}\sqrt{1 - \kappa V_{-,\text{eff}} \bar{r}^2} \right] - (\phi_- \to \phi_+) \right\} \right)' \\ &= \frac{8\pi}{T\kappa} \frac{V_{-,\text{eff}} \kappa \bar{r}^2 - 1}{\sqrt{1 - \kappa V_{-,\text{eff}} \bar{r}^2}} - (\phi_- \to \phi_+). \end{aligned} \tag{5.101}$$

Solving the equation of the derivatives we can find

$$
\begin{aligned}
&B' = B'_{wall} + B'_{in} = 0 \Rightarrow \frac{8\pi}{T}\bar{r}S_1 + \frac{8\pi}{T}\frac{1}{\kappa}\frac{V_{-,\text{eff}}\kappa\bar{r}^2 - 1}{\sqrt{1-\kappa V_{-,\text{eff}}\bar{r}^2}} - \frac{8\pi}{T}\frac{1}{\kappa}\frac{V_{+,\text{eff}}\kappa\bar{r}^2 - 1}{\sqrt{1-\kappa V_{+,\text{eff}}\bar{r}^2}} = 0 \\
&\Rightarrow \bar{r}S_1\kappa = \sqrt{1-\kappa V_{+,\text{eff}}\bar{r}^2} - \sqrt{1-\kappa V_{-,\text{eff}}\bar{r}^2} \\
&\Rightarrow \bar{r}^2 S_1^2\kappa^2 = 1 - \kappa V_{+,\text{eff}}\bar{r}^2 - 2\sqrt{(1-\kappa V_{+,\text{eff}}\bar{r}^2)(1-\kappa V_{-,\text{eff}}\bar{r}^2)} + 1 - \kappa V_{-,\text{eff}}\bar{r}^2 \\
&\Rightarrow \bar{r}^2 S_1^2\kappa^2 - 2 + (V_{+,\text{eff}} + V_{-,\text{eff}})\kappa\bar{r}^2 = -2\sqrt{(1-\kappa V_{+,\text{eff}}\bar{r}^2)(1-\kappa V_{-,\text{eff}}\bar{r}^2)} \\
&\Rightarrow \bar{r}^2\kappa(S_1^2\kappa + V_{+,\text{eff}} + V_{-,\text{eff}}) - 2 = -2\sqrt{(1-\kappa V_{+,\text{eff}}\bar{r}^2)(1-\kappa V_{-,\text{eff}}\bar{r}^2)} \\
&\Rightarrow \bar{r}^4\kappa^2(S_1^2\kappa + V_{+,\text{eff}} + V_{-,\text{eff}})^2 - 4\bar{r}^2\kappa(S_1^2 + V_{+,\text{eff}} + V_{-,\text{eff}}) + 4 = 4(1-\kappa V_{+,\text{eff}}\bar{r}^2)(1-\kappa V_{-,\text{eff}}\bar{r}^2) \\
&\Rightarrow \bar{r}^4\kappa^2(S_1^2\kappa + V_{+,\text{eff}} + V_{-,\text{eff}})^2 - 4\bar{r}^2\kappa(S_1^2 + V_{+,\text{eff}} + V_{-,\text{eff}}) + \cancel{4} = \cancel{4} - 4V_{+,\text{eff}}\kappa\bar{r}^2 - 4V_{-,\text{eff}}\kappa\bar{r}^2 + 4V_{+,\text{eff}}V_{-,\text{eff}}\kappa^2 \\
&\Rightarrow \bar{r}^{\cancel{4}^2}\kappa^{\cancel{2}}(S_1^2\kappa + V_{+,\text{eff}} + V_{-,\text{eff}})^2 - 4\bar{r}^{\cancel{2}}\kappa(S_1^2 + V_{+,\text{eff}} + V_{-,\text{eff}}) = -4\kappa\bar{r}^{\cancel{2}}(V_{+,\text{eff}} + V_{-,\text{eff}}) + 4V_{+,\text{eff}}V_{-,\text{eff}}\bar{r}^{\cancel{4}^2}\kappa^{\cancel{2}} \\
&\Rightarrow \bar{r}^{\cancel{2}}\kappa - 4V_{+,\text{eff}}V_{-,\text{eff}}\kappa\bar{r}^2 = 4S_1^{\cancel{2}}\kappa + 4(V_{+,\text{eff}} + V_{-,\text{eff}} - V_{+,\text{eff}} - V_{-,\text{eff}}) \\
&\Rightarrow \bar{r}^2[(S_1^2\kappa + V_{+,\text{eff}} + V_{-,\text{eff}})^2 - 4V_{+,\text{eff}}V_{-,\text{eff}})] = 4S_1^2. \\
&\Rightarrow \bar{r}^2 = \frac{4S_1^2}{S_1^4\kappa^2 + 2S_1^2\kappa(V_{+,\text{eff}} + V_{-,\text{eff}}) + (V_{+,\text{eff}} + V_{-,\text{eff}})^2 - 4V_{+,\text{eff}}V_{-,\text{eff}}}.
\end{aligned}
\tag{5.102}
$$

This long procedure leads to

$$
\begin{aligned}
\bar{r}^2 &= \frac{4S_1^2}{\kappa^2 S_1^4 + 2\kappa S_1^2(V_{+,\text{eff}} + V_{-,\text{eff}}) + (V_{-,\text{eff}} - V_{+,\text{eff}})^2} \\
&= \frac{\bar{r}_L^2}{1 + 2(\bar{r}_L/2d)^2 + (\bar{r}_L/2D)^4}.
\end{aligned}
\tag{5.103}
$$

As before $\bar{r}_L$ is the radius in the absence of gravity

$$
\bar{r}_L = \frac{2S_1}{V_{+,\text{eff}} - V_{-,\text{eff}}}. \tag{5.104}
$$

Also,

$$
d^2 = \frac{1}{\kappa(V_{+,\text{eff}} + V_{-,\text{eff}})} \tag{5.105}
$$

and

$$
D^2 = \frac{1}{\kappa(V_{+,\text{eff}} - V_{-,\text{eff}})}. \tag{5.106}
$$

Now, let us evaluate the bounce action at this radius the small gravity limit. We have

$$
\begin{aligned}
B &= B_{wall} + B_{in} \\
&= \frac{4\pi}{T}\bar{r}^2 S_1 + \frac{4\pi}{T\kappa}\left(\bar{r}\sqrt{1-\kappa V_{+,\text{eff}}\bar{r}^2} - \bar{r}\sqrt{1-\kappa V_{-,\text{eff}}\bar{r}^2}\right) + B_{arc} \\
&\approx \frac{4\pi}{T}\bar{r}^2 S_1 - \frac{2\pi r_L^3}{T} + B_{arc} = \frac{2\pi r_L^3}{T} - \frac{2\pi r_L^3}{T} + B_{arc} \\
&= B_{arc},,
\end{aligned}
\tag{5.107}
$$

where, is the part with the arcsines of B_{in} at Eq.(5.94). Therefore we can write for the total bounce action

$$B = B_{arc} = \frac{4\pi}{T\kappa}\left[\frac{\arcsin\sqrt{\kappa V_{+,\text{eff}}}\bar{r}}{\sqrt{\kappa V_{+,\text{eff}}}} - \frac{\arcsin\sqrt{\kappa V_{-,\text{eff}}}\bar{r}}{\sqrt{\kappa V_{-,\text{eff}}}}\right]. \tag{5.108}$$

To check this let us take the limit in which κ goes to zero and find if it gives Linde's result,

$$\lim_{\kappa\to 0}\frac{4\pi}{T\kappa}\left[\frac{\arcsin\sqrt{\kappa V_{+,\text{eff}}}\bar{r}}{\sqrt{\kappa V_{+,\text{eff}}}} - \frac{\arcsin\sqrt{\kappa V_{-,\text{eff}}}\bar{r}}{\sqrt{\kappa V_{-,\text{eff}}}}\right] = \frac{2\pi}{3T}\bar{r}_L^3\epsilon = \frac{16\pi S_1^3}{3T\epsilon^2}, \tag{5.109}$$

in agreement with the result at Eq.(5.41).

According to [206] we can separate the zero gravity portion of the action, as Parke did at [178], and write

$$B = B_L r[(\bar{r}_L/2D)^2, D^2/d^2]. \tag{5.110}$$

There are many ways to write $r(x,y)$, two of them are given in the next expression,

$$\begin{aligned} r(x,y) &= \frac{3}{2x^{3/2}}\int_0^x \frac{z^{1/2}}{1+2yz+z^2}dz \\ &= \frac{3}{2\sqrt{2}x^{3/2}}\left[\frac{1}{\sqrt{y+1}}\arccos\frac{1-x}{\sqrt{1+2yx+x^2}} - \frac{1}{\sqrt{y-1}}\arccos\frac{1+x}{\sqrt{1+2yx+x^2}}\right]. \end{aligned} \tag{5.111}$$

This function shows all the features studied in the zero temperature case of Section 3.10 in Fig.3.4. In Fig.5.3 function $r(x,y)$ has been plotted for several values of y.

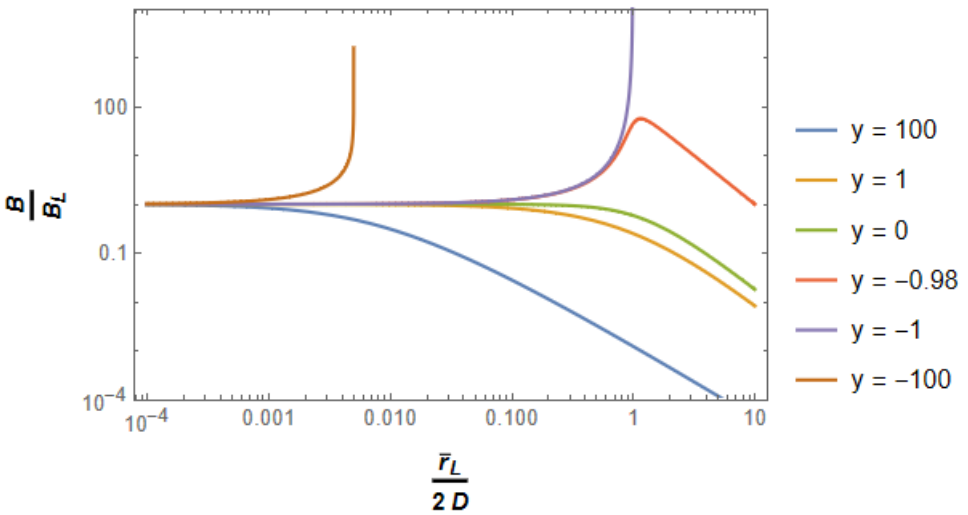

Figure 5.3: The function $B/B_L(x) = r(x)$, plotted for several values of $y = D^2/d^2$.

5.3.4 Applicability of the method

For these calculations to be valid, first $B \gg 1$ because the semi-classical limit must be valid, also the TWA will be valid under the condition that the length scales $|d|$, D, and $\bar{\rho}_0$ be much greater than the bubble wall thickness.

We assumed that the difference between the potential energy densities is small, equal to ϵ, but the requirement that the potentials be small never happened. So, a restrictive length scale is that of $|d|$.

The thickness can be determined as before by an approximate expression

$$\Delta\eta = \int_{(\phi_+ + 3\phi_-)/4}^{(3\phi_+ + \phi_-)/4} d\phi \{2[V_{0,\text{eff}}(\phi, T) - V_{0,\text{eff}}(\phi_\pm, T)]\}^{-1/2} \sim \frac{\Delta\phi}{\sqrt{\Delta V_{\text{eff}}}}. \tag{5.112}$$

From this and the definition of $|\lambda|$, we can find a restriction of the following form:

$$|\lambda| \gg \Delta\eta \Rightarrow \frac{\Delta V_{\text{eff}}}{|V_{\min,\text{eff}}|} \gg (\Delta\phi)^2\kappa \tag{5.113}$$

In the limit of weak gravity, the above can be satisfied by a moderately potential high barrier, as long as $\phi_+ - \phi_-$ is not great enough. As this difference or the gravitation becomes stronger the potential barrier has to be much higher than the two potential minima's values.

Finally, recall that we work in the high-temperature case where $T \gg 1/r$. The bounce action in this limit will be significantly smaller than it from the zero T limit by a factor:

$$B(T)/B(0) \sim \frac{1}{\bar{r}T} \sim \frac{\epsilon}{S_1 T}. \tag{5.114}$$

5.4 High-temperature vacuum decay: The non-minimal coupling case

5.4.1 Calculation of the bounce action

In a theory with a coupling term between R and the scalar field, as we have seen, the action is

$$S_M = \int d^4x\sqrt{-g}\left[\frac{R}{2\kappa} - \frac{1}{2}g^{\mu\nu}\partial_\mu\phi\partial_\nu\phi - \frac{1}{2}\xi R\phi^2 - U(\phi)\right]. \tag{5.115}$$

In the high-temperature phase transition scenario, the treatment of the problem and the field equations will be not much different from the previous paragraph where the coupling ξ was absent.

Here will be used again a metric of the form of Eqs.(5.71-5.73). This will lead to the same Ricci scalar of Eq.(5.77). Now, Let us derive the form of the Euclidean action in the usual way

$$\begin{aligned} S_E &= \frac{4\pi}{T}\int d\eta r^2\left(\frac{1}{2}\dot{\phi}^2 + V_{\text{eff}} - \frac{R}{2\kappa} + \frac{1}{2}\xi R\phi^2\right) \\ &\overset{(5.77)}{=} \frac{4\pi}{T}\int d\eta\left[r^2\left(\frac{1}{2}\dot{\phi}^2 + V_{\text{eff}}\right) + \frac{1}{\kappa}(2r\ddot{r} + \dot{r}^2 - 1) - \xi\phi^2(2r\ddot{r} + \dot{r}^2 - 1)\right] \\ &= \frac{4\pi}{T}\int d\eta\left[r^2\left(\frac{1}{2}\dot{\phi}^2 + V_{\text{eff}}\right) + \frac{1 - \kappa\xi\phi^2}{\kappa}(2r\ddot{r} + \dot{r}^2 - 1)\right] \\ &= \frac{4\pi}{T}\int d\eta\left[r^2\left(\frac{1}{2}\dot{\phi}^2 + V_{\text{eff}}\right) + \frac{1}{\kappa_{\text{eff}}}(2r\ddot{r} + \dot{r}^2 - 1)\right], \end{aligned} \tag{5.116}$$

where

$$\kappa_{\text{eff}}(\phi) = \frac{\kappa}{1 - \kappa\xi\phi^2}, \tag{5.117}$$

as Valerio Faraoni [207] notes in his book. Writing the action in this way we made to bring it in a similar form to this in the absence of coupling in Eq.(5.81).

For the next step, we will drop the second derivative term by integration by parts

$$\int d\eta \frac{1}{\kappa_{\text{eff}}}(2r\ddot{r} + \dot{r}^2 - 1) \to -\int d\eta \frac{1}{\kappa_{\text{eff}}}(\dot{r}^2 + 1) + \mathcal{O}(r\ddot{r})\Big|_0^{\eta_{max}} \tag{5.118}$$

and

$$\int d\eta \xi\phi^2(2r\ddot{r} + \dot{r}^2 - 1) \to -\int d\eta[\xi\phi^2(\dot{r}^2 + 1) + 4\xi\phi\dot{\phi}r\dot{r}] + \mathcal{O}(r\ddot{r})\Big|_0^{\eta_{max}}. \tag{5.119}$$

One can show that the scale factor r crosses zero at least once [190]. Without loss of generality, we chose value η of the first zero to be $\eta = 0$ and the second to be at η_{max}. Therefore, we can ignore the surface terms as always. Putting these results in Eq.(5.116) we get

$$S_E = \frac{4\pi}{T}\int d\eta \left[r^2\left(\frac{1}{2}\dot{\phi}^2 + V_{\text{eff}}\right) - \frac{1}{\kappa_{\text{eff}}}(\dot{r}^2 + 1) + 4\xi\phi\dot{\phi}r\dot{r}\right]. \tag{5.120}$$

We can now derive from this action the Euclidean equations of motion in an alternative way used in the other chapters. From the Euler-Lagrange equation, we can obtain the differential equation of the scalar field which is

$$\frac{\partial\mathcal{L}_E}{\partial\phi} - \frac{d}{dt}\left(\frac{\partial\mathcal{L}_E}{\partial\dot{\phi}}\right) = 0 \quad \Rightarrow \quad \ddot{\phi} + 2\frac{\dot{r}}{r}\dot{\phi} - \xi R\phi = V'_{\text{eff}}. \tag{5.121}$$

For the scale factor r, Euler-Lagrange gives a linear combination of the two Friedman-like equations. The second equation of interest can be derived from the Hamiltonian if it settled to zero. The trajectories in the phase space of this model are constrained on the energy surface $\mathcal{H} = 0$, and the Friedmann equation is an expression of such energy balance [208]

$$\begin{aligned}
&\mathcal{H} = \dot{\phi}\frac{\partial\mathcal{L}_E}{\partial\dot{\phi}} + \dot{r}\frac{\partial\mathcal{L}_E}{\partial\dot{r}} - \mathcal{L}_E = 0 \\
&\Rightarrow r^2\dot{\phi}^2 + 4\xi\phi\dot{\phi}r\dot{r} - \frac{2}{\kappa_{\text{eff}}}\dot{r}^2 + \cancel{4\xi\phi\dot{\phi}r\dot{r}} - r^2\left(\frac{1}{2}\dot{\phi}^2 + V_{\text{eff}}\right) + \frac{1}{\kappa_{\text{eff}}}(\dot{r}^2 + 1) - \cancel{4\xi\phi\dot{\phi}r\dot{r}} = 0 \\
&\Rightarrow r^2\dot{\phi}^2 + 4\xi\phi\dot{\phi}r\dot{r} - r^2\left(\frac{1}{2}\dot{\phi}^2 + V_{\text{eff}}\right) = \frac{1}{\kappa_{\text{eff}}}(\dot{r}^2 - 1).
\end{aligned} \tag{5.122}$$

If we solve this with respect to $\dot{r}^2$ we will get the first Friedmann equation

$$\begin{aligned}
\dot{r}^2 &= 1 + \kappa_{\text{eff}}r^2\left(\frac{1}{2}\dot{\phi}^2 - V_{\text{eff}} + 4\xi\phi\dot{\phi}\frac{\dot{r}}{r}\right) \\
&= 1 + \frac{\kappa r^2}{1 - \kappa\xi\phi^2}\left(\frac{1}{2}\dot{\phi}^2 - V_{\text{eff}} + 4\xi\phi\dot{\phi}\frac{\dot{r}}{r}\right).
\end{aligned} \tag{5.123}$$

It can easily be observed that both Eq.(5.121) and Eq.(5.123) are slightly modified from the equations of the previous subsection due to the coupling ξ. Euclidean action can be more simplified as we know by inserting this last equation in Eq.(5.120) in order to eliminate the first derivative term. This gives

$$S_E = \frac{8\pi}{T}\int d\eta \left(r^2 V_{\text{eff}} - \frac{1}{\kappa_{\text{eff}}}\right). \tag{5.124}$$

Going through the usual thin-wall approximation we will get for the wall contribution to the bounce action

$$\begin{aligned}
B_{wall} &= S_E(\phi) - S_E(\phi_+) \\
&= \frac{4\pi}{T}\bar{r}^2 \int_0^{\eta_{max}} d\eta[2(V_{\text{eff}} - V_{+,\text{eff}}) + \xi\frac{2}{\bar{r}^2}(\phi^2 - \phi_+^2)] \\
&\approx \frac{4\pi}{T}\bar{r}^2 \int_0^{\eta_{max}} d\eta[2(V_{0,\text{eff}} - V_{0,+,\text{eff}}) + \xi\frac{2}{\bar{r}^2}(\phi^2 - \phi_+^2)] \\
&\approx \frac{4\pi}{T}\bar{r}^2 \int_{\phi_-}^{\phi_+} d\phi\sqrt{2(V_{0,\text{eff}} - V_{0,+,\text{eff}}) + \xi\frac{2}{\bar{r}^2}(\phi^2 - \phi_+^2)} \\
&= \frac{4\pi}{T}\bar{r}^2 \int_{\phi_-}^{\phi_+} d\phi\sqrt{2(V_{0,\text{eff}} - V_{0,+,\text{eff}}) - \xi\frac{2}{\bar{r}^2}(\phi_+^2 - \phi^2)} \\
&= \frac{4\pi}{T}\bar{r}^2 \int_{\phi_-}^{\phi_+} d\phi\sqrt{2(V_{0,\text{eff}} - V_{0,+,\text{eff}})}\sqrt{1 - \xi\frac{2}{\bar{r}^2}\frac{\phi_+^2 - \phi^2}{2(V_{0,\text{eff}} - V_{0,+,\text{eff}})}} \\
&\approx \frac{4\pi}{T}\bar{r}^2 \int_{\phi_-}^{\phi_+} d\phi\left[\sqrt{2(V_{0,\text{eff}} - V_{0,+,\text{eff}})} - \frac{\xi}{\bar{r}^2}\frac{\phi_+^2 - \phi^2}{\sqrt{2(V_{0,\text{eff}} - V_{0,+,\text{eff}})}}\right] \\
&= \frac{4\pi}{T}\bar{r}^2\left[\int_{\phi_-}^{\phi_+} d\phi\sqrt{2(V_{0,\text{eff}} - V_{0,+,\text{eff}})} - \frac{C\xi}{\bar{r}}\right] = \frac{4\pi}{T}\bar{r}^2 S,
\end{aligned} \tag{5.125}$$

where $S = S_1 - C\xi/\bar{r}$ and S_1 is the usual surface tension. The C reflects the small correction of surface energy density and depends directly on the theory under study. For an effective potential of the form of Eq.(4.6), where $\phi \equiv \phi(T)$ we will get for the parameter C,

$$C = \frac{4\alpha}{\sqrt{\lambda}\bar{r}^2}. \tag{5.126}$$

Inside the wall, from Eq.(5.123) we have

$$d\eta = dr(1 - \kappa_{\text{eff}} r^2 V_{\text{eff}})^{-1/2}, \tag{5.127}$$

so that

$$\begin{aligned}
B_{in} &= -\frac{8\pi}{T}\int_0^{\bar{r}} dr\left\{\kappa_{\text{eff},-}^{-1}[1 - \kappa_{\text{eff},-} r^2 V_{-,\text{eff}}]^{1/2} - (\phi_- \to \phi_+)\right\} \\
&= \frac{4\pi}{T}\left\{\left[\frac{\arcsin\sqrt{\kappa_{\text{eff},-}|V_{-,\text{eff}}|}\bar{r}}{\kappa_{\text{eff},-}\sqrt{\kappa_{\text{eff},-}|V_{-,\text{eff}}|}} + \bar{r}\kappa_{\text{eff},-}^{-1}\sqrt{1 - \kappa_{\text{eff},-}V_{\text{-,eff}}\bar{r}^2}\right] - (\phi_- \to \phi_+)\right\}.
\end{aligned} \tag{5.128}$$

5.4.2 Analytical solutions

Let us investigate our problem in the usual simple case where the true vacuum is 0 (null) and the false vacuum is small and positive like Eq.(5.88). We find that the first derivative of the wall contribution to the bounce action is the same as in the non-coupling situation

$$B'_{wall} = \frac{8\pi}{T}\bar{r}S_1. \tag{5.129}$$

For the part inside the wall, we can write from the integral form of Eq.(5.128)

$$\begin{aligned} B_{in} &= -\frac{8\pi}{T}\int_0^{\bar{r}}\left[\frac{1}{\kappa_{\text{eff,-}}}-\frac{1}{\kappa_{\text{eff,+}}}(1-\kappa_{\text{eff,+}}r^2\epsilon)^{1/2}\right] \\ &= -\frac{8\pi}{T}\left[\frac{1}{\kappa_{\text{eff,-}}}\bar{r}-\int_0^{\bar{r}}\frac{1}{\kappa_{\text{eff,+}}}(1-\kappa_{\text{eff,+}}r^2\epsilon)^{1/2}\right] \\ &= -\frac{8\pi}{T}\left[\frac{1}{\kappa_{\text{eff,-}}}\bar{r}-\frac{\arcsin\sqrt{\epsilon\kappa_{\text{eff,+}}}\bar{r}}{2\sqrt{\epsilon\kappa_{\text{eff,+}}}\kappa_{\text{eff,+}}}-\frac{\bar{r}}{2\kappa_{\text{eff,+}}}\sqrt{1-\epsilon\kappa_{\text{eff,+}}r^2}\right]. \end{aligned} \tag{5.130}$$

If we differentiate the above expression with respect to $\bar{r}$ we will find

$$B'_{in} = -\frac{8\pi}{T}\left\{\frac{1}{\kappa_{\text{eff,-}}}+\frac{\epsilon\kappa_{\text{eff,+}}\bar{r}^2-1}{\kappa_{\text{eff,+}}\sqrt{1-\epsilon\kappa_{\text{eff,+}}\bar{r}^2}}\right\}. \tag{5.131}$$

Solving for $\bar{r}$ the below equation as usual

$$B' = B'_{wall} + B'_{in} = 0, \tag{5.132}$$

after a great amount of trivial algebra, we end up to

$$\bar{r} = \frac{2S_1(1-\kappa\xi\alpha^2)}{\kappa S_1^2+\epsilon-\kappa\epsilon\xi\alpha^2}, \tag{5.133}$$

where it is assumed that $\phi_-^2 \sim \phi_+^2 \sim \alpha^2$ to first order. Then, we can divide the radius into two parts,

$$\begin{aligned} \bar{r} &= \frac{2S_1}{\kappa S_1^2+\epsilon-\kappa\epsilon\xi\alpha^2}-\frac{2S_1\kappa\xi\alpha^2}{\kappa S_1^2+\epsilon-\kappa\epsilon\xi\alpha^2} \\ &= \frac{\bar{r}_L}{1+(\bar{r}_L/2D)^2-\kappa\xi\alpha^2}-\bar{r}_L\xi\frac{\kappa\alpha^2}{1+(\bar{r}_L/2D)^2-\kappa\xi\alpha^2}, \end{aligned} \tag{5.134}$$

where $\bar{r}_L = 2S_1/\epsilon$ is Linde's result in the absence of gravity and $D = (\kappa\epsilon)^{-1/2}$. We will expand the radius in first order to the coupling, keeping only linear terms of ξ

$$\bar{r}(\xi) \sim \bar{r}(0) + \bar{r}'(0)\xi. \tag{5.135}$$

The above expansion leads to the final expression of the radius which is

$$\begin{aligned} \bar{r} &= \frac{\bar{r}_L}{1+(\bar{r}_L/2D)^2}-\xi\frac{\bar{r}_L\alpha^2\kappa\left(\frac{\bar{r}_L}{2D}\right)^2}{[1+(\bar{r}_L/2D)^2]^2} \\ &= \bar{r}_{Lov,+}-\xi\frac{\bar{r}_L\alpha^2\kappa\left(\frac{\bar{r}_L}{2D}\right)^2}{[1+(\bar{r}_L/2D)^2]^2}, \end{aligned} \tag{5.136}$$

where $\bar{r}_{Lov,+}$ denotes the result obtained by Loveridge in Eq.(5.92) [206].

Someone can notice that Eq.(5.136) corresponds to Lee's result in the zero temperature case, demonstrated in the fourth chapter in Eq.(4.38). Here, we can observe also that there is no dependence on the parameter C. This is a reasonable result and can be justified, by recalling that the term containing C gives a zero derivative as a constant function of $\bar{r}$ in the wall contribution.

At this point

$$\begin{aligned} B_{wall} &= \frac{4\pi}{T}\bar{r}^2 S = \frac{4\pi}{T}\bar{r}^2(S_1 - \frac{C\xi}{\bar{r}^2}) \\ &= \frac{4\pi}{T}\left[\frac{\bar{r}_L^3}{(1+b^2)^2}\epsilon - C\xi - \frac{\xi\alpha^2\kappa b^2\epsilon\bar{r}_L^3}{(1+b^2)^2} + \frac{\bar{r}_L^3\epsilon\xi^2\alpha^4\kappa^2 b^4}{2(1+b^2)^4)}\right] \\ &= \frac{4\pi}{T}\left[\frac{\bar{r}_L^3}{(1+b^2)^2}\epsilon - C\xi - \mathcal{O}(b^2) + \mathcal{O}(b^4)\right] \end{aligned} \tag{5.137}$$

with $b = \bar{r}_L/2D$, and we will break B_{in} in three terms because they will be long enough. We first have

$$B_{in,I} = \frac{8\pi}{T\kappa_{\text{eff,-}}}\bar{r} = -\frac{8\pi}{T}D^2 A\epsilon\left(\frac{\bar{r}_L}{1+b^2} - \frac{\bar{r}_L\xi\alpha^2\kappa b^2}{1+b^2}\right), \tag{5.138}$$

$$B_{arc} = \frac{4\pi}{T\kappa_{\text{eff},+}}\frac{\arcsin\left(\sqrt{\kappa_{\text{eff},+}\epsilon}\bar{r}\right)}{\sqrt{\kappa_{\text{eff},+}\epsilon}} = \frac{4\pi}{T}D^3 A^{3/2}\epsilon\arcsin\left[A^{-1/2}\left(\frac{2b}{1+b^2} - \xi\frac{\alpha^2\kappa b^3}{(1+b^2)^2}\right)\right], \tag{5.139}$$

$$B_{sqrt} = \frac{4\pi}{T\kappa_{\text{eff},+}}\bar{r}\sqrt{1-\kappa_{\text{eff},+}\epsilon\bar{r}^2} = \frac{4\pi}{T}D^3\epsilon A\left(\frac{2b}{1+b^2} - \xi\frac{2\alpha^2\kappa b^3}{(1+b^2)^2}\right)\text{sqrt}\left[1 - \frac{4b^2}{A}\left(\frac{1}{1+b^2} - \xi\frac{\alpha^2\kappa b^2}{(1+b^2)^2}\right)\right]. \tag{5.140}$$

where $A = 1 - \kappa\xi\alpha^2$. The overall B_{in} is

$$B_{in} = B_{in,I} + B_{arc} + B_{sqrt}. \tag{5.141}$$

If we make a small gravity approach, and we will keep only $\mathcal{O}(b)$ terms like Loveridge we take

$$\begin{aligned} B_{in} &= -\frac{8\pi}{T\kappa_{\text{eff,-}}}\bar{r} + \frac{4\pi}{T\kappa_{\text{eff},+}}\left[\frac{\arcsin\left(\sqrt{\kappa_{\text{eff},+}\epsilon}\bar{r}\right)}{\sqrt{\kappa_{\text{eff},+}\epsilon}} + \bar{r}\sqrt{1-\kappa_{\text{eff},+}\epsilon\bar{r}^2}\right] \\ &= -\frac{8\pi}{T}D^2\epsilon\frac{\bar{r}_L}{1+b^2}A + \frac{4\pi}{T}D^3\epsilon\left[A^{3/2}\arcsin\left(\frac{2b}{1+b^2}A^{-1/2}\right) + \frac{2b}{1+b^2}A\sqrt{1-\mathcal{O}(b^2)}\right] \\ &\approx -\frac{8\pi}{T}D^2\epsilon\frac{\bar{r}_L}{1+b^2}A + \frac{4\pi}{T}D^3\epsilon A\left[A^{1/2}\arcsin\left(\frac{2b}{1+b^2}A^{-1/2}\right) + \frac{2b}{1+b^2}\right], \end{aligned} \tag{5.142}$$

The sum of these two contributions gives the overall B

$$\begin{aligned} B &= B_{wall} + B_{in} \\ &= \frac{4\pi}{T}\frac{\bar{r}_L^3}{(1+b^2)^2}\epsilon - \frac{4\pi}{T}C\xi - \frac{8\pi}{T}D^2\epsilon\frac{\bar{r}_L}{1+b^2}A + \frac{4\pi}{T}D^3\epsilon A\left[A^{1/2}\arcsin\left(\frac{2b}{1+b^2}A^{-1/2}\right) + \frac{2b}{1+b^2}\right] \\ &= \frac{4\pi}{T}D^3\epsilon\left[\frac{8b^3}{(1+b^2)^2} - \frac{4b}{1+b^2}A + A^{3/2}\arcsin\left(\frac{2b}{1+b^2}A^{-1/2}\right) + \frac{2b}{1+b^2}A\right] - \frac{4\pi}{T}C\xi \\ &= \frac{4\pi}{T}D^3\epsilon\left[A^{3/2}\arcsin\left(\frac{2b}{1+b^2}A^{-1/2}\right) - \frac{2b}{1+b^2}A\right] - \frac{4\pi}{T}C\xi. \end{aligned} \tag{5.143}$$

Now, if we perform a first-order Taylor expansion to $B(\xi)$, we will get our final expression

$$\begin{aligned} B(\xi) &\sim B(0) + \xi B'(0) \\ &= B_{Lov,+} - \frac{4\pi}{T}\xi\left[\frac{1}{2}D^3\epsilon\alpha^2\kappa\left(3\arcsin\left(\frac{2b}{1+b^2}\right) - \frac{6b}{1-b^4}\right) + C\right] + \mathcal{O}(\xi^2) \\ &= B_{Lov,+} - \frac{4\pi}{T}\xi\left[\frac{1}{2}D^3\epsilon\alpha^2\kappa\left(3\arccos\left(\frac{1-b^2}{1+b^2}\right) - \frac{6b}{1-b^4}\right) + C\right] + \mathcal{O}(\xi^2). \end{aligned} \tag{5.144}$$

As someone could expect the bounce action consists of two terms, the first one $B_{Lov,+}$ is Loveridge's result obtained in Eq.(5.96) for the null true vacuum case and the second one is linear to the coupling ξ.

The opposite case where the false vacuum is zero and the true is small and negative equal to $-\epsilon$ can also be worked out rather simply. Here we take

$$\begin{aligned} \bar{r} &= \frac{\bar{r}_L}{1-(\bar{r}_L/2D)^2} + \xi\frac{\bar{r}_L\alpha^2\kappa\left(\frac{\bar{r}_L}{2D}\right)^2}{[1-(\bar{r}_L/2D)^2]^2} \\ &= \bar{r}_{Lov,-} + \xi\frac{\bar{r}_L\alpha^2\kappa\left(\frac{\bar{r}_L}{2D}\right)^2}{[1-(\bar{r}_L/2D)^2]^2} \end{aligned} \tag{5.145}$$

and

$$\begin{aligned} B(\xi) &\sim B(0) + \xi B'(0) \\ &= B_{Lov,+} + \frac{4\pi}{T}\xi\left[\frac{1}{2}D^3\epsilon\alpha^2\kappa\left(3\sinh^{-1}\left(\frac{2b}{1+b^2}\right) - \frac{6b}{1-b^4}\right) - C\right] + \mathcal{O}(\xi^2) \\ &= B_{Lov,+} + \frac{4\pi}{T}\xi\left[\frac{1}{2}D^3\epsilon\alpha^2\kappa\left(3\cosh^{-1}\left(\frac{1-b^2}{1+b^2}\right) - \frac{6b}{1-b^4}\right) - C\right] + \mathcal{O}(\xi^2), \end{aligned} \tag{5.146}$$

here again, the first term in each equation is the standard result obtained by Loveridge.

In both cases we see that the positive non-minimal coupling constant makes the materialization of the bubble more likely, that is, it diminishes B standing at the exponential of the decay rate and makes the radius of the bubble when it materializes smaller. For the negative non-minimal coupling constant ξ, it makes the materialization of the bubble less likely and makes the radius of the bubble at its moment of materialization bigger. The same conclusions were drawn for the zero temperature transitions in the fourth chapter.

Chapter 6

Cosmological phase transitions at ultra-late times

In a context where the observed cosmological constant has emerged as a meta-stable vacuum of a scalar field, it may decay to the true vacuum at present or in the future. In this chapter we estimate the scale of the produced true vacuum bubbles, assuming that the decay rate Γ/V of this process is similar to the Hubble expansion rate H_0, denoting a vacuum decay at present times. We find that the typical scale of the bubbles at formation is sub-mm. Then we investigate their evolution which is dependent on the scalar field mass. We will see that if the field mass is larger than $0.003\,eV$ the dominant bubble tension is leading them to total collapse. For smaller scalar field mass a bubble can expand after formation with the speed of light as we already know. The research begins with a simple model for a metastable Λ and is extended to the modified gravity case (bubbles of gravitational constant G_{eff}).

All of these will be studied since first a brief review of the Hubble tension will be made. One of the most important challenges the standard cosmological model is submitted to is the tension of the Hubble parameter. Could a proposed present-day phase transition of the gravitational constant within a true vacuum, which is supported by observational data and suggested as a potential resolution to the Hubble tension, effectively address this significant problem in modern Cosmology?

6.1 The Hubble tension

Let us discuss the well-known Hubble tension curiosity in brief. Local measurements of the Hubble constant H_0, using a distance ladder approach are measured constantly at significantly higher values than those given by the angular scale of fluctuations of the CMB in the frameworks of the ΛCDM model.

Combined local direct measurements of the Hubble constant are in 5σ tension with indirect measurements of H_0 with CMB. This tension can be larger if combinations of local measurements are used [59][209][210]. The best fit value given by the Planck/ΛCDM is $H_0 = 67.4 \pm 0.5\,km\,s^{-1}\,Mpc^{-1}$ [76]. The local measurements, using Cepheid calibrators by the SH0ES Team, giving a larger value at $H_0 = 73.04 \pm 1.04 \pm 0.5\,km\,s^{-1}\,Mpc^{-1}$. These numbers giving rise to a near 5σ tension [59][211–213]. In the previous analysis by the SH0ES Team a value of $H_0 = 73.2 \pm 1.3\,km\,s^{-1}\,Mpc^{-1}$ leading to a 4.2σ tension with the predictions given by the CMB observations [214][215]. In general, a wide range of local observations are appearing to be consistently larger than the Planck/ΛCDM measurement of the Hubble constant. The statistical significance using different methods of local measurements can vary but is always large

[59][209][210].

A variety of theoretical models entered the challenge of addressing the Hubble tension. Many of these amendments introduce new physics, such as early dark energy, modifications of the standard model neutrino sector, extra radiation, primordial magnetic fields, or varying fundamental constants, with the aim of reducing the sound horizon at recombination [216–218]. Others demand a deformation of the Hubble expansion rate $H(z)$ at late times [219][220] or indicate a transition/recalibration of the SnIa absolute luminosity due to late time new physics. A proposed rapid transition in the value of the relative effective gravitational constant $\mu_G = G_{eff}/G_N$ at $z \approx 0.01$ could explain the lower luminosity of local supernovae, thus giving a solution to the H_0 crisis [130]. A relevant talk about this subject and the ΛCDM crisis in general by Prof. Leandros Perivolaropoulos could be enlightening [221]. Also, for more detailed discussions of the proposed newphysics models someone can check [57][59][61].

In the year 2021 Mortsell et al. and Perivolaropoulos with Skara [222–224] re-analyzed the Cepheid[1] data used to extract a value of the Hubble constant H_0 by the calibration of Type Ia supernovae (SnIa)[2] More concretely, they analyzed the color-luminosity relation of Cepheids in anchor galaxies and SnIa host galaxies by identifying the color-luminosity relation for each individual galaxy instead of enforcing a universal color-luminosity relation to correct the near-infrared (NIR) Cepheid magnitudes. This process reveals a systematic brightening of Cepheids at distances larger than about $20\,Mpc$ which could be enough to resolve the Hubble tension. An even more recent re-analysis of the Cepheid data by Perivolaropoulos and Skara [226] on August of 2022 indicates a transition at a critical distance of $50\,Mpc$ as we will see later in this chapter.

In addition to that Perivolaropoulos and Skara investigated the effects of variation of the Cepheid calibration empirical parameters, these are the color-luminosity and the Cepheid absolute magnitude, and found some precious hints for the presence of a fundamental physics transition taking place at a time more recent than $150\,Myrs$ ago. This transition could be a false vacuum decay of the metastable constant Λ to its true vacuum, and this is the point where one of the goals of this thesis is taking an essential shape. The magnitude of this hypothetical transition leads to the consistent with the CMB's indications for the value of H_0, thus the Hubble tension is eliminated. To be noted as well that a first-order phase transition at present times is indicated in the context of the Tully-Fisher data in a recent paper by Alestas et al. [227].

6.2 A model for a metastable cosmological constant

6.2.1 Bubble radius scale

Let us suppose that the metastable cosmological constant Λ decays from its false vacuum to its true one through quantum tunneling, then as we know a bubble will be formed. In this section, we will try to address this bubble's scale using results familiar to us from the previous chapters.

In the second chapter we derived the analytical bounce action form as it was given in the papers by Coleman and de Lucia [131][133], we found that the bounce action in the exponential of the decay rate will be

$$B = \frac{27\pi^2}{2\epsilon^3}\left(\frac{\epsilon\bar{\rho}}{3}\right)^4 = \frac{\pi^2}{6}\epsilon\bar{\rho}^4, \tag{6.1}$$

[1] A Cepheid variable is a type of star that pulsates radially, varying in both diameter and temperature and producing changes in brightness with a well-defined stable period and amplitude.

[2] A Type Ia supernova (read: "type one-A") is a type of supernova that occurs in binary systems (two stars orbiting one another) in which one of the stars is a white dwarf. The other star can be anything from a giant star to an even smaller white dwarf [225].

where, $\bar{\rho}$ is the bubble radius and

$$\epsilon = U(\phi_+) - U(\phi_-) = \Delta U, \tag{6.2}$$

in a theory where the potential can be written as

$$U = U_0 + O(\epsilon). \tag{6.3}$$

Here, the first term of the potential will take our familiar form

$$U_0 = \frac{\lambda}{8}\left(\phi^2 - \frac{m^2}{\lambda}\right)^2. \tag{6.4}$$

Also, let us recall the decay rate expression resulting from the WKB approximation

$$\frac{\Gamma}{V} = Ae^{-B}. \tag{6.5}$$

All of these results, in the context of a complete treatment of the quantum mechanical tunneling from a metastable false vacuum state to the true, were discussed extensively in the second chapter of this thesis.

According to Linde, [171] and similar to the work of Abdala and Lima et al. [228–230] we can posit A in dimensional grounds and write $A \sim m^4$. So, given the potential we could use the expression for B, Eq.(6.1), to calculate the decay rate. Substituting Eq.(6.1) in Eq.(6.5) we find for it

$$\frac{\Gamma}{V} = Ae^{-B} \sim m^4 e^{-\frac{\pi^2\bar{\rho}^4\epsilon}{6}}. \tag{6.6}$$

We wish to study a present time decay, so we have to make some claims. To begin with, let us recall that the present age of the Universe in the current ΛCDM model is exactly the inverse of the Hubble parameter, H_0^{-1} [231]. The number of bubble nucleation events integrated over a Hubble volume ($d_H^3 \approx H_0^{-3}$) and the age of the Universe ($t_U \approx H_0^{-1}$) estimated us [232][233]

$$\mathcal{N} = (\Gamma/V)H_0^{-4}, \tag{6.7}$$

therefore, if we set $\mathcal{N} = 1$, for one bubble nucleation event we will come up with

$$\frac{\Gamma}{V} = H_0^4. \tag{6.8}$$

What we did was simply to set the decay rate to an upper bound for a slow, time-independent, uncompleted transition, then the decay time $t_d \sim H_0^{-1}$ will be comparable to the age of the Universe. Using Eq.(6.6) and Eq.(6.8) we can now solve for the bubble radius as

$$\frac{\Gamma}{V} = H_0^4 \Rightarrow \frac{m}{H_0^4} \approx e^{\epsilon\bar{\rho}^4} \Rightarrow \bar{\rho} \approx 4\epsilon^{-1/4}\ln\left(\frac{m}{H_0}\right)^{1/4}, \tag{6.9}$$

and for the potential barrier, we infer from the above result that

$$S_1 = \frac{\epsilon\bar{\rho}}{3} = \left(\frac{8\epsilon^3}{27\pi^2}\ln\frac{m}{H_0}\right)^{1/4}. \tag{6.10}$$

For an order of magnitude estimation we can ignore the logarithmic terms, since for a wide range of values of $m > H_0$ we get $[\ln(m/H_0)]^{1/4} \sim \mathcal{O}(1)$, thus we can write

$$\bar{\rho} \sim \epsilon^{-1/4} \tag{6.11}$$

and

$$S_1 \sim \epsilon^{3/4}. \tag{6.12}$$

The order of magnitude analysis made in the previous statement is equivalent to setting $B \sim \mathcal{O}(1)$. This is not a concern for our calculation because B needs to be at least $\mathcal{O}(10^3)$ in order to change our estimates. All these are for a slow, time-independent, uncompleted transition. Similarly, in a time-dependent transition, it is usually the case that, as the false vacuum starts decaying, the decay rate is highly suppressed with $B \sim \mathcal{O}(10^4)$, and as the transition proceeds the bounce action evolves to smaller values till $B \sim \mathcal{O}(1) - \mathcal{O}(10^3)$(depending on the exact model) and the transition can proceed rapidly. Thus our estimates are valid for the relevant range where the transition is taking place with non-negligible probabilities.

In the context of the thin-wall approximation for a metastable cosmological[3] constant transition, ϵ has to be small enough for accurate results [234]. Then we can write for the ϵ,

$$H_0^2 \sim \frac{8\pi G}{3}\epsilon \Rightarrow \epsilon \sim \frac{3}{8\pi G}H_0^2 \sim 10^{-2}M_{Pl}^2 H_0^2 \Rightarrow \epsilon \sim 10^{-48}\text{Gev}^4. \tag{6.13}$$

Conclusively, this leads to $\bar{\rho} \sim 100\,\mu$m and $S_1 \sim 10^{-36}\text{Gev}^3$. As we expected from the literature the radius scale of the bubble is negligible with respect to cosmological distances. Since the bubble wall traces out the hyperboloid $\bar{\rho}^2 = -t^2 + x^2 + y^2 + z^2$, we can assume, as it has been already discussed in Chapter 2 and in the literature, that the bubble forms with essentially zero radius and expands at the speed of light.

As an example of a time-dependent, pre-recombination transition we might take the New Early Dark Energy (NEDE) model. Assuming a bubble with a thin wall, for a decay rate close to $10^{-108}\,eV^4$, we get $B \sim 250$, this gives $\bar{\rho} \sim 3.5 \times \epsilon^{-1/4}$ and $S_1 \sim 1.2 \times \epsilon^{3/4}$, for when the transition becomes relevant. It is worth noting that we take similar results at the order of μm for the bubble radius scale if we perform the corresponding analysis for the finite temperature case, using the results of chapter four.

6.2.2 The critical bubble mass

In the present segment we will try to address the following question: "What is the critical mass of these bubbles below which the bubbles expand?". Let us first start with the computation of the total energy of a thin-walled bubble, in the absence of gravitation, at the time of its materialization. The energy is the sum of two terms, a negative volume term, and a positive surface term. The energy of the world outside, E_{out}, vanishes before the bubble's materialization and whatever else barrier penetration may do, it does not violate the conservation of energy [133]. Thus, we can write

$$\begin{aligned} E &= E_{in} + E_{wall} + \cancelto{0}{E_{out}} \\ &= -\frac{4}{3}\pi\bar{\rho}^3\epsilon + 4\pi\bar{\rho}^2 S_1 \\ &= -\frac{4}{3}\pi\bar{\rho}^3\epsilon + 4\pi\bar{\rho}^2 m^3, \end{aligned} \tag{6.14}$$

in the last line the substitution $S_1 \sim m^3$ was made, which is true in the theory under study discussed in the second chapter [131].

Now, let us define what the critical radius is. The smallest particle size below which an aggregate is thermodynamically stable is known as the critical radius. In other words, it is the

[3]Here the role of the cosmological constant is played by the energy scale of the false vacuum $\Lambda = \epsilon = \Delta U$

minimum radius at which a new phase inclusion, such as a bubble, droplet, or solid particle, becomes viable and starts to expand as a result of atoms or molecules grouping together (in a gas, liquid, or solid matrix) [235].

This basic concept does not change as far as the cosmological phase transitions are concerned. When the false vacuum decays, the lower-energy true vacuum forms through our familiar process known as bubble nucleation [236–239]. In this procedure, the real vacuum is contained in a bubble that forms due to instanton effects. Because energy is utilized as the fields pass over a potential barrier preventing access to the true vacuum, the bubble's walls have a positive surface tension. While the latter is proportional to the square of the bubble's radius, the former tends to be in the third power as we depicted in Eq.(6.14) above. The critical radius of the bubble will be at the peak of the total energy, thus is found by optimization, setting the derivative of the total energy to zero,

$$\frac{\mathrm{d}E_{tot}}{\mathrm{d}\bar{\rho}} = 0 \Rightarrow 8\pi\bar{\rho}m^3 - 4\pi\bar{\rho}^2\epsilon = 0 \Rightarrow \bar{\rho} \equiv \bar{\rho}_c = \frac{2m^3}{\epsilon} \overset{(6.13)}{=} \frac{2m^3}{M_{Pl}^2 H_0^2}. \tag{6.15}$$

From the definition of the critical radius with the aid of Eq.(6.11) and Eq.(6.13) we can write

$$\frac{\bar{\rho}}{\bar{\rho}_c} \approx \frac{(M_{Pl}H_0)^{-1/2}}{(M_{Pl}H_0)^{-2}m^3} = \frac{(M_{Pl}H_0)^{3/2}}{m^3} \approx \frac{10^{-7.5}\,eV}{m^3} \geq 1 \Rightarrow m \leq 10^{-2.5}\,eV, \tag{6.16}$$

Since,

$$\begin{aligned} H_0 &\sim 10^{-42}\,GeV = 10^{-33}\,eV, \\ M_{Pl} &\sim 10^{19}\,GeV = 10^{28}\,eV. \end{aligned} \tag{6.17}$$

Consequently, the critical mass of the bubble is

$$m_c \sim 0.003\,eV. \tag{6.18}$$

Therefore, from Eq.(6.16) we conclude that for $m \leq m_c$ the bubble will expand and for $m > m_c$ it will collapse.

6.3 The effects of gravity

In Section 3.7 we derived the bounce action Eq.(3.60), in the presence of gravity. That was

$$B = \frac{B_0}{[1 + (\bar{\rho}/2D)^2]^2}, \tag{6.19}$$

where the parameters denoted as "0" are the classic Coleman's results in the absence of gravity and $D \sim \sqrt{3/\epsilon}M_{Pl}$. Let us investigate the $(\bar{\rho}/2D)^2$ term in Eq.(6.19), this leads us to

$$\frac{\bar{\rho}^2}{(2D)^2} = \frac{\bar{\rho}^2\epsilon}{12M_{Pl}^2} \overset{(6.13)}{=} \frac{\bar{\rho}^2 H_0^2}{100} \approx \left(\frac{3\times 10^5}{100\times 10^{25}}\right)^2 \approx 10^{-63} \ll 1. \tag{6.20}$$

Thus the gravitational correction is not relevant in the case of a cosmological constant transition as described above. These corrections become important close to the Planck scale (as $\rho_0 \sim D$) where we expect the semi-classical approximation scheme for the decay rate to break down. In these scales, we can write for the bounce action

$$B \sim \epsilon\bar{\rho}^4 \sim \epsilon D^4 \sim M_{Pl}^4/\epsilon, \tag{6.21}$$

and the decay rate gets a huge exponential suppression unless the potentials are comparable to the Planck mass. Thus, when gravity is strong enough to significantly modify the transition rates the bubble nucleation events will have become irrelevant for times less than or comparable to H_0^{-1}.

6.4 A model for the nucleation of cosmological phase transitions

6.4.1 Description and mathematical structure

In order to estimate the bubble scale after the course of the transition we will use a simple model developed by Hogan [240]. We will go through the development of the final expression of the scale step by step. It is noted that the expression going to be derived is a better fit for a universe dominated by radiation but the differences between that and the more correct expression occur in the argument of the logarithm, so it can be used for a modern-day phase transition, as we will see later [241].

Let us think about a time-dependent phase transition at the radiation epoch in a finite temperature and denote the decay rate per unit time per unit volume as $\Gamma(t)$ (where we have suppressed the explicit volume element in the denominator)

$$\Gamma(t) = CT^4 e^{-B(t)}, \tag{6.22}$$

where, C, is some dimensionless constant. We will adopt the following functional form for the exponential term in terms of temperature, which is sufficiently general to describe thermal or quantum tunneling

$$B = b(T)(T_c/T - 1)^{-\beta}, \tag{6.23}$$

where $\beta > 0$, $b > 0$ and $d\ln b/d\ln T > 0$ (but is of $\mathcal{O}(1)$ if the second factor is not $\gg 1$). Here β is assumed to be constant but this model can be efficient if it is also left to vary slowly with some restrictions. It is noted that in this functional form we can write the theories discussed in Subsection 5.2.3. In the above equation, T_c is our well-known critical temperature where the phase of the universe described by a potential becomes metastable. In this temperature $B \to \infty$ as $T \to T_c$.

At the time t the fraction of space occupied by bubbles of true vacuum nucleated is $F = 1 - p$ [242][243], where p denote the percentage of the volume still in the old phase of the false vacuum, during the course of the transition [243], then

$$p(t) = \exp\left[-\int_0^t dt' \Gamma(t') a^3(t') V(t,t')\right] = \exp(-P(t)), \tag{6.24}$$

where

$$V(t,t') = \frac{4\pi}{3}\left[\int_{t'}^t dt'' \frac{1}{a(t'')}\right]^3 \tag{6.25}$$

is the comoving volume of a bubble at time t when nucleated at time t' with negligible radius, as shown in the previous pages, and expanding at almost light speed. In the above $a(t)$ is the usual FLRW scale factor and $P(t)$ is the integral in the exponential function. We will derive step by step Eq.(6.24) in Appendix G.

Let us make some comments about p before we proceed with our process. In a time-dependent transition, one can separate three regimes where p goes from $p \gg 1$ to $p \sim \mathcal{O}(1)$ and $p \gg 1$. In the first extreme value of p, an observer is situated in a universe undergoing a slow, yet-to-be-completed phase transition, and if this observer is not in a bubble interior, which is very possible for $p \gg 1$ then the conclusion made is that he will observe a regular FLRW homogenous and isotropic universe. If however, some observers live inside a bubble then their observations will be of an inhomogeneous and in general anisotropic universe, therefore there will be a break to

the cosmological principle. On the other extreme, $p \ll 1$, the phase transition has already been completed and the universe under observation will have a distinct expansion history from our base ΛCDM model.

The function $P(t)$ is approximately valid until the time t_1 the new phase percentage of space, F, approaches one ($F(t_1) \cong 1$). When this happens the space will almost be in its true vacuum, $p \ll 1$, and an adequate approximation for F in a time $t \leq t_1$ would be

$$\begin{aligned} F = 1 - p = 1 - e^{-P(t)} \approx 1 - 1 + P(t) = P(t) \Rightarrow \\ \Rightarrow F \approx \int_0^t dt' \Gamma(t') a^3(t') V(t, t'). \end{aligned} \tag{6.26}$$

We will define $\delta t = (F/\dot{F})_{t_1}$ as the characteristic time of the transition, in this time most of the matter changes from one phase to another. This δt is also the characteristic radius of the bubbles because a bubble expands with almost the speed of light ($c = 1 \Rightarrow R_b = c\delta t = \delta t$). As $\dot{F}$ gets bigger the rate of bubbles occupying space increases and the characteristic time gets smaller. The comoving number density of larger bubbles of radius r which nucleated at t_r is exponentially small and goes like $\Gamma(t_r)dr$. Next, we will write

$$\Gamma(t) \approx \Gamma(t_1)\delta(t - t_1), \tag{6.27}$$

assuming that initially, the rate of bubbles formed is small, but as $t \to t_1$ and $\Gamma(t) \to \Gamma(t_1)$ there is a timescale δt in which a lot of bubbles form with non-negligible volume. Therefore, Eq.(6.27) allows us to rewrite Eq.(6.26) as

$$\begin{aligned} F(t) &\approx \int_0^t dt' \Gamma(t') a^3(t') V(t, t') \\ &\approx \int_0^t dt' \Gamma(t_1) \delta(t' - t_1) a^3(t') V(t, t') \\ &= \Gamma(t_1) V(t, t_1) a^3(t_1), \end{aligned} \tag{6.28}$$

where in the third line the properties of delta "function" were used. Now,

$$\begin{aligned} \left.\frac{\mathrm{d}F(t)}{\mathrm{d}t}\right|_{t=t_1} &= \frac{\mathrm{d}F(t_1)}{\mathrm{d}t_1} \\ &\approx \frac{\mathrm{d}\Gamma(t_1)}{\mathrm{d}t_1} V(t_1, t_1) a^3(t_1) + \cdots \\ &= \left.\frac{\mathrm{d}\Gamma(t)}{\mathrm{d}t}\right|_{t=t_1} V(t, t_1) a^3(t_1). \end{aligned} \tag{6.29}$$

Then,

$$\begin{aligned} \delta t = \left(\frac{F}{\dot{F}}\right)_{t_1} \approx \left(\frac{\Gamma}{\dot{\Gamma}}\right)_{t_1} = \frac{CT^4 e^{-B(t_1)}}{-CT^4 \dot{B}(t_1) e^{-B(t_1)}} \Rightarrow \\ \Rightarrow \delta t \approx \left(\frac{\Gamma}{\dot{\Gamma}}\right)_{t_1} = -\frac{1}{\dot{B}(t_1)}. \end{aligned} \tag{6.30}$$

Well, δt is the time bubbles have to nucleate and expand with the speed of light ($c = 1$) and $\delta t \ll t$. To find the volume of the bubble we will use the "Midpoint Rule". For an integral with

bounds of integration, let us call them, d and e we will divide our interval $[d, e]$ in N smaller intervals with equal width

$$\Delta x = \frac{e-d}{N}. \tag{6.31}$$

The intervals will be denoted in the following way,

$$[x_0, x_1], [x_1, x_2], \cdots [x_{N-1}, x_N], \tag{6.32}$$

with $x_0 = d$ and $x_N = e$. Let us denote as x_i^* the midpoint of each interval, then the "Midpoint Rule" states

$$\int_b^e f(x)dx \approx \Delta x[f(x_1^*) + f(x_2^*) + \cdots + f(x_N^i)]. \tag{6.33}$$

Hence, the volume of such a bubble is

$$V \cong \left[\int_{t_1}^{t_1+\delta t} dt' \frac{1}{a(t')}\right]^3 \times \frac{4\pi}{3} \overset{(\delta t << t)}{\approx} \left[\frac{\delta t}{a(t_1)}\right]^3 \times \frac{4\pi}{3} \sim (\delta t)^3 \times \frac{4\pi}{3}, \tag{6.34}$$

as it was referred before in this thesis, the bubbles have a characteristic radius of δt. Bubbles formed in negligible volume and radius $V(t_1, t_1 + \delta t) \sim V(t_1, t_1) \neq 0$.

From the above results, we can approximate the $F(t_1)$ integral in a different manner

$$\begin{aligned} F(t_1) &\cong \int_0^{t_1} dt' \Gamma(t') V(t, t') a^3(t') \\ &\cong \delta t \Gamma(t_1) V(t_1, t_1) a^3(t_1) \\ &= \delta t \times C T^4 e^{-B_1} \frac{(\delta t)^3}{\cancel{a^3(t_1)}} \times \frac{4\pi}{3} \times \cancel{a^3(t_1)} \\ &= C(4\pi/3)(T\delta t)^4 e^{-B_1} \cong 1, \end{aligned} \tag{6.35}$$

where $B_1 \equiv B(t_1)$. The value of the action B at the time of the catastrophic bubble formation is then approximately

$$B_1 \cong 4 \ln[T\delta t (4\pi C/3)^{1/4}]. \tag{6.36}$$

Let A denote the logarithmic derivative of the action in units of the cosmological time,

$$A(t) \equiv -(\dot{B}/B)_t. \tag{6.37}$$

Finally, let us define the ratio of the transition time δt to the cosmological time as

$$\Delta \equiv (\delta t/t) \cong (B_1 A_1)^{-1}, \tag{6.38}$$

where we used Eq.(6.30) and the definition of the logarithmic derivative. This interesting quantity determines the characteristic size of bubbles. We will see in the following subsection that A_1 is of $\mathcal{O}(1)$.

In order to proceed we have to find a relation between the time and the temperature. Something we can do is try to rewrite the Friedmann equation in terms of time and temperature. To obtain the general evolution of the Universe it is enough to assume that is given by the simple perfect fluid form

$$T^\mu_\nu = \mathrm{diag}(\epsilon, -p, -p, -p). \tag{6.39}$$

where ϵ is the energy density and p the pressure. The Friedman equation can be written as

$$\frac{\dot{a}^2}{a^2} = \frac{8\pi G}{3}\epsilon - \frac{k}{a^2}, \tag{6.40}$$

where k is $1, 0, -1$ depending on the shape of the universe.

In the case of the very early Universe, the radiation-dominated epoch, when matter behaves like radiation, pressure, and energy are given by

$$p = \frac{1}{3}\epsilon = \frac{\pi^2}{90} g_* T^4, \tag{6.41}$$

where g_* is the effective number of relativistic degrees of freedom. The value of this number is increased by every relativistic bosonic and fermionic degree of freedom with unity and 7/8 respectively. The above relation is an idealization, valid for free particles. The inclusion of the interactions between particles modifies it slightly even at temperatures far away from any phase transition [244].

For a flat Universe ($k = 0$) in the radiation era we have

$$a(t) \sim t^{1/2} \Rightarrow \dot{a}(t) \sim \frac{1}{2} t^{-1/2}. \tag{6.42}$$

Also, $G \sim 1/M_{Pl}^2$ and the Friedmann equation becomes

$$\begin{aligned} &\frac{\dot{a}^2}{a^2} = \frac{4}{45}\pi^3 \frac{1}{M_{Pl}^2} g_* T^4 \Rightarrow \left(\frac{1}{2}\frac{t^{-1/2}}{t^{1/2}}\right)^2 = \frac{4}{45}\pi^3 \frac{1}{M_{Pl}^2} g_* T^4 \Rightarrow \\ &\Rightarrow t^2 T^4 = \frac{45}{16\pi^3}\frac{M_{Pl}^2}{g_*}, \end{aligned} \tag{6.43}$$

from Eq.(6.43) we obtain the final expression which is

$$t = T^{-2}\frac{M_{Pl}}{\sqrt{g_*}}\sqrt{\frac{45}{16\pi^3}}. \tag{6.44}$$

This important equation gives the relation between temperature and time in a radiation-dominated Universe.

From Eq.(6.38) $\delta t = t\Delta$. Using this information in Eq.(6.36) we can write

$$B_1 \cong 4\ln[T\delta t(4\pi C/3)^{1/4}] = 4\ln[Tt\Delta(4\pi C/3)^{1/4}]. \tag{6.45}$$

Then, the reverse of the quantity Δ becomes

$$\begin{aligned} \Delta^{-1} \cong B_1 A_1 &= 4A_1 \ln[(45/16\pi^3(T^{-1} M_{Pl} g_*^{-1/2}\Delta(4\pi C/3)^{1/4}] \\ &= 4A_1\{\ln(M_{Pl}/T) + \ln[g_*^{-1/2}\Delta(45/16\pi^3)^{1/2}(4\pi C/3)^{1/4}]\}. \end{aligned} \tag{6.46}$$

The second term of the above expression may be neglected due to the enormous discrepancy in the scales of T and M_{Pl} [240]. Finally, the ratio of the typical bubble size at the end of the phase transition will be

$$\Delta \cong [4A_1 \ln(M_{Pl}/T)]^{-1}. \tag{6.47}$$

This is a result that is insensitive to parameters C or g_*, and remains valid even if the crude estimation of Eq.(6.35) is wrong by several orders of magnitude according to Hogan [240].

We stated before that A_1 is of $\mathcal{O}(1)$ or greater, but how do we know that this quantity is not actually very small? For the form adopted for the action in Eq.(6.23) and the definition of A we get after some trivial algebra

$$A = \frac{1}{2}\frac{\mathrm{d}\ln b}{\mathrm{d}\ln T} + \frac{1}{2}\beta(1 - T/T_c)^{-1}, \tag{6.48}$$

which is always $\geq O(1)$ from our assumption about b. We will need the results obtained here in a following section.

6.4.2 Approximation of the logarithmic derivative of the action

Let us make an approximate calculation of A_1 to check if it is of $\mathcal{O}(1)$. If we impose a transition time growing for $\delta t \sim 150\, Myrs$, then we have from Eq.(6.45)

$$B_1 \sim 4\ln\left[1.6\times 10^{27}\left(\frac{4\pi}{3}\right)^{1/4}\right] + \ln C \sim 253 + \ln C, \tag{6.49}$$

where $\delta t \sim 0.8\times 10^{31}\, eV^{-1}$ and $T = 2.7^o K \sim 0.002\, eV$ were used. Parameter C is inside the logarithm so it will not affect B_1 that much if $C \gg 1$ or $C \ll 1$. Assuming that C is of $\mathcal{O}(1)$ then

$$A_1 \sim \frac{t}{\delta t}B_1^{-1} \sim \frac{4.3\times 10^{17}\,\cancel{sec}}{4.7\times 10^{15}\,\cancel{sec}} 4\times 10^{-3} \sim 0.4 \sim \mathcal{O}(1). \tag{6.50}$$

6.5 The non-minimal coupling case: Bubbles of Gravitational Constant

6.5.1 The bubble radius at the moment of nucleation

In this section, we will calculate the radius scale at the moment of the nucleation in the non-minimal coupling case [181] for a late time transition of the gravitational constant. The mechanism consists of the scalar field slowly rolling towards one of its minima during the expansion history, eventually arriving there at low redshift. If this minimum is metastable, there will be a decay rate associated with the transition which will then turn on at very late times. We will consider only the first scenario for transitions from de-Sitter ($U_+ = \epsilon$) to flat space ($U_- = 0$). We are going to ignore the gravitational correction, as it was shown, its contribution was at the class scale of 10^{-63}.

If the coupling $\xi \ll 1$, then naturally $\bar{\rho} \sim \bar{\rho}_0 \sim 10\mu\, m$, but let us check what is going on if the coupling is stronger, around $\mathcal{O}(1)$. We will use Eq.(4.46) in the case of interest, a transition from de-Sitter space to Minkowski space. In this scenario, the equation becomes

$$B_{\mathrm{TW}} = 2\pi^2\left(\bar{\rho}^3 S_1 + \xi\bar{\rho}C_1 - \frac{2}{3}\frac{\left((1-\bar{\rho}^2\kappa_+\epsilon)^{3/2} - 1\right)}{\kappa_+^2\epsilon} - \frac{\bar{\rho}^2}{\kappa_-}\right) \tag{6.51}$$

The requirements will be the same as in the model of the metastable cosmological constant studied previously. That is, $\epsilon \sim 10^{-48}\, GeV^4$ and the following equation

$$\Gamma/V = H_0^4 \to m^4 e^{-B_{TW}} = H_0^4. \tag{6.52}$$

In order to solve this equation we will expand B_{TW} in small gravity ($\kappa \to 0$). This expansion gives

$$B_{\rm TW} = \frac{1}{2}\pi^2\left(4C_1\xi\bar{\rho} - \bar{\rho}^4\epsilon + 4\bar{\rho}^3 S_1\right) - \frac{1}{12}\kappa\pi^2\bar{\rho}^6\epsilon^2 + \mathcal{O}(\kappa^2). \tag{6.53}$$

Hence, our demand for an ultra-late time transition becomes

$$\frac{1}{2}\pi^2\left(4C_1\xi\bar{\rho} - \bar{\rho}^4\epsilon + 4\bar{\rho}^3 S_1\right) - \frac{1}{12}\kappa\pi^2\bar{\rho}^6\epsilon^2 = \ln\left(m^4/H_0^4\right). \tag{6.54}$$

We will use the scales obtained in the simple case, and we will try to find the radius for a field mass scale of the order

$$m \sim m_{crit} \sim 10^{-3}\, eV. \tag{6.55}$$

Also, we will take that $\ln(m^4/H_0^4) \sim \epsilon\bar{\rho}_0^4$ for the simple case and we will substitute in the equation of B_{TW} the dimensionless variables in order to solve the problem approximately in *Mathematica* for several values of ξ in the interval $[0, 5]$. The dimensionless variables are the same used in the numerical bounce solutions obtained in the second, third and fourth chapter

$$\frac{\lambda}{m^4}U(\phi) = \tilde{U}(\tilde{\phi}), \quad \frac{\lambda\phi^2}{m^2} = \tilde{\phi}^2, \quad \frac{\lambda\epsilon}{m^4} = \tilde{\epsilon}, \quad m\eta = \tilde{\eta}, \quad m\rho = \tilde{\rho}, \quad \frac{m^2}{\lambda}\kappa = \tilde{\kappa}. \tag{6.56}$$

Consequently, the equation to solve, in the mass scale we chose is the following

$$\frac{1}{2}\pi^2\left(4\tilde{C_1}\xi\tilde{\bar{\rho}} - \tilde{\bar{\rho}}^4\tilde{\epsilon} + 4\tilde{\bar{\rho}}^3\tilde{S}_1\right) - \frac{1}{12}\tilde{\kappa}\pi^2\tilde{\bar{\rho}}^6\tilde{\epsilon}^2 = 0.03. \tag{6.57}$$

In the table above we demonstrate couples of real solutions of the equation for different values of ξ. As may one observe, for $\xi = 0$, $\bar{\rho}_1$ and $\bar{\rho}_2$ tend to ρ_0 result. We would achieve more accurate results if we did not choose to focus on the order of magnitude of the different quantities, but in the end, our goal is to show that in the modified gravity case with non-minimal coupling the radius at the moment of the nucleation in a present-day transition remains negligible with respect to the cosmological distances for values of $\xi \sim \mathcal{O}(1)$. For instance, if $\xi = 1$, then $\bar{\rho}_1 = m_{crit}^{-1}\tilde{\bar{\rho}}_1 \sim 0.002\,\mu m$ and $\bar{\rho}_2 = m_{crit}^{-1}\tilde{\bar{\rho}}_2 \sim 3600\,\mu m$, negligible in both cases but with a five order of magnitude difference. Recall that $\bar{\rho}_0 \sim 10\,\mu m$.

ξ	$\tilde{\bar{\rho}}_1$	$\tilde{\bar{\rho}}_2$
0.0	0.561442	3.99042
0.00001	0.552694	3.99345
0.0001	0.476	4.02033
0.1	0.0012678	9.41467
0.2	0.0006339	11.3941
0.5	0.00025356	14.8634
1.0	0.00012678	18.3129
3.0	0.00004226	25.7379
5.0	0.000025356	30.2418

Table 6.1: Real solutions $\tilde{\bar{\rho}}_1$, and $\tilde{\bar{\rho}}_2$ of Eq.(6.57) for several values of the coupling ξ.

6.5.2 Theoretical estimation of the scale

We can get a theoretical prediction of the spatial extent of the gravitational constant bubbles at the end of the phase transition using the formula derived in Hogan's model section. Although Eq.(6.47) is strictly valid only for radiation-dominated epochs, the differences between that and the more correct expression occur in the argument of the logarithm and are therefore becoming insignificant because $M_{Pl} \gg T$ [241]. For a very recent false vacuum decay with vacuum energy comparable to the cosmological constant the scale of the produced bubbles is

$$R_b = \Delta/H_0, \tag{6.58}$$

using $T = 2.7^{o}\, K \sim 2 \times 10^{-4}\, eV$, as the temperature of the photon background at the onset of the phase transition and A_1 is an $\mathcal{O}(1)$[4] constant. We also have that $\Delta \sim 1/300 A_1$, and with $H_0 = 70\, km\, sec^{-1}\, Mpc^{-1}$ in Eq.(6.47) we obtain

$$R_b \sim 45 \times A_1^{-1}\, Mpc, \tag{6.59}$$

in our case R_b will be in the range of $9\, Mpc - 90\, Mpc$, which is clearly within the area of transition scales favored by the Cepheid data according to the analysis by Perivolaropoulos and Skara [226][5] and by the Tully-Fisher data as indicated by [131][132][227][245].

The data indications coincide with the bubble scale evolved if the transition was triggered almost at $\delta t \sim 150\, Myrs$ ago, then we would have

$$R_b \sim \delta t = 48.6\, Mpc. \tag{6.60}$$

The indicated transition by the Cepheid data could be interpreted as a result of a first-order phase transition occurring very recently due to a decay of the false vacuum. Then, hypothetically we could live in a bubble universe with a radius within $40-50\, Mpc$ where a first-order scalar-tensor physics transition has occurred. If this bubble was created at the recent $150\, Myrs$ ($z \sim 0.01$) ago, then we would not have been able to observe other true vacuum bubbles since light from them may not have reached us yet. In that case, there would be no apparent large-scale violation of the cosmological principle. A fundamental physics transition like this, such as a gravitational constant transition, could eliminate the Hubble tension.

A perfect question to be asked is why a fundamental physics transition occurred at $z \sim 0.01$? In the following two subsections, we will give a brief picture of the latest constraints on the evolution of the gravitational constant obtained by local and non-local methods, then we will search for the observational effects and hints indicating a bubble nucleation at $z \sim 0.01$.

6.5.3 The effective gravitational constant G_{eff}

The most general action of the non-minimal coupling case in four dimensions has the following form [187]

$$S = \int d^4x\sqrt{-g}\left[\frac{F(\phi)}{2}R - \frac{1}{2}g^{\mu\nu}\partial_\mu\phi\partial_\nu\phi - V(\phi)\right] + S_m \tag{6.61}$$

[4]Generally, the order of magnitude of a number is the smallest power of 10 used to represent that number. To work out the order of magnitude of a number N, first N is expressed in the following form: $N = a \times 10^b$ where $0.5 \leq a \leq 5$. Then b represents the order of magnitude of the number.

[5]The present paper is a reanalysis of [224] where there the transition indicated by the Cepheid data was located at $15 - 20\, Mpc$.

where S_m is the action related to the Lagrangian $\mathcal{L}_m\left[\psi_m; g_{\mu\nu}\right]$ of the matter source. The $F(\phi)$ function of the field describes the non-minimal coupling, encapsulating the effects of a varying gravitational constant in the physical Jordan frame.

In this brief section, we will show that the varying G_{eff} is proportional to F^{-1}. In order to achieve that we are going to vary the action with respect to the inverse metric,

$$\begin{aligned}
\delta S = 0 \Rightarrow \int d^4x\, \delta\sqrt{-g}\left[\frac{F(\phi)}{2}R - \frac{1}{2}g^{\mu\nu}\partial_\mu\phi\partial_\nu\phi - V(\phi)\right] + \delta S_{matter} + \\
+ \int d^4x\sqrt{-g}\left[F(\phi)\delta R - \frac{1}{2}\,\delta g^{\mu\nu}\partial_\mu\phi\partial_\nu\phi\right] = 0 \Rightarrow \\
\Rightarrow \int d^4x\,\sqrt{-g}\Big[-\frac{1}{2}g_{\mu\nu}\left(\frac{F(\phi)}{2}R - \frac{1}{2}g^{a\beta}\partial_a\phi\partial_\beta\phi - V(\phi)\right) + \frac{\delta S_m}{\sqrt{-g}\delta g^{\mu\nu}} + \frac{F(\phi)}{2}R_{\mu\nu} - \nabla_\mu\nabla_\nu\frac{F(\phi)}{2} + \\
+ g_{\mu\nu}\nabla_\sigma\nabla^\sigma\frac{F(\phi)}{2} - \frac{1}{2}\partial_\mu\phi\partial_\nu\phi\Big]\delta g^{\mu\nu} = 0 \Rightarrow -\frac{F(\phi)}{2}\frac{g_{\mu\nu}}{2}R + \frac{1}{4}g_{\mu\nu}g^{a\beta}\partial_a\phi\partial_\beta\phi + \frac{V(\phi)}{2}g_{\mu\nu} - \\
-\frac{T^{matter}_{\mu\nu}}{2} + \frac{F(\phi)}{2}R_{\mu\nu} - \nabla_\mu\nabla_\nu\frac{F(\phi)}{2} + g_{\mu\nu}\nabla_\sigma\nabla^\sigma\frac{F(\phi)}{2} - \frac{1}{2}\partial_\mu\phi\partial_\nu\phi = 0 \xrightarrow{\times\frac{2}{F(\phi)}} R_{\mu\nu} - \frac{1}{2}g_{\mu\nu}R + \\
+\frac{1}{2F(\phi)}g_{\mu\nu}g^{a\beta}\partial_a\phi\partial_\beta\phi + \frac{V(\phi)}{F(\phi)}g_{\mu\nu} - \frac{T^{matter}_{\mu\nu}}{F(\phi)} - \frac{1}{F(\phi)}\nabla_\mu\nabla_\nu F(\phi) + \frac{g_{\mu\nu}}{F(\phi)}\nabla_\sigma\nabla^\sigma F(\phi) - \frac{1}{F(\phi)}\partial_\mu\phi\partial_\nu\phi = 0 \\
\Rightarrow F(\phi)G_{\mu\nu} = T^{matter}_{\mu\nu} + \nabla_\mu\nabla_\nu F(\phi) + \partial_\mu\phi\partial_\nu\phi - \frac{1}{2}g_{\mu\nu}g^{a\beta}\partial_a\phi\partial_\beta\phi - V(\phi)g_{\mu\nu} - g_{\mu\nu}\nabla_\sigma\nabla^\sigma F(\phi),
\end{aligned} \tag{6.62}$$

where the identities proved in Appendix E were used. In the above, $G_{\mu\nu} = R_{\mu\nu} - \frac{1}{2}Rg_{\mu\nu}$ is the Einstein tensor. The representation of Eq.(6.62) constitutes the generalized Einstein's equations for the case of modified gravity.

We can write our expression in an alternative form

$$G_{\mu\nu} = \frac{1}{F(\phi)}(T^{matter}_{\mu\nu} + T^{(\phi)}_{\mu\nu}) = \frac{1}{F(\phi)}T^{total}_{\mu\nu}. \tag{6.63}$$

In Eq.(6.63) $T^{(\phi)}_{\mu\nu} = \nabla_\mu\nabla_\nu F(\phi) + \partial_\mu\phi\partial_\nu\phi - \frac{1}{2}g_{\mu\nu}g^{a\beta}\partial_a\phi\partial_\beta\phi - V(\phi)g_{\mu\nu} - g_{\mu\nu}\nabla_\sigma\nabla^\sigma F(\phi)$. Someone can notice that the term $1/F(\phi)$ is playing the role of the effective gravitational constant $8\pi G_{eff}$ in this theory. In models described by modified gravity theories, the Universe consists of matter and a scalar field that plays the role of dark energy.

In scalar-tensor theories, in general, the effective Newton's constant with respect to the redshift z is given by [120, 246]

$$G_{eff} = \frac{1}{F(\phi)}\left(\frac{2F + 4\left(\frac{dF}{d\phi}\right)^2}{2F + 3\left(\frac{dF}{d\phi}\right)^2}\right) = \frac{1}{F(\phi)}\frac{F(\phi) + 2\left(\frac{dF}{d\phi}\right)^2}{F(\phi) + \frac{3}{2}\left(\frac{dF}{d\phi}\right)^2} \propto \frac{1}{F(\phi)}. \tag{6.64}$$

In the case of interest, studied in Chapter 4, where $F(\phi) = \frac{1}{\kappa} - \xi\phi^2$, the effective constant will be

$$G_{eff} \propto \frac{1}{\frac{1}{\kappa} - \xi\phi^2}. \tag{6.65}$$

The approximation in the above equations is for consistency with solar system tests, which indicate that $\frac{dF}{d\phi} \sim \frac{dF}{dz} \sim 0$ (see [247, 248]) and holds true only for low redshifts.

6.5.4 Constraints on the variability of the gravitational constant

Variation of the gravitational constant was originally postulated by Dirac in his classic paper [125] and still remains a key component of many theories that try to resolve the tensions resulting between local observations and them from cosmological measurements. A varying gravitational constant, related to the expectation value of some dynamical scalar field, in the prism of a gravitational transition at $z \sim 0.01$ could resolve the Hubble tension (more about varying fundamental constants of physics can be found at [249, 250]).

In many modified gravity theories, including scalar-tensor theories, the strength of gravitational interactions G_{eff} measured in Cavendish-type experiments measuring the force between masses, with the famous Newton's law of universal gravitation

$$F = G_{eff}\frac{m_1 m_2}{r^2} \tag{6.66}$$

is distinct from the Planck mass corresponding to G_N that determine the cosmological background expansion rate

$$H^2 = \frac{8\pi G_N}{3}\rho_{tot}. \tag{6.67}$$

In the case of scalar-tensor theories involving a scalar field ϕ and a non-minimal coupling $F(\phi)$ we have shown that the gravitational interaction strength will be of the form of Eq.(6.64). Whereas, the Planck mass-related G_N will be

$$G_N = \frac{1}{F}. \tag{6.68}$$

It should be stated that most current astrophysical and cosmological constraints on gravitational constant constrain the time derivative of G_{eff} at specific times, the most usual assumption in such models is a smooth power-law evolution of G_{eff}, or constrain changes of the Planck mass-related G_N instead of the effective Newton's constant (CMB and nucleosynthesis constraints [251]). So, a conclusion that can be drawn is that these studies may be less sensitive in detecting rapid transitions of G_{eff} at low z.

A collection of the current constraints on the evolution of G_{eff} and G_N can be found in Table 5.1, where the experimental constraints from local and cosmological time scales on the time variation of the gravitational constant are reviewed. The physics involved in these methods is in such diversity from method to method, and the resulting upper bounds differ by several orders of magnitude. Most of these constraints are obtained from systems in which gravity has not an insignificant role, in some methods can be the motion of celestial bodies of the solar system, and in others, the constraints come out from astrophysical and cosmological systems. They are mainly related to the comparison of a gravitational time scale, e.g., period of orbits, with a non-gravitational time scale. The constraints can be distinguished into two types, one from observations on cosmological scales and the other from local, inner galactic, or astrophysical scales. The strongest constraints to date come from lunar ranging experiments.

Let us now clarify the content of the table. In the first column, the used method is listed. The second column contains the upper bound $\left|\frac{\Delta G}{G}\right|_{max}$ of the fractional change of G during the corresponding timescale. An assumption of a smooth evolution of the gravitational constant is involved in most of these bounds. The third column presents the upper bound on the normalized time derivative $\left|\frac{\dot{G}}{G}\right|_{max}$. The fourth column is an approximate time scale over which each experiment is averaging each variation, and in the fifth column, the corresponding article on the appearance of each bound is referred. Also, to be noted that entries with a star (*) indicate constraints on G_N, while the rest of them refer to G_{eff}.

Method	$\left\lvert\frac{\Delta G_{\text{eff}}}{G_{\text{eff}}}\right\rvert_{max}$	$\left\lvert\frac{\dot{G}_{\text{eff}}}{G_{\text{eff}}}\right\rvert_{max}$ (yr^{-1})	Time Scale (Yr)	References
Lunar ranging		7.1×10^{-14}	24	[252]
Solar system		4.6×10^{-14}	50	[253, 254]
Pulsar timing		3.1×10^{-12}	1.5	[255]
Strong Lensing		10^{-2}	0.6	[256]
Orbits of binary pulsar		1.0×10^{-12}	22	[257]
Ephemeris of Mercury		4×10^{-14}	7	[258]
Exoplanetary motion		10^{-6}	4	[259]
Hubble diagram SnIa	0.1	1×10^{-11}	$\sim 10^8$	[260]
Pulsating white-dwarfs		2.0×10^{-12}	0	[261]
Viking lander ranging		4×10^{-12}	6	[262]
Helioseismology		1.25×10^{-13}	4×10^9	[263]
Gravitational waves	8	5×10^{-8}	1.3×10^8	[264]
Paleontology	0.1	2×10^{-11}	4×10^9	[265]
Globular clusters		35×10^{-12}	$\sim 10^{10}$	[266]
Binary pulsar masses		4.8×10^{-12}	$\sim 10^{10}$	[267]
Gravitochemical heating		4×10^{-12}	$\sim 10^8$	[268]
Strong lensing		3×10^{-1}	$\sim 10^{10}$	[256]
Big Bang Nucleosynthesis *	0.05	4.5×10^{-12}	1.4×10^{10}	[251]
Anisotropies in CMB *	0.095	1.75×10^{-12}	1.4×10^{10}	[269]

Table 6.2: Solar system, astrophysical and cosmological constraints on the evolution of the gravitational constant. Methods with a star (*) constrain G_N, while the rest constrain G_{eff}. The latest and strongest constraints are shown for each method.

Some further constraints maybe could be obtained from an extended analysis of other astrophysical and geophysical–climatological data of Earth paleontology. Multiple types of solar system anomalies were discussed in [270], and this article could be a good starting point for further research in the framework of the gravitational transition hypothesis. For example, an interesting issue, is the 'Faint young Sun paradox' [271, 272], which involves an inconsistency between geological findings and solar models about the temperature of the Earth about four billion years ago.

6.5.5 Hints of a gravitational transition at $z = 0.01$

In a recent article by Perivolaropoulos and Skara [226] after the reproduction of the SH0ES baseline model results a transition was allowed[6] to the value of any one of the four parameters of the Cepheid+SnIa sample at a given distance D_c or cosmic time t_c. These parameters are: the fiducial luminosity of SnIa M_B and Cepheids M_W and the two parameters (b_W and Z_W) standardizing Cepheid luminosities with period and metallicity.

The results were exciting on the occasion of an M_B transition at $D_c \cong 50\,Mpc$ or about 160 million years ago. More specifically, the best fit value of the Hubble parameter falls from

[6]This means the addition of a single degree of freedom in the analysis. In Appendix H it is shown what is meant by this statement.

$H_0 = 73.04 \pm 1.04\, km\, s^{-1}\, Mpc^{-1}$ to $H_0 = 67.32 \pm 4.64\, km\, s^{-1}\, Mpc^{-1}$ which is in agreement with the Planck measurement. This is a decent hint for a transition behavior that resolves the Hubble tension, and it is still apparent when the inverse distance ladder constraint on M_B is taken into account in the data processing [130, 273, 274]. This constraint states that

$$M_B^{P18} = -19.401 \pm 0.027. \tag{6.69}$$

Then, the uncertainty for H_0 drops significantly ($H_0 = 68.2 \pm 0.8\, km\, s^{-1}\, Mpc^{-1}$).

At the same critical distance, D_c, related indications of a transitional behavior are observed for the other three key parameters of the study, even if in that situation, the Hubble constant's best fit value is not dramatically altered, so we will focus our attention on the M_B transition hint.

As it has been repeated many times in this thesis a transition could be a result of a sudden change in a physics constant, during the last $200\, Myrs$ in the context of a first-order phase transition which gives arise to a gravitational constant bubble whose profile studied in the previous sections. But how do we allow for a transition to the four parameters of the SH0ES analysis? A transition of one of the Cepheid calibration parameters can be implemented by replacing one of the four modeling parameters in the $\mathbf{q}$ vector with two corresponding parameters one for high and one for low distances (recent cosmic times). More about the SH0ES analysis and answers to questions like: "What exactly the $\mathbf{q}$ vector is?" can be found in Appendix H.

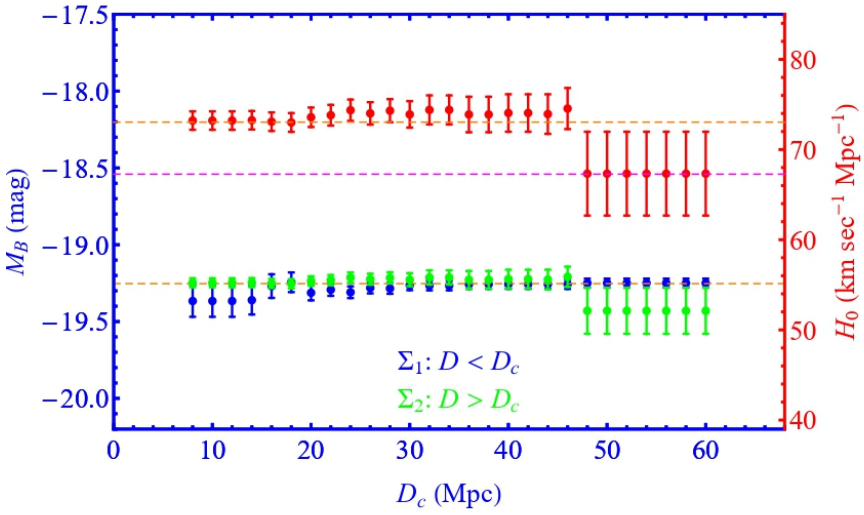

Figure 6.1: The best fit values with uncertainties for the high-low D bin of SnIa absolute magnitude M_B (green and blue points) and for H_0 (red points). This generalization of the SH0ES baseline analysis allows for a transition of M_B. The best fit parameter values as shown as functions of the critical transition D_c. Dotted lines correspond to the SH0ES R21 best fit and to the Planck18/ΛCDM best fit for H_0 (taken from [226])

Let us proceed to a brief, qualitative commentary on this research. In Fig.6.1, where a M_B transition is allowed at $D_c > 47\, Mpc$, the best fit value of H_0 drops spontaneously near the best fit Planck18/ΛCDM around $67\, km\, sec^{-1}\, Mpc$. The appearance of this effect is of great value because it arises with no prior or other information from the inverse distance ladder results. The increased uncertainties in the area of the transition around $47\, Mpc$ can be justified by the fact

that the most distant usable Cepheid hosts are few, and specifically three, compared to the sample in lower distances.

The same behavior is observed, in a modified version of the model analysis with the addition of the inverse distance ladder constraint on M_B of Eq.(6.69). The result is depicted in Fig.6.2. Conclusively, the M_B transition degree of freedom resolves the H_0 tension both in the absence of the inverse distance ladder constraint and in the presence of it. Also, to be noted that in the case where the M_B constraint is present, the model with the M_B transition degree of freedom at almost $50\,Mpc$ is strongly preferred over the baseline SH0ES model as indicated by the model selection criteria. For an extensive analysis of all of these, we refer the reader to the work of Perivolaropoulos and Skara [226] and more specifically in Table 4, where the results of all transition models are shown in great detail.

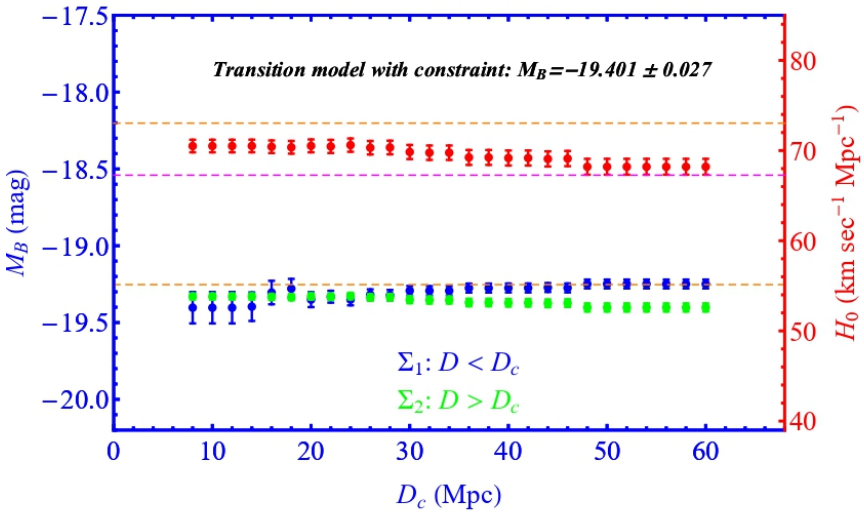

Figure 6.2: The new constraints on H_0 and on the parameters $M_B^{>}$ and $M_B^{<}$ emerging after implementing the inverse distance ladder constraint from Eq.(6.69) on the high distance bin of the M_B transition model (taken from [226]).

Finally, in Fig.6.3 we can clearly see the appearance of a transition hint, the green point of the absolute magnitude M_B transition model is below the red data point corresponding to the constant M_B SH0ES model. In this figure with the red points are shown the corresponding binned Cepheid+SnIa host values of M_B obtained from the baseline SH0ES model, with the green color being the points obtained by the transition model and the blue ones are the inverse distance ladder calibrated binned M_B of the Hubble flow SnIa of the Pantheon dataset.

It is worth commenting that in one of their articles [227], a year older than [226], Alestas, Antoniou, and Perivolaropoulos used a specific statistic on a robust dataset of 118 Tully–Fisher datapoints to demonstrate the existence of evidence for a transition in the evolution of the baryonic Tully-Fisher relation (BTFR). Using Monte Carlo simulations that compare the real Tully-Fisher dataset with homogenized datasets constructed by the BTFR, a transition is indicated in the best-fit values of BTFR parameters at distances $D_c \cong 9\,Mpc$ and/or $D_c \cong 17\,Mpc$. It is noted that this result is in agreement with the first Skara's and Perivolaropoulos' paper on Cepheid calibrators parameters transition indicating one at a distance in the range between 10 and $20\,Mpc$. As they

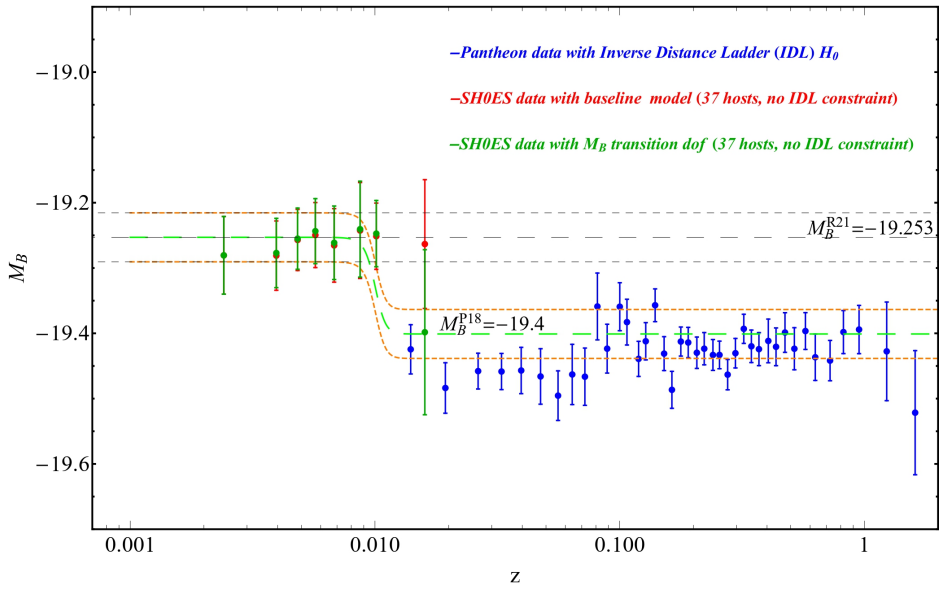

Figure 6.3: The binned (5 host bins with 2 hosts in last bin where $z > 0.01$) Cepheid+SnIa host values of M_B obtained assuming the baseline SH0ES model (red points) and the M_B transition model ($D_c = 50\,Mpc$, green points) are shown along with the inverse distance ladder calibrated binned M_B of the Hubble flow SnIa of the Pantheon dataset (blue points). When the transition degree of freedom is allowed, the data excite it and a hint for a transition appears (the green data point of the transition model is clearly below the red point corresponding to the constant M_B SH0ES baseline model) (taken from [226]).

refer, such a transition could be interpreted as a systematic effect or as a transition of the effective Newton constant with a 10% lower value at early times, with the transition taking place about 80 million years ago or less.

This $\Delta M_B \sim -0.2$ transition shown in the figure can be achieved if we assume a power law dependence of the luminosity

$$L \sim G_{eff}^{-b} \tag{6.70}$$

where $b > 0$ and $\mathcal{O}(1)$. The simplest hypothesis that can be made is $L \sim m_c$,[130] where m_c is the Chandrasekhar mass. This choice leads to $b = 3/2$ [275].

But why we chose the Chandrasekhar mass? This depends on the effective gravitational constant and the mass per electron m' [276] with the following expression:

$$m_c \simeq \frac{3}{m'}\left(\frac{1}{G_{eff}}\right)^{3/2}. \tag{6.71}$$

A possible fundamental constant transition would trigger a transition to Chandrasekhar mass and the SnIa peak absolute luminosity too [277]. A hypothesis that makes sense is that the luminosity is proportional to m_c.

The connection between the absolute luminosity and the SnIa absolute magnitude is given by

$$M_B - M_{0B} = -\frac{5}{2}\log_{10}\frac{L}{L_0}, \tag{6.72}$$

where L_0 represents the local values. It is obvious that a G_{eff} decrease leads to an increase of L and a decrease of M_B.

A useful phenomenological approximation to the M_B transition is of the following form:

$$M_B(z) = \begin{cases} M_B^{R21}, & \text{if } z \leq z_t \\ M_B^{R21} + \Delta M_B, & \text{if } z > z_t, \end{cases} \tag{6.73}$$

the needed gap in L is approximately related to the corresponding gap in H_0 [130]:

$$\Delta M_B \equiv M_B^{P18} - M_B^{R21} \approx 5 \log_{10} \frac{H_0^{P18}}{H_0^{R21}} \approx -0.2. \tag{6.74}$$

From all these, can be concluded that the M_B transition and the corresponding H_0 crisis could be explained by a transition of the G_{eff} via:

$$\mu_G(z) \equiv \frac{G_{eff}}{G_{Nt}} = \begin{cases} 1 \equiv \mu_G^<, & \text{if } z \leq z_t \\ 1 + \Delta\mu_G \equiv \mu_G^>, & \text{if } z > z_t, \end{cases} \tag{6.75}$$

with G_{Nt} the local measured Newton's constant. Now, the change of μ_G is related to the SnIa M_B change via:

$$\Delta M_B = -\frac{5}{2} \log_{10} \frac{L^{P18}}{L^{R21}} = \frac{15}{4} \log_{10} \mu_G^>. \tag{6.76}$$

In the above L^{P18} is the CMB-calibrated SnIa luminosities and L^{R21} is the Cepheid-calibrated ones. So we have that

$$\Delta\mu_G = 10^{\frac{4}{15}\Delta M_B} - 1 \approx -0.12. \tag{6.77}$$

Chapter 7

Summary, Conclusions and Future Prospects

7.1 Summary and Conclusions

In the greater extent of this thesis, the main aspects of false vacuum decay in zero and in finite temperature were studied in detail. In the zero temperature case, we derived analytical expressions for the bubble's radius in flat space transition at the moment of nucleation via the thin-wall approximation. Also, we used the path integral approach to derive a full form of the decay rate expression of the false vacuum. Adjusting, our problem with a Wick rotation to the Euclidean spacetime, we solved the equations of motion of the field theory in the semi-classical approximation (where the exponential $B \gg 1$), and we make an extensive analysis of the instantons solutions in a double well potential [149]. We studied n bounce configurations and showed that the modification to the ground state energy from an one minimum potential (for example, the simple harmonic oscillator) is very small in the semi-classical limit. Actually, the functional integral has modified the ground-state energy as follows

$$E_0 = (\omega/2 - Ke^{-B}). \tag{7.1}$$

Also, we found that the bounce solution is not a minimum of the action, but in fact, a saddle point, and the system has a zero and a negative eigenvalue. The problem of the negative eigenvalue can be treated if the metastable potential of the theory is seen as an analytical continuation of a stable potential. Using the right treatment, and saddle-point approximation we derived the decay rate of the metastable field

$$\frac{\Gamma}{V} = e^{-B}(B/2\pi)^2 \left| \frac{\det'[-\partial^2 + U(\bar{\phi})]}{\det[-\partial^2 + U''(\phi_+)^2]} \right|^{-1/2}, \tag{7.2}$$

where, det′, denotes the determinant computed with the zero eigenvalues omitted.

Analytical expressions for the bubble radius and the exponential term of the decay rate derived in the case where the gravitation is included in the zero temperature false vacuum decay. There, we studied transitions of de-Sitter ($U(\phi_+) = \epsilon$) to flat space ($U(\phi_-) = 0$) and from flat space ($U(\phi_+ = 0$) to Anti-de-Sitter ($U(\phi_-) = -\epsilon$, using the thin-wall formalism. The important results derived in the context of Coleman-de Luccia (CDL) bounces are the following [133]: For the first case,

$$\bar{\rho} = \frac{\bar{\rho}_0}{1 + (\bar{\rho}_0/2D)^2}, \tag{7.3}$$

$$B = \frac{B_0}{[1 + (\rho_0/2D)^2)]^2} \tag{7.4}$$

and for the second case,

$$\bar{\rho} = \frac{\bar{\rho}_0}{1 - (\bar{\rho}_0/2D)^2} \tag{7.5}$$

$$B = \frac{B_0}{[1 - (\rho_0/2D)^2)]^2}. \tag{7.6}$$

An arbitrarily small cosmological constant (ϵ) is considered in these calculations, exactly like Coleman-De Lucia works [131][133]. The thin-wall approach can be justified if the radius $\bar{\rho}$ and D are very large in comparison to the range of variation of the field ϕ. In the first case, gravitational effects make the materialization more likely, as they diminish the value of B, and make the bubble radius at the nucleation moment smaller. The second special case gives the exact opposite result, gravity makes a bubble with a larger radius at the moment of nucleation but this nucleation becomes less likely.

As far as the bubble growth after the nucleation, in the flat case after an analytical continuation the $\mathcal{O}(4)$ symmetry of the Euclidean bounce becomes an $\mathcal{O}(3,1)$ symmetry of the Minkowskian bounce. The bubble evolves according to a classical Klein-Gordon equation of the form

$$-\frac{\partial^2\phi}{\partial t} + \nabla^2\phi = \frac{\partial U}{\partial \phi}. \tag{7.7}$$

and the wall traces out the hyperboloid

$$\vec{x}^2 - t^2 = \bar{\rho}^2. \tag{7.8}$$

Because the phenomenon of a bubble appearance is a purely quantum phenomenon, the bubble radius is expected to be a microscopic number, which leads to the conclusion that the bubble will start to extend with a speed reaching the speed of light. If a bubble is directed to an observer who is at rest, he will be notified of the coming moment when his worldline will be intersected by the light cone of the point of the thin-wall creation.

When gravity is present, in the first special case, a new phase Minkowski space bubble grows inside the old phase de-Sitter universe. This was the conclusion made after the analytic continuation. The radius ρ is bounded above by D in the new metric after the analytical continuation

$$\rho = D\sin(\eta/D), \tag{7.9}$$

which explains the form of Eq.(7.9). The bubble cannot be larger than D, a larger bubble could not fit into the closed space background.

In the second special case, we are outside the bubble, living in the false vacuum Minkowski universe, the true vacuum bubble will be an open Anti-de Sitter space. We saw that a true vacuum bubble of this space can end up collapsing after a finite time after its materialization due to TWA corrections ϕ is obtaining a time dependence as a result its time derivative not be zero for a scale factor equal to zero.

Moreover, Coleman-De Luccia's semiclassical instanton approximation is extended in modified theories of gravity, $F(\phi) = 1/\kappa - \xi\phi^2$ where ξ is non-minimally coupling of the curvature scalar and the scalar field. Analytical, complicated expressions derived for the parameter B appearing on the decay rate expression, and the bubble radius in the same two special cases. In both cases, we observe that the appearance of a positive coupling ξ makes nucleation of the bubble more likely, and the radius smaller. For a negative coupling, it makes the materialization less likely and the radius bigger.

Furthermore, we conducted numerical computations in several chapters of this thesis. We computed numerically the classical bounce solutions by solving the Euclidean field equations.

For the case without gravity in zero temperature, we worked out the problem with a rescaled potential, we used the shooting method via the command `Method` in *Mathematica* directly in the `NDSolve` command. In the CDL case, where gravitational effects are present, we constructed our shooting method from the beginning, we built the initial conditions of the system of differential equations via Taylor expansion and turn the boundary value problem into a numerically solvable initial value problem. These methods are presented in detail in Appendix I, where a bubble profile for a finite temperature phase transition is obtained with the `AnyBubble` package too. In all these numerical results the expected $tanh$(like) instanton solution form was achieved.

In the non-minimal coupling case numerical computations we used a very informative toy model described by

$$U = -\frac{1}{4}a^2(3b-1)\phi^2 + \frac{1}{2}a(b-1)\phi^3 + \frac{1}{4}\phi^4 + a^4 c. \tag{7.10}$$

We saw that in the $dS \to M$ transition (first case) the scale factor numerical solution obtains a second zero, which comes in total agreement with the theoretical expectation proved by Guth and Weinberg, who talked about a second zero of the scale factor ρ in the dS background [190]. In the second case, $(M \to AdS)$ ρ asymptotes a linear function in the Euclidean space as was expected.

We also studied some aspects of finite temperature vacuum decay. Here thermal tunneling takes the place of quantum tunneling, the symmetry is changing because now thermal quantum field theory is equivalent to a Euclidean field theory with periodicity to Euclidean time (anti-periodic for fermionic fields). In this case, We are looking for an $\mathcal{O}(3)$ solution periodic in "time" $1/\beta$ (the thermodynamical beta) direction with a period T^{-1}. Going through all the way, we obtained analytical expressions in the flat case in the high-temperature limit via the thin-wall approximation for the radius $r(T)$ and the exponential term $B = S_3/T$ (the Euclidean action becomes now 3-dimensional for 4-dimensional due to periodicity). We also modified the CDL results and we can conclude that the basic features of the gravitational presence remain the same at finite temperature. The decline of positive energy vacua is still accelerated by gravity, while the decay of negative energy vacua is suppressed. The basic features are still there in the modified high-temperature results in the non-minimal coupling case.

Finally, an additional goal was the qualitative study of ultra-late time transitions. In such transitions, we assumed that the decay rate Γ is similar to the Hubble expansion rate H_0, which means a first-order phase transition at present cosmological times. Also, a second demand was that the metastable cosmological constant $\epsilon = \Delta U \sim M_{Pl}^2 H_0^2 \sim 10^{-48} GeV^{-4}$, ($\Delta U$, is the potential difference between the false and the true vacuum). Under this consideration, we estimated the scale of the produced true vacuum bubbles and investigated their evolution. We found that the radius at the moment of nucleation is sub-mm and that their tension dominates leading them to rapid collapse if the scalar field mass is larger than about $0.003\, eV$, otherwise the bubbles expand with the speed of light. We also investigated the non-minimal coupling case, bubbles of gravitational constant in a context of a rapid transition at G_{eff}. We showed that the gravitational correction of Coleman-de Luccia $(\bar{\rho}_0/2D)^2$ can be neglected for the scale considered and found that the typical bubble radius at the moment of the nucleation is again negligible for values of coupling $\xi \sim \mathcal{O}(1)$ for field mass scale $m \sim m_{crit} \sim 10^{-3} eV$. Also, the scale spatial extent at the end of the phase transition was calculated and found to be $A_1 45\, Mpc$, where A_1 is an $\mathcal{O}(1)$ parameter. This interesting theoretical result which was obtained using Hogan's model [240] includes within its range the critical distance $D_c \sim 50\, Mpc$ indicated in the reanalysis of the latest SH0ES data for H_0 by Perivolaropoulos and Skara [226]. By allowing for a transition to the SnIa absolute magnitude M_B (where a transition to M_B could be triggered by a rapid transition to the gravitational constant) the best-fit value of the Hubble parameter drops from

$H_0 = 73.04 \pm 1.04\, km\, s^{-1}\, Mpc^{-1}$ to $H_0 = 67.32 \pm 4.64\, km\, s^{-1} Mpc^{-1}$ in full consistency with the Planck value.

The confirmation of a rapid fundamental physics transition about 100-150 million years ago would bring a new revolutionary era to the science of physics. It would challenge the foundations of current theories, inspire new lines of research, and stimulate interdisciplinary collaboration across various branches of physics. Alternative cosmological models would enter the game questioning with vigor the standard ΛCDM model. The perspective we see and explain the physical world would be modified. A fundamental physics transition would open the way to a new era of exciting research in the field of Cosmology and not only.

7.2 Future Prospects

What could be some possible extensions to this work? One further step in this analysis could be the study of false vacuum decay in the context of other modified gravity (MG) theories [278]. For example, one could use the thin-wall approximation process for general forms of the non-minimal coupling function $F(\phi)$ and of the potential $U(\phi)$. In general, there exists a huge gamut of MG theories out there, beyond non-minimal coupling theories, and it would be interesting for someone to investigate bubble profiles in such theories, numerically and analytically.

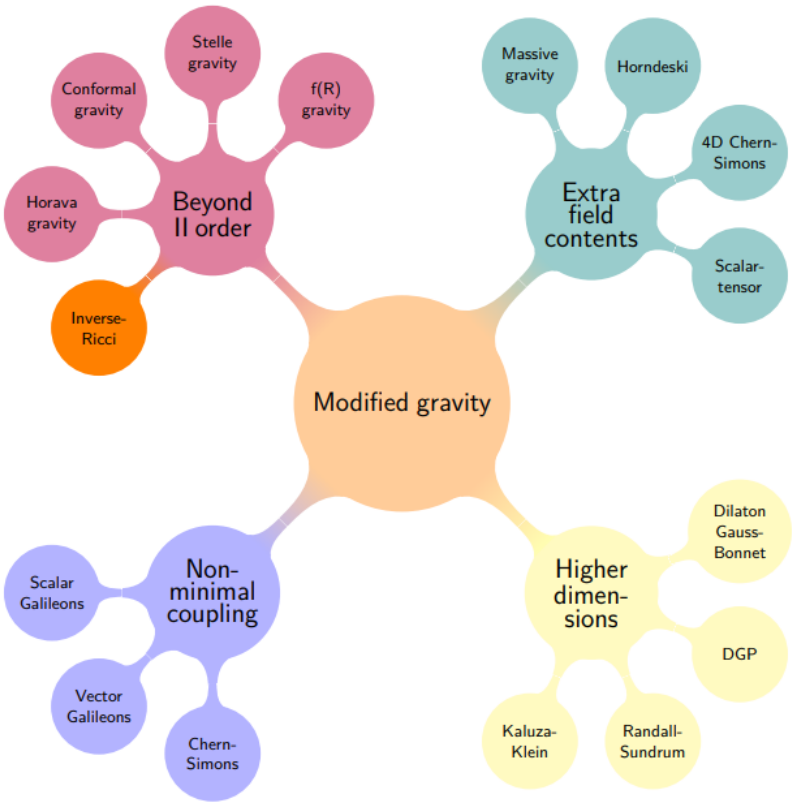

Figure 7.1: Classification of modified gravity theories (taken from [278])

Another specific example of extending this project could be a symmetron with explicit breaking as the scalar field model [279]. For a mechanism like symmetron to operate the vacuum

expectation value (VEV) of the scalar field must be dependent on the local mass density. The VEV becomes large in regions of low mass density, and small in regions of high mass density. In addition, the coupling of the scalar to matter is proportional to the VEV, so that the scalar couples with gravitational strength in regions of low density, but is decoupled and screened in regions of high density. This could be achieved with a symmetry-breaking potential of the form [280]:

$$U(\phi) = -\frac{1}{2}m^2\phi^2 + \frac{1}{4}\lambda\phi^4. \tag{7.11}$$

The dependence of the symmetron effective potential on the matter density has implications for the cosmological evolution of the scalar field. Since the matter density redshifts in time, the effective potential is time-dependent and results in a phase transition when the matter density falls below a critical value. Could such a symmetron phase transition be triggered in the recent past ($z_{tran} \leq 1$)?

Finally, one more prospect that could be made is the search of a first-order phase transition signature in a gravitational wave (GW) signal. In the case of a rapid transition of the Hubble parameter $H = a'/a$, which could qualitatively be described with a Heaviside step function, the factor a''/a in the differential equation below [281]

$$\partial_r^2 g - g'' + \frac{a''}{a}g = 0 \tag{7.12}$$

would not be negligible, but in fact we would have a δ Dirac "function" and discontinuity to g, something that affects the GW's signal. As a result of these, a first order phase transition information could be enclosed in observable GW's signals. On the other hand, a power law change of the scale factor ($a(\eta) \sim \eta^2$) leads to $\frac{a''}{a} \sim \eta^{-2}$, where η is the conformal time, and as long as $\omega^2 >> \eta^{-2}$, the term with g in Eq.(7.12) is negligible with respect to $-g'' = \omega^2 g$. In this case we have a usual wave equation of the form

$$\partial_r^2 - g'' \approx 0. \tag{7.13}$$

In the last few years, more and more papers, investigate the connection between GW's and cosmological phase transitions. Recently, there has been a resurgence of interest in theories with first order phase transitions due to the possibility of observing a gravitational wave signal, emerging from the collisions of bubbles [282–289]. Worth noting that bubble collisions have been studied theoretically in the past literature and here are some indicated works [290–292].

Conclusively, there is a wide field of research, not only theoretical but with observational interest and the excitement that accompanies a possible existing fundamental psychics change in the background of this investigation.

Appendices

Chapter A

Decay rate from the WKB method

In our first appendix, we rederive the decay rate from solving the static Schrödinger equation using the WKB expansion. The derivation will follow the calculation of the ground-state energy in a symmetric double-well potential made by Coleman in his book [153], where it modifies it to be applicable to vacuum decay, it can also be found at [293] and [167].

Inside the potential barrier, for $x_p < x < x_+$ (take a look at Fig.A.1), according to the WKB formula we have the following wave function

$$\psi_{\rm WKB} = \frac{c_1}{\sqrt{\kappa(x)}} e^{\frac{1}{\hbar}\int_{x_p}^{x} dx'\kappa(x')} + \frac{c_2}{\sqrt{\kappa(x)}} e^{-\frac{1}{\hbar}\int_{x_p}^{x} dx'\kappa(x')}, \tag{A.1}$$

where $\kappa(x) = \sqrt{2(V(x)-E)}$. Our goal is to match this function with those near the two turning points x_p and x_+. First, the region around x_+ will be considered, there the potential is $V(x) \approx m^2(x_+ - x)^2/2$. What we expect is the wave function of the ground state to be approximated by the solution to this harmonic oscillator potential. We will consider, for the false vacuum bound state, the zero-point energy written as $E = \hbar m(1/2+\epsilon)$, where ϵ is just a small correction. Next, we will make an expansion to $\kappa(x)$ as

$$\kappa(x) \sim \sqrt{2V(x)}\left(1 - \frac{E}{2V(x)}\right), \tag{A.2}$$

then we substitute this into the WKB wave function. Using

$$\begin{aligned}\int_{x_p}^{x} dx'\sqrt{2V(x')} &= \int_{x_p}^{x_+} dx'\sqrt{2V(x')} + \int_{x_+}^{x} dx'\sqrt{2V(x')} \\ &= \frac{B}{2} - \frac{1}{2}m(x_+ - x)^2,\end{aligned} \tag{A.3}$$

where B is the usual bounce action. After all this process we arrive at

$$\begin{aligned}\psi_{\rm WKB} = &\frac{c_1}{\sqrt{m(x_+-x)}} e^{\frac{1}{\hbar}\left(\frac{B}{2} - \frac{1}{2}m(x_+-x)^2 + Em^{-1}\log\left(B^{-1/2}m^{3/2}A^{-1}(x_+-x)\right)\right)} \\ &+ \frac{c_2}{\sqrt{m(x_+-x)}} e^{-\frac{1}{\hbar}\left(\frac{B}{2} - \frac{1}{2}m(x_+-x)^2 + Em^{-1}\log\left(B^{-1/2}m^{3/2}A^{-1}(x_+-x)\right)\right)},\end{aligned} \tag{A.4}$$

where we have used Eq.(D.16) from the Appendix D dedicated to the functional determinant calculation. Now, if we substitute $E = \hbar(1/2+\epsilon)$ into the above expression we finally have

$$\psi_{\rm WKB} = \left(c_1 e^{B/2\hbar} B^{-1/4} A^{-1/2} m^{1/4} e^{-\frac{m}{2\hbar}(x_+-x)^2} + \frac{c_2}{m^{1/4}(x_+-x)} e^{-B/2\hbar} B^{1/4} A^{1/2} m^{1/4} e^{\frac{m}{2\hbar}(x_+-x)^2}\right) \times [1 + O(\epsilon)]. \tag{A.5}$$

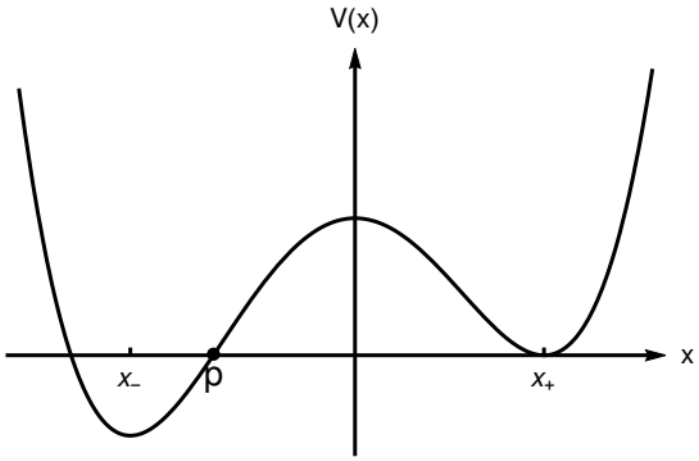

Figure A.1: The classical potential $V(x)$ in a theory with a false vacuum

To fix the coefficients c_1 and c_2, we need to match the WKB wave function to the solutions of the Schrödinger equation beyond the turning points. At first, we take into consideration the false vacuum region. This region is described approximately by the following equation

$$-\frac{\hbar}{2}\partial_x^2\psi(x) + \frac{1}{2}m^2(x-x_+)^2\psi(x) = E\psi(x), \tag{A.6}$$

where, for the purpose of matching, we look for approximate solutions valid for $(x - x_+) \gg \hbar/m$. Since ϵ is a small number, we will solve this equation perturbatively around ϵ equals zero. We already know one solution for Schrödinger's equation, for $\epsilon = 0$, this is

$$\psi_1(x) = m^{1/4}e^{-\frac{m}{2\hbar}(x_+-x)^2}. \tag{A.7}$$

Of course, there is another odd solution, which has a simple form, easily computed by the WKB approximation or just read off from Eq.(A.5)

$$\psi_2(x) = \frac{1}{m^{1/4}(x_+ - x)}e^{\frac{m}{2\hbar}(x_+-x)^2}, \tag{A.8}$$

where the latter is valid for $|x - x_+| \gg \hbar/m$. The Wronskian of these solutions is

$$W(x) = \psi_1(x)\partial_x\psi_2(x) - \psi_2(x)\partial_x\psi_1(x) = -\frac{2m}{\hbar} + \mathcal{O}\left(\frac{1}{(x-x_+)^2}\right). \tag{A.9}$$

For non-vanishing ϵ, we can write

$$\psi(x) = \psi_1(x) + \delta\psi(x), \tag{A.10}$$

and the perturbation to Eq.(A.6) is

$$-\frac{\hbar}{2}\partial_x^2\delta\psi(x) + \frac{1}{2}m^2(x-x_+)^2\delta\psi(x) = (\hbar m)\epsilon\psi_1(x), \tag{A.11}$$

The solution to this can be found by a standard method; we will turn the above into an integral equation and then we will irritate once [153][293][167], this will give

$$\psi(x) = \psi_1(x) - \epsilon\int_x^\infty dx'\psi_1(x')[\psi_1(x')\psi_2(x) - \psi_2(x')\psi_1(x)]. \tag{A.12}$$

Here, $\psi(x)$ vanishes for x goes to plus infinity. This automatically takes care of vanishing boundary conditions in the region $(x - x_+) \gg \sqrt{\hbar/m}$. The only matching left to be done is in the region $(x_+ - x) \ll \sqrt{\hbar/m}$, where we can use the following approach

$$\int_x^\infty dx' \psi_1^2(x') \approx \int_{-\infty}^\infty dx' \psi_1^2(x') = \sqrt{\pi\hbar}, \tag{A.13}$$

where a typical Gaussian integral appeared in the above expression. Inserting this into our solution accompanied by a normalization factor we will get

$$\begin{aligned} \psi(x) &= N\left[\psi_1(x) - \epsilon \int_x^\infty dx' \psi_1(x')[\psi_1(x')\psi_2(x) - \psi_2(x')\psi_1(x)]\right] \\ &= N\left[m^{1/4} e^{-m(x_+ - x)^2/2\hbar}[1 + \mathcal{O}(\epsilon)] - \frac{\epsilon\sqrt{\pi\hbar}}{m^{1/4}(x_+ - x)} e^{m(x_+ - x)^2/2\hbar}\right]. \end{aligned} \tag{A.14}$$

If we compare the latter with Eq.(A.5) we find that

$$m\epsilon = -\frac{c_1}{c_2}\sqrt{\frac{B}{\pi\hbar}} e^{-B/\hbar} A. \tag{A.15}$$

Someone can observe the similarity to the decay rate, this observation gives us the feeling that we are close to the desired result.

The ratio c_2/c_1 can be determined in the region around x_p. There, we can approximate $V(x) \sim V'(x_p)(x - x_p)$, and we neglect the zero-point energy of the false vacuum, taking $E = 0$. The Schrödinger equation we are going to face now will be the following

$$-\frac{\hbar^2}{2}\partial_x^2 \psi(x) + V'(x_p)(x - x_p)\psi(x) = 0. \tag{A.16}$$

Let us define $z = a(x - x_p)$, with $a = (\hbar^2/2V'(x_p))^{1/3}$, we have

$$\partial_z^2 \psi(z) - z\psi(z) = 0, \tag{A.17}$$

which is the Airy equation with the solution to be the well-known Airy functions

$$\mathrm{Ai}(z) \to \frac{1}{2\sqrt{\pi}} z^{-1/4} \exp\left(-\frac{2}{3} z^{3/2}\right) \text{ for } z \to +\infty, \tag{A.18}$$

$$\mathrm{Ai}(z) \to \frac{1}{\sqrt{\pi}} |z|^{-1/4} \sin\left(\frac{2}{3}|z|^{3/2} + \frac{\pi}{4}\right) \text{ for } z \to -\infty, \tag{A.19}$$

and

$$\mathrm{Bi}(z) \to \frac{1}{\sqrt{\pi}} z^{-1/4} \exp\left(\frac{2}{3} z^{3/2}\right) \text{ for } z \to +\infty, \tag{A.20}$$

$$\mathrm{Bi} \to \frac{1}{\sqrt{\pi}} |z|^{-1/4} \cos\left(\frac{2}{3}|z|^{3/2} + \frac{\pi}{4}\right) \text{ for } z \to -\infty, \tag{A.21}$$

This gives the following matching formulæ: If for $x > x_p$ we have

$$\frac{c_1}{\sqrt{\kappa(x)}} \exp\left[\frac{1}{\hbar}\int_{x_p}^x dx' \kappa(x')\right] + \frac{c_2}{\sqrt{\kappa(x)}} \exp\left[-\frac{1}{\hbar}\int_{x_p}^x dx' \kappa(x')\right] \tag{A.22}$$

then for $x < x_p$ the solution will be in the following form

$$\frac{2c_2}{\sqrt{k(x)}} \sin\left[\frac{1}{\hbar}\int_x^{x_p} dx' k(x') + \frac{\pi}{4}\right] + \frac{c_1}{\sqrt{k(x)}} \cos\left[\frac{1}{\hbar}\int_x^{x_p} dx' k(x') + \frac{\pi}{4}\right] \tag{A.23}$$

where $k(x) = \sqrt{-V(x)}$ and we have used $\kappa(x) \sim \sqrt{z}$ for $z > 0$ and $k(x) \sim \sqrt{|z|}$ for $z < 0$.

The wave function beyond x_p must be a purely outgoing wave in order to describe tunneling, something of the form $\sim \exp\big(-\frac{1}{\hbar}[\int_x^{x_p} dx' k(x') + \frac{\pi}{4}]\big)$, in our problem the outgoing wave spreads towards the negative direction of x. In order to satisfy this condition for $x < x_p$, we have to set $c_1 = 2ic_2$, so this gives

$$m\epsilon = \frac{i}{2}\sqrt{\frac{B}{\pi\hbar}} e^{-B/\hbar} A, \tag{A.24}$$

which is imaginary as we can see. Finally, we arrive at the decay rate expression in agreement with the result derived in the second chapter from the path integral. This is

$$\frac{\Gamma}{V} = \frac{2}{\hbar} \operatorname{Im} E = \sqrt{\frac{B}{\pi\hbar}} e^{-B/\hbar} A. \tag{A.25}$$

Chapter B

Proof: O(4) symmetric solutions of Eq.(2.54) are these of least action

B.1 Prologue

In this appendix, we will show that the non-trivial solutions of the lowest action are spherically symmetric, for a wide class of Euclidean scalar field equations. We will follow the paper by Coleman et al. [149].

In his classic paper, on the study of vacuum instability, Coleman faced a differential equation in four-dimensional Euclidean space, of the form

$$\Delta\phi = U'(\phi) \tag{B.1}$$

where Δ, is the Euclidean Laplace operator and the prime on the potential denotes differentiation with respect to the field ϕ (our familiar equation of motion (2.54) of Chapter 2 is an equation of this form). A trivial solution to this equation is a constant ϕ. In the text, a spherically symmetric non-trivial solution was constructed, and it was stated that this solution is of the lowest action of any non-trivial solution.

B.2 Statement of the main theorem

Before we proceed to our main statement we shall define that a real function of a single real variable $U(\phi)$ is admissible in N dimensions if:

1. U is continuously differentiable for all ϕ;
2. $U(0) = U'(0) = 0$;
3. U is negative somewhere;
4. There exist positive numbers, a, b, α and β such that

$$\alpha < \beta < 2N/(N-2) \tag{B.2}$$

and

$$U - a|\phi|^{\alpha} + b|\phi|^{\beta} \geq 0 \tag{B.3}$$

for all ϕ.

Theorem: *In N-dimensional Euclidean space, $N > 2$, for any admissible U, Eq.(B.1) possesses at least one monotone spherically symmetric solution vanishing at infinity, other than the trivial solution $\phi = 0$. Moreover, the Euclidean action of this solution is*

$$S = \int d^N x \left[\frac{1}{2}(\nabla\phi)^2 + U(\phi)\right], \tag{B.4}$$

and is less than or equal to that of any other solution vanishing at infinity. If the other solution is not both spherically symmetric and monotone, the action of Eq.(B.4) is strictly less than that of the other solution.

B.3 The Reduced Problem

For the first step, the Euclidean action will be divided into two parts

$$S = T + V \tag{B.5}$$

where

$$T = \frac{1}{2}\int d^N x(\nabla\phi)^2 \tag{B.6}$$

and

$$V = \int d^N x U(\phi). \tag{B.7}$$

Now, if we define a scale transformation by

$$\phi_\sigma = \phi(x/\sigma) \to \phi(x/\sigma) = \sigma^N \phi(x), \tag{B.8}$$

where σ is positive, then the scaling properties of T and V are the following

$$V[\phi_\sigma] = \sigma^N V[\phi] \tag{B.9}$$

and

$$T[\phi_\sigma] = \sigma^{N-2} T[\phi] \tag{B.10}$$

A good observation that can be made is that any solution of Eq.(B.1) makes S stationary. Under this observation, one can conclude that S must be stationary ($S' = 0$) under scale transformations, whence

$$(N-2)T + NV = 0 \Rightarrow S = 2T/N \tag{B.11}$$

for any solution of the differential equation.

We shall give the definition of "the reduced problem"; it is the problem of finding a function vanishing at infinity that minimizes T for some fixed negative V.

From the scale transformations of T and V, it is obvious that if we can find a solution to the reduced problem for some negative V we can find a solution for any negative V; the solutions are just scale transformations of each other. Indeed, all the solutions have the same value as the scale-invariant ratio,

$$R = -\frac{T^{N/(N-2)}}{V}, \tag{B.12}$$

and the reduced problem can be stated simply as the problem of searching for a function with a negative V which minimizes R. Let us now refer to another theorem from the paper

Theorem A: *If a solution of the reduced problem exists, then, for appropriately chosen V, it is a solution of Eq.(B.1) that has action less than or equal to that of any non-trivial solution of Eq.(B.1).*

A solution to the reduced problem ϕ is a function that makes

$$S' = T + \lambda^2 V \tag{B.13}$$

stationary. In the above equation, λ^2 is a Lagrange multiplier. Using the same arguments as before, we can arrive to

$$(N-2)T + \lambda^2 NV = 0. \tag{B.14}$$

Because T is positive and V is negative, λ^2 must be positive and our notation is not deceptive. Then the function ϕ_λ, which is scale transformed, is a solution of Eq.(B.1).

Next, we have to show that the latter is a solution that has S less than or equal to that of any solution of our differential equation. Consider $\bar{\phi}$ to be a non-trivial solution of Eq.(B.1). Since this solution is non-trivial, $T[\bar{\phi}]$ is not zero and from Eq.(B.11), $V[\bar{\phi}]$ is automatically negative. Now, let ϕ be the solution to the reduced problem with

$$V[\phi] = V[\bar{\phi}]. \tag{B.15}$$

By the definition of the reduced problem

$$T[\phi] \leq T[\bar{\phi}]. \tag{B.16}$$

If we make a comparison of equation (B.11) with (B.14), we have

$$\lambda \leq 1. \tag{B.17}$$

As we expect, ϕ_λ satisfies Eq.(B.1), but

$$T[\phi_\lambda] = \lambda^{(N-2)/2} T[\phi] \leq T[\bar{\phi}]. \tag{B.18}$$

Therefore, from Eq.(B.11) someone has that

$$S[\phi_\lambda] \leq S[\bar{\phi}] \tag{B.19}$$

B.4 Analysis of the Reduced Problem

Let us put on a second theorem to the story:

Theorem B: *There exists at least one solution to the reduced problem. All solutions to the reduced problem are spherically symmetric and monotone.*

Theorem B completes the puzzle and together with Theorem A implies our main theorem. The proof of B is somewhat long, and following this paper of Coleman, we will organize it and present it as a long sequence of ten statements with short proofs.

Here is important to recall the fourth condition of admissibility of the function U, it was stating the existence of four positive numbers a, b, α, and β with

$$2N/(N-2) > \beta > \alpha, \tag{B.20}$$

such that

$$U - a|\phi|^\alpha + b|\phi|^\beta \geq 0. \tag{B.21}$$

Now, let us present the statements of Theorem B.

Statement 1: *For any function ϕ such that $V[\bar{\phi}]$ is negative,*

$$\int d^N x|\phi|^\beta \geq \frac{a}{b}\int d^N x|\phi|^\alpha. \tag{B.22}$$

The proof of this statement is simple if we integrate Eq.(B.21), we find

$$b\int d^N x|\phi|^\beta \geq a\int d^N x|\phi|^\alpha - V[\phi]. \tag{B.23}$$

But V is negative.

Statement 2: *For any function ϕ such that $V[\bar{\phi}]$ is negative, and for any $\gamma > \beta$*

$$\int d^N x|\phi|^\gamma \geq \left(\frac{a}{b}\right)^{(\gamma-\alpha)/(\beta-\alpha)}\int d^N x|\phi|^\alpha. \tag{B.24}$$

To prove it, we can use Hölder's inequality,

$$\int d^N x|\phi|^\beta \leq \left[\int d^N x|\phi|^\alpha\right]^{(\gamma-\beta)/(\gamma-\alpha)}\left[\int d^N x|\phi|^\gamma\right]^{(\beta-\alpha)/(\gamma-\alpha)}. \tag{B.25}$$

If we combine it with Statement 1, it is trivial to reach the desired result.

Having established these preliminary inequalities, we can now focus our attention on the reduced problem. We know that T is a positive functional, so it bounded below on the set of all functions with fixed negative V and thus has a greatest lower bound, $\inf T$. Therefore, a minimizing sequence can be constructed, an infinite sequence of functions ϕ_n, such that $V[\phi_n]$ is a fixed negative number and

$$\lim_{n\to\infty} T[\phi_n] = \inf T. \tag{B.26}$$

Our important task is to show that the elements of the minimizing sequence can be chosen such that they converge to an actual minimum of T.

It would be a good idea to choose the elements of this sequence to be differentiable functions of compact support. Of course, this does not imply that their limit (if it exists) is such a function.

Statement 3: *Either there exists a minimizing sequence such that $\phi_n(x)$ is greater than or equal to zero for all n and all x, or there exists a minimizing sequence such that $\phi_n(x)$ is less than or equal to zero for all n and all x.*

Well, in the analysis class we have learned that any function can be written as a sum of two parts, its positive and its negative one. So, this makes us write

$$\phi(x) = \phi_+(x) + \phi_-(x), \tag{B.27}$$

where

$$\phi_+(x) = \max\{\phi(x), 0\} \tag{B.28}$$

and

$$\phi_-(x) = \min\{\phi(x), 0\}. \tag{B.29}$$

It is clear from the above that

$$T[\phi] = T[\phi_+] + T[\phi_-]. \tag{B.30}$$

Also, because $U(0) = 0$

$$V[\phi] = V[\phi_+] + V[\phi_-]. \tag{B.31}$$

Now, let us construct the scale-invariant ratio of Eq.(B.12)

$$R[\phi] = \frac{-(T[\phi_+] + T[\phi_-])^{N/(N-2)}}{V[\phi_+] + V[\phi_-]}. \tag{B.32}$$

From this, someone can easily see that either

$$R[\phi] \geq R[\phi_+], \quad \text{if} \quad V[\phi_-] \geq 0, \tag{B.33}$$

$$R[\phi] \geq R[\phi_-], \quad \text{if} \quad V[\phi_+] \geq 0, \tag{B.34}$$

or

$$R[\phi] \geq \min\{R[\phi_+], R[\phi_-]\}, \quad \text{if} \quad V[\phi_\pm] < 0. \tag{B.35}$$

These inequalities must be obeyed by each function in a minimizing sequence; thus, either the minimizing sequence has an infinite subsequence for which

$$R[\phi_n] \geq R[\phi_{n+}] \tag{B.36}$$

or

$$R[\phi_n] \geq R[\phi_{n-}]. \tag{B.37}$$

We will assume for the moment the first alternative. Consider now an new sequence of functions ϕ'_n, where each element is a scale transform of ϕ_{n+}, with the scale transformation chosen such that

$$V[\phi'_n] = V[\phi_n]. \tag{B.38}$$

But from the first alternative we chose Eq.(B.36), we can write immediately the following inequality

$$T[\phi'_n] \leq T[\phi_n]. \tag{B.39}$$

Consequently, what we have done is to construct a minimizing sequence composed exclusively of non-negative functions. The same reasoning applies if we chose the second alternative. But, in order to keep our analysis as simple as possible, from now on we will work under the assumption that the minimizing sequence we deal with is composed of non-negative functions. The arguments for the alternative case can be constructed trivially by replacing $\phi \to -\phi$ everywhere.

Statement 4: *There exists a minimizing sequence such that $\phi_n(x)$ is spherically symmetric and monotone for all n.*

An important reminder before we proceed in the proof of the fourth statement is the definition of the spherical rearrangement ϕ_R of a non-negative function ϕ. The spherical rearrangement is

a spherically symmetric function, monotone decreasing as one moves away from the origin, such that, for any positive number M,

$$\mu\{x|\phi_R(x) \geq M\} = \mu\{x|\phi(x) \geq M\}, \tag{B.40}$$

where μ is the Lebesgue measure. It is trivial to show that

$$V[\phi_R] = V[\phi], \tag{B.41}$$

but it is not trivial to show that

$$T[\phi_R] \leq T[\phi]. \tag{B.42}$$

We will not prove it in this appendix, because the proof would make this appendix way too long. We will cite the work of Martin, Glase et al [294] for a greater deepening of the issue. Thus, from all of these, the spherical rearrangement of the minimizing sequence is a minimizing sequence too.

A wise choice, when spherical symmetry appears, is to rewrite things in terms of spherical coordinates. So, we will define y by

$$r = e^y \tag{B.43}$$

where r is the usual distance from the origin. If we also define $f_n(y)$ as

$$f_n = \phi_n e^{\frac{1}{2}(N-2)y}. \tag{B.44}$$

With the aid of the latter, going to spherical coordinates is not a difficult task:

$$T[\phi_n] = \frac{1}{2}\int d^N x(\nabla\phi_n)^2 \quad \rightarrow T[\phi_n] = C_N \int dy\left[\frac{1}{2}\left(\frac{\mathrm{d}f_n}{\mathrm{d}y}\right)^2 + \frac{(N-2)^2}{8}f_n^2\right] \tag{B.45}$$

where C_N is just a positive constant that results after the integration over $N-2$ angles.

Statement 5: *There exists a minimizing sequence of non-negative spherically symmetric monotone functions such that all of the following are uniformly bounded from above:*

$$\int dy(df_n/dy)^2, \tag{A}$$

$$\int dy f_n^2, \tag{B}$$

$$\frac{|f_n(y_1) - f_n(y_2)|}{|y_1 - y_2|^{1/2}}, \tag{C}$$

$$|f_n(y)|, \tag{D}$$

$$\int d^N x|\phi_n|^{2N/(N-2)}, \tag{E}$$

$$\int d^N x|\phi_n|^{\alpha}. \tag{F}$$

It is trivial the choice of a minimizing sequence that can bound T. Hence, bounds (A) and (B) is a consequence of Eq.(B.45). Bound (C) follows from the first bound with the help of the

Schwartz inequality, we have that

$$\begin{aligned} |f_n(y_1) - f_n(y_2)| &= \left| \int_{y_1}^{y_2} dy (df_n/dy) \right| \\ &\leq \left| \int_{y_1}^{y^2} dy (df_n/dy)^2 \right|^{1/2} \left| \int_{y_1}^{y_2} dy \right|^{1/2} \\ &\leq \left| \int_{y_1}^{y^2} dy (df_n/dy)^2 \right|^{1/2} |y_1 - y_2|^{1/2}. \end{aligned} \tag{B.46}$$

The function $f_n(y)$ vanishes at infinity and because of this

$$|f_n(y_1)|^2 = \left| 2 \int_{y_1}^{\infty} dy f_n (df_n/dy) \right| \leq \int dy [f_n^2 + (df_n/dy)^2] \tag{B.47}$$

from which bound (D) comes up. For bound (E) we can write immediately

$$d^N x |\phi_N|^{2N/(N-2)} = \int dy |f_n|^{2N/(N-2)} \leq \sup |f_n|^{4/(N-2)} \int dy |f_n|^2 \tag{B.48}$$

Bound (F) is a consequence of bound (E) and Statement 2. Note here that bounds (C),(D), and (E) are standard Sobolev theorems [295] but we included explicit Coleman's proofs.

Statement 6: *There exists a minimizing sequence of spherically symmetric functions and a bounded continuous function f such that*

$$\lim_{n \to \infty} f_n(y) = f(y) \tag{B.49}$$

pointwise for all y and uniformly on any finite interval.

By bounds (C) and (D), the minimizing sequence is a family of uniformly bounded equicontinuous functions; Ascoli's theorem then asserts the existence of a subsequence with the stated property.

Let us define ϕ as

$$\phi = f e^{-\frac{1}{2}(N-2)y} \tag{B.50}$$

then this statement just tells us that ϕ_n converges to ϕ pointwise almost everywhere. Because f is bounded, ϕ vanishes at infinity. It is noted that we have not yet shown ϕ is not zero.

Statement 7: *For the minimizing sequence of the preceding statement,*

$$\lim_{n \to \infty} \int d^N x |\phi_n|^\beta = \int d^N x |\phi|^\beta. \tag{B.51}$$

We can write that

$$\int d^N x |\phi_n|^\beta = C_N \int dy |f_n|^\beta \exp \left[\left(N - \frac{1}{2} \beta [N-2] \right) y \right] \equiv C_N \int dy h_n(y). \tag{B.52}$$

Now, the integral can be divided into three parts

$$\int dy h_n(y) = \int_{-\infty}^{y_1} dy h_n(y) + \int_{y_1}^{y_2} dy h_n(y) + \int_{y_2}^{\infty} dy h_n(y), \tag{B.53}$$

where y_1 and y_2 are going to be fixed numbers. For the first part,

$$\left|\int_{-\infty}^{y_1} dy h_n(y)\right| \leq \frac{\sup|f_n|^\beta \exp\left[(N-\frac{1}{2}\beta(N-2))y_1\right]}{N-\frac{1}{2}\beta(N-2)}. \tag{B.54}$$

Thus, we have the total control of the first part in the integral, it can be made as small as we please, by choosing y_1 sufficiently large and negative. For the second term,

$$\left|\int_{y_2}^{\infty} dy h_n(y)\right| \leq C_N^{-1} \sup|f_n|^{\beta-\alpha} \exp\left[-\frac{1}{2}(N-2)(\beta-\alpha)y_2\right] \int d^N x |\phi_N|^\alpha. \tag{B.55}$$

The last term can be made as small as we want uniformly in n if we choose y_2 to be sufficiently large and positive. Finally, we get

$$\lim_{n\to\infty} \int_{y_1}^{y_2} dy h_n(y) = \int_{y_1}^{y_2} dy |f|^\beta \exp\left[\left(N-\frac{1}{2}\beta(N-2)\right)y\right], \tag{B.56}$$

by the sixth statement.

Statement 8: *For the minimizing sequence of the preceding statement,*

$$V[\phi] \leq V[\phi_n]. \tag{B.57}$$

From Eq.(B.21) we can get

$$U(\phi) + b|\phi|^\beta \geq 0. \tag{B.58}$$

If we consider Fatou's Lemma, we can arrive at

$$\begin{aligned} V[\phi] + b\int d^N x |\phi|^\beta &\leq \lim_{n\to\infty}\left[V[\phi_n] + b\int d^N x |\phi_n|^\beta\right] \\ &= V[\phi_n] + b\int d^N x |\phi|^\beta. \end{aligned} \tag{B.59}$$

Thus, now we know that ϕ is not zero.

Statement 9: *For the minimizing sequence of the preceding statement,*

$$T[\phi] \leq \lim_{n\to\infty} T[\phi_n]. \tag{B.60}$$

The functional T can be thought of as defining a Hilbert space norm. Hence, in this context the minimizing sequence constructed is a sequence of bounded vectors; such a sequence always has a weakly convergent subsequence. This statement is then the proposition, familiar to mathematics, that the norm in Hilbert space is weakly lower semicontinuous.

Statement 10: The function ϕ defined above is a solution of the reduced problem.

For the final statement's proof, we will use Statements 8 and 9, from them we can derive for the ratio R that

$$R[\phi] \leq \lim_{n\to\infty} R[\phi_n]. \tag{B.61}$$

But the limit on the right is the infimum of the scale-invariant ratio R. Thus, ϕ must attain the infimum, to be a minimum of R because "less than" is not possible.

We have almost arrived at the proof of Theorem B; a monotone spherically-symmetric solution of the reduced problem has been constructed with success. The remainder of the theorem, which is the non-existence of non-spherically-symmetric solutions, is trivial. From [294] it is well-known that T for any function is equal to T for the spherical rearrangement of the function only if the original function is spherically symmetric and monotone. This statement completes our long proof for the $O(4)$ symmetric solutions constructed throughout this thesis.

Chapter C

Solving the soliton equation

C.1 The general problem

In this appendix we are going to solve the familiar equation called soliton in a one-dimensional field theory, using the aid from the book written by Rajamaran [154]. Soliton has the form depicted in the following expression

$$\frac{\mathrm{d}^2\phi}{\mathrm{d}x^2} = \frac{\mathrm{d}U}{\mathrm{d}\phi}, \tag{C.1}$$

where x is the spatial variable in the one-dimensional theory and the prime denotes derivation with respect to ϕ. We will solve the equation for $\phi(x)$, which is an ordinary differential equation, but this problem should be examined at the outset.

First, let us state that any localized static (time-independent) solution is a soliton. Consider a single scalar field $\phi(x,t)$ whose dynamics are governed by the Lagrangian

$$\mathcal{L} = \frac{1}{2}(\dot{\phi})^2 - \frac{1}{2}(\phi') - U(\phi), \tag{C.2}$$

where henceforth a dot or a prime represents differentiation with respect to the time or the space variable. The potential is reaching a minimum value of zero for some value or values of ϕ. If the variational action principle applied on our Lagrangian will lead, as usual, to a wave equation of the form

$$\Box\phi \equiv \ddot{\phi} - \phi'' = -\frac{\partial U}{\partial \phi}. \tag{C.3}$$

This equation conserves as time varies and the total energy functional is given by

$$E[\phi] = \int_{-\infty}^{\infty} dx \left[\frac{1}{2}(\dot{\phi})^2 - \frac{1}{2}(\phi') + U(\phi)\right]. \tag{C.4}$$

Let the absolute minimum of the potential occur at M points $M \geq 1$. That is let

$$U(\phi) = 0 \text{ for } \phi = g^{(i)}\,, i = 1, \ldots, M. \tag{C.5}$$

Then, as it is reasonable, the energy functional is also minimized when the field is constant in space-time and takes any of these g values. As we said before, we are interested in static solutions, for which Eq.(C.3) reduces to our soliton of Eq.(C.1).

Further, a solitary wave (soliton) must have finite energy and a localized energy density. As it was noted, the field must approach one of the values $g^{(i)}$ as x goes to plus and minus infinity.

If the potential $U(\phi)$ had one and only minimum at $\phi = g$, then for our static solution $\phi(x) \to g$ as $x \to \pm\infty$. If there are several degenerate minima, then the field must approach any of these $g's$ as the spatial variable goes to minus infinity, and either the same value of $g^{(i)}$ or any other as x approaches infinity in the opposite direction. Subject to these boundary conditions we solve the soliton equation.

As we have already shown in the text, in the second chapter, the soliton equation has a mechanical analogue. If we think of the variable x as "time" and ϕ as the coordinate of a unit-mass point-particle, then Eq.(C.1) is just Newton's second law for the motion of this particle but in an upside down potential given by $-U(\phi)$. The solution to this equation for $\phi(x)$ represents the motion of the particle to this analogy. The total energy of this motion is conserved and given by

$$W \equiv \frac{1}{2}(\phi')^2 - U(\phi). \tag{C.6}$$

The boundary conditions discussed earlier demand that as x tends to infinity then $U \to 0$ and $\partial\phi/\partial x \to 0$. Hence the energy goes to zero. This energy W is not to be confused with the energy functional of Eq.(C.4) of the original field system. For a static solution, we are looking for the functional of the energy that will represent the total "action" of the analogue particle's motion and is given by

$$S = \int dx \left[\frac{1}{2}\left(\frac{\mathrm{d}\phi}{\mathrm{d}x}\right)^2 + U(\phi)\right]. \tag{C.7}$$

If we multiply Eq.(C.1) by ϕ' and integrate once, we have

$$\int \phi'\phi'' dx = \int \frac{\mathrm{d}U}{\mathrm{d}\phi}\phi' dx \Rightarrow \frac{1}{2}(\phi')^2 = U(\phi). \tag{C.8}$$

Since both the first derivative of the field and the potential vanish at minus infinity, the integration constant is going to be zero. So the above is just a virial theorem for the analogue-particle.

Now, is the time to extend the analysis made in the text. Let us first consider a $U(\phi)$ which has a unique minimum at $\phi = \phi_1$ (Fig.C.1). The analogue-particle sees an upside potential with a maximum at ϕ_1 and a negative value for all other ϕ. The boundary conditions demand a zero energy trajectory with the starting and the ending point being identical at $\phi = \phi_1$ in the far past and the far future of the motion ($x = \pm\infty$). A look at the graph is enough to tell us that no such non-trivial motion is possible.

Once the particle takes off from ϕ_1 in either direction, it never returns. With this qualitative look, without explicitly solving Eq.(C.1) and independently of the details of the potential, we can see that a case with one minimum cannot be a soliton.

For a potential with two or more degenerate minima ($M > 1$), let us say for example with three minima at ϕ_1, ϕ_2 and ϕ_3 (Fig.C.2) the boundary conditions now indicate that the particle must leave any of these points at $x = -\infty$ and end up at $x = \infty$ at any one of them. With a potential of this form this trajectory now can be possible. It can take off from the top of the hill of ϕ_1 at minus infinity and roll up to the top of ϕ_2 as $x \to +\infty$ asymptotically. Or it can begin at ϕ_2 and end up at ϕ_3. Or it can take the reverse paths. These are the only four possibilities for this example. The particle cannot, for instance, begin from ϕ_1, go up to ϕ_2 and either return to the starting point or go to ϕ_3. To make a quick proof of this statement, note that at the top of the hill ϕ_2, both U and U' vanish. As a consequence from Eq.(C.1) and Eq.(C.8), both the

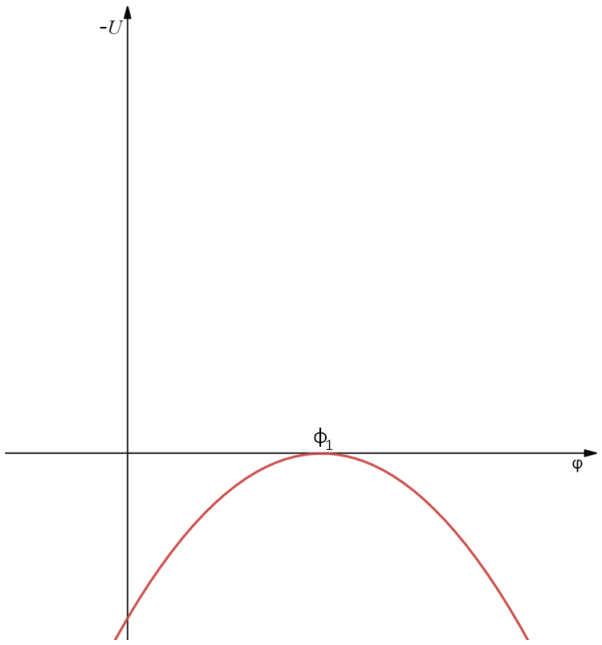

Figure C.1: The upside down potential of the analogue particle for a $U(\phi)$ with a unique minimum. There are non-trivial static solutions in this case.

'velocity' ϕ' and the 'acceleration' ϕ'' vanish there. Further,

$$\begin{aligned} \phi''' &= \frac{\mathrm{d}}{\mathrm{d}x}\left(\frac{\mathrm{d}U}{\mathrm{d}\phi}\right) = \frac{\mathrm{d}^2U}{\mathrm{d}\phi^2}\phi' = 0, \\ \phi'''' &= \frac{\mathrm{d}^2U}{\mathrm{d}\phi^2}\phi'' + \frac{\mathrm{d}^3U}{\mathrm{d}\phi^3}\phi'^2 = 0 \text{ etc.} \end{aligned} \tag{C.9}$$

Consequently, all derivatives vanish at ϕ_2. Thus, our particle after leaving ϕ_1 can barely make it to the second top as the "time" goes to infinity, where all derivatives of its motion vanish. The particle cannot return to ϕ_1 neither can climb to ϕ_3.

This mechanical analogy makes us draw two important conclusions: a) when $U(\phi)$ has a unique absolute minimum, there can be no static solitary wave and b) when it has n discrete degenerate minima, the problem can have $2(n-1)$ types of solutions, connecting to neighboring minima, as x varies from $-\infty$ to $+\infty$.

If we solve by quadrature, we can get from Eq.(C.8),

$$\frac{\mathrm{d}\phi}{\mathrm{d}x} = \pm[2U(\phi)]^{1/2}. \tag{C.10}$$

Upon integration

$$x - x_0 = \pm\int_{\phi(x_0)}^{\phi(x)} \frac{d\bar{\phi}}{[2U(\bar{\phi})]^{1/2}}, \tag{C.11}$$

where x_0, is the integration constant, an arbitrary point in space where the field takes the value of $\phi(x_0)$.

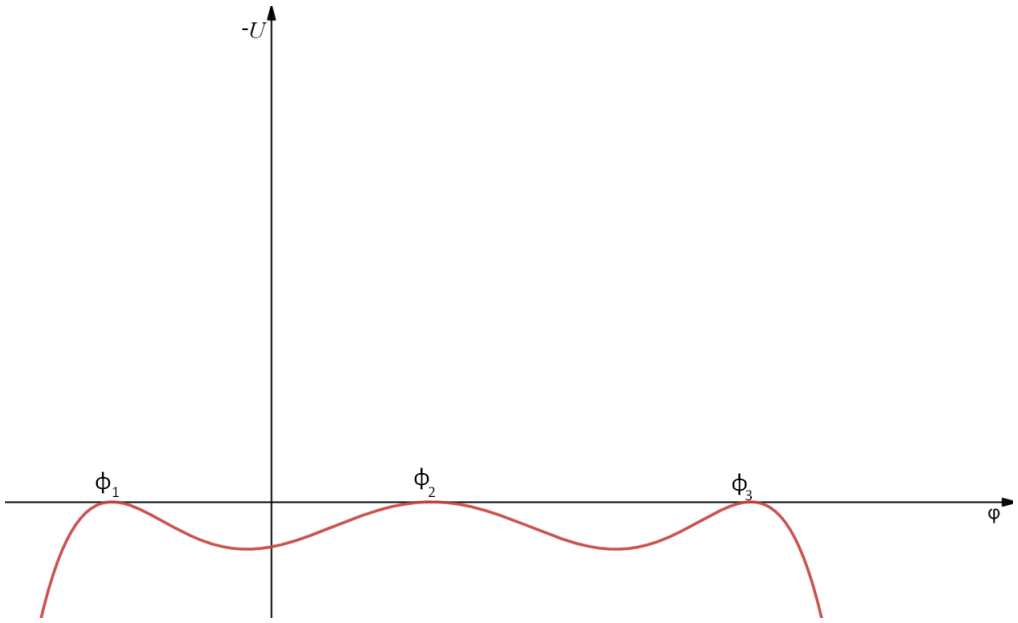

Figure C.2: The situation where the potential has three discrete degenerate minima. In this case the possibility for four non-trivial solutions exists.

C.2 The 'kink' solution of ϕ^4 theory

Let us consider the 'kink' solution of a ϕ^4 theory [296][297][298] in order to illustrate an analytical solution. Here, the potential will have the familiar form

$$U(\phi) = \frac{1}{4}\lambda(\phi^2 - m^2/\lambda)^2. \tag{C.12}$$

The equation of motion is the following

$$\ddot{\phi} - \phi'' = m^2 - \lambda\phi^3. \tag{C.13}$$

The potential vanishes at $\pm m/\sqrt{\lambda}$. The localized solution must tend to $\pm m/\sqrt{\lambda}$ as $x \to \pm\infty$. In particular, we have two types of static solutions. The analogue particle can begin from $-m/\sqrt{\lambda}$ at minus infinity and end up at $+m\sqrt{\lambda}$ at plus infinity, or vice versa. The static equation will be

$$\phi'' = \frac{\mathrm{d}U}{\mathrm{d}\phi} = \lambda\phi^3 - m^2\phi \tag{C.14}$$

and the solution to this, according to Eq.(C.11), will be

$$x - x_0 = \pm\int_{\phi(x_0)}^{\phi(x)} \frac{d\bar{\phi}}{\sqrt{\lambda/2}(\bar{\phi}^2 - m^2/\lambda)}. \tag{C.15}$$

This is a well-known integral; let us illustrate its solution. Upon choosing $\phi(x_0) = 0$ it becomes

$$\begin{aligned} x &= \pm\int_0^{\phi(x)} \frac{d\bar{\phi}}{\sqrt{\lambda/2}(\bar{\phi}^2 - m^2/\lambda)} \\ &= \pm\frac{\ln\left(\phi\lambda\left|2\phi\lambda - 2m\sqrt{\lambda}\right| - m\sqrt{\lambda}\left|2\phi\lambda - 2m\sqrt{\lambda}\right|\right) - \ln\left(2\phi^2\lambda^2 - 2m^2\lambda\right)}{\sqrt{2}\,m}. \end{aligned} \tag{C.16}$$

If we solve the above for ϕ it gives

$$\phi(x) = \pm\frac{m}{\sqrt{\lambda}}\frac{e^{\sqrt{2}mx}+1}{e^{\sqrt{2}mx}-1} = \pm\frac{m}{\sqrt{\lambda}}\tanh[(m/\sqrt{\lambda})x]. \tag{C.17}$$

Chapter D

Functional Determinant

In this appendix, we will introduce a way of evaluating the functional determinants of ordinary differential operators (the Gel'fand-Yaglom method). We will follow again the book written by Coleman [153]. This method can also be applied to false vacuum decay because the $\mathcal{O}(4)$-symmetry of the background allows the decomposition of a four-dimensional partial differential operator into a hyperradial operator and the Laplace-Beltrami operator.

D.1 Gel'fand-Yaglom theorem

Consider the equation

$$(-\partial_\tau^2 + W(\tau))\psi(\tau) = \lambda\psi(\tau) \tag{D.1}$$

where $W(\tau)$ is some bounded function of $\tau \in [-T/2, T/2]$. We will define $\psi_\lambda(\tau)$ as the solution of Eq.(D.1) obeying the boundary conditions

$$\psi_\lambda(-T/2) = 0, \qquad \partial_\tau\psi_\lambda(\tau)|_{\tau=-T/2} = 1. \tag{D.2}$$

The determinant of the operator $-\partial_\tau^2 + W(\tau)$ is defined as

$$\det\big(-\partial_\tau^2 + W(\tau)\big) = \prod_n \lambda_n \tag{D.3}$$

in the same way, as we did in the text. In the above equation, λ_n is the eigenvalue of the operator satisfying

$$(-\partial_\tau^2 + W(\tau))\psi_{\lambda_n}(\tau) = \lambda_n\psi_{\lambda_n}(\tau) \tag{D.4}$$

with boundary conditions $\psi_{\lambda_n}(-T/2) = \psi_{\lambda_n}(T/2) = 0$. The Gel'fand-Yaglom theorem states that

$$\frac{\det\big[-\partial_\tau^2 + W^{(1)}(\tau) - \lambda\big]}{\det[-\partial_\tau^2 + W^{(2)}(\tau) - \lambda]} = \frac{\psi_\lambda^{(1)}(T/2)}{\psi_\lambda^{(2)}(T/2)}. \tag{D.5}$$

Coleman gave a very elegant proof: $\psi_\lambda^{(1)}$, $\psi_\lambda^{(2)}$ are the eigenfunctions when and only when $\psi_\lambda^{(1)}(T) = 0$, $\psi_\lambda^{(2)}(T) = 0$. The left-hand side of the above formula is a meromorphic function of λ, with a simple zero at each eigenvalue λ_n^1 and a simple pole at each λ_n^2. By elementary Fredholm theory, it goes to one as λ goes to infinity in any direction except along the positive real axis. The right-hand side is a meromorphic function with exactly the same zeros and poles. By elementary differential-equation theory, it also goes to one in the same limit. Thus the ratio of two sides is

an analytic function of λ that goes to one as λ goes to infinity in any direction except along the positive real axis. That is, the ratio of two sides is one.

Applying the above formula to the case $\lambda = 0$ and taking the limit $T \to \infty$, we obtain the ratio that we have in our decay rate formula.

D.2 Evaluating the ratio of the functional determinants

We can define a quantity N by

$$\frac{\det(-\partial_\tau^2 + W)}{\psi_0(T/2)} = \pi\hbar N^2, \tag{D.6}$$

from the formula of the Gel'fand-Yaglom theorem, N is independent of W. The latter expression can be used to define the normalization constant N appearing in the functional integral. So, we obtained a desired formula for evaluating Gaussian functional integrals

$$N[\det\left(-\partial_\tau^2 + W\right)]^{-1/2} = [\pi\hbar\psi_0(T/2)]^{-1/2}. \tag{D.7}$$

For the linear harmonic oscillator case, a potential with one minimum in the center of the axes, considered in the work of Coleman and Callan [132], the functional determinant ratio in the tunneling rate now can be readily evaluated. In this case $W = U''(0) = \omega^2$, thus

$$\langle 0|\, e^{-HT/\hbar}\, |0\rangle = N[\det\left(-\partial_\tau^2 + \omega^2\right)]^{-1/2}. \tag{D.8}$$

For the case where $\lambda = 0$ Eq.(D.1) becomes

$$(-\partial_\tau^2 + W(\tau))\psi_0(\tau) = 0 \tag{D.9}$$

with the usual initial conditions, we get the following solution for ψ_0

$$\psi_0(\tau) = \frac{1}{\omega}\sinh\omega(\tau + T/2) \tag{D.10}$$

from which immediately follows that for $T \to \infty$ then $\sinh T \sim e^T$, therefore

$$\begin{aligned} N[\det\left(-\partial_\tau^2 + \omega^2\right)]^{-1/2} &= [\pi\hbar\omega^{-1}\sinh\omega T]^{-1/2} \\ &= \left(\frac{\omega}{\pi\hbar}\right)^{1/2} e^{-\omega T/2}, \end{aligned} \tag{D.11}$$

which is Eq.(2.142).

Now, let us consider the case where $W^{(2)}(\tau) = V''(\bar{x}(\tau))$, looking at fluctuations around the bounce. We have to evaluate the prime determinant. According to Coleman, we can do this by evaluating the full determinant on a finite interval $[-T/2, T/2]$, dividing it by its smallest finite eigenvalue near zero, λ_0, and finally letting T approach infinity. A function $\psi_0^{(2)}(t)$ can be constructed from an arbitrary basis of solutions. In order to apply the Gel'fand-Yaglom formula of Eq.(D.5) it is sufficient to be aware of the asymptotic behavior at $\pm T/2$. So, this time we have to construct solutions for the equation

$$[-\partial_\tau^2 + V''(\bar{x}(\tau))]\psi(\tau) = 0, \tag{D.12}$$

as we have already seen in the text one solution (the Goldstone mode) in the basis can be

$$x_1(\tau) = B^{-1/2}\frac{\mathrm{d}\bar{x}(\tau)}{\mathrm{d}\tau} \to \pm\frac{A}{\sqrt{m}}e^{-m|\tau|},\ \tau \to \pm\infty. \tag{D.13}$$

The constant A is determined by the asymptotic behavior of $x_1(\tau)$. Note that $x_1(\tau)$ does not satisfy the boundary conditions, $x_1(-T/2) = x_1(T/2) = 0$ so the solution we are looking for, $\psi_0^{(2)}(\tau)$ cannot be $x_1(\tau)$. As we know for the classical bounce we have that

$$\frac{1}{2}\left(\frac{\mathrm{d}\bar{x}}{\mathrm{d}\tau}\right)^2 - V(\bar{x}(\tau)) = 0. \tag{D.14}$$

Therefore $d\bar{x}/d\tau = \sqrt{2V(\bar{x})}$ which leads to

$$\tau = \int_{xp}^{x} dx \frac{1}{\sqrt{2V(x)}}. \tag{D.15}$$

Using the asymptotic behaviour, Eq.(D.13), one has

$$m\tau \equiv \int_{xp}^{x} dx \frac{1}{\sqrt{2V(x)}} = -\ln[B^{-1/2}m^{3/2}A^{-1}(x_+ - x)] + \mathcal{O}(x_+ - x). \tag{D.16}$$

Equation Eq.(D.12) must have a second solution, which is denoted by $x_2(\tau)$. We will normalize this solution such that its Wronskian with the first solution to be given by

$$x_1\partial_\tau x_2 - x_2\partial_\tau x_1 = 2A^2. \tag{D.17}$$

Thus its asymptotic behavior can be deduced

$$x_2(\tau) \to \frac{A}{\sqrt{m}} e^{m|\tau|}, \ \tau \to \pm\infty. \tag{D.18}$$

According to the boundary conditions (D.2), someone can construct now the desired solution $\psi_0^{(2)}(\tau)$ as

$$\psi_0^{(2)}(\tau) = -\frac{1}{2\sqrt{m}A}(e^{mT/2}x_1 + e^{-mT/2}x_2), \tag{D.19}$$

leading to $\psi_0^{(2)}(T/2) = -1/m$.

This can take care of the determinant. To find the lowest eigenvalue of the problem, we have to search for $\psi_\lambda(\tau)$ for small λ, let us name it λ_0. This can be done exactly in the same way as in Appendix A by a standard method. We will turn our equation of interest (D.12) into an integral equation and then iterate once. Hence, as before we expand $\psi_{\lambda_0}(\tau) = \psi_0^{(2)}(\tau) + \delta\psi_{\lambda_0}(\tau)$ in the eigen-equation. One has

$$(-\partial_\tau^2 + V''(\bar{x}))\delta\psi_{\lambda_0}(\tau) = \lambda_0\psi_0^{(2)}(\tau). \tag{D.20}$$

We can then construct a solution directly as

$$\psi_{\lambda_0}(\tau) = \psi_0^{(2)}(\tau) - \frac{\lambda_0}{2A^2}\int_{-T/2}^{\tau} d\tau'[x_2(\tau)x_1(\tau') - x_1(\tau)x_2(\tau')]\psi_0^{(2)}(\tau') \tag{D.21}$$

and

$$\psi_{\lambda_0}(T/2) = -\frac{1}{m} + \frac{\lambda_0}{4mA^2}\int_{-T/2}^{T/2} d\tau'[e^{mT}x_1^2(\tau') - e^{-mT}x_2^2(\tau')]. \tag{D.22}$$

For large T, the second term in this expression is bounded, and thus negligible to the first one. Since, x_1 is normalized, for large T we get

$$\psi_{\lambda_0}(T/2) \approx -\frac{1}{m} + \frac{\lambda_0}{4mA^2}e^{mT}. \tag{D.23}$$

By requiring the boundary condition $\psi_{\lambda_0}(T/2) = 0$, we obtain $\lambda_0 = 4A^2/e^{mT}$. Returning now to the Gel'fand-Yaglom formula

$$\frac{\det[-\partial_\tau^2 + V''(\bar{x})]}{\det[-\partial_\tau^2 + V''(x_+)]} = \frac{\psi_0^{(2)}(T/2)}{\psi_0^{(1)}(T/2)} = -\frac{1}{2A^2}. \tag{D.24}$$

Note that this is a negative number, indicating the existence of a negative eigenvalue in the eigenspectrum of our operator. Substituting the above result into Eq.(2.199) we can arrive to

$$\frac{\Gamma}{V} = \sqrt{\frac{B}{\pi\hbar}} e^{-B/\hbar} A, \tag{D.25}$$

which is in total agreement with the result derived by the WKB approximation in the first appendix.

Chapter E

Calculations for standard Cosmology

E.1 Variation of Ricci scalar

From the definition of the Ricci scalar, we can write

$$R = g^{\mu\nu}R_{\mu\nu} \Rightarrow \delta R = R_{\mu\nu}\delta g^{\mu\nu} + g^{\mu\nu}\delta R_{\mu\nu}. \tag{E.1}$$

The Riemann curvature tensor is

$$R^{\rho}_{\sigma\mu\nu} = \partial_\mu \Gamma^{\rho}_{\nu\sigma} - \partial_\nu \Gamma^{\rho}_{\mu\sigma} + \Gamma^{\rho}_{\mu\lambda}\Gamma^{\lambda}_{\nu\sigma} - \Gamma^{\rho}_{\nu\lambda}\Gamma^{\lambda}_{\mu\sigma}, \tag{E.2}$$

and the variation of this gives

$$\delta R^{\rho}_{\sigma\mu\nu} = \partial_\mu \delta\Gamma^{\rho}_{\nu\sigma} - \partial_\nu \delta\Gamma^{\rho}_{\mu\sigma} + \delta\Gamma^{\rho}_{\mu\lambda}\Gamma^{\lambda}_{\nu\sigma} + \Gamma^{\rho}_{\mu\lambda}\delta\Gamma^{\lambda}_{\nu\sigma} - \delta\Gamma^{\rho}_{\nu\lambda}\Gamma^{\lambda}_{\mu\sigma} - \Gamma^{\rho}_{\nu\lambda}\delta\Gamma^{\lambda}_{\mu\sigma}. \tag{E.3}$$

The covariant derivative of a tensor with mixed indices, in general, is

$$\nabla_\lambda C^{i}_{jk} = \partial_\lambda C^{i}_{jk} + \Gamma^{i}_{\lambda m}C^{m}_{jk} - \Gamma^{m}_{\lambda j}C^{i}_{mk} - \Gamma^{m}_{\lambda k}C^{i}_{jm}, \tag{E.4}$$

where the simple rule behind this is that for each contravariant (upper) index in the tensor, there is a positive term with a Christoffel symbol, and for each covariant (lower) index, there is a negative term. Hence, according to the above, we can calculate

$$\nabla_\lambda(\delta\Gamma^{\rho}_{\nu\mu}) = \partial_\lambda(\delta\Gamma^{\rho}_{\nu\mu}) + \Gamma^{\rho}_{\sigma\lambda}\delta\Gamma^{\sigma}_{\nu\mu} - \Gamma^{\sigma}_{\nu\lambda}\delta\Gamma^{\rho}_{\sigma\mu} - \Gamma^{\sigma}_{\mu\lambda}\delta\Gamma^{\rho}_{\nu\sigma}. \tag{E.5}$$

If we check carefully, we can observe that Eq.(E.5) is equal to the difference between two such terms

$$\begin{aligned}\nabla_\mu(\delta\Gamma^{\rho}_{\nu\sigma}) &= \partial_\mu(\delta\Gamma^{\rho}_{\nu\sigma}) + \Gamma^{\rho}_{\kappa\mu}\delta\Gamma^{\kappa}_{\nu\sigma} - \Gamma^{\kappa}_{\nu\mu}\delta\Gamma^{\rho}_{\kappa\sigma} - \Gamma^{\kappa}_{\sigma\mu}\delta\Gamma^{\rho}_{\nu\kappa}\\ \nabla_\nu(\delta\Gamma^{\rho}_{\mu\sigma}) &= \partial_\nu(\delta\Gamma^{\rho}_{\mu\sigma}) + \Gamma^{\rho}_{\kappa\nu}\delta\Gamma^{\kappa}_{\mu\sigma} - \Gamma^{\kappa}_{\mu\nu}\delta\Gamma^{\rho}_{\kappa\sigma} - \Gamma^{\kappa}_{\sigma\nu}\delta\Gamma^{\rho}_{\mu\kappa}\end{aligned} \tag{E.6}$$

and by setting $\kappa = \lambda$ above someone obtains

$$\begin{aligned}&\nabla_\mu(\delta\Gamma^{\rho}_{\nu\sigma}) - \nabla_\nu(\delta\Gamma^{\rho}_{\mu\sigma}) = \partial_\mu(\delta\Gamma^{\rho}_{\nu\sigma}) + \Gamma^{\rho}_{\lambda\mu}\delta\Gamma^{\lambda}_{\nu\sigma} - \cancel{\Gamma^{\lambda}_{\nu\mu}\delta\Gamma^{\rho}_{\lambda\sigma}} - \Gamma^{\lambda}_{\sigma\mu}\delta\Gamma^{\rho}_{\nu\lambda} - \partial_\nu(\delta\Gamma^{\rho}_{\mu\sigma}) -\\ &- \Gamma^{\rho}_{\lambda\nu}\delta\Gamma^{\lambda}_{\mu\sigma} + \cancel{\Gamma^{\lambda}_{\mu\nu}\delta\Gamma^{\rho}_{\lambda\sigma}} + \Gamma^{\lambda}_{\sigma\nu}\delta\Gamma^{\rho}_{\mu\lambda} = \delta R^{\rho}{}_{\sigma\mu\nu}.\end{aligned} \tag{E.7}$$

By contracting two indices of the variation of the Riemann tensor we can obtain the variation of the Ricci tensor

$$\delta R^{\rho}{}_{\mu\sigma\nu} = \nabla_\sigma(\delta\Gamma^{\rho}_{\nu\mu}) - \nabla_\nu(\delta\Gamma^{\rho}_{\mu\sigma}) \xrightarrow{\text{contraction}} \delta R_{\mu\nu} = \nabla_\rho(\delta\Gamma^{\rho}_{\nu\mu}) - \nabla_\nu(\delta\Gamma^{\rho}_{\rho\mu}). \tag{E.8}$$

Hence, the desired quantity, the variation of the Ricci scalar is given by

$$\delta R = R_{\mu\nu}\delta g^{\mu\nu} + \nabla_\sigma(g^{\mu\nu}\delta\Gamma^{\sigma}_{\mu\nu} - g^{\mu\sigma}\delta\Gamma^{\rho}_{\rho\mu}). \tag{E.9}$$

E.2 Variation of the Square Root of the Determinant of the Metric Tensor

The calculation of the square root of the determinant of the metric tensor will be done fully general for n-dimensional Riemannian spaces. Then, an application of this will be done for the pseudo-Riemannian 4-dimensional space of General Relativity. The first step is to write the determinant as

$$g \equiv \det\left(g_{a\beta}\right). \tag{E.10}$$

We have that

$$\delta\left(\sqrt{g}\right) = \frac{1}{2\sqrt{g}}\delta g. \tag{E.11}$$

For for any square $n \times n$ matrix A it hold that

$$\det\left(A\right) = e^{Tr(A)}. \tag{E.12}$$

According to this, we can write for our determinant

$$g = \det\left(g_{a\beta}\right) = e^{Tr\left(g_{a\beta}\right)} \tag{E.13}$$

and under the variation $g_{a\beta} \to g_{a\beta} + \delta g_{a\beta}$ it follows that

$$\det(g_{a\beta} + \delta g_{a\beta}) = e^{Tr\left(g_{a\beta}+\delta g_{a\beta}\right)} = e^{Tr\left(g_{a\beta}\right)+Tr\left(\delta g_{a\beta}\right)} = \underbrace{e^{Tr\left(g_{a\beta}\right)}}_{\equiv g}\, e^{Tr\left(\delta g_{a\beta}\right)}. \tag{E.14}$$

We employed the linearity of the trace in order to go through the second equality to the third one. Now, we can expand $e^{Tr(\delta g_{ab})}$, neglecting second and higher order terms, since the variations δg are small, and we arrive to

$$e^{Tr(\delta g_{ab})} \approx 1 + Tr(\delta g_{ab}) \tag{E.15}$$

and therefore

$$\det(g_{a\beta} + \delta g_{a\beta}) \approx g\left(1 + Tr(\delta g_{a\beta})\right) \tag{E.16}$$

but, by the definition of the trace

$$Tr(\delta g_{a\beta}) = g^{a\beta}\delta g_{a\beta}. \tag{E.17}$$

Going back to Eq.(E.16) we can write

$$\det(g_{a\beta} + \delta g_{a\beta}) \approx g\left(1 + g^{a\beta}\delta g_{a\beta}\right) \tag{E.18}$$

Using this result to the definition of the variation we will find that

$$\begin{aligned} \delta g = \delta\left(\det(g_{a\beta})\right) = \det(g_{a\beta} + \delta g_{a\beta}) - \det(g_{a\beta}) \approx \\ \approx g\left(1 + g^{a\beta}\delta g_{a\beta}\right) - g = g g^{a\beta}\delta g_{a\beta} \Rightarrow \delta g = -g g_{a\beta}\delta g^{a\beta}. \end{aligned} \tag{E.19}$$

Now, we are ready to prove Eq.(3.19). Let us use Eq.(E.19)

$$\begin{aligned} \delta\left(\sqrt{g}\right) = \frac{1}{2\sqrt{g}}\delta g = -\frac{1}{2}\frac{(\sqrt{g})^{\not 2}}{\not{\sqrt{g}}} g_{a\beta}\delta g^{a\beta} = -\frac{1}{2}\sqrt{g} g_{a\beta}\delta g^{a\beta} \Rightarrow \\ \Rightarrow \delta\left(\sqrt{g}\right) = -\frac{1}{2}\sqrt{g} g_{a\beta}\delta g^{a\beta}. \end{aligned} \tag{E.20}$$

For the final step, in order to go from the generality to the 4-dimensional pseudo-Riemannian space of General Relativity, we simply replace $g \to -g$ and let the indices run from 0 to 3

$$\delta\left(\sqrt{-g}\right) = -\frac{1}{2}\sqrt{-g} g_{\mu\nu}\delta g^{\mu\nu}, \tag{E.21}$$

where $\mu, \nu = 0, 1, 2, 3$ as usual.

Chapter F

Calculation of the integral in Eq.(5.87)

In this appendix, we are going to calculate the integral that came up in Eq.(5.87). This was an integral of the form

$$I = \int \sqrt{1 - ax^2} dx. \tag{F.1}$$

Let us try to calculate it going through all the way step by step. First of all, we can perform a trigonometric substitution in our initial expression. If we substitute

$$x = \frac{\tan(u)}{\sqrt{-a}} \rightarrow u = \arctan\big(\sqrt{-a}x\big),\ dx = \frac{sec^2(u)}{\sqrt{-a}} du \tag{F.2}$$

then the integral becomes

$$I = \int \frac{\sec^2(u)\sqrt{\tan^2(u)+1}}{\sqrt{-a}} du = \frac{1}{\sqrt{-a}} \int \sec^3(u) du = \frac{1}{\sqrt{-a}} I_2 \tag{F.3}$$

where we used the identity $\tan^2(u) + 1 = \sec^2(u)$ for our transition to the second equality. Next, let us focus on the solution of I_2, we have

$$\begin{aligned} I_2 &= \int \sec^3(u) du = \frac{\sec(u)\tan(u)}{2} + \frac{1}{2}\int \sec(u) du \\ &= \frac{\sec(u)\tan(u)}{2} + \frac{\ln(\tan(u) + \sec(u))}{2}. \end{aligned} \tag{F.4}$$

In the first line of the above, we applied a reduction formula

$$\int \sec^n(u) du = \frac{n-2}{n-1} \int \sec^{n-2}(u) du + \frac{\sec^{n-2}(u)\tan(u)}{n-1} \tag{F.5}$$

for $n = 3$. Also, in the last line of I_2 we replaced directly $\int \sec(u) du = \ln(\tan(u) + \sec(u))$, because it is a standard integral. Now, we will undo our substitution $u = \arctan\big(\sqrt{-a}x\big)$. We have

$$\tan\big(\arctan\big(\sqrt{-a}x\big)\big) = \sqrt{-a}x \tag{F.6}$$

and

$$\sec\big(\arctan\big(\sqrt{-a}x\big)\big) = \sqrt{1 - ax^2}. \tag{F.7}$$

Finally, we can apply our results to our integral

$$\begin{aligned} I &= \frac{1}{\sqrt{-a}} I_2 = \frac{\sec(u)\tan(u)}{2\sqrt{-a}} + \frac{\ln(\tan(u)+\sec(u))}{\sqrt{-a}} \\ &= \frac{x\sqrt{1-ax^2}}{2} + \frac{\ln\left(\sqrt{1-ax^2}-\sqrt{-a}x\right)}{2\sqrt{-a}}. \end{aligned} \tag{F.8}$$

The problem is solved. Apply the absolute value function to arguments of logarithm functions in order to extend the antiderivative's domain:

$$I = \int \sqrt{1-ax^2}dx = \frac{x\sqrt{1-ax^2}}{2} + \frac{\ln\left(\left|\sqrt{1-ax^2}-\sqrt{-a}x\right|\right)}{2\sqrt{-a}} + C. \tag{F.9}$$

For the last step, we can prove that

$$\arcsin x = \frac{1}{i}\ln\left(ix + \sqrt{1-x^2}\right). \tag{F.10}$$

Assume $y \in \mathbb{R}$ where $-\frac{\pi}{2} \leq y \leq \frac{\pi}{2}$,

$$\begin{aligned} & y = \arcsin x \Leftrightarrow x = \sin y \Leftrightarrow x = \frac{1}{2i}(e^{iy} - e^{-iy}) \Leftrightarrow \\ & \Leftrightarrow 2ix = e^{iy} - e^{-iy} \Leftrightarrow 2ixe^{iy} = e^{2iy} - 1 \Leftrightarrow \\ & \Leftrightarrow e^{2iy} - 2ixe^{1y} = -1 \Leftrightarrow e^{2iy} - 2ixe^{1y} - x^2 = 1 - x^2 \Leftrightarrow \\ & \Leftrightarrow (e^{iy} - ix)^2 = 1 - x^2 \Leftrightarrow e^{iy} - ix = \sqrt{1-x^2} \Leftrightarrow \\ & \Leftrightarrow iy = \ln\left(ix + \sqrt{1+x^2}\right) \Leftrightarrow y = \frac{1}{i}\ln\left(ix + \sqrt{1-x^2}\right). \end{aligned} \tag{F.11}$$

So, our integral becomes

$$I = \frac{\arcsin\left(\sqrt{a}\,x\right)}{2\sqrt{a}} + \frac{x\sqrt{1-ax^2}}{2} + C \tag{F.12}$$

and the definite integral of Eq.(5.87)

$$I_d = \int_0^{x_0} \sqrt{1-ax^2}dx = \frac{\sqrt{a}\arcsin\left(\sqrt{a}\,x_0\right) + ax_1\sqrt{1-ax_0^2}}{2a}. \tag{F.13}$$

Chapter G

Derivation of Eq.(6.24)

In this Appendix we will try to reproduce Eq.(6.24) just like Guth and Weinberg did in [243]. Recall that $p(t)$ is the fraction of space remaining in the old phase. First of all, consider a space containing randomly placed spheres, including overlapping and nested spheres, then someone shall ask for the probability that a given point in this space is not inside any sphere. Next, we will let $n(V)dV$ to be the density of spheres with some volume between V and $V + dV$ and $g(V_1, V_2)$ to be the probability that a given point is not contained in any sphere of volume between V_1 and V_2. We shall also state that $n(V)VdV$ is the total volume of bubbles with volumes between V and V+dV per unit volume. This allows us to write

$$g(V, V + dV) = 1 - n(V)VdV \tag{G.1}$$

as the probability of a point not belonging in a spherical volume between V and $V + dV$, then from this

$$\begin{aligned} g(V_1, V_2 + dV_2) &= g(V_1, V_2)g(V_2, V_2 + dV_2) \\ &= g(V_1, V_2)[1 - n(V_2)V_2dV_2], \end{aligned} \tag{G.2}$$

so, on the left hand side after some rearrangement of the terms, the definition of the first derivative appears and we get

$$\frac{\mathrm{d}g(V_1, V_2)}{\mathrm{d}V_2} = -n(V_2)g(V_1, V_2)V_2. \tag{G.3}$$

Solving this simple differential equation someone has

$$g(V_1, V_2) = \exp\left[-\int_{V_1}^{V_2} dVn(V)V\right]. \tag{G.4}$$

In particular, the probability of not being in any sphere is

$$g(0, \infty) = e^{-\mathcal{U}}, \tag{G.5}$$

where

$$\mathcal{U} = \int_0^{\infty} dVn(V)V. \tag{G.6}$$

This $\mathcal{U}$ is the total volume in spheres per unit volume of space or the probability of a point belonging to a bubble.

Under the restriction that does not allow bubbles to nucleate within other bubbles, their distribution is not completely random in the phase transition. We are going to relax this condition

and include a number of bubbles nucleating within bubbles, since these fictitious bubbles are entirely contained within real ones, this will cause no error in our determination of $p(t)$. As we know $\Gamma(t)$ is the nucleation rate, and the comoving volume at time t of a bubble formed at t',

$$V(t',t) = \frac{4\pi}{3} r(t',t)^3 = \frac{4\pi}{3}\left[\int_{t'}^{t} dt'' \frac{1}{a(t'')}\right]^3. \tag{G.7}$$

Initially, the radius of the bubble is negligible ($r(t') = 0$) and the bubble expands with the speed of light in a flat universe. The comoving volume expression is resulting from the latter statement

$$ds^2 = 0 \Rightarrow dt = adr \Rightarrow r = \int \frac{dt}{a}. \tag{G.8}$$

The total number of bubbles (real and fictitious) formed per unit time per unit coordinate volume is $\Gamma(t)a(t)^3$ and

$$\mathcal{U} = \int_{t_0}^{t} dt \Gamma(t) a(t)^3 V(t',t). \tag{G.9}$$

If we substitute the latter in Eq.(G.4) we obtain Eq.(6.24).

Chapter H

The new SH0ES data analysis

H.1 A brief presentation of the standard baseline SH0ES analysis

In this section, we will show the main equations used in the modeling of the Cepheid SnIa measured apparent magnitudes with parameters including H_0, as it was presented in [226]. These equations are outlined below:

- The equation that connects the measured Wesenheit magnitude of the jth Cepheid in the ith galaxy, with the host distance moduli μ_i and the modeling parameters M_W, b_W and Z_W is of the form[1]

$$m^W_{H,i,j} = \mu_i + M^W_H + b_W[P]_{i,j} + Z_W[O/H]_{i,j}, \tag{H.1}$$

  where μ_i is the inferred distance modulus to the galaxy, M^W_H is the zero-point Cepheid absolute magnitude of a period $P = 10\,d$ Cepheid (d for days). The relationship between magnitude and metallicity as well as period is depicted by the slope parameters b_W-Z_W. The $[O/H]$ is a measure of the metallicity of the Cepheid. The Cepheid metal abundance in comparison to that of our Sun is represented by the standard bracket shorthand notation $[O/H]$.

$$[O/H] \equiv \log(O/H) - \log(O/H)_\odot = \Delta \log(O/H). \tag{H.2}$$

  Some more comments to be stated here are that O and H represent the quantity of oxygen and hydrogen atoms per unit of volume respectively. A unit used to measure metallicity dex (decimal exponent) is defined as $n\,dex \equiv 10^n$. Also, the bracket shorthand notation for the period $[P]$ is used as

$$[P] \equiv \log P - 1, \tag{H.3}$$

  where $[P]$ is measured in days

- There is a relation that connects the color and shape corrected SnIa B-band peak magnitude in the ith host with μ_i of the ith host and with the SnIa M_B

$$m^0_{B,i} = \mu_i + M_B. \tag{H.4}$$

[1] For Cepheids in the LMC/SMC anchor observed from the ground the zero-point parameter zp is added on the right-hand side and therefore Eq.(H.1) is going to be $m^W_{H,i,j} = \mu_i + M^W_{H,i} + b_W[P]_{i,j} + Z_W[O/H]_{i,j} + zp$ to allow for a different P-L zero-point between ground and HST observations.

The relation between the distance modulus and the luminosity distance d_L measured in Mpc is

$$\mu = 5\log(d_L/Mpc) + 25, \tag{H.5}$$

where in a flat universe

$$d_L(z) = c(1+z)\int_0^z \frac{dz'}{H(z')} = cH_0^{-1}(1+z)\int_0^z \frac{H_0\, dz'}{H(z')} \equiv H_0^{-1}\, D_L(z), \tag{H.6}$$

where $D_L(z)$ is the Hubble free luminosity distance which is independent of H_0.

- Combining Eqs.(H.4)-(H.6) it is trivial to derive the equation showing that H_0 is connected with M_B and $D_L(z)$. This is

$$5\log H_0 = M_B + 5\log D_L(z) - m_B^0(z) + 25. \tag{H.7}$$

In the framework of a cosmographic expansion of $H(z)$ valid for $z \ll 1$ [299] we have

$$\log D_L(z)_c \simeq \log\left[cz\left(1 + \frac{1}{2}(1-q_0)z - \frac{1}{6}(1-q_0-3q_0^2+j_0)z^2 + \mathcal{O}(z^3)\right)\right] \tag{H.8}$$

where $q_0 \equiv -\frac{1}{H_0^2}\frac{d^2a(t)}{dt^2}\Big|_{t=t_0}$ and $j_0 \equiv \frac{1}{H_0^3}\frac{d^3a(t)}{dt^3}\Big|_{t=t_0}$ are the deceleration and jerk parameters respectively. Conclusively, Eqs.(H.7) and (H.8) lead to the expression that relates H_0 with the SnIa absolute magnitude M_B, which can be written as

$$5\log H_0 = M_B + 5\log D_L(z) - m_B^0(z) + 25 \equiv M_B + 5\, a_B + 25. \tag{H.9}$$

The parameter $a_B \equiv \log D_L(z) - 0.2 m_B^0(z)$ is defined in the SH0ES work in [300].

In summary, the most substantial equations for modeling in the SH0ES analysis for the measurement of H_0 are Eqs.(H.1), (H.4) and (H.9). The data entered in these equations are the apparent magnitudes of Cepheids $m_{H,i,j}^W$ and the SnIa apparent magnitudes $m_{B,i}^0$ (hosted in galaxies with Cepheid and SnIa or in the Hubble flow) which can be measured. The parameters to be fit using a maximum likelihood approach are the distance moduli μ_i (of the anchors and supporting hosts, the Cepheid+SnIa hosts and, Hubble flow SnIa), the parameters (M_H^W, b_W, Z_W and M_B), the Hubble constant H_0, the zero-point zp of the Cepheid P-L relation in the LMC ground measurements and the dummy parameter X. A number of forty-seven parameters. The SH0ES team has released the data as a .fits file and given them in a format of a data column vector Y with 3492 entries which include eight constraints on the parameters obtained from observations in anchor galaxies where the μ_i are measured directly with geometric methods.

Also, we should refer that the entries of Y matrix do not involve purely measured magnitudes. In fact, these entries are the residuals derived by subtraction of specific quantities. In particular:

- The Cepheid Wesenheit magnitudes are presented as residuals with respect to a fiducial P-L term as

$$\bar{m}_{H,i,j}^W \equiv m_{H,i,j}^W - b_W^0[P] \tag{H.10}$$

where $b_W^0 = -3.286$ is a fiducial Cepheid P-L slope. As a consequence of the definition given, the derived best-fit slope is in fact a residual slope $\Delta b_W \equiv b_W - b_W^0$.

- The residual Cepheid Wesenheit magnitudes of the Cepheids in the anchors $N4258$, LMC, and the supporting pure Cepheid host SMC (non-SnIa hosts) are shown following subtraction of the matching geometrically determined fiducial μ_i.

- The standardized apparent magnitudes of supernovae type Ia in the Hubble flow are given as residuals after subtracting the $D_L(z)$ with cosmographic expansion $5\log D_L(z)_c + 25$ (see Eq.(H.8)).

From the above, we can present the column vector Y:

$$
\mathbf{Y} = \left(\begin{array}{c}
\bar{m}^W_{H,1} \\
\dots \\
\bar{m}^W_{H,2150} \\
\hline
\bar{m}^W_{H,N4258,1} - \mu_{0,N4258} \\
\dots \\
\bar{m}^W_{H,N4258,443} - \mu_{0,N4258} \\
\bar{m}^W_{H,M31,1} \\
\dots \\
\bar{m}^W_{H,M31,55} \\
\bar{m}^W_{H,LMC,ground,1} - \mu_{0,LMC} \\
\dots \\
\bar{m}^W_{H,LMC,ground,270} - \mu_{0,LMC} \\
\bar{m}^W_{H,SMC,ground,1} - \mu_{0,SMC} \\
\dots \\
\bar{m}^W_{H,SMC,ground,143} - \mu_{0,SMC} \\
\bar{m}^W_{H,LMC,HST,1} - \mu_{0,LMC} \\
\dots \\
\bar{m}^W_{H,LMC,HST,69} - \mu_{0,LMC} \\
\hline
\bar{m}^0_{B,1} \\
\dots \\
m^0_{B,77} \\
\hline
-5.803 \ (M^W_{H,HST}) \\
-5.903 \ (M^W_{H,Gaia}) \\
-0.21 \ (Z_{W,Gaia}) \\
0 \ (X) \\
0 \ (\Delta zp) \\
0 \ (\Delta b_W) \\
0 \ (\Delta \mu_{N4258}) \\
0 \ (\Delta \mu_{LMC}) \\
\hline
m^0_{B,1} - 5\log[cz_1(...)] - 25 \\
\dots \\
m^0_{B,277} - 5\log[cz_{277}(...)] - 25
\end{array}\right)
\begin{array}{l}
\} \ 2150 \, Cepheids \, in \, 37 \, SnIa \, hosts \\
\} \ 980 \, Cepheids \, in \, non \, SnIa \, hosts \\
\} \ 77 \, SnIa \, in \, Cepheid \, hosts \\
\} \ 8 \, External \, constraints \\
\} \ 277 \, SnIa \, in \, Hubble \, flow
\end{array}
$$

The 8 external anchor parameter constraints appearing in Y are shown below:

$$\begin{aligned} M_H^W &= -5.803 \pm 0.082 \\ M_H^W &= -5.903 \pm 0.025 \\ Z_W &= -0.21 \pm 0.12 \\ X &= 0 \pm 0.00003 \\ \Delta zp &= 0 \pm 0.1 \\ \Delta b_W &= 0 \pm 10 \\ \Delta\mu_{N4258} &= 0 \pm 0.03 \\ \Delta\mu_{LMC} &= 0 \pm 0.026 \end{aligned} \tag{H.11}$$

The parameters to be fit utilizing the data from the column vector Y can be written in a vector form q with 47 entries:

$$\mathbf{q}= \left.\begin{pmatrix} \mu_1 \\ \dots \\ \mu_{37} \\ \Delta\mu_{N4258} \\ M_H^W \\ \Delta\mu_{LMC} \\ \mu_{M31} \\ \Delta b_W \\ M_B \\ Z_W \\ X \\ \Delta zp \\ 5\log H_0 \end{pmatrix}\right\} 47 \text{ parameters}$$

If we make usage of the column vectors formulation we have $\mathbf{Y}$ and $\mathbf{q}$ for the Y and q matrices respectively. Then, we can express the content of Eqs.(H.1), (H.4) and (H.9) in the form below

$$\mathbf{Y} = \mathbf{L}\mathbf{q}, \tag{H.12}$$

with the matrices to be $\mathbf{Y}$ for the measurements, the parameters' matrix $\mathbf{q}$ and $\mathbf{L}$ a model matrix with 3492 rows corresponding to measurement matrix $\mathbf{Y}$ and 47 columns corresponding to $\mathbf{q}$. The design matrix $\mathbf{L}$ also contains some Cepheid's data, more specifically their periods and metallicities. In the baseline, modeling process $\mathbf{L}$ can be formed as

$$\mathbf{L} = \left(\begin{array}{cccccccccccccc}
1 & \dots & 0 & 0 & 1 & 0 & 0 & [P]_1 & 0 & [O/H]_1 & 0 & 0 & 0 \\
\dots & \dots & \dots & \dots & \dots & \dots & \dots & \dots & \dots & \dots & \dots & \dots & \dots \\
0 & \dots & 1 & 0 & 1 & 0 & 0 & [P]_{2150} & 0 & [O/H]_{2150} & 0 & 0 & 0 \\
\hline
0 & \dots & 0 & 1 & 1 & 0 & 0 & [P]_{N4258,1} & 0 & [O/H]_{N4258,1} & 0 & 0 & 0 \\
\dots & \dots & \dots & \dots & \dots & \dots & \dots & \dots & \dots & \dots & \dots & \dots & \dots \\
0 & \dots & 0 & 1 & 1 & 0 & 0 & [P]_{N4258,443} & 0 & [O/H]_{N4258,443} & 0 & 0 & 0 \\
0 & \dots & 0 & 0 & 1 & 0 & 1 & [P]_{M31,1} & 0 & [O/H]_{M31,1} & 0 & 0 & 0 \\
\dots & \dots & \dots & \dots & \dots & \dots & \dots & \dots & \dots & \dots & \dots & \dots & \dots \\
0 & \dots & 0 & 0 & 1 & 0 & 1 & [P]_{M31,55} & 0 & [O/H]_{M31,55} & 0 & 0 & 0 \\
0 & \dots & 0 & 0 & 1 & 1 & 0 & [P]_{LMC,ground,1} & 0 & [O/H]_{LMC,ground,1} & 0 & 1 & 0 \\
\dots & \dots & \dots & \dots & \dots & \dots & \dots & \dots & \dots & \dots & \dots & \dots & \dots \\
0 & \dots & 0 & 0 & 1 & 1 & 0 & [P]_{LMC,ground,270} & 0 & [O/H]_{LMC,ground,270} & 0 & 1 & 0 \\
0 & \dots & 0 & 0 & 1 & 1 & 0 & [P]_{SMC,ground,1} & 0 & [O/H]_{SMC,ground,1} & 0 & 1 & 0 \\
\dots & \dots & \dots & \dots & \dots & \dots & \dots & \dots & \dots & \dots & \dots & \dots & \dots \\
0 & \dots & 0 & 0 & 1 & 1 & 0 & [P]_{SMC,ground,143} & 0 & [O/H]_{SMC,ground,143} & 0 & 1 & 0 \\
0 & \dots & 0 & 0 & 1 & 1 & 0 & [P]_{LMC,HST,1} & 0 & [O/H]_{LMC,HST,1} & 0 & 0 & 0 \\
\dots & \dots & \dots & \dots & \dots & \dots & \dots & \dots & \dots & \dots & \dots & \dots & \dots \\
0 & \dots & 0 & 0 & 1 & 1 & 0 & [P]_{LMC,HST,69} & 0 & [O/H]_{LMC,HST,69} & 0 & 0 & 0 \\
\hline
1 & \dots & 0 & 0 & 0 & 0 & 0 & 0 & 1 & 0 & 0 & 0 & 0 \\
\dots & \dots & \dots & \dots & \dots & \dots & \dots & \dots & \dots & \dots & \dots & \dots & \dots \\
0 & \dots & 1 & 0 & 0 & 0 & 0 & 0 & 1 & 0 & 0 & 0 & 0 \\
\hline
0 & \dots & 0 & 0 & 1 & 0 & 0 & 0 & 0 & 0 & 0 & 0 & 0 \\
0 & \dots & 0 & 0 & 1 & 0 & 0 & 0 & 0 & 0 & 0 & 0 & 0 \\
0 & \dots & 0 & 0 & 0 & 0 & 0 & 0 & 0 & 1 & 0 & 0 & 0 \\
0 & \dots & 0 & 0 & 0 & 0 & 0 & 0 & 0 & 0 & 1 & 0 & 0 \\
0 & \dots & 0 & 0 & 0 & 0 & 0 & 0 & 0 & 0 & 0 & 1 & 0 \\
0 & \dots & 0 & 0 & 0 & 0 & 0 & 1 & 0 & 0 & 0 & 0 & 0 \\
0 & \dots & 0 & 1 & 0 & 0 & 0 & 0 & 0 & 0 & 0 & 0 & 0 \\
0 & \dots & 0 & 0 & 0 & 1 & 0 & 0 & 0 & 0 & 0 & 0 & 0 \\
\hline
0 & \dots & 0 & 0 & 0 & 0 & 0 & 0 & 1 & 0 & 0 & 0 & -1 \\
\dots & \dots & \dots & \dots & \dots & \dots & \dots & \dots & \dots & \dots & \dots & \dots & \dots \\
0 & \dots & 0 & 0 & 0 & 0 & 0 & 0 & 1 & 0 & 0 & 0 & -1
\end{array}\right)$$

The entries separated with horizontal lines correspond from top to bottom to:

- **2150 Cepheids in 37 SnIa hosts**
- **980 Cepheids in non SnIa hosts**
- **77 SnIa in Cepheid hosts**
- **8 External constraints**
- **277 SnIa in Hubble flow**

It is obvious that the system of Eq.(H.12) consists of 3492 equations and 47 unknown parameter values. A system of equations is characterized as overdetermined in mathematics if there are more equations than unknowns [301]. When a system is overdetermined and has random coefficients, it is usually always inconsistent (it has no solution) and in our case at best it can be used in the context of the maximum likelihood analysis to find the best fit parameter values that have maximum likelihood and thus the χ^2 is the minimum. In order to define χ^2 statistic we need the measurement error matrix (covariance matrix) $\mathbf{C}$. In general, the 3492×3492 matrix $\mathbf{C}$ along with $\mathbf{Y}$, $\mathbf{L}$ matrices are provided publicly as fits files by SH0ES team at Github: PantheonPlusSH0ES/DataRelease. Using the measurement error matrix $\mathbf{C}$ that quantifies the uncertainties and the correlation of the data, the χ^2 can be expressed as

$$\chi^2 = (\mathbf{Y} - \mathbf{Lq})^{\mathbf{T}} \mathbf{C}^{-\mathbf{1}} (\mathbf{Y} - \mathbf{Lq}). \tag{H.13}$$

The linearity of the system (H.12) allows the analytical minimization of χ^2 and simultaneously this means that the uncertainty of each parameter can be analytically evaluated. If we minimize analytically χ^2, we can calculate the best fit parameter maximum likelihood vector. Let us show how we can achieve it. Firstly, using the properties of a transpose matrix we can express the χ^2 statistic as

$$\begin{aligned}\chi^2 &= (\mathbf{Y}-\mathbf{Lq})^{\mathbf{T}}\mathbf{C}^{-\mathbf{1}}(\mathbf{Y}-\mathbf{Lq})\\ &= (\mathbf{Y}^{\mathbf{T}}-\mathbf{q}^{\mathbf{T}}\mathbf{L}^{\mathbf{T}})\\ &= \mathbf{q}^{\mathbf{T}}\mathbf{L}^{\mathbf{T}}\mathbf{C}^{-\mathbf{1}}\mathbf{Lq}-\mathbf{2q}^{\mathbf{T}}\mathbf{L}^{\mathbf{T}}\mathbf{C}^{-\mathbf{1}}\mathbf{Y}+\mathbf{Y}^{\mathbf{T}}\mathbf{C}^{-\mathbf{1}}\mathbf{Y}.\end{aligned} \tag{H.14}$$

Next, we will minimize χ^2 with respect to $\mathbf{q}$

$$\frac{\partial\chi^2}{\partial\mathbf{q}}\Big|_{\mathbf{q}_{best}} = 0 \Rightarrow \mathbf{2L^{T}C^{-1}Lq_{best}-2L^{T}C^{-1}Y=0}. \tag{H.15}$$

It follows, from Eq.(H.15), that

$$\mathbf{q}_{best} = (\mathbf{L}^{\mathbf{T}}\mathbf{C}^{-\mathbf{1}}\mathbf{L})^{-\mathbf{1}}\mathbf{L}^{\mathbf{T}}\mathbf{C}^{-\mathbf{1}}\mathbf{Y}. \tag{H.16}$$

This is the best fit parameter maximum likelihood vector. Now, the standard errors squared of $\mathbf{q_{best}}$ entries are given as the elements on the diagonals of the transformed covariance matrix

$$\Sigma_{\mathbf{kl}} = \sum_{\mathbf{i}}\sum_{\mathbf{j}}\left[\frac{\partial\mathbf{q_{best,k}}}{\partial\mathbf{Y_i}}\right]\mathbf{C_{ij}}\left[\frac{\partial\mathbf{q_{best,l}}}{\partial\mathbf{Y_j}}\right], \tag{H.17}$$

or, someone can write

$$\Sigma = \left[\frac{\partial\mathbf{q_{best}}}{\partial\mathbf{Y}}\right]\mathbf{C}\left[\frac{\partial\mathbf{q_{best}}}{\partial\mathbf{Y}}\right]^{\mathbf{T}}. \tag{H.18}$$

Therefore,

$$\begin{aligned}\Sigma &= (\mathbf{L}^{\mathbf{T}}\mathbf{C}^{-\mathbf{1}}\mathbf{L})^{-\mathbf{1}}\mathbf{L}^{\mathbf{T}}\mathbf{C}^{-\mathbf{1}}\mathbf{C}\left[(\mathbf{L}^{\mathbf{T}}\mathbf{C}^{-\mathbf{1}}\mathbf{L})^{-\mathbf{1}}\mathbf{L}^{\mathbf{T}}\mathbf{C}^{-\mathbf{1}}\right]^{\mathbf{T}}\\ &= (\mathbf{L}^{\mathbf{T}}\mathbf{C}^{-\mathbf{1}}\mathbf{L})^{-\mathbf{1}}\mathbf{L}^{\mathbf{T}}\mathbf{C}^{-\mathbf{1}}\mathbf{C}\mathbf{C}^{-\mathbf{1}}\mathbf{L}(\mathbf{L}^{\mathbf{T}}\mathbf{C}^{-\mathbf{1}}\mathbf{L})^{-\mathbf{1}}\\ &= (\mathbf{L}^{\mathbf{T}}\mathbf{C}^{-\mathbf{1}}\mathbf{L})^{-\mathbf{1}}.\end{aligned} \tag{H.19}$$

For a paradigm, the best fit of the parameter $5\log H_0$ is obtained as the entry with the number 47 of the vector $\mathbf{q_{best}}$ and the corresponding 1σ standard error is the $\sqrt{\Sigma_{\mathbf{47,47}}}$ element of the error matrix. Using Eq.(H.16), Eq.(H.19) and the released data of the SH0ES team, the latest R21 published result for the Hubble parameter is $H_0 = 73.04 \pm 1.04 km\ s^{-1}\ Mpc^{-1}$.

H.2 What if a Cepheid calibration parameter is allowed to transit?

As it has already been written in the text a transition can be allowed to the system if one of the four Cepheid parameters for calibration in $\mathbf{q}$ vector is replaced by two new respective parameters, one for high and the other for low distances. In this situation, the entries of the matrix $\mathbf{q}$ are increased by one and now there are 48 (from 47 originally). Since one of the entries of $\mathbf{q}$ is changed into a pair of entries, the corresponding column of $\mathbf{L}$ should now acquire a dyad of columns. One of these two columns corresponding to the high distances adopts the entries from

the original column related to them and is filled with zeros in entries related to the low distance data (or constraints) and the reverse should happen for the low distance parameter column. These matrices' transformations are shown in the schematic diagrams depicted below.

$$\mathbf{L_{(3492\times 47)}} = \left(\begin{array}{ccc} \dots & L_{1,j} & \dots \\ \dots & L_{2,j} & \dots \\ \dots & L_{3,j} & \dots \\ \dots & \dots & \dots \\ \dots & \dots & \dots \\ \dots & L_{3491,j} & \dots \\ \dots & L_{3492,j} & \dots \end{array}\right) \left.\begin{array}{l} \\ \\ \\ \\ \\ \\ \\ \end{array}\right\} \begin{array}{c} D_{Y_1} < D_c \\ D_{Y_2} > D_c \\ D_{Y_3} > D_c \\ \dots \\ \dots \\ D_{Y_{3491}} < D_c \\ D_{Y_{3492}} > D_c \end{array} \implies \mathbf{L_{(3492\times 48)}} = \left(\begin{array}{ccc} \dots & L_{1,j} & 0 & \dots \\ \dots & 0 & L_{2,j+1} & \dots \\ \dots & 0 & L_{3,j+1} & \dots \\ \dots & \dots & \dots & \dots \\ \dots & \dots & \dots & \dots \\ \dots & L_{3491,j} & 0 & \dots \\ \dots & 0 & L_{3492,j+1} & \dots \end{array}\right) \tag{H.20}$$

$$\mathbf{q_{(47\times 1)}} = \begin{pmatrix} \dots \\ \dots \\ \dots \\ q_j \\ \dots \\ \dots \end{pmatrix} \rightarrow \mathbf{q_{(48\times 1)}} = \begin{pmatrix} \dots \\ \dots \\ q_j \\ q_{j+1} \\ \dots \\ \dots \end{pmatrix} \tag{H.21}$$

For example, if a transition was allowed to b_W then this parameter would be split to to $b_W^>$ and $b_W^<$ and Eq. (H.1) would be replaced by

$$m^W_{H,i,j}(D) = \mu_i + M_H^W + b_W^> \Theta(D - D_c)[P]_{i,j} + b_W^< \Theta(D_c - D)[P]_{i,j} + Z_W[O/H]_{i,j}. \tag{H.22}$$

Our actions would be similar for the splitting of each one of the other 3 calibration parameters M_H^W, Z_W, and M_B. In (H.22) D is a distance that might be applied to each data-vector entry $\mathbf{Y}$. The form of the data vector and the covariance matrix $\mathbf{C}$ are not affected by the duality of any parameter in versions of high-distance and low-distance.

H.3 Adding the inverse instant ladder constraint on M_B

First let us recall the inverse distance ladder constraint on M_B [130, 273, 274]:

$$M_B^{P18} = -19.401 \pm 0.027. \tag{H.23}$$

The analysis is modified by adding a further constraint to the $\mathbf{Y}$ data vector (the eighth constraint corresponds to entry 3125 and after this, entry 3216 is added with the value of -19.401 for the

M_B constraint). Now, the model matrix $\mathbf{L}$ needs one more line too, after line 3215 all entries are set to zero except the entry at the 43rd column that corresponds to $M_B^<$, the low distance parameter. One more column after the 43rd column is added in the model matrix to accommodate the parameter $M_B^>$ for high distances. A distance that is larger than this of the most distant type Ia supernovae of the sample is assigned to the new constraint so that it has an effect only on $M_B^>$ (the entry at line 3216 column 43 of the matrix $\mathbf{L}$ gets zero for value for all D_c while the next element at 44th column is set to one for all D_c). A line is added to $\mathbf{C}$ following line 3215 with a single entry at the diagonal equal to $\sigma_{MB}^2 = 0.027^2 = 0.000729$ to account for the equivalent uncertainty of the additional constraint. Consequently, upon the introduction of the limitation in the M_B transition model the measurement matrix $\mathbf{Y}$ has 3493 elements, $\mathbf{L}$ has dimensions 3493×48, $\mathbf{q}$ vector has 48 elements and $\mathbf{C}$ has dimensions 3493×3493.

Chapter I

Numerical methods for the vacuum decay

I.1 Zero temperature false vacuum decay at flat space-time

I.1.1 The rescaled action and the rescaled potential

In this first section of our final appendix, we will follow the methods used in [157]. The main quest is to go a step further, beyond our standard thin-wall assumption, and achieve a precise numerical solution for the bounce equation.

Our first goal is to proceed to the Euclidean action and the potential rescaling. consider our familiar potential

$$U(\phi) = \frac{\lambda}{8}(\phi^2 - a^2)^2 - \frac{\epsilon}{2a}(\phi - a), \tag{I.1}$$

with $a > 0$, $\lambda > 0$, and $\epsilon > 0$ the external cause which breaks the symmetry of the double well. The two minima of the potential, in first order with respect to ϵ, will be

$$\phi_\pm(\epsilon) = \phi_\pm(0) + \frac{1}{2}\frac{\mathrm{d}\phi_\pm}{\mathrm{d}\epsilon}\bigg|_{\epsilon=0} \epsilon + \dots, \tag{I.2}$$

with $\phi_\pm(0) = \pm a$, for $\epsilon \ll 1$. Then,

$$\frac{\mathrm{d}U}{\mathrm{d}\phi}\bigg|_{\phi_\pm} = 0 \Rightarrow \phi_\pm(\phi_\pm^2 - a^2) = \frac{\epsilon}{\lambda a}. \tag{I.3}$$

If we differentiate with respect to ϵ and calculate the expression in $\epsilon = 0$, it becomes

$$3\phi_\pm^2 \frac{\mathrm{d}\phi_\pm}{\mathrm{d}\epsilon}\bigg|_{\epsilon=0} - a^2 \frac{\mathrm{d}\phi_\pm}{\mathrm{d}\epsilon}\bigg|_{\epsilon=0} = \frac{1}{\lambda a} \Rightarrow \frac{\mathrm{d}\phi_\pm}{\mathrm{d}\epsilon}\bigg|_{\epsilon=0} = \frac{1}{\lambda a^3}. \tag{I.4}$$

Finally, (I.2) becomes

$$\phi_\pm = a\left(1 + \frac{\epsilon}{\lambda a^4} + \dots\right) \tag{I.5}$$

Now, we are going to expand our scalar field about ϕ_+, its false vacuum, in the following way

$$\phi = \phi_+ + \varphi. \tag{I.6}$$

In this way, if we Taylor expand the potential we get rid of the linear term as follows

$$U(\varphi) = U(\phi_+) + \cancel{U'(\phi_+)(\varphi-\phi_+)^0} + \frac{U''(\phi_+)}{2}(\varphi-\phi_+)^2 + \frac{U'''(\phi_+)}{3!}(\varphi-\phi_+)^3 + \frac{U''''(\phi_+)}{4!}(\varphi-\phi_+)^4 + \dots$$

$$\Rightarrow U(\varphi) = U(\phi_+) + \frac{U''(\phi_+)}{2}(\varphi-\phi_+)^2 + \frac{U'''(\phi_+)}{6}(\varphi-\phi_+)^3 + \frac{U''''(\phi_+)}{24}(\varphi-\phi_+)^4 + \dots. \quad \text{(I.7)}$$

Now, after a great amount of very trivial algebra, which is not shown here due to its size and simplicity, the potential up to dimension four is given by

$$U(\varphi) = \frac{m}{2}\varphi^2 - \eta\varphi^3 + \frac{\lambda}{8}\varphi^4, \quad \text{(I.8)}$$

where we have defined

$$m^2 = \frac{\lambda}{2}(3\phi_+^2 - a^2), \qquad \eta = \frac{\lambda}{2}|\phi_+|. \quad \text{(I.9)}$$

If we rescale the field φ as well as the coordinates of space-time as

$$\varphi = \frac{m^2}{2\eta}\Phi, \qquad \tilde{x} = mx, \quad \text{(I.10)}$$

the classical Euclidean action

$$S_E[\varphi] = \int d^4x \left[\frac{1}{2}(\partial_\mu\varphi)^2 + \frac{m}{2}\varphi^2 - \eta\varphi^3 + \frac{\lambda}{8}\varphi^4\right] \quad \text{(I.11)}$$

after some simple algebra will simplify to

$$S_E[\Phi] = \left(\frac{m^2}{4\eta^2}\right)\int d^4\tilde{x}\left[\frac{1}{2}(\tilde{\partial}_\mu\Phi)^2 + \frac{1}{2}\Phi^2 - \frac{1}{3}\Phi^3 + \frac{k}{8}\Phi^4\right], \quad \text{(I.12)}$$

where the dimensionless k next to the quartic coupling strength is defined as

$$k = \frac{\lambda m^2}{4\eta^2} = 1 - \frac{\epsilon}{2\lambda a^4} + \dots. \quad \text{(I.13)}$$

It is obvious from the above that α tends to one in the "thin-wall" limit. From Eq.(I.12) we get the dimensionless potential

$$U(\Phi) = \frac{1}{2}\Phi^2 - \frac{1}{2}\Phi^3 + \frac{k}{8}\Phi^4. \quad \text{(I.14)}$$

The shape of the potential is determined by k, and its divergence from the unity represents a measurement of the vacuum energy difference in relation to the height of the barrier. Someone can observe this behavior in Fig.I.1

I.1.2 The equation of motion

The rescaled equation of motion of the classical bounce $\Phi_{cl}(r)$ can be obtained with the principle of least action of the rescaled Euclidean equation under the usual assumption of the spherical symmetry of the bounce. Let us derive the EoM in a slightly different way from the

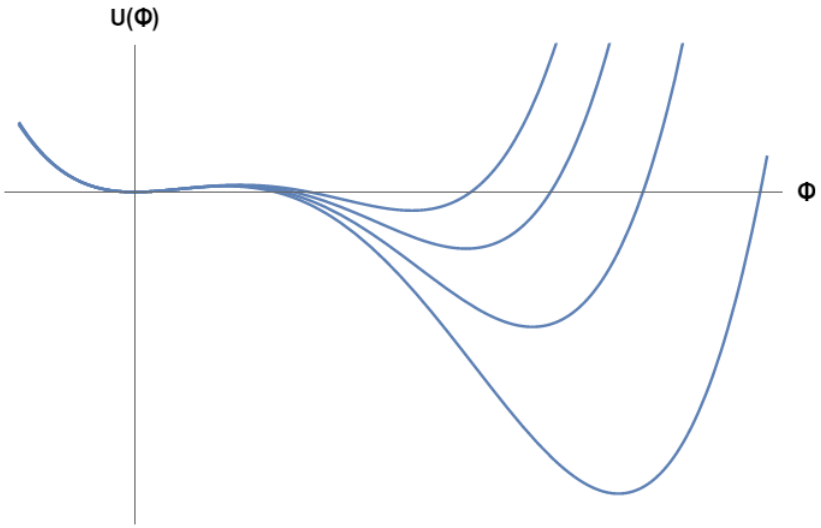

Figure I.1: The rescaled potential ploted for $k = 0.6, 0.7, 0.8, 0.9$. As this parameter approaches unity, the rescaled potential approaches the double well potential.

main text. First, we transform from the Cartesian coordinates $\{x^1, x^2, x^3, x^4\}$ to the spherical polar ones $\{r, \phi_1, \phi_2, \phi_3\}$

$$\begin{aligned} x_1 &= r\cos\phi_1 \\ x_2 &= r\sin\phi_2\cos\phi_2 \\ x_3 &= r\sin\phi_1\sin\phi_2\cos\phi_3 \\ x_4 &= r\sin\phi_2\sin\phi_2\sin\phi_3. \end{aligned} \tag{I.15}$$

The 4-volume element in Euclidean space can be obtained easily by using the Jacobian:

$$d^4x = \left|\det\frac{\partial(x_i)}{\partial(r,\phi_j)}\right| dr d\phi_1 d\phi_2 d\phi_3 = r^3\sin^2\phi_1\sin\phi_2 dr d\phi_1 d\phi_2 d\phi_3. \tag{I.16}$$

Consequently,

$$\begin{aligned} S_E[\Phi] &= \left(\frac{m^2}{4\eta^2}\right)\int d^4\tilde{x}\left[\frac{1}{2}(\tilde{\partial}_\mu\Phi)^2 + \frac{1}{2}\Phi^2 - \frac{1}{3}\Phi^3 + \frac{k}{8}\Phi^4\right] \\ &= \left(\frac{m^2}{4\eta^2}\right)\int_0^{2\pi} d\phi_3\int_0^{\pi} d\phi_2\sin\phi_2\int_0^{\pi} d\phi_1\sin^2\phi_1\int_0^{r_f} r^3 dr\left(\frac{1}{2}(\partial_r\Phi)^2 + \frac{1}{2}\Phi^2 - \frac{1}{3}\Phi^3 + \frac{k}{8}\Phi^4\right) \\ &= (2\pi)(2)\left(\frac{\pi}{2}\right)\left(\frac{m^2}{4\eta^2}\right)\int_0^{r_f} r^3 dr\left(\frac{1}{2}(\partial_r\Phi)^2 + \frac{1}{2}\Phi^2 - \frac{1}{3}\Phi^3 + \frac{k}{8}\Phi^4\right) \\ &= (2\pi)^2\left(\frac{m^2}{4\eta^2}\right)\int_0^{r_f} r^3 dr\left(\frac{1}{2}(\partial_r\Phi)^2 + \frac{1}{2}\Phi^2 - \frac{1}{3}\Phi^3 + \frac{k}{8}\Phi^4\right). \end{aligned} \tag{I.17}$$

The Lagrangian in the new coordinates will be

$$\mathcal{L}[\Phi] \propto r^3\left(\frac{1}{2}(\partial_r\Phi)^2 + \frac{1}{2}\Phi^2 - \frac{1}{3}\Phi^3 + \frac{k}{8}\Phi^4\right). \tag{I.18}$$

The equation of the bounce solution can be found by the Euler-Lagrange equation to be the following for our case

$$-\Phi_{cl}'' - \frac{3}{r}\Phi_{cl} + \Phi_{cl} - \frac{3}{2}\Phi_{cl}^2 + \frac{k}{2}\Phi_{cl}^3 = 0, \tag{I.19}$$

with the boundary conditions given by

$$\Phi_{cl}'(0) = 0, \qquad \Phi_{cl}(\infty) = \Phi_+. \tag{I.20}$$

This boundary value problem (BVP) is going to be solved numerically in the next subsection.

I.1.3 *Mathematica* coding

In this section, we will show the *Mathematica* code, explained in analytical steps, for the numerical solution of the BVP with ordinary differential equation (ODE) (I.19) and the boundary conditions of Eq.(I.20). The k parameter is a constant for which $0 < k < 1$.

Our first step is to construct an improved boundary condition for larger values of the radius r. As one may expect, from the second boundary condition at large r, Φ_{cl} is very small in this specific region. Therefore, we can drop the ODE's nonlinear terms and solve with the `DSolve` command as follows

```
In=DSolve[phi''[r] + 3/r phi'[r] − phi[r] == 0,phi[r],r]
Out={{phi[r] −> −((BesselJ[1, I r] C[1])/r) + (BesselY[1, −I r] C[2])/r}}
```

And with a proper choice of `C[1]` and `C[2]` yields `BesselK[1, r]/r`. This solution satisfies the boundary condition for Φ_{cl} at infinity. As a consequence, an improved condition for large finite r is the following

```
phi'[rmax] == c phi[rmax]
```

with

```
c = N[D[(BesselK[1, r/r), r]/(BesselK[1, r]/r) /. r −> rmax];
```

The algorithm below is the main code for plotting one of the figures of Fig.2.13 for $k = 0.7$. To perform this numerical solution *Shooting Method* was used into the `NDSolve` command

```
rmin = .01; rmax = 13; k = .7;
c = N[D[(BesselK[1, r]/r), r]/(BesselK[1, r]/r) /. r −> rmax];
sol = NDSolveValue[{phi''[r] + 3/r phi'[r] − phi[r] + 3/2 phi[r]^2
− k/2 [r]^3 == 0,
phi'[rmax] == c phi[rmax], phi'[rmin] == 0}, phi, {r, r, rmax},
Method −> {"Shooting","StartingInitialConditions"−>{phi[rmin] == 3.31151,
r'[rmin] ==0}}
]
```

The precise value of $\Phi_{cl} = 3.31151$ is obtained by performing the algorithm for `rmax=5`, which is forgiving for inaccurate guesses of the starting point, and then calling this accurate value with `sol[rmin]`. Also, to avoid the singularity at $r = 0$, the algorithm's starting point is `rmin=0.01`. A final comment, to plot the bounce solution depicted in Fig.I.2 the command `Plot` was used. The same algorithm was repeated in order to draw the figures for various values of k.

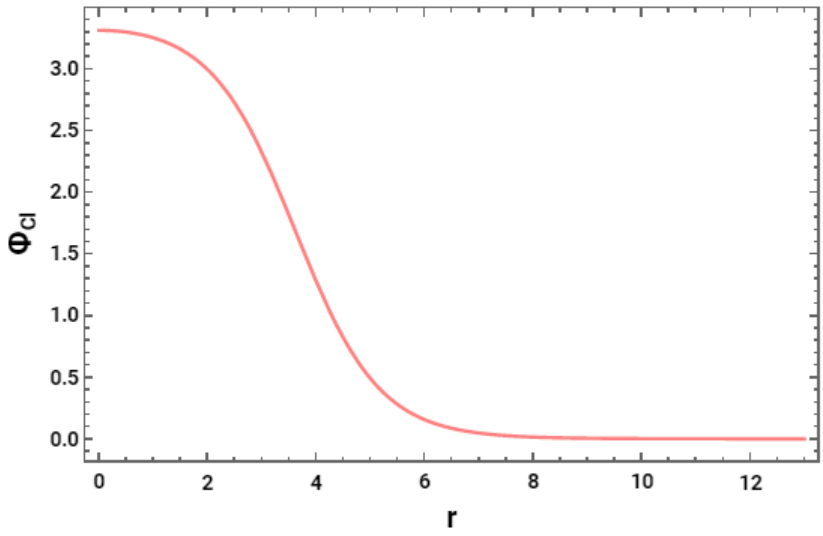

Figure I.2: The bounce solution plotted for $k = 0.7$

I.2 Zero temperature false vacuum decay at curved space-time

I.2.1 The Shooting Method explained

In this section, we will describe the method used to solve numerically the coupled field equations in the CDL case. Let us remind the equations of interest, for ϕ we have

$$\ddot{\phi} + \frac{3\dot{\rho}}{\rho}\dot{\phi} = U'(\phi) \tag{I.21}$$

and for ρ is

$$\dot{\rho}^2 = 1 + \frac{1}{3}\kappa\rho^2\left(\frac{1}{2}\dot{\phi}^2 - U(\phi)\right). \tag{I.22}$$

In this system, an issue occurs straight away because of the square root of $\dot{\rho}$ in the second equation. A clever way to avoid this ambiguity is to differentiate the equation of ρ with respect to η [302]. Let us perform this differentiation:

$$\begin{aligned}
2\dot{\rho}\ddot{\rho} &= \frac{2}{3}\kappa\rho\dot{\rho}\left(\frac{1}{2}\dot{\phi}^2 - U(\phi)\right) + \frac{1}{3}\kappa\rho^2\left(\dot{\phi}\ddot{\phi} - U'(\phi)\dot{\phi}\right) \\
\Rightarrow 2\dot{\rho}\ddot{\rho} &= \frac{2}{3}\kappa\rho\dot{\rho}\left(\frac{1}{2}\dot{\phi}^2 - U(\phi)\right) + \frac{1}{3}\kappa\rho^2\left(-\frac{3\dot{\rho}}{\rho}\dot{\phi}^2\right) \\
\Rightarrow 2\dot{\rho}\ddot{\rho} &= 2\dot{\rho}\rho\frac{\kappa}{3}\dot{\phi}^2 - 2\dot{\rho}\rho\frac{\kappa}{3}U - \dot{\rho}\rho\kappa\dot{\phi}^2.
\end{aligned}$$

In the second line, Eq.(I.21) was used. From the above, we get

$$\ddot{\rho} = -\frac{\kappa}{3}\rho(\dot{\phi} + U(\phi)). \tag{I.23}$$

Similar to the previous section we will introduce some dimensionless variables

$$x = mr, \qquad \tilde{\phi}(x) = \frac{\phi(\eta)}{m}, \qquad \tilde{U}(\tilde{\phi}) = \frac{U(\phi)}{m^4}, \qquad \tilde{\rho}(x) = \tilde{\rho}(\eta), \tag{I.24}$$

where m is the mass, arbitrarily selected. The system of the equations will be expressed in the new dimensionless variables as follows

$$\tilde{\ddot{\phi}} = -3\frac{\tilde{\dot{\rho}}}{\tilde{\rho}}\tilde{\dot{\phi}} + \frac{\mathrm{d}\tilde{U}}{\mathrm{d}\tilde{\phi}}, \tag{I.25}$$

$$\tilde{\ddot{\rho}} = -\frac{8\pi}{3}M\tilde{\rho}\left(\tilde{\dot{\phi}}^2 + \tilde{U}\right), \tag{I.26}$$

where $M = m/m_{Pl}$.

Contrary to the previous section where we used the *Shooting Method* as a saved command built-in *Mathematica*, here we will construct a shooting algorithm step by step before we begin the coding part.

The boundary conditions for the field $\tilde{\phi}$ become

$$\lim_{x\to\infty}\tilde{\phi}(x) = \frac{\phi_+}{m} \tag{I.27}$$

$$\left.\frac{\mathrm{d}\tilde{\phi}(x)}{\mathrm{d}x}\right|_{x=0} = 0. \tag{I.28}$$

The boundary conditions for $\tilde{\rho}$ read

$$\tilde{\rho}(0) = 0, \tag{I.29}$$

$$\tilde{\dot{\rho}}(0) = 1. \tag{I.30}$$

The first condition means that the bubble at the beginning of its nucleation has a tiny radius, almost zero, and the second condition arises from Eq.(I.22).

Finding a solution with numerical methods in the system of the differential equations is not a straightforward process since our boundary conditions define a BVP, not an initial value problem (IVP), but with the *Shooting Method* we can get a solution. We will define an IVP by choosing a new boundary condition for $\tilde{\phi}(0)$. This condition will have the following form

$$\tilde{\phi}(0) = a, \tag{I.31}$$

and with the conditions Eqs.(I.28)-(I.30) constitute a Cauchy problem (IVP) which can be solved numerically as a function of a. Then, this parameter is adjusted in order for Eq.(I.27) to be fulfilled.

As before, at $x = 0$ a singular point exists at Eq.(I.25); for this reason, the solution must be placed in a range $[x_{min}, x_{max}]$ with x_{min} to be positive. Consequently, the initial conditions must be adapted to $x = x_{min}$ from those at $x = 0$. To achieve this, we can connect $\tilde{\phi}(x_{min})$ to $\tilde{\phi}(0)$ if we Taylor expand as follows

$$\tilde{\phi}(x_{min}) = a + \cancel{\tilde{\dot{\phi}}(0)x_{min}} + \frac{1}{2}\tilde{\ddot{\phi}}(0)x_{min}^2 + \mathcal{O}(x_{min}^3) = a + \frac{1}{2}\tilde{\ddot{\phi}}(0)x_{min}^2 + \mathcal{O}(x_{min}^3). \tag{I.32}$$

We used Eq.(I.28) on the above expression. Now, from Eq.(I.25) we can get

$$\ddot{\tilde{\phi}}(0) = \tilde{U}'(\tilde{\phi}(0)) - \frac{3\dot{\tilde{\rho}}(x)}{\tilde{\rho}(x)}\dot{\tilde{\phi}}(x)\Big|_{x=0} = \tilde{U}'(a) - 3\ddot{\tilde{\phi}}(0). \tag{I.33}$$

This lead to

$$\ddot{\tilde{\phi}}(0) = \frac{1}{4}\tilde{U}'(a). \tag{I.34}$$

Therefore, the initial conditions for $\tilde{\phi}$ become

$$\tilde{\phi}(x_{min}) = a + \frac{1}{8}\tilde{U}'(a)x_{min}^2 + \mathcal{O}(x_{min}^3), \tag{I.35}$$

$$\dot{\tilde{\phi}}(x_{min}) = \frac{1}{4}\tilde{U}'(a)x_{min} + \mathcal{O}(x_{min}^2). \tag{I.36}$$

Acting in a similar way, we Taylor expand for $\tilde{\rho}(x_{min})$ around $\tilde{\rho}(0)$ and we get

$$\tilde{\rho}(x_{min}) = \cancel{\tilde{\rho}(0)} + \dot{\tilde{\rho}}(0)x_{min} + \frac{1}{2}\ddot{\tilde{\rho}}(0)x_{min}^2 = x_{min} \tag{I.37}$$

from Eq.(I.26) and the conditions Eq.(I.29) and Eq.(I.30). Finally, the initial conditions for $\tilde{\rho}$ will be

$$\tilde{\rho}(x_{min}) = x_{min}, \tag{I.38}$$

$$\dot{\tilde{\rho}}(x_{min}) = 1. \tag{I.39}$$

I.2.2 *Mathematica* coding

In this section, we will show the *Mathematica* code for the method described in the previous pages. Here is the first part of the program:

```
u[eps_][phi_[x_]] := 1/8 (phi[x]^2 - 1)^2 + eps/2 (phi[x] - 1);
solve[phi_, r_, x_, xmin_, xmax_, a_, a0_, fv_, mrat_, u_] :=
Module[{dua, eq},
   dua = D[u, phi[x]] /. phi[x] -> a;
   eq["phi"] = phi''[x] + 3 r'[x]/r[x] phi'[x] - D[u, phi[x]]==0;
   eq["r"] = r''[x] + 8 Pi/3 mrat^2 r[x] (phi'[x]^2 + u) == 0;
   eq["ic"] = {phi[xmin] == a + 1/8 dua xmin^2,
   phi'[xmin] == 1/4 dua xmin, r[xmin] == xmin, r'[xmin] == 1};
   ParametricNDSolve[Flatten[{eq["phi"], eq["r"], eq["ic"]}], {phi, r},
   {x, xmin, xmax},{a}]
   ];
```

In the beginning, we are setting the rescaled potential of the form

$$\tilde{U}(\tilde{\phi}) = \frac{1}{8}(\tilde{\phi}^2 - 1)^2 + \frac{\tilde{\epsilon}}{2}(\tilde{\phi} - 1). \tag{I.40}$$

Afterwards, we introduce the main function `solve`, which contains the system of the differential equations and the initial conditions constructed via the *Shooting Method* in the previous section. For the last step, the system is solved with `ParametricNDSolve` command. Now, let us present the second, and final, part of this algorithm:

```
Manipulate[Module[{pnds, phi, r, x, a},
  pnds = solve[phi, r, x, xmin, xmax, a, a0, fv, mrat,
  u[eps][phi[x]]];
  {Plot[Evaluate[{phi[a0][x]} /. pnds], {x, xmin, xmax},
    Frame->True, LabelStyle -> {Black, Bold},
    FrameLabel->{Style["η",13],Style["ϕ",13]}, Axes->False,
    PlotRange->All,
    Enclose[ConfirmQuiet[
     a = (a /. FindRoot[phi[a][xmax] == fv /. pnds, {a, a0}])]]}],
     {{xmin, .01}, .0001,.1}, {{xmax, 15}, 1, 200}, {{a0, -1.05103}, -1.1, 0},
     {{fv, 0.939646}, 1,0}, {{eps, .292}, .0002, 1}, {{mrat, .00436}, .000001, 1}
     ]
```

In this part, we use the `Manipulate` command to adjust our parameters in order to get more accurate results. In this command is enclosed the plot for the bounce solution in the curved case depicted in Fig.2.14. Also, the `FindRoot` command was used for solving for the optimal a which fulfills Eq.(I.27). In summary, that was the method and the code used to achieve a numerical solution in the presence of gravity.

I.3 Finite temperature bubble profile plotted with `AnyBubble` package

In this section, we will plot a bubble profile at finite temperature for a specific potential using the `AnyBubble` package [303]. The `AnyBubble` is a numerical package, written in *Mathematica*, to calculate the bounce solution. There are several packages existing out there for this purpose such as `CosmoTransitions`[304, 305], `BubbleProfiler`[306, 307], `SimpleBounce`[308], and many more algorithms [309–321], but we will focus on an example solved with `AnyBubble`.

This package can solve the generalized EoM for multi-field configurations,

$$\frac{\mathrm{d}^2\phi_i}{\mathrm{d}r^2} + \frac{D-1}{r}\frac{\mathrm{d}\phi_i}{\mathrm{d}r} = \frac{\partial U}{\partial \phi_i}, \tag{I.41}$$

where D is the dimensions number of space-time.

In our one-field case, with $D = 3$ the equation of motion is reduced to

$$\frac{\mathrm{d}^2\phi}{\mathrm{d}r^2} + \frac{2}{r}\frac{\mathrm{d}\phi}{\mathrm{d}r} = \frac{\partial U}{\partial \phi}. \tag{I.42}$$

`AnyBubble` has one main function, `FindBubble`, with its structure given below

```
FindBubble[potential, field, tv, fv]
```

As the arguments of the function impose, the corresponding argument will be entered in each position. Let us for example work with the following potential

$$U(\phi) = \phi^4 - 14\phi^2 + 24\phi. \tag{I.43}$$

For this potential, we will write

```
solution=FindBubble[f[1]^4 − 14 f[1]^2 + 24 f[1], f, {−3}, {2}]
```

Something to be commented in this point is that in a one-field configuration like ours, the user must use the notation `fieldname[1]`, we chose `f[1]` to be the name of the field. If we had n fields we should write `fieldname[n]`, where the number of the fields must be specified exactly in order for the program to run.

The function will return a vector of the form {`action,profile`}, where `action` corresponds to the Euclidean action

$$S_E[\phi] = A_{D-1}\int_0^\infty dr r^{D-1}\left[\frac{1}{2}\partial_r\phi\partial_r\phi + U(\phi) - U(\text{fv})\right], \tag{I.44}$$

here for $D = 3$. On the above A_{D-1} is the area of $(D-1)$-sphere. The second vector's coefficient `profile` corresponds to the field value as a function of the radius r.

Finally, we can draw the bubble profile if we write

```
Plot[solution[[2]][r], {r, 0, 3}, Frame −> True, LabelStyle −> {Black, Bold},
FrameLabel −> {Style["r", 13], Style["ϕ", 13]}, Axes −> False,
PlotRange −> All, PlotStyle −> Red]
```

and we get Fig.I.3

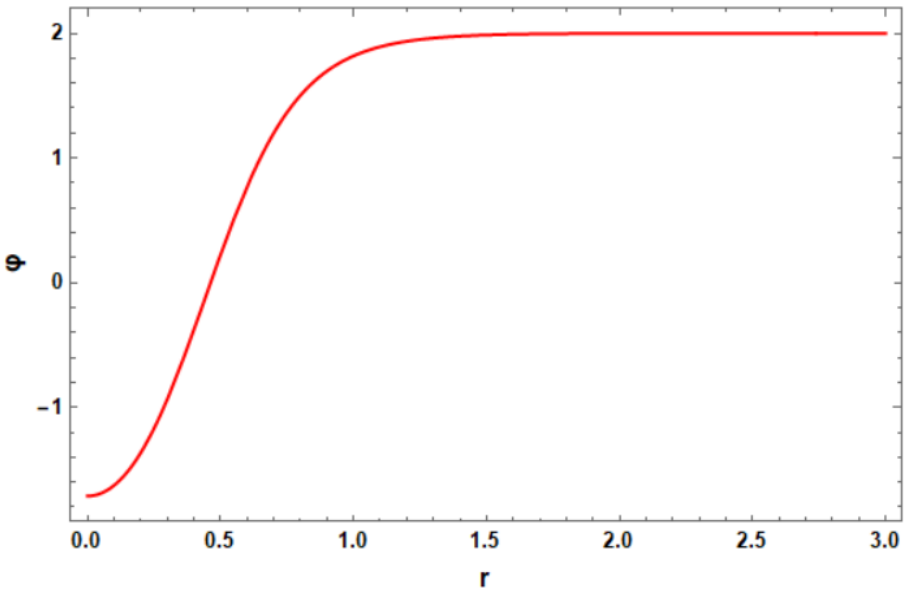

Figure I.3: A bubble profile for a finite temperature phase transition, for the potential of Eq.(I.43), obtained with `AnyBubble` package.

I.4 Modified gravity case

In the modified gravity case of Chapter 4 with $F(\phi) = 1/\kappa - \xi\phi^2$ we used the same approach to solve the Euclidean field equations as in the curved case of Chapter 3 where $\xi = 0$. The code below is solving a $M \to AdS$ transition ($c = 0$), with $\xi = 0.1$, for the toy-model potential used in Chapter 4 at the numerical section.

```
{fv, xi, a, b, c} = {0, 0.1, 1, .1, 0};
u = −1/4 a^2 (3 b − 1) phi[x]^2 + 1/2 a (b − 1) phi[x]^3 + 1/4 phi[x]^4 + a^4 c;
Manipulate[
 R = k/(1 − k∗xi∗phi[x]^2)∗(phi′[x]^2 + 4 u −
    6 xi (phi′[x]^2 + phi[x] phi′′[x] + 3 phi′[x]∗phi[x]∗r′[x]/r[x]));
 due = D[u, phi[x]] /. phi[x] −> e;
 eq1 = phi′′[x] + (3 r′[x]/r[x] phi′[x] − xi∗phi[x]∗R − D[u, phi[x]]) == 0;
 eq2 = r′′[x] + k∗r[x]/(3 (1 − k∗xi∗phi[x]^2)) (phi′[x]^2 + u − 3 xi (phi′[x]^2
 +phi′′[x] phi[x] + phi′[x] phi[x] r′[x]/r[x])) == 0;
 ic = {phi[xmin] == e + 1/8 due xmin^2, phi′[xmin] == 1/4 due xmin,
   r[xmin] == xmin, r′[xmin] == 1};
 sol = ParametricNDSolve[
   Flatten[{eq1, eq2, ic}], {phi, r}, {x, xmin, xmax}, {e}];
 sol1 = FindRoot[phi[e][xmax] == fv /. sol, {e, e0}];
 p1 = Plot[Evaluate[{phi[e][x]} /. sol1 /. sol], {x, xmin, xmax},
   PlotLegends −> {"xi=0.1"}];
 q1 = Plot[Evaluate[{r[e][x]}/10 /. sol1 /. sol], {x, tmin, tmax},
   PlotLegends −> {"xi=0.1"}];
 Show[p1, q1], {{k, 1.9, "kappa"}, 1, 3, 0.1}, {{xmin, 0.01, "eta_min"},
  0.0001, 0.01, 0.0001}, {{xmax, 30, "eta_max"}, 15, 35, 0.1},
  {{e0, 1.033, "e0"}, 0.89, 1.1, 0.01}]
```

In this algorithm `x` is referred to Euclidean time parameter η, and `e0`, is the shooting parameter, our initial guess which must be sufficiently close, but not equal to the true vacuum value to avoid overshoot. The `Manipulate` command is helping us to adjust the parameters of interest in order to achieve the best possible accuracy.

References

[1] G. F. R. E. Stephen W. Hawking, *The large scale structure of space-time*, Cambridge Monographs on Mathematical Physics (Cambridge University Press, 1975).

[2] S. Weinberg, *Gravitation and cosmology: principles and applications of the general theory of relativity* (Wiley, 1972).

[3] E. R. Harrison, "Comments on the big-bang", Nature **228**, 258–260 (1970).

[4] F. Hoyle, "A New Model for the Expanding Universe", mnras **108**, 372 (1948).

[5] H. Bondi and T. Gold, "The Steady-State Theory of the Expanding Universe", mnras **108**, 252 (1948).

[6] C. O'Raifeartaigh and S. Mitton, "A new perspective on steady-state cosmology: from Einstein to Hoyle", in (2015).

[7] K. Helge, *Cosmology and controversy: the historical development of two theories of the universe*, 1st ed. (Princeton University Press, 1996).

[8] M. Livio, "Lost in translation: mystery of the missing text solved", Nature **479**, 171–173 (2011).

[9] G. Lemaître, "Expansion of the universe, A homogeneous universe of constant mass and increasing radius accounting for the radial velocity of extra-galactic nebulae", mnras **91**, 483–490 (1931).

[10] R. A. Alpher, H. Bethe, and G. Gamow, "The origin of chemical elements", Phys. Rev. **73**, 803–804 (1948).

[11] A. A. Penzias and R. Wilson, "A Measurement of Excess Antenna Temperature at 4080 Mc/s.", apj **142**, 419–421 (1965).

[12] S. M. Carroll, "The cosmological constant", Living Reviews in Relativity **4**, `10.12942/lrr-2001-1` (2001).

[13] P. J. E. Peebles, "Tests of cosmological models constrained by inflation", **284**, 439–444 (1984).

[14] P. J. E. Peebles and B. Ratra, "The cosmological constant and dark energy", Rev. Mod. Phys. **75**, 559–606 (2003).

[15] P. Bull et al., "Beyond ΛCDM: Problems, solutions, and the road ahead", Phys. Dark Univ. **12**, 56–99 (2016).

[16] G. Bertone, D. Hooper, and J. Silk, "Particle dark matter: evidence, candidates and constraints", Physics Reports **405**, 279–390 (2005).

[17] A. Bosma, "21-cm line studies of spiral galaxies. II. The distribution and kinematics of neutral hydrogen in spiral galaxies of various morphological types.", **86**, 1825–1846 (1981).

[18]K. C. Freeman, "On the Disks of Spiral and S0 Galaxies", **160**, 811 (1970).

[19]V. C. Rubin, J. Ford W. K., and N. Thonnard, "Rotational properties of 21 SC galaxies with a large range of luminosities and radii, from NGC 4605 (R=4kpc) to UGC 2885 (R=122kpc).", **238**, 471–487 (1980).

[20]V. C. Rubin and J. Ford W. Kent, "Rotation of the Andromeda Nebula from a Spectroscopic Survey of Emission Regions", **159**, 379 (1970).

[21]F. Zwicky, "Die Rotverschiebung von extragalaktischen Nebeln", Helv. Phys. Acta **6**, 110–127 (1933).

[22]F. Zwicky, "On the Masses of Nebulae and of Clusters of Nebulae", **86**, 217 (1937).

[23]S. M. Carroll, W. H. Press, and E. L. Turner, "The cosmological constant", Annual Review of Astronomy and Astrophysics **30**, 499–542 (1992).

[24]A. Einstein, "Cosmological Considerations in the General Theory of Relativity", Sitzungsber. Preuss. Akad. Wiss. Berlin (Math. Phys.) **1917**, 142–152 (1917).

[25]A. Albrecht and P. J. Steinhardt, "Cosmology for grand unified theories with radiatively induced symmetry breaking", Phys. Rev. Lett. **48**, 1220–1223 (1982).

[26]A. H. Guth, "Inflationary universe: a possible solution to the horizon and flatness problems", Phys. Rev. D **23**, 347–356 (1981).

[27]A. D. Linde, "A New Inflationary Universe Scenario: A Possible Solution of the Horizon, Flatness, Homogeneity, Isotropy and Primordial Monopole Problems", Phys. Lett. B **108**, edited by L.-Z. Fang and R. Ruffini, 389–393 (1982).

[28]A. A. Starobinsky, "A New Type of Isotropic Cosmological Models Without Singularity", Phys. Lett. B **91**, edited by I. M. Khalatnikov and V. P. Mineev, 99–102 (1980).

[29]L. Perivolaropoulos and F. Skara, "Challenges for <math altimg="si238.svg" display="inline" id="d1e11032"><mi mathvariant="normal">Λ</mi></math>CDM: An update", New Astron. Rev. **95**, 101659 (2022).

[30]E. W. Kolb and M. S. Turner, *The Early Universe*, Vol. 69 (1990).

[31]M. S. Longair, *Galaxy Formation*, Astronomy and Astrophysics Library (Springer, Heidelberg, Germany, 2008).

[32]P. Coles and F. Lucchin, "Cosmology, the origin and evolution of cosmic structure", Chichester: Wiley, |c1995 **-1** (1995).

[33]S. Dodelson, *Modern Cosmology* (Academic Press, Amsterdam, 2003).

[34]A. R. Liddle, "The Early universe", ASP Conf. Ser. **126**, 31 (1997).

[35]A. R. Liddle and D. H. Lyth, *Cosmological inflation and large scale structure* (2000).

[36]V. Mukhanov, *Physical Foundations of Cosmology* (Cambridge University Press, Oxford, 2005).

[37]M. S. Turner, "Large Scale Structure from Quantum Fluctuations in the Early Universe", Phil. Trans. Roy. Soc. Lond. A **357**, 7 (1999).

[38]D. Scott, "The standard cosmological model", Can. J. Phys. **84**, 419–435 (2006).

[39]M. Kamionkowski and A. Kosowsky, "The Cosmic microwave background and particle physics", Ann. Rev. Nucl. Part. Sci. **49**, 77–123 (1999).

[40]D. J. Fixsen, E. S. Cheng, J. M. Gales, J. C. Mather, R. A. Shafer, and E. L. Wright, "The Cosmic Microwave Background spectrum from the full COBE FIRAS data set", Astrophys. J. **473**, 576 (1996).

[41]J. C. Mather, D. J. Fixsen, R. A. Shafer, C. Mosier, and D. T. Wilkinson, "Calibrator design for the COBE far infrared absolute spectrophotometer (FIRAS)", Astrophys. J. **512**, 511–520 (1999).

[42]G. F. Smoot, C. L. Bennett, A. Kogut, E. L. Wright, J. Aymon, N. W. Boggess, E. S. Cheng, G. de Amici, S. Gulkis, M. G. Hauser, G. Hinshaw, P. D. Jackson, M. Janssen, E. Kaita, T. Kelsall, P. Keegstra, C. Lineweaver, K. Loewenstein, P. Lubin, J. Mather, S. S. Meyer, S. H. Moseley, T. Murdock, L. Rokke, R. F. Silverberg, L. Tenorio, R. Weiss, and D. T. Wilkinson, "Structure in the COBE Differential Microwave Radiometer First-Year Maps", **396**, L1 (1992).

[43]C. L. Bennett, A. Banday, K. M. Gorski, G. Hinshaw, P. Jackson, P. Keegstra, A. Kogut, G. F. Smoot, D. T. Wilkinson, and E. L. Wright, "Four year COBE DMR cosmic microwave background observations: Maps and basic results", Astrophys. J. Lett. **464**, L1–L4 (1996).

[44]L. Page, M. R. Nolta, C. Barnes, C. L. Bennett, M. Halpern, G. Hinshaw, N. Jarosik, A. Kogut, M. Limon, S. S. Meyer, H. V. Peiris, D. N. Spergel, G. S. Tucker, E. Wollack, and E. L. Wright, "First-year iwilkinson microwave anisotropy probe/i (iWMAP/i) observations: interpretation of the TT and TE angular power spectrum peaks", The Astrophysical Journal Supplement Series **148**, 233–241 (2003).

[45]R. H. Cyburt, B. D. Fields, K. A. Olive, and T.-H. Yeh, "Big bang nucleosynthesis: present status", Reviews of Modern Physics **88**, 10.1103/revmodphys.88.015004 (2016).

[46]F. Iocco, G. Mangano, G. Miele, O. Pisanti, and P. D. Serpico, "Primordial nucleosynthesis: from precision cosmology to fundamental physics", Physics Reports **472**, 1–76 (2009).

[47]D. N. Schramm and M. S. Turner, "Big-bang nucleosynthesis enters the precision era", Reviews of Modern Physics **70**, 303–318 (1998).

[48]G. Steigman, "Primordial nucleosynthesis: successes and challenges", Int. J. Mod. Phys. E **15**, 1–36 (2006).

[49]G. Steigman, "Primordial nucleosynthesis in the precision cosmology era", Annual Review of Nuclear and Particle Science **57**, 463–491 (2007).

[50]F. Zwicky, "On the Masses of Nebulae and of Clusters of Nebulae", apj **86**, 217 (1937).

[51]D. Spergel et al., "Wilkinson Microwave Anisotropy Probe (WMAP) three year results: implications for cosmology", Astrophys.J.Suppl. **170**, 377 (2007).

[52]W. J. G. de Blok and A. Bosma, "High-resolution rotation curves of low surface brightness galaxies", Astron. Astrophys. **385**, 816 (2002).

[53]S. Perlmutter, G. Aldering, G. Goldhaber, R. A. Knop, P. Nugent, P. G. Castro, S. Deustua, S. Fabbro, A. Goobar, D. E. Groom, I. M. Hook, A. G. Kim, M. Y. Kim, J. C. Lee, N. J. Nunes, R. Pain, C. R. Pennypacker, R. Quimby, C. Lidman, R. S. Ellis, M. Irwin, R. G. McMahon, P. Ruiz-Lapuente, N. Walton, B. Schaefer, B. J. Boyle, A. V. Filippenko, T. Matheson, A. S. Fruchter, N. Panagia, H. J. M. Newberg, W. J. Couch, and T. S. C. Project, "Measurements of Ω and Λ from 42 high-redshift supernovae", The Astrophysical Journal **517**, 565–586 (1999).

[54]A. G. Riess, A. V. Filippenko, P. Challis, A. Clocchiatti, A. Diercks, P. M. Garnavich, R. L. Gilliland, C. J. Hogan, S. Jha, R. P. Kirshner, B. Leibundgut, M. M. Phillips, D. Reiss, B. P. Schmidt, R. A. Schommer, R. C. Smith, J. Spyromilio, C. Stubbs, N. B. Suntzeff, and J. Tonry, "Observational evidence from supernovae for an accelerating universe and a cosmological constant", The Astronomical Journal **116**, 1009–1038 (1998).

[55]F. Bernardeau, S. Colombi, E. Gaztañaga, and R. Scoccimarro, "Large-scale structure of the universe and cosmological perturbation theory", Physics Reports **367**, 1–248 (2002).

[56]E. Abdalla, G. F. Abellán, A. Aboubrahim, A. Agnello, Özgür Akarsu, Y. Akrami, G. Alestas, D. Aloni, L. Amendola, L. A. Anchordoqui, R. I. Anderson, N. Arendse, M. Asgari, M. Ballardini, V. Barger, S. Basilakos, R. C. Batista, E. S. Battistelli, R. Battye, M. Benetti, D. Benisty, A. Berlin, P. de Bernardis, E. Berti, B. Bidenko, S. Birrer, J. P. Blakeslee, K. K. Boddy, C. R. Bom, A. Bonilla, N. Borghi, F. R. Bouchet, M. Braglia, T. Buchert, E. Buckley-Geer, E. Calabrese, R. R. Caldwell, D. Camarena, S. Capozziello, S. Casertano, G. C.-F. Chen, J. Chluba, A. Chen, H.-Y. Chen, A. Chudaykin, M. Cicoli, C. J. Copi, F. Courbin, F.-Y. Cyr-Racine, B. Czerny, M. Dainotti, G. D'Amico, A.-C. Davis, J. de Cruz Pérez, J. de Haro, J. Delabrouille, P. B. Denton, S. Dhawan, K. R. Dienes, E. D. Valentino, P. Du, D. Eckert, C. Escamilla-Rivera, A. Ferté, F. Finelli, P. Fosalba, W. L. Freedman, N. Frusciante, E. Gaztañaga, W. Giarè, E. Giusarma, A. Gómez-Valent, W. Handley, I. Harrison, L. Hart, D. K. Hazra, A. Heavens, A. Heinesen, H. Hildebrandt, J. C. Hill, N. B. Hogg, D. E. Holz, D. C. Hooper, N. Hosseininejad, D. Huterer, M. Ishak, M. M. Ivanov, A. H. Jaffe, I. S. Jang, K. Jedamzik, R. Jimenez, M. Joseph, S. Joudaki, M. Kamionkowski, T. Karwal, L. Kazantzidis, R. E. Keeley, M. Klasen, E. Komatsu, L. V. Koopmans, S. Kumar, L. Lamagna, R. Lazkoz, C.-C. Lee, J. Lesgourgues, J. L. Said, T. R. Lewis, B. L'Huillier, M. Lucca, R. Maartens, L. M. Macri, D. Marfatia, V. Marra, C. J. Martins, S. Masi, S. Matarrese, A. Mazumdar, A. Melchiorri, O. Mena, L. Mersini-Houghton, J. Mertens, D. Milaković, Y. Minami, V. Miranda, C. Moreno-Pulido, M. Moresco, D. F. Mota, E. Mottola, S. Mozzon, J. Muir, A. Mukherjee, S. Mukherjee, P. Naselsky, P. Nath, S. Nesseris, F. Niedermann, A. Notari, R. C. Nunes, E. Ó. Colgáin, K. A. Owens, E. Özülker, F. Pace, A. Paliathanasis, A. Palmese, S. Pan, D. Paoletti, S. E. P. Bergliaffa, L. Perivolaropoulos, D. W. Pesce, V. Pettorino, O. H. Philcox, L. Pogosian, V. Poulin, G. Poulot, M. Raveri, M. J. Reid, F. Renzi, A. G. Riess, V. I. Sabla, P. Salucci, V. Salzano, E. N. Saridakis, B. S. Sathyaprakash, M. Schmaltz, N. Schöneberg, D. Scolnic, A. A. Sen, N. Sehgal, A. Shafieloo, M. Sheikh-Jabbari, J. Silk, A. Silvestri, F. Skara, M. S. Sloth, M. Soares-Santos, J. S. Peracaula, Y.-Y. Songsheng, J. F. Soriano, D. Staicova, G. D. Starkman, I. Szapudi, E. M. Teixeira, B. Thomas, T. Treu, E. Trott, C. van de Bruck, J. A. Vazquez, L. Verde, L. Visinelli, D. Wang, J.-M. Wang, S.-J. Wang, R. Watkins, S. Watson, J. K. Webb, N. Weiner, A. Weltman, S. J. Witte, R. Wojtak, A. K. Yadav, W. Yang, G.-B. Zhao, and M. Zumalacárregui, "Cosmology intertwined: a review of the particle physics, astrophysics, and cosmology associated with the cosmological tensions and anomalies", Journal of High Energy Astrophysics **34**, 49–211 (2022).

[57]L. A. Anchordoqui, E. Di Valentino, S. Pan, and W. Yang, "Dissecting the H0 and S8 tensions with Planck + BAO + supernova type Ia in multi-parameter cosmologies", JHEAp **32**, 28–64 (2021).

[58]T. Buchert, A. A. Coley, H. Kleinert, B. F. Roukema, and D. L. Wiltshire, "Observational Challenges for the Standard FLRW Model", Int. J. Mod. Phys. D **25**, edited by M. Bianchi, R. T. Jantzen, and R. Ruffini, 1630007 (2016).

[59]E. Di Valentino, O. Mena, S. Pan, L. Visinelli, W. Yang, A. Melchiorri, D. F. Mota, A. G. Riess, and J. Silk, "In the realm of the Hubble tension—a review of solutions", Class. Quant. Grav. **38**, 153001 (2021).

[60]K. Schmitz, "Modern Cosmology, an Amuse-Gueule", (2022).

[61]N. Schöneberg, G. Franco Abellán, A. Pérez Sánchez, S. J. Witte, V. Poulin, and J. Lesgourgues, "The H_0 Olympics: A fair ranking of proposed models", Phys. Rept. **984**, 1–55 (2022).

[62]C. P. Burgess, "The Cosmological Constant Problem: Why it's hard to get Dark Energy from Micro-physics", in 100e Ecole d'Ete de Physique: Post-Planck Cosmology (2015), pp. 149–197.

[63]J. Martin, "Everything You Always Wanted To Know About The Cosmological Constant Problem (But Were Afraid To Ask)", Comptes Rendus Physique **13**, 566–665 (2012).

[64]S. Weinberg, "The cosmological constant problem", Rev. Mod. Phys. **61**, 1–23 (1989).

[65]H. E. S. Velten, R. F. vom Marttens, and W. Zimdahl, "Aspects of the cosmological "coincidence problem"", Eur. Phys. J. C **74**, 3160 (2014).

[66]V. L. Fitch, R. D. Marlow, and M. A. E. Dementi, *Critical problems in physics*, Princeton Series in Physics (1998), p. 123.

[67]E. J. Copeland, M. Sami, and S. Tsujikawa, "Dynamics of dark energy", Int. J. Mod. Phys. D **15**, 1753–1936 (2006).

[68]J. Sola, "Cosmological constant and vacuum energy: old and new ideas", J. Phys. Conf. Ser. **453**, edited by T. Papakostas and D. A. Pliakis, 012015 (2013).

[69]S. Weinberg, *Cosmology* (2008).

[70]J. A. W. John D. Barrow Frank J. Tipler, *The anthropic cosmological principle*, 1st ed., Oxford Paperbacks (Oxford University Press, USA, 1988).

[71]B. Carter, "Anthropic principle in cosmology", in Current issues in cosmology. Proceedings, Colloquium on 'Cosmology: Facts and problems', Paris, France, June 8-11, 2004 (2006), pp. 173–179.

[72]B. Carter, "Anthropic interpretation of quantum theory", Int. J. Theor. Phys. **43**, 721–730 (2004).

[73]L. Susskind, "The Anthropic landscape of string theory", edited by B. J. Carr, 247–266 (2003).

[74]S. Weinberg, "Anthropic bound on the cosmological constant", Phys. Rev. Lett. **59**, 2607–2610 (1987).

[75]N. Aghanim et al., "Planck 2018 results. I. Overview and the cosmological legacy of Planck", Astron. Astrophys. **641**, A1 (2020).

[76]N. Aghanim et al., "Planck 2018 results. VI. Cosmological parameters", Astron. Astrophys. **641**, [Erratum: Astron.Astrophys. 652, C4 (2021)], A6 (2020).

[77]B. P. Abbott et al., "A gravitational-wave standard siren measurement of the Hubble constant", Nature **551**, 85–88 (2017).

[78]S. Basilakos and S. Nesseris, "Conjoined constraints on modified gravity from the expansion history and cosmic growth", Phys. Rev. D **96**, 063517 (2017).

[79]S. Joudaki et al., "KiDS-450 + 2dFLenS: Cosmological parameter constraints from weak gravitational lensing tomography and overlapping redshift-space galaxy clustering", Mon. Not. Roy. Astron. Soc. **474**, 4894–4924 (2018).

[80]L. Kazantzidis and L. Perivolaropoulos, "Evolution of the $f\sigma_8$ tension with the Planck15/ΛCDM determination and implications for modified gravity theories", Phys. Rev. D **97**, 103503 (2018).

[81]E. Macaulay, I. K. Wehus, and H. K. Eriksen, "Lower Growth Rate from Recent Redshift Space Distortion Measurements than Expected from Planck", Phys. Rev. Lett. **111**, 161301 (2013).

[82]S. Nesseris, G. Pantazis, and L. Perivolaropoulos, "Tension and constraints on modified gravity parametrizations of $G_{\rm eff}(z)$ from growth rate and Planck data", Phys. Rev. D **96**, 023542 (2017).

[83]F. Skara and L. Perivolaropoulos, "Tension of the E_G statistic and redshift space distortion data with the Planck - ΛCDM model and implications for weakening gravity", Phys. Rev. D **101**, 063521 (2020).

[84]Y. Akrami et al., "Planck 2018 results. VII. Isotropy and Statistics of the CMB", Astron. Astrophys. **641**, A7 (2020).

[85]D. J. Schwarz, C. J. Copi, D. Huterer, and G. D. Starkman, "CMB Anomalies after Planck", Class. Quant. Grav. **33**, 184001 (2016).

[86]A. Kashlinsky, F. Atrio-Barandela, D. Kocevski, and H. Ebeling, "A measurement of large-scale peculiar velocities of clusters of galaxies: results and cosmological implications", Astrophys. J. Lett. **686**, L49–L52 (2009).

[87]R. Watkins, H. A. Feldman, and M. J. Hudson, "Consistently Large Cosmic Flows on Scales of 100 Mpc/h: a Challenge for the Standard LCDM Cosmology", Mon. Not. Roy. Astron. Soc. **392**, 743–756 (2009).

[88]D. L. Wiltshire, P. R. Smale, T. Mattsson, and R. Watkins, "Hubble flow variance and the cosmic rest frame", Phys. Rev. D **88**, 083529 (2013).

[89]C. A. P. Bengaly, R. Maartens, and M. G. Santos, "Probing the Cosmological Principle in the counts of radio galaxies at different frequencies", JCAP **04**, 031 (2018).

[90]N. J. Secrest, S. von Hausegger, M. Rameez, R. Mohayaee, S. Sarkar, and J. Colin, "A Test of the Cosmological Principle with Quasars", Astrophys. J. Lett. **908**, L51 (2021).

[91]J. A. King, J. K. Webb, M. T. Murphy, V. V. Flambaum, R. F. Carswell, M. B. Bainbridge, M. R. Wilczynska, and F. E. Koch, "Spatial variation in the fine-structure constant – new results from VLT/UVES", Mon. Not. Roy. Astron. Soc. **422**, 3370–3413 (2012).

[92]J. K. Webb, J. A. King, M. T. Murphy, V. V. Flambaum, R. F. Carswell, and M. B. Bainbridge, "Indications of a spatial variation of the fine structure constant", Phys. Rev. Lett. **107**, 191101 (2011).

[93]G. E. Addison, D. J. Watts, C. L. Bennett, M. Halpern, G. Hinshaw, and J. L. Weiland, "Elucidating ΛCDM: Impact of Baryon Acoustic Oscillation Measurements on the Hubble Constant Discrepancy", Astrophys. J. **853**, 119 (2018).

[94]A. Cuceu, J. Farr, P. Lemos, and A. Font-Ribera, "Baryon Acoustic Oscillations and the Hubble Constant: Past, Present and Future", JCAP **10**, 044 (2019).

[95]J. Evslin, "Isolating the Lyman Alpha Forest BAO Anomaly", JCAP **04**, 024 (2017).

[96]Y. Minami, "Determination of miscalibrated polarization angles from observed cosmic microwave background and foreground EB power spectra: Application to partial-sky observation", PTEP **2020**, 063E01 (2020).

[97]Y. Minami and E. Komatsu, "Simultaneous determination of the cosmic birefringence and miscalibrated polarization angles II: Including cross frequency spectra", PTEP **2020**, 103E02 (2020).

[98]Y. Minami, H. Ochi, K. Ichiki, N. Katayama, E. Komatsu, and T. Matsumura, "Simultaneous determination of the cosmic birefringence and miscalibrated polarization angles from CMB experiments", PTEP **2019**, 083E02 (2019).

[99]Y. Minami and E. Komatsu, "New Extraction of the Cosmic Birefringence from the Planck 2018 Polarization Data", Phys. Rev. Lett. **125**, 221301 (2020).

[100]J. S. Bullock and M. Boylan-Kolchin, "Small-Scale Challenges to the ΛCDM Paradigm", Ann. Rev. Astron. Astrophys. **55**, 343–387 (2017).

[101]A. Del Popolo and M. Le Delliou, "Small scale problems of the ΛCDM model: a short review", Galaxies **5**, 17 (2017).

[102]L. Verde, P. Protopapas, and R. Jimenez, "Planck and the local Universe: Quantifying the tension", Phys. Dark Univ. **2**, 166–175 (2013).

[103]B. D. Fields, "The primordial lithium problem", Ann. Rev. Nucl. Part. Sci. **61**, 47–68 (2011).

[104]A. Banerjee, E. O. Colgáin, M. Sasaki, M. M. Sheikh-Jabbari, and T. Yang, "On problems with cosmography in cosmic dark ages", Phys. Lett. B **818**, 136366 (2021).

[105]E. Lusso, E. Piedipalumbo, G. Risaliti, M. Paolillo, S. Bisogni, E. Nardini, and L. Amati, "Tension with the flat ΛCDM model from a high-redshift Hubble diagram of supernovae, quasars, and gamma-ray bursts", Astron. Astrophys. **628**, L4 (2019).

[106]G. Risaliti and E. Lusso, "Cosmological constraints from the Hubble diagram of quasars at high redshifts", Nature Astron. **3**, 272–277 (2019).

[107]I. Antoniou and L. Perivolaropoulos, "Constraints on spatially oscillating sub-mm forces from the Stanford Optically Levitated Microsphere Experiment data", Phys. Rev. D **96**, 104002 (2017).

[108]L. Perivolaropoulos, "Submillimeter spatial oscillations of Newton's constant: Theoretical models and laboratory tests", Phys. Rev. D **95**, 084050 (2017).

[109]J. D. Bowman, A. E. E. Rogers, R. A. Monsalve, T. J. Mozdzen, and N. Mahesh, "An absorption profile centred at 78 megahertz in the sky-averaged spectrum", Nature **555**, 67–70 (2018).

[110]E. Asencio, I. Banik, and P. Kroupa, "A massive blow for ΛCDM – the high redshift, mass, and collision velocity of the interacting galaxy cluster El Gordo contradicts concordance cosmology", Mon. Not. Roy. Astron. Soc. **500**, 5249–5267 (2020).

[111]D. Kraljic and S. Sarkar, "How rare is the Bullet Cluster (in a ΛCDM universe)?", JCAP **04**, 050 (2015).

[112]N. Arkani-Hamed, S. Dimopoulos, and G. R. Dvali, "The Hierarchy problem and new dimensions at a millimeter", Phys. Lett. **B429**, 263–272 (1998).

[113]I. Antoniadis, N. Arkani-Hamed, S. Dimopoulos, and G. R. Dvali, "New dimensions at a millimeter to a Fermi and superstrings at a TeV", Phys. Lett. **B436**, 257–263 (1998).

[114]T. Kaluza, "On the Problem of Unity in Physics", Sitzungsber. Preuss. Akad. Wiss. Berlin (Math. Phys.) **1921**, 966–972 (1921).

[115]D. Huterer and M. S. Turner, "Prospects for probing the dark energy via supernova distance measurements", Phys. Rev. **D60**, 081301 (1999).

[116]S. Carloni, P. K. S. Dunsby, S. Capozziello, and A. Troisi, "Cosmological dynamics of R**n gravity", Class. Quant. Grav. **22**, 4839–4868 (2005).

[117]S. Nojiri and S. D. Odintsov, "Unifying phantom inflation with late-time acceleration: Scalar phantom-non-phantom transition model and generalized holographic dark energy", Gen. Rel. Grav. **38**, 1285–1304 (2006).

[118]G. Allemandi, A. Borowiec, and M. Francaviglia, "Accelerated cosmological models in Ricci squared gravity", Phys. Rev. **D70**, 103503 (2004).

[119]G. Esposito-Farese and D. Polarski, "Scalar tensor gravity in an accelerating universe", Phys. Rev. **D63**, 063504 (2001).

[120]B. Boisseau, G. Esposito-Farese, D. Polarski, and A. A. Starobinsky, "Reconstruction of a scalar tensor theory of gravity in an accelerating universe", Phys. Rev. Lett. **85**, 2236 (2000).

[121]C. Armendariz-Picon, V. F. Mukhanov, and P. J. Steinhardt, "Essentials of k essence", Phys. Rev. **D63**, 103510 (2001).

[122]A. Yu. Kamenshchik, U. Moschella, and V. Pasquier, "An Alternative to quintessence", Phys. Lett. **B511**, 265–268 (2001).

[123]M. C. Bento, O. Bertolami, and A. A. Sen, "Generalized Chaplygin gas, accelerated expansion and dark energy matter unification", Phys. Rev. **D66**, 043507 (2002).

[124]N. Bilic, G. B. Tupper, and R. D. Viollier, "Unification of dark matter and dark energy: The Inhomogeneous Chaplygin gas", Phys. Lett. **B535**, 17–21 (2002).

[125]P. A. M. Dirac, "The Cosmological constants", Nature **139**, 323 (1937).

[126]P. Demarque, L. M. Krauss, D. B. Guenther, and D. Nydam, "The Sun as a Probe of Varying G", **437**, 870 (1994).

[127]D. B. Guenther, L. M. Krauss, and P. Demarque, "Testing the Constancy of the Gravitational Constant Using Helioseismology", **498**, 871–876 (1998).

[128]E. P. Bellinger and J. Christensen-Dalsgaard, "Asteroseismic constraints on the cosmic-time variation of the gravitational constant from an ancient main-sequence star", Astrophys. J. Lett. **887**, L1 (2019).

[129]P. J. Mohr, D. B. Newell, and B. N. Taylor, "Codata recommended values of the fundamental physical constants: 2014", Rev. Mod. Phys. **88**, 035009 (2016).

[130]V. Marra and L. Perivolaropoulos, "Rapid transition of Geff at zt≃0.01 as a possible solution of the Hubble and growth tensions", Phys. Rev. D **104**, L021303 (2021).

[131]S. R. Coleman, "The Fate of the False Vacuum. 1. Semiclassical Theory", Phys. Rev. D **15**, [Erratum: Phys.Rev.D 16, 1248 (1977)], 2929–2936 (1977).

[132]C. G. Callan Jr. and S. R. Coleman, "The Fate of the False Vacuum. 2. First Quantum Corrections", Phys. Rev. D **16**, 1762–1768 (1977).

[133]S. R. Coleman and F. De Luccia, "Gravitational Effects on and of Vacuum Decay", Phys. Rev. D **21**, 3305 (1980).

[134]S. R. Coleman, "The Uses of Instantons", Subnucl. Ser. **15**, edited by M. A. Shifman, 805 (1979).

[135]T. Lancaster and S. J. Blundell, *Quantum field theory for the gifted amateur* (Oxford University Press, Oxford, 2014).

[136]J. J. Sakurai, *Modern quantum mechanics; rev. ed.* (Addison-Wesley, Reading, MA, 1994).

[137]C. M.Bender and S. A. Orszag, *Advanced Mathematical Methods for Scientists and Engineers; rev. ed.* (McGraw-Hill, 1978).

[138]J. Kevorkian and J. Cole, *Multiple scale and singular perturbation methods; rev. ed.* (McGraw-Hill, 1996).

[139]L. Perko, "Nonlinear systems: global theory", in *Differential equations and dynamical systems* (Springer New York, New York, NY, 2001), pp. 181–314.

[140]W. Bpyce and C. Richard, *Elementary differential equations and boundary value problems; rev. ed.* (Willey, 1969).

[141]T. Banks, C. M. Bender, and T. T. Wu, "Coupled anharmonic oscillators. i. equal-mass case", Phys. Rev. D **8**, 3346–3366 (1973).

[142]T. Banks and C. M. Bender, "Coupled anharmonic oscillators. ii. unequal-mass case", Phys. Rev. D **8**, 3366–3378 (1973).

[143]A. Masoumi, "Topics in vacuum decay", PhD thesis (Columbia U., 2013).

[144]H. Goldestein, *Classical Mechanics; rev. ed.* (Addison Wesley, 1969), pp. 362–371.

[145]F. David, "The standard formulations of classical and quantum mechanics", in *The formalisms of quantum mechanics: an introduction* (Springer International Publishing, Cham, 2015), pp. 7–46.

[146]M. E. Peskin and D. V. Schroeder, *An Introduction to quantum field theory* (Addison-Wesley, Reading, USA, 1995).

[147]A. Zee, *Quantum field theory in a nutshell* (2003).

[148]P. V. Nieuwenhuizen and A. Warl, "A continuous Wick rotation for spinor fields and supersymmetry in Euclidean space", in Gauge theories, applied supersymmetry and quantum gravity II (1997).

[149]S. R. Coleman, V. Glaser, and A. Martin, "Action Minima Among Solutions to a Class of Euclidean Scalar Field Equations", Commun. Math. Phys. **58**, 211–221 (1978).

[150]T. Osborne, *Lecture notes on Quantum Field Theory II* (2019).

[151]A. Rajantie and S. Stopyra, "Standard model vacuum decay in a de sitter background", Phys. Rev. D **97**, 025012 (2018).

[152]F. Devoto, S. Devoto, L. Di Luzio, and G. Ridolfi, "False vacuum decay: an introductory review", J. Phys. G **49**, 103001 (2022).

[153]S. Coleman, *Aspects of Symmetry: Selected Erice Lectures* (Cambridge University Press, Cambridge, U.K., 1985).

[154]R. Rajaraman, *SOLITONS AND INSTANTONS. AN INTRODUCTION TO SOLITONS AND INSTANTONS IN QUANTUM FIELD THEORY* (1982).

[155]J. L. Gervais, "Solitons and Instantons in Quantum Field Theory", Acta Phys. Austriaca Suppl. **18**, 385–428 (1977).

[156]D. Boyanovsky, H. de Vega, and D. Schwarz, "Phase transitions in the early and present universe", Annual Review of Nuclear and Particle Science **56**, 441–500 (2006).

[157]G. V. Dunne and H. Min, "Beyond the thin-wall approximation: Precise numerical computation of prefactors in false vacuum decay", Phys. Rev. D **72**, 125004 (2005).

[158]C. Grosche and F. Steiner, *Handbook of Feynman Path Integrals*, Vol. 145 (1998).

[159]R. Feynman, A. Hibbs, and D. Styer, *Quantum mechanics and path integrals*, Dover Books on Physics (Dover Publications, 2010).

[160]L. Schulman, *Techniques and applications of path integration*, Dover Books on Physics (Dover Publications, 2012).

[161]"Application of the calculus of variations to eigenvalue problems", in *Methods of mathematical physics* (John Wiley Sons, Ltd, 1989) Chap. 6, pp. 397–465.

[162]A. Wickens, "Vacuum decay, gravitational waves and magnetic fields in the early universe", PhD thesis (King's Coll. London, King's Coll. London, 2021).

[163]A. Kusenko, "Tunneling in quantum field theory with spontaneous symmetry breaking", Physics Letters B **358**, 47–50 (1995).

[164]J.-L. Gervais and B. Sakita, "Extended Particles in Quantum Field Theories", Phys. Rev. D **11**, edited by K. Kikkawa, M. Virasoro, and S. R. Wadia, 2943 (1975).

[165]A. I. Vainshtein, V. I. Zakharov, V. A. Novikov, and M. A. Shifman, "ABC's of Instantons", Sov. Phys. Usp. **25**, 195 (1982).

[166]M. Paranjape, "Instantons, supersymmetry and morse theory", in *The theory and applications of instanton calculations*, Cambridge Monographs on Mathematical Physics (Cambridge University Press, 2017), 259–296.

[167]W.-Y. Ai, "Aspects of false vacuum decay", PhD thesis (Munich, Tech. U., 2019).

[168]E. Witten, "Analytic Continuation Of Chern-Simons Theory", AMS/IP Stud. Adv. Math. **50**, edited by J. E. Andersen, H. U. Boden, A. Hahn, and B. Himpel, 347–446 (2011).

[169]E. Witten, "A New Look At The Path Integral Of Quantum Mechanics", (2010).

[170]A. D. Linde, *Particle physics and inflationary cosmology*, Vol. 5 (1990).

[171]A. D. Linde, "Decay of the False Vacuum at Finite Temperature", Nucl. Phys. B **216**, [Erratum: Nucl.Phys.B 223, 544 (1983)], 421 (1983).

[172]S. Carroll, *Spacetime and geometry. an introduction to general relativity* (AW, 2004).

[173]P. Kanti, *Lecture notes for the course of cosmology* (2014).

[174]B. Schutz, *A first course in general relativity* (Cambridge University Press, 2009).

[175]G. W. Gibbons and S. W. Hawking, "Action Integrals and Partition Functions in Quantum Gravity", Phys. Rev. D **15**, 2752–2756 (1977).

[176]A. Masoumi, S. Paban, and E. J. Weinberg, "Tunneling from a Minkowski vacuum to an AdS vacuum: A new thin-wall regime", Phys. Rev. D **94**, 025023 (2016).

[177]P. Burda, R. Gregory, and I. Moss, "The fate of the Higgs vacuum", JHEP **06**, 025 (2016).

[178]S. J. Parke, "Gravity, the Decay of the False Vacuum and the New Inflationary Universe Scenario", Phys. Lett. B **121**, 313–315 (1983).

[179]S. W. Hawking and I. G. Moss, "Supercooled Phase Transitions in the Very Early Universe", Phys. Lett. B **110**, 35–38 (1982).

[180]E. J. Weinberg, "Hawking-Moss bounces and vacuum decay rates", Phys. Rev. Lett. **98**, 251303 (2007).

[181]W. Lee and C. H. Lee, "The fate of the false vacuum in Einstein gravity theory with nonminimally-coupled scalar field", Int. J. Mod. Phys. D **14**, 1063–1073 (2005).

[182]W. Lee, B.-H. Lee, C. H. Lee, and C. Park, "False vacuum bubble nucleation due to a nonminimally coupled scalar field", Physical Review D **74**, 10.1103/physrevd.74.123520 (2006).

[183]O. Czerwińska, Z. Lalak, M. Lewicki, and P. Olszewski, "Non-minimally coupled gravity and vacuum stability", PoS **CORFU2016**, 064 (2017).

[184]V. Faraoni, "Nonminimal coupling of the scalar field and inflation", Phys. Rev. D **53**, 6813–6821 (1996).

[185]V. Faraoni, "Inflation and quintessence with nonminimal coupling", Phys. Rev. D **62**, 023504 (2000).

[186]F. Perrotta, C. Baccigalupi, and S. Matarrese, "Extended quintessence", Physical Review D **61**, 10.1103/physrevd.61.023507 (1999).

[187]A. Lykkas and L. Perivolaropoulos, "Scalar-Tensor Quintessence with a linear potential: Avoiding the Big Crunch cosmic doomsday", Phys. Rev. **D93**, 043513 (2016).

[188]S. Capozziello, S. Nesseris, and L. Perivolaropoulos, "Reconstruction of the Scalar-Tensor Lagrangian from a LCDM Background and Noether Symmetry", JCAP **0712**, 009 (2007).

[189]W. J. Misner C.W. Thorne K.S., *Gravitation* (Freeman, 1973).

[190]A. H. Guth and E. J. Weinberg, "Could the Universe Have Recovered from a Slow First Order Phase Transition?", Nucl. Phys. B **212**, 321–364 (1983).

[191]M. B. Hindmarsh, M. Lüben, J. Lumma, and M. Pauly, "Phase transitions in the early universe", SciPost Phys. Lect. Notes **24**, 1 (2021).

[192]A. D. Linde, "Fate of the False Vacuum at Finite Temperature: Theory and Applications", Phys. Lett. B **100**, 37–40 (1981).

[193]R. Kubo, "Statistical mechanical theory of irreversible processes. 1. General theory and simple applications in magnetic and conduction problems", J. Phys. Soc. Jap. **12**, 570–586 (1957).

[194]P. C. Martin and J. Schwinger, "Theory of many-particle systems. i", Phys. Rev. **115**, 1342–1373 (1959).

[195]M. Laine and A. Vuorinen, *Basics of Thermal Field Theory*, Vol. 925 (Springer, 2016).

[196]I. Affleck, "Quantum Statistical Metastability", Phys. Rev. Lett. **46**, 388 (1981).

[197]L. D. McLerran, M. E. Shaposhnikov, N. Turok, and M. B. Voloshin, "Why the baryon asymmetry of the universe is approximately 10**-10", Phys. Lett. B **256**, 451–456 (1991).

[198]L. D. Landau and E. M. Lifshitz, *Statistical Physics, Part 1*, Vol. 5, Course of Theoretical Physics (Butterworth-Heinemann, Oxford, 1980).

[199]P. B. Arnold and O. Espinosa, "The Effective potential and first order phase transitions: Beyond leading-order", Phys. Rev. D **47**, [Erratum: Phys.Rev.D 50, 6662 (1994)], 3546 (1993).

[200]M. Quiros, "Finite temperature field theory and phase transitions", in ICTP Summer School in High-Energy Physics and Cosmology (Jan. 1999), pp. 187–259.

[201]D. A. Kirzhnits and A. D. Linde, "Macroscopic Consequences of the Weinberg Model", Phys. Lett. B **42**, 471–474 (1972).

[202]S. Weinberg, "Gauge and global symmetries at high temperature", Phys. Rev. D **9**, 3357–3378 (1974).

[203]L. Dolan and R. Jackiw, "Symmetry Behavior at Finite Temperature", Phys. Rev. D **9**, 3320–3341 (1974).

[204]D. A. Kirzhnits and A. D. Linde, "Symmetry Behavior in Gauge Theories", Annals Phys. **101**, 195–238 (1976).

[205]A. D. Linde, "Phase Transitions in Gauge Theories and Cosmology", Rept. Prog. Phys. **42**, 389 (1979).

[206]L. C. Loveridge, "Effects of gravity and finite temperature on the decay of the false vacuum", arXiv: High Energy Physics - Theory (2004).

[207]V. Faraoni, *Cosmology in scalar tensor gravity* (2004).

[208]G. N. Remmen and S. M. Carroll, "Attractor Solutions in Scalar-Field Cosmology", Phys. Rev. D **88**, 083518 (2013).

[209]A. G. Riess, "The Expansion of the Universe is Faster than Expected", Nature Rev. Phys. **2**, 10–12 (2019).

[210]K. C. Wong et al., "H0LiCOW – XIII. A 2.4 per cent measurement of H0 from lensed quasars: 5.3σ tension between early- and late-Universe probes", Mon. Not. Roy. Astron. Soc. **498**, 1420–1439 (2020).

[211]A. G. Riess et al., "A Comprehensive Measurement of the Local Value of the Hubble Constant with 1 km s^1 Mpc^1 Uncertainty from the Hubble Space Telescope and the SH0ES Team", Astrophys. J. Lett. **934**, L7 (2022).

[212]D. Sapone, S. Nesseris, and C. A. P. Bengaly, "Is there any measurable redshift dependence on the SN Ia absolute magnitude?", Phys. Dark Univ. **32**, 100814 (2021).

[213]P. Shah, P. Lemos, and O. Lahav, "A buyer's guide to the Hubble constant", Astron. Astrophys. Rev. **29**, 9 (2021).

[214]A. G. Riess, S. Casertano, W. Yuan, J. B. Bowers, L. Macri, J. C. Zinn, and D. Scolnic, "Cosmic Distances Calibrated to 1% Precision with Gaia EDR3 Parallaxes and Hubble Space Telescope Photometry of 75 Milky Way Cepheids Confirm Tension with ΛCDM", Astrophys. J. Lett. **908**, L6 (2021).

[215]G. C. et al., "Igaia/i early data release 3", Astronomy &amp Astrophysics **650**, C3 (2021).

[216]P. Agrawal, F.-Y. Cyr-Racine, D. Pinner, and L. Randall, "Rock 'n' Roll Solutions to the Hubble Tension", (2019).

[217]T. Karwal and M. Kamionkowski, "Dark energy at early times, the hubble parameter, and the string axiverse", Phys. Rev. D **94**, 103523 (2016).

[218]V. Poulin, T. L. Smith, T. Karwal, and M. Kamionkowski, "Early Dark Energy Can Resolve The Hubble Tension", Phys. Rev. Lett. **122**, 221301 (2019).

[219]G. Alestas, L. Kazantzidis, and L. Perivolaropoulos, "H_0 tension, phantom dark energy, and cosmological parameter degeneracies", Phys. Rev. D **101**, 123516 (2020).

[220]E. Di Valentino, A. Melchiorri, and J. Silk, "Reconciling Planck with the local value of H_0 in extended parameter space", Phys. Lett. B **761**, 242–246 (2016).

[221]L. Perivolaropoulos, *"H_0 crisis: systematics of distance calibrators or the end of ΛCDM?"*, Youtube, (2020) https://www.youtube.com/watch?v=RQ0DU88A2ik.

[222]E. Mortsell, A. Goobar, J. Johansson, and S. Dhawan, "The Hubble Tension Revisited: Additional Local Distance Ladder Uncertainties", Astrophys. J. **935**, 58 (2022).

[223]E. Mortsell, A. Goobar, J. Johansson, and S. Dhawan, "Sensitivity of the Hubble Constant Determination to Cepheid Calibration", Astrophys. J. **933**, 212 (2022).

[224]L. Perivolaropoulos and F. Skara, "Hubble tension or a transition of the Cepheid SnIa calibrator parameters?", Phys. Rev. D **104**, 123511 (2021).

[225]B. BASU, T. CHATTOPADHYAY, and S. BISWAS, *An introduction to astrophysics* (PHI Learning, 2010).

[226]L. Perivolaropoulos and F. Skara, "A reanalysis of the latest SH0ES data for H_0: Effects of new degrees of freedom on the Hubble tension", (2022).

[227]G. Alestas, I. Antoniou, and L. Perivolaropoulos, "Hints for a Gravitational Transition in Tully–Fisher Data", Universe **7**, 366 (2021).

[228]R. G. Landim and E. Abdalla, "Metastable dark energy", Phys. Lett. B **764**, 271–276 (2017).

[229]E. Abdalla, L. L. Graef, and B. Wang, "A Model for Dark Energy decay", Phys. Lett. B **726**, 786–790 (2013).

[230]J. A. S. Lima, G. J. M. Zilioti, and L. C. T. Brito, "Extended Metastable Dark Energy", Phys. Dark Univ. **30**, 100713 (2020).

[231]J. A. S. Lima, "Age of the Universe, Average Deceleration Parameter and Possible Implications for the End of Cosmology", (2007).

[232]M. S. Turner, E. J. Weinberg, and L. M. Widrow, "Bubble nucleation in first-order inflation and other cosmological phase transitions", Phys. Rev. D **46**, 2384–2403 (1992).

[233]L. M. Krauss and A. J. Long, "Metastability of the False Vacuum in a Higgs-Seesaw Model of Dark Energy", Phys. Rev. D **89**, 085023 (2014).

[234]D. A. Samuel and W. A. Hiscock, "'Thin wall' approximations to vacuum decay rates", Phys. Lett. B **261**, 251–256 (1991).

[235]N. H. Fletcher, "Size Effect in Heterogeneous Nucleation", **29**, 572–576 (1958).

[236]M. Stone, "The Lifetime and Decay of Excited Vacuum States of a Field Theory Associated with Nonabsolute Minima of Its Effective Potential", Phys. Rev. D **14**, 3568 (1976).

[237]P. H. Frampton, "Vacuum Instability and Higgs Scalar Mass", Phys. Rev. Lett. **37**, [Erratum: Phys.Rev.Lett. 37, 1716 (1976)], 1378 (1976).

[238]M. Stone, "Semiclassical Methods for Unstable States", Phys. Lett. B **67**, 186–188 (1977).

[239]P. H. Frampton, "Consequences of Vacuum Instability in Quantum Field Theory", Phys. Rev. D **15**, 2922 (1977).

[240]C. J. Hogan, "NUCLEATION OF COSMOLOGICAL PHASE TRANSITIONS", Phys. Lett. B **133**, 172–176 (1983).

[241]A. V. Patwardhan and G. M. Fuller, "Late-time vacuum phase transitions: Connecting sub-eV scale physics with cosmological structure formation", Phys. Rev. D **90**, 063009 (2014).

[242]C. J. Hogan, "Cosmological structure produced by a phase transition near nuclear density", **252**, 418–432 (1982).

[243]A. H. Guth and E. J. Weinberg, "Cosmological Consequences of a First Order Phase Transition in the SU(5) Grand Unified Model", Phys. Rev. D **23**, 876 (1981).

[244]J. Ignatius, "Cosmological phase transitions", Other thesis (Oct. 1993).

[245]M. Doran and G. Robbers, "Early dark energy cosmologies", JCAP **06**, 026 (2006).

[246]S. Nesseris and L. Perivolaropoulos, "Evolving newton's constant, extended gravity theories and snia data analysis", Phys. Rev. **D73**, 103511 (2006).

[247]E. Poisson and C. M. Will, "Gravitational waves from inspiraling compact binaries: Parameter estimation using second postNewtonian wave forms", Phys. Rev. **D52**, 848–855 (1995).

[248]P. D. Scharre and C. M. Will, "Testing scalar tensor gravity using space gravitational wave interferometers", Phys. Rev. **D65**, 042002 (2002).

[249]E. Garcia-Berro, J. Isern, and Y. A. Kubyshin, "Astronomical measurements and constraints on the variability of fundamental constants", Astron. Astrophys. Rev. **14**, 113 (2007).

[250]J.-P. Uzan, "Varying Constants, Gravitation and Cosmology", Living Rev. Rel. **14**, 2 (2011).

[251]J. Alvey, N. Sabti, M. Escudero, and M. Fairbairn, "Improved BBN Constraints on the Variation of the Gravitational Constant", Eur. Phys. J. C **80**, 148 (2020).

[252]F. Hofmann and J. Müller, "Relativistic tests with lunar laser ranging", Class. Quant. Grav. **35**, 035015 (2018).

[253]E. V. Pitjeva, N. P. Pitjev, D. A. Pavlov, and C. C. Turygin, "Estimates of the change rate of solar mass and gravitational constant based on the dynamics of the Solar System", Astron. Astrophys. **647**, A141 (2021).

[254]E. V. Pitjeva and N. P. Pitjev, "Relativistic effects and dark matter in the Solar system from observations of planets and spacecraft", Mon. Not. Roy. Astron. Soc. **432**, 3431 (2013).

[255]A. T. Deller, J. P. W. Verbiest, S. J. Tingay, and M. Bailes, "Extremely high precision VLBI astrometry of PSR J0437-4715 and implications for theories of gravity", Astrophys. J. Lett. **685**, L67 (2008).

[256]L. Giani and E. Frion, "Testing the Equivalence Principle with Strong Lensing Time Delay Variations", JCAP **09**, 008 (2020).

[257]W. W. Zhu et al., "Tests of Gravitational Symmetries with Pulsar Binary J1713+0747", Mon. Not. Roy. Astron. Soc. **482**, 3249–3260 (2019).

[258]A. Genova et al., "Solar system expansion and strong equivalence principle as seen by the NASA MESSENGER mission", Nature Communications, 10.1038/s41467-017-02558-1 (2018).

[259]K. Masuda and Y. Suto, "Transiting planets as a precision clock to constrain the time variation of the gravitational constant", Publ. Astron. Soc. Jap. **68**, L5 (2016).

[260]E. Gaztanaga, A. Cabre, and L. Hui, "Clustering of Luminous Red Galaxies IV: Baryon Acoustic Peak in the Line-of-Sight Direction and a Direct Measurement of H(z)", Mon. Not. Roy. Astron. Soc. **399**, 1663–1680 (2009).

[261]E. García-Berro, S. Torres, L. G. Althaus, and A. H. Córsico, "White dwarf constraints on a secularly varying gravitational constant", in 14th Marcel Grossmann Meeting on Recent Developments in Theoretical and Experimental General Relativity, Astrophysics, and Relativistic Field Theories, Vol. 4 (2017), pp. 3651–3656.

[262]R. W. Hellings, P. J. Adams, J. D. Anderson, M. S. Keesey, E. L. Lau, E. M. Standish, V. M. Canuto, and I. Goldman, "Experimental test of the variability of G using viking lander ranging data", Phys. Rev. Lett. **51**, 1609–1612 (1983).

[263]A. Bonanno and H.-E. Fröhlich, "A new helioseismic constraint on a cosmic-time variation of G", Astrophys. J. Lett. **893**, L35 (2020).

[264]A. Vijaykumar, S. J. Kapadia, and P. Ajith, "Constraints on the time variation of the gravitational constant using gravitational-wave observations of binary neutron stars", Phys. Rev. Lett. **126**, 141104 (2021).

[265]J.-P. Uzan, "The Fundamental Constants and Their Variation: Observational Status and Theoretical Motivations", Rev. Mod. Phys. **75**, 403 (2003).

[266]S. Degl'Innocenti, G. Fiorentini, G. G. Raffelt, B. Ricci, and A. Weiss, "Time variation of Newton's constant and the age of globular clusters", Astron. Astrophys. **312**, 345–352 (1996).

[267]S. E. Thorsett, "The Gravitational constant, the Chandrasekhar limit, and neutron star masses", Phys. Rev. Lett. **77**, 1432–1435 (1996).

[268]P. Jofre, A. Reisenegger, and R. Fernandez, "Constraining a possible time-variation of the gravitational constant through gravitochemical heating of neutron stars", Phys. Rev. Lett. **97**, 131102 (2006).

[269]F. Wu and X. Chen, "Cosmic microwave background with Brans-Dicke gravity II: constraints with the WMAP and SDSS data", Phys. Rev. D **82**, 083003 (2010).

[270]L. Iorio, "Gravitational Anomalies in the Solar System?", Int. J. Mod. Phys. D **24**, 1530015 (2015).

[271]G. Feulner, "The faint young sun problem", Reviews of Geophysics **50**, 10.1029/2011rg000375 (2012).

[272]V. Sahni and Y. Shtanov, "Can a variable gravitational constant resolve the faint young Sun paradox?", Int. J. Mod. Phys. D **23**, 1442018 (2014).

[273]D. Camarena and V. Marra, "On the use of the local prior on the absolute magnitude of Type Ia supernovae in cosmological inference", Mon. Not. Roy. Astron. Soc. **504**, 5164–5171 (2021).

[274]A. Gómez-Valent, "Measuring the sound horizon and absolute magnitude of SNIa by maximizing the consistency between low-redshift data sets", Phys. Rev. D **105**, 043528 (2022).

[275]E. Gaztanaga, E. Garcia-Berro, J. Isern, E. Bravo, and I. Dominguez, "Bounds on the possible evolution of the gravitational constant from cosmological type Ia supernovae", Phys. Rev. D **65**, 023506 (2002).

[276]L. Amendola, P. S. Corasaniti, and F. Occhionero, "Time variability of the gravitational constant and type Ia supernovae", (1999).

[277]W. D. Arnett, "Type I supernovae. I - Analytic solutions for the early part of the light curve", **253**, 785–797 (1982).

[278]S. Shankaranarayanan and J. P. Johnson, "Modified theories of gravity: Why, how and what?", Gen. Rel. Grav. **54**, 44 (2022).

[279]K. Hinterbichler, J. Khoury, A. Levy, and A. Matas, "Symmetron Cosmology", Phys. Rev. D **84**, 103521 (2011).

[280]K. Hinterbichler and J. Khoury, "Symmetron Fields: Screening Long-Range Forces Through Local Symmetry Restoration", Phys. Rev. Lett. **104**, 231301 (2010).

[281]M. Maggiore, *Gravitational Waves. Vol. 1: Theory and Experiments*, Oxford Master Series in Physics (Oxford University Press, 2007).

[282]C. Caprini et al., "Detecting gravitational waves from cosmological phase transitions with LISA: an update", JCAP **03**, 024 (2020).

[283]J. Ellis, M. Lewicki, and J. M. No, "On the Maximal Strength of a First-Order Electroweak Phase Transition and its Gravitational Wave Signal", JCAP **04**, 003 (2019).

[284]M. Hindmarsh, S. J. Huber, K. Rummukainen, and D. J. Weir, "Gravitational waves from the sound of a first order phase transition", Phys. Rev. Lett. **112**, 041301 (2014).

[285]R. Jinno and M. Takimoto, "Gravitational waves from bubble collisions: An analytic derivation", Phys. Rev. D **95**, 024009 (2017).

[286]M. Hindmarsh, S. J. Huber, K. Rummukainen, and D. J. Weir, "Numerical simulations of acoustically generated gravitational waves at a first order phase transition", Phys. Rev. D **92**, 123009 (2015).

[287]M. Hindmarsh, S. J. Huber, K. Rummukainen, and D. J. Weir, "Shape of the acoustic gravitational wave power spectrum from a first order phase transition", Phys. Rev. D **96**, [Erratum: Phys.Rev.D 101, 089902 (2020)], 103520 (2017).

[288]V. Vaskonen, "Electroweak baryogenesis and gravitational waves from a real scalar singlet", Phys. Rev. D **95**, 123515 (2017).

[289]R. Apreda, M. Maggiore, A. Nicolis, and A. Riotto, "Gravitational waves from electroweak phase transitions", Nucl. Phys. B **631**, 342–368 (2002).

[290]A. Melfo and L. Perivolaropoulos, "Formation of vortices in first order phase transitions", Phys. Rev. D **52**, 992–998 (1995).

[291]Y.-i. Takamizu and D. Chernoff, "Collisions of false vacuum bubbles in cylindrical symmetry", (2017).

[292]A. Milsted, J. Liu, J. Preskill, and G. Vidal, "Collisions of False-Vacuum Bubble Walls in a Quantum Spin Chain", PRX Quantum **3**, 020316 (2022).

[293]W.-Y. Ai, B. Garbrecht, and C. Tamarit, "Functional methods for false vacuum decay in real time", JHEP **12**, 095 (2019).

[294]V. Glaser, A. Martin, H. Grosse, and W. E. Thirring, "A Family of Optimal Conditions for the Absence of Bound States in a Potential", in *Studies in Mathematical Physics, Essays in Honor of Valentine Bargmann*, edited by E. H. Lieb, B. Simon, and A. S. Wightman (June 1975), pp. 169–194.

[295]V. Maz'ya, *Sobolev spaces*, Grundlehren der mathematischen Wissenschaften (Springer Berlin, Heidelberg).

[296]J. Goldstone and R. Jackiw, "Quantization of nonlinear waves", Phys. Rev. D **11**, 1486–1498 (1975).

[297]R. F. Dashen, B. Hasslacher, and A. Neveu, "Semiclassical bound states in an asymptotically free theory", Phys. Rev. D **12**, 2443–2458 (1975).

[298]A. M. Polyakov, "Particle Spectrum in Quantum Field Theory", JETP Lett. **20**, edited by J. C. Taylor, 194–195 (1974).

[299]J. P. Hu and F. Y. Wang, "High-redshift cosmography: Application and comparison with different methods", Astron. Astrophys. **661**, A71 (2022).

[300]A. G. Riess et al., "A 2.4% Determination of the Local Value of the Hubble Constant", Astrophys. J. **826**, 56 (2016).

[301]J. E. Gentle, "Numerical linear algebra for applications in statistics", in (1998).

[302]A. Rajantie and S. Stopyra, "Standard Model vacuum decay with gravity", Phys. Rev. D **95**, 025008 (2017).

[303]A. Masoumi, K. D. Olum, and B. Shlaer, "Efficient numerical solution to vacuum decay with many fields", JCAP **01**, 051 (2017).

[304]S. Profumo, L. Ubaldi, and C. Wainwright, "Singlet Scalar Dark Matter: monochromatic gamma rays and metastable vacua", Phys. Rev. D **82**, 123514 (2010).

[305]C. L. Wainwright, "CosmoTransitions: Computing Cosmological Phase Transition Temperatures and Bubble Profiles with Multiple Fields", Comput. Phys. Commun. **183**, 2006–2013 (2012).

[306]S. Akula, C. Balázs, and G. A. White, "Semi-analytic techniques for calculating bubble wall profiles", Eur. Phys. J. C **76**, 681 (2016).

[307]P. Athron, C. Balázs, M. Bardsley, A. Fowlie, D. Harries, and G. White, "BubbleProfiler: finding the field profile and action for cosmological phase transitions", Comput. Phys. Commun. **244**, 448–468 (2019).

[308]R. Sato, "SimpleBounce : a simple package for the false vacuum decay", Comput. Phys. Commun. **258**, 107566 (2021).

[309]M. Claudson, L. J. Hall, and I. Hinchliffe, "Low-Energy Supergravity: False Vacua and Vacuous Predictions", Nucl. Phys. B **228**, 501–528 (1983).

[310]A. Kusenko, "Tunneling in quantum field theory with spontaneous symmetry breaking", Phys. Lett. B **358**, 47–50 (1995).

[311]A. Kusenko, P. Langacker, and G. Segrè, "Phase transitions and vacuum tunneling into charge- and color-breaking minima in the mssm", Phys. Rev. D **54**, 5824–5834 (1996).

[312]J. M. Moreno, M. Quiros, and M. Seco, "Bubbles in the supersymmetric standard model", Nucl. Phys. B **526**, 489–500 (1998).

[313]J. M. Cline, J. R. Espinosa, G. D. Moore, and A. Riotto, "String mediated electroweak baryogenesis: A Critical analysis", Phys. Rev. D **59**, 065014 (1999).

[314]P. John, "Bubble wall profiles with more than one scalar field: A Numerical approach", Phys. Lett. B **452**, 221–226 (1999).

[315]J. M. Cline, G. D. Moore, and G. Servant, "Was the electroweak phase transition preceded by a color broken phase?", Phys. Rev. D **60**, 105035 (1999).

[316]T. Konstandin and S. J. Huber, "Numerical approach to multi dimensional phase transitions", JCAP **06**, 021 (2006).

[317]J.-h. Park, "Constrained potential method for false vacuum decays", JCAP **02**, 023 (2011).

[318]V. Guada, A. Maiezza, and M. Nemevšek, "Multifield Polygonal Bounces", Phys. Rev. D **99**, 056020 (2019).

[319]R. Jinno, "Machine learning for bounce calculation", (2018).

[320]J. R. Espinosa and T. Konstandin, "A Fresh Look at the Calculation of Tunneling Actions in Multi-Field Potentials", JCAP **01**, 051 (2019).

[321]M. L. Piscopo, M. Spannowsky, and P. Waite, "Solving differential equations with neural networks: Applications to the calculation of cosmological phase transitions", Phys. Rev. D **100**, 016002 (2019).